Investigating the post-transcriptional regulation of plant immunity by the RNA binding protein GRP7



Brett Wadley

Linacre College

Department of Biology,

University of Oxford

A thesis submitted for the degree of *Doctor of Philosophy*

Michaelmas 2025

Abstract

In Eukaryotes, mRNA exists as a ribonucleoprotein complex consisting of an mRNA transcript associated with RNA-binding proteins (RBPs). RBPs regulate gene expression by orchestrating mRNA processing. The RBP GLYCINE RICH PROTEIN 7 (GRP7) plays a critical role in many physiological processes and stress responses in the model plant *Arabidopsis thaliana* by regulating RNA processing events including alternative splicing (AS) and translation. The RNA binding activity of GRP7 is important for an effective plant immune response as interfering with its RNA recognition motif through targeted mutagenesis, or via the action of the *Pseudomonas syringae* pv. *tomato* DC3000 (*Pto* DC3000) virulence effector HopU1, suppresses pathogen-associated molecular pattern (PAMP)-triggered immunity (PTI). Here, plant optimised individual nucleotide crosslinking and immunoprecipitation version 2 (iCLIP2) has been used to profile changes in the RNA targets and binding sites of GRP7 in *A. thaliana* seedlings following PTI activation by the bacterial elicitor peptide flg22. The targets of GRP7 in the PTI activated condition were significantly enriched in biotic stress associated gene transcripts, many of which have previously been reported as being differentially alternatively spliced following biotic stress exposure. For one of these targets, *CALCIUM-DEPENDENT PROTEIN KINASE 28*, we provide evidence that GRP7 regulates the alternative splicing of this immune regulator in a manner that is consistent with GRP7's role in promoting immunity to *Pto* DC3000. We show that a putative GRP7-regulated gene called *ALLY of AML-1 and LEF-1 3/THO complex subunit 4C* (*ALY3*), which encodes an mRNA export factor, may be associated with susceptibility to *Pto* DC3000. The data presented in this thesis provides a novel insight in the how plant RBPs function during biotic stress and represents an important resource for the wider community to facilitate the identification of new components of the plant immune system. This would help inform future gene editing strategies to improve the disease resistance of economically important crops.

Acknowledgements

Firstly, I would like to thank Professor Gail Preston for her supervision, guidance, and support over the past four years, and for giving me the freedom to follow my research interests.

I would like to thank the Interdisciplinary Bioscience Doctoral Training Partnership and the BBSRC for funding this research and supporting my studentship.

I would also like to thank the many scientists and colleagues who have been mentors and role models for me: Professor Elena Baena-González, Dr Maddy Seale, Dr Nattapong Sanguankiattichai, Dr Marlene Reichel, Dr Floren Scrafton, Dr Morgan Wade, and Dr Marcel Bach-Pages. Thank you to Professor Dorothee Staiger and members of the Staiger lab for hosting me over the summer of 2022.

I would like to thank the past and present members of the Preston and Van der Hoorn labs and the incredible technical support staff in the Department of Biology who made this work possible.

I would also like to thank my A-level Biology teachers Emma Cox and Deborah Hobbs, whose enthusiasm for their subject inspired me to study Biology.

Finally, I would like to thank my parents, Tina and Phil, and the rest of my family and friends. Without your unwavering support I would not be where I am today.

This thesis is dedicated to all first-generation university students.

Table of Contents

CHAPTER 1 GENERAL INTRODUCTION 6

1.1 OVERVIEW OF THE PLANT IMMUNE SYSTEM 7
1.2 TRANSCRIPTIONAL NETWORKS IN PAMP-TRIGGERED IMMUNITY 10
1.2.1 PTI signal transduction and transcriptional regulation 10
1.2.2 Spatial and temporal regulation 11
1.3 OVERVIEW OF THE RNA LIFECYCLE 13
1.3.1 RNA processing in the nucleus 13
1.3.2 mRNA export from the nucleus 16
1.4 RNA BINDING PROTEINS REGULATE PAMP-TRIGGERED IMMUNITY 18
1.4.1 Structural features of RNA binding proteins 18
1.4.2 Studying RBP-RNA interactions in planta 19
1.4.3 Regulation of RNA stability & translation 20
1.4.4 Alternative splicing during immune responses 21
1.4.5 Regulation of nuclear mRNA export 22
1.5 PATHOGENS TARGET HOST RBPS TO SUPPRESS IMMUNITY 24
1.5.1 Oomycete pathogens 24
1.5.2 Fungal pathogens 25
1.5.3 Parasitic nematodes 25
1.5.4 Bacterial pathogens 26
1.6 GRP7: AN RBP AT THE CROSSROADS OF PLANT PHYSIOLOGY, DEVELOPMENT, AND STRESS RESPONSES 28
1.7 METHODS TO STUDY RBPS IN PLANTS 30
1.8 THESIS AIMS AND RATIONALE 32

CHAPTER 2 UNCOVERING THE RNA INTERACTOME OF GLYCINE RICH PROTEIN 7 (GRP7) DURING PAMP-TRIGGERED IMMUNITY 34

2.1 INTRODUCTION 35
2.2 MATERIALS AND METHODS 39
2.2.1 Plant growth conditions 39
2.2.2 Flg22 treatment and validation 39
2.2.3 MAPK phosphorylation assay 39
2.2.4 RT-qPCR quantification of relative gene expression 40
2.2.5 Plant iCLIP2 40
2.2.6 iCLIP2 control immunoblot 43
2.2.7 Bioinformatic analysis 44
2.2.8 Assay of flg22-induced degradation of GRP7 by immunoblot 45
2.2.9 GRP7-GFP confocal microscopy 45
2.2.10 Phylogenetic tree construction 45
2.3 RESULTS 46
2.3.1 Flg22 treatment elicited PTI in seedlings 46
2.3.2 iCLIP2 Control immunoprecipitation and validation 48
2.3.3 GRP7-GFP immunoprecipitation and RNA isolation 49

2.3.4 cDNA library preparation *51*
2.3.5. Library sequencing & quality control *52*
2.3.6 GRP7 target identification and analysis *54*
2.3.7 flg22-only GRP7 target specificity is not driven by transcriptional changes *56*
2.3.8 GRP7 association with known and novel immunity-related RNA targets *57*
2.3.9 Assessing flg22-induced changes in the subcellular localisation of GRP7 ..... *59*
2.3.10 GRP7 is not degraded at 2 hours following PTI activation *60*
2.3.11 Phylogenetic analysis of A. thaliana GRP7 orthologues in crop species *61*
2.4 DISCUSSION 63
2.4.1 Expansion of the GRP7 RNA interactome during PTI *63*
2.4.2 Selective binding of GRP7 to substrate RNA *64*
2.4.3 Study limitations and future directions *66*

CHAPTER 3 INVESTIGATING THE ROLE OF GRP7 IN PTI-ASSOCIATED ALTERNATIVE SPLICING 69

3.1 INTRODUCTION 70
3.2 MATERIALS AND METHODS 72
3.2.1 Plant growth conditions *72*
3.2.2 Flg22 treatment and RNA extraction *72*
3.2.3 Reverse-transcription quantitative PCR (RT-qPCR) *72*
3.2.4 Agromonas lux *73*
3.2.5 Agromonas ROS *73*
3.2.6 RT-PCR validation of transient gene expression *74*
3.2.7 AlphaFold Multimer modelling of candidate protein interactions *74*
3.2.8 sen1-1 mutant identification *74*
3.2.9 Pathogen infection assay *75*
3.3 RESULTS 76
3.3.1 Selection of candidate genes *76*
3.3.2 Validating GRP7 mutant and overexpression A. thaliana lines *81*
3.3.3 GRP7 regulates the alternative splicing of CPK28 mRNA *81*
3.3.4 Validation of transient expression of candidate isoforms in N. benthamiana *84*
3.3.5 Alternative isoforms influence resistance to P. syringae *86*
3.3.6 CPK28 isoforms differentially influence flg22-induced ROS burst *88*
3.3.7 Protein-protein interactions may be affected by truncated isoforms *90*
3.3.8 SEN1 loss-of-function mutants do not have altered resistance to Pto DC3000 ..... *91*
3.4 DISCUSSION 93
3.4.1 GRP7 promotes a PTI-associated CPK28 splicing state that aligns with defence amplification *94*
3.4.2 Isoform identity matters for defence: Behaviours of CPK28 and CIPK3 ..... *95*
3.4.3 SEN1 does not appear to contribute to defence response to Pto DC3000 ..... *97*
3.4.4 Study limitations and future directions *100*

CHAPTER 4 ALY3 – AN RNA BINDING PROTEIN THAT PROMOTES SUSCEPTIBILITY TO *PSEUDOMONAS SYRINGAE* 104

4.1 INTRODUCTION 105
4.2 MATERIALS AND METHODS 107
4.2.1 Plant growth conditions *107*
4.2.2 T-DNA mutant genotyping *107*
4.2.3 Pathogen infection assays *107*
4.2.4 Luminol-based detection of ROS *108*
4.2.5 MAPK phosphorylation assay *109*
4.2.6 RT-qPCR quantification of ALY3 gene expression *109*
4.2.7 RNA binding domain prediction *109*
4.3 RESULTS 110
4.3.1 Screening candidate genes for altered disease resistance *110*
4.3.2 ALY3 promotes susceptibility to virulent and avirulent strains of P. syringae *113*
4.3.3 ALY3 negatively regulates MAPK functioning *114*
4.3.4 GRP7 does not modulate the expression of ALY3 mRNA *115*
4.3.5 Predicting the RNA binding regions of ALY3 ..... *116*
4.4 DISCUSSION 117
4.4.1 ALY3 may promote susceptibility to Pto DC3000 by enhancing MAPK signalling *117*
4.4.2 Study limitations and future directions *119*

CHAPTER 5 GENERAL DISCUSSION 122

5.1 OVERVIEW 123
5.2 IDENTIFICATION OF THE GRP7 INTERACTOME DURING PTI 124
5.3 ALTERNATIVE SPLICING AS A MECHANISM TO FINE-TUNE PTI 126
5.4 RNA BINDING PROTEINS AS TARGETS FOR CROP IMPROVEMENT 128
5.5 CONCLUSIONS 130

APPENDICES 132

APPENDIX I. 133
APPENDIX II. 139
APPENDIX III. 141
APPENDIX IV. 143

REFERENCES 145

Chapter 1

General Introduction

1.1 Overview of the plant immune system

Over the course of their evolution, plants have developed a highly effective innate immune system to defend against pathogenic microorganisms. Unlike vertebrates, plants lack mobile immune cells and an adaptive immune system. Instead, plants rely on pre-formed barriers and cell-autonomous, inducible defence responses (Dodds and Rathjen, 2010; Spoel and Dong, 2012). Over the past two decades enormous progress has been made in uncovering the molecular basis of the immune systems of plants. Combined with the promise of novel engineering biology tools and conventional breeding approaches, this has opened up new strategies to improve the disease resistance traits of crops in the face of global challenges to plant health and food security (Boutrot and Zipfel, 2017; Zaidi *et al.*, 2020).

The first integrated model of plant immunity described a system consisting of two distinct but interconnected sectors called pathogen-associated molecular pattern (PAMP)-triggered immunity (PTI) and effector-triggered immunity (ETI) (Jones and Dangl, 2006). PTI is activated upon the recognition of conserved microbial features, or the damage-associated products of their activity, by cell surface-localised receptors called pattern recognition receptors (PRRs) (Boller and Felix, 2009). This activates a cascade of intracellular signal transduction pathways resulting in defence outputs such as the production of defence metabolites, a reactive oxygen species (ROS) burst in the apoplast and fortification of the cell wall (Yu *et al.*, 2017). These responses are accompanied and augmented by global changes in gene expression, which are regulated at both the transcriptional and post-transcriptional level (Staiger *et al.*, 2013; Tsuda and Somssich, 2015).

A well characterised PAMP-PRR interaction is the perception of the elicitor peptide flg22, derived from bacterial flagellin, by the plant PRR FLAGELLIN-SENSING 2 (FLS2) and its co-receptor BRI1-ASSOCIATED RECEPTOR KINASE 1 (BAK1) in *Arabidopsis thaliana* (Chinchilla *et al.*, 2007; Sun *et al.*, 2013) (figure 1). After gaining entry to the apoplast though natural openings or wounds, bacterial pathogens such as *Pseudomonas syringae* encounter hydrolytic enzymes produced by the host plant, which facilitate the release of PAMPs from pathogen macromolecules that can be detected by the host. One such hydrolase, β-galactosidase 1 (BGAL1) deglycosylates flagellin, which facilitates the release of immunogenic peptide fragments from the bacterial flagellum by additional host proteases (Buscaill *et al.*, 2019). These resulting fragments, such as flg22, bind to FLS2 and result in the heterodimerisation of FLS2 and BAK1 to generate an active signalling module. The intracellular kinase domains of the FLS2-BAK1 complex then transphosphorylate downstream signalling partners such as MITOGEN-ACTIVATED PROTEIN KINASES (MAPK), which subsequently

modulate PTI-responsive gene expression – contributing to pathogen defence (Asai *et al.*, 2002; Maldonado-Bonilla *et al.*, 2014; Pecher *et al.*, 2014; Yu *et al.*, 2017). Furthermore, innate immune recognition of (hemi) biotrophic pathogens such as *P. syringae* triggers changes in host cellular redox signalling and the biosynthesis of the phytohormone salicylic acid (SA), which is essential for the induction of local and systemic defences to this class of pathogens by influencing the expression of thousands of genes through its receptor NONEXPRESSOR OF PR GENES 1 (NPR1) (Vlot, Dempsey and Klessig, 2009). Specifically, SA-induced changes in redox signalling triggers the reduction of disulfide bonds that link NPR1 together in an inactive oligomeric form in the cytoplasm. This results in the translocation of NPR1 into the nucleus where it co-activates the expression of SA-responsive genes (Spoel and Dong, 2024).

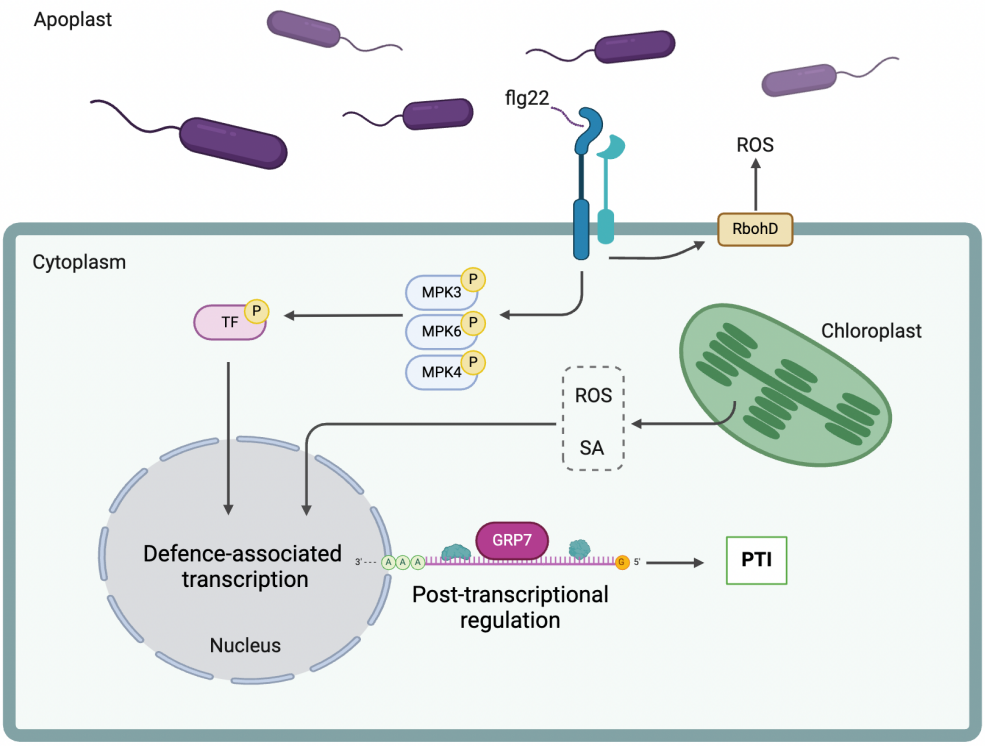

Figure 1. Flg22-induced PAMP-triggered immune (PTI) response. Perception of flg22 by the FLS2/BAK1 receptor pair activates MAPK phosphorylation cascades, converging on MPK3/6/4, which alters the activity of transcription factors (TF) that regulate the transcription of defence-associated genes. The expression of these genes can be regulated at the post-transcriptional level by RNA binding proteins such as GLYCINE RICH PROTEIN 7 (GRP7). Flg22 perception also triggers the production of reactive oxygen species (ROS) in the apoplast and the chloroplast, and the biosynthesis of defence hormones such as salicylic acid (SA), which can both influence gene transcription in the nucleus.

This system is remarkably effective at preventing the growth and proliferation of a range of invading microorganisms and multicellular pests. However, plant pathogens deploy arsenals of virulence effectors that interfere with core components of the immune system to inhibit PTI or to manipulate the host to create a favorable environment for growth (S. Zhang *et al.*, 2022). In the case of *P. syringae* pathovar (pv.) *tomato* DC3000 (*Pto* DC3000), the pathogen secretes effectors into the apoplast, or directly into the host cell via the type III secretion system (T3SS) – a needle-like macromolecular complex that penetrates the host's cell wall and interacts with the host plasma membrane (Cunnac, Lindeberg and Collmer, 2009). Some of these effectors possessed by *Pto* DC3000 can suppress multiple levels of the flg22-FLS2 pathway. For example, a small molecule effector directly suppresses the activity of host BGAL1 to inhibit the generation of flg22, which enables the pathogen to evade recognition by the immune system (Buscaill *et al.*, 2019). Furthermore, the type III secreted effector AvrPtoB is translocated into the host where it interacts with and polyubiquitinates FLS2 – targeting it for degradation and supressing the activity of its kinase signalling domain. This renders the host less sensitive to flg22 (De Torres *et al.*, 2006; Göhre *et al.*, 2008). Other *P. syringae* pathovars deploy effectors, such as AvrRPS4, to suppress flg22-induced PTI at later stages of the signalling cascade by interacting with WRKY-class transcription factors, which regulate the expression of many PTI-responsive genes (Pandey and Somssich, 2009; Sarris *et al.*, 2015).

In turn, plants have evolved a network of intracellular nucleotide-binding/leucine-rich repeat (NB-LRR, or NLR) receptors that either directly recognise pathogen effectors, or detect the activity of such effectors, resulting in ETI (Jones and Dangl, 2006). ETI is characterised by the hypersensitive cell death response (HR), in conjunction with higher amplitude defence responses, which restricts pathogen growth (Cui, Tsuda and Parker, 2015). For example, AvrRPS4 is recognised by the RESISTANCE TO PSEUDOMONAS SYRINGAE 4 (RPS4) and RESISTANCE TO RALSTONIA SOLANACEARUM 1 (RRS1) complex in *A. thaliana*, which activates pathogen defence responses (Williams *et al.*, 2014; Sarris *et al.*, 2015; Mukhi *et al.*, 2021). It has previously been demonstrated that the PTI and ETI pathways converge, particularly at the level of defence gene expression (Peng, van Wersch and Zhang, 2018). We now understand that PTI and ETI in fact are mutually potentiating, as activation of ETI amplifies of the defence and transcriptional responses triggered by PTI (Ngou *et al.*, 2021).

1.2 Transcriptional networks in PAMP-triggered immunity

Due to their sessile nature, plants cannot avoid external stresses such as infection by pathogens. Consequently, they have evolved highly complex transcriptional programmes that possess the capacity to integrate diverse environmental signals to both anticipate and respond to adverse conditions. Early microarray studies investigating the transcriptional basis of plant immunity identified thousands of genes that are differentially regulated in *A. thaliana* following exposure to flg22 (Tao *et al.*, 2003; Navarro *et al.*, 2004). Interestingly, many of these genes were also regulated upon recognition of virulence effectors by NLR proteins, indicating that both PTI and ETI trigger similar transcriptional responses. The wide-scale adoption of next generation sequencing (NGS) approaches has further facilitated the study of global transcriptional responses to a range of pathogens and PAMP elicitors, to identify novel components of the immune system. Bjornson and colleagues demonstrated that core sets of genes are similarly regulated in response to a range of pathogen and host-derived elicitors irrespective of their origin, suggesting that plants rely on a general transcriptional programme to respond to the early stages of an infection (Bjornson *et al.*, 2021).

1.2.1 PTI signal transduction and transcriptional regulation

Immediately following perception of PAMPs by PRRs, signalling cascades are activated which converge on sets of transcription factors, subsequently regulating the rate of transcription of PTI-responsive target genes. A rapid and transient increase in the concentration of cytoplasmic calcium (Ca^{2+}) is one of the earliest signalling events to occur following pathogen recognition (Yu *et al.*, 2017). This event is perceived by calcium binding proteins such as calmodulin (CaM), calcium-dependent protein kinases (CPKs), and calcineurin B-like proteins (CBLs), which interact with downstream signalling partners to regulate various PTI-related responses including transcriptional reprogramming in the nucleus (Reddy and Reddy, 2004; Wang and Luan, 2024). For example, Ca^{2+} stimulates the interaction of CaM with its transcription factor signalling partner CBP60g to directly regulate the expression of thousands of PTI-responsive genes, including genes involved in the biosynthesis of SA (Wang *et al.*, 2009; Sun *et al.*, 2015).

The WRKY family of transcription factors have been firmly linked to the innate immune response of *A. thaliana* and are dynamically regulated by MAPKs and CDPKs in response to pathogen challenge (Tsuda and Somssich, 2015). Following the detection of flg22 by FLS2, two MAPK phosphorylation cascades are initiated, resulting in the activation of MPK6, MPK3, and MPK4, which are critical upstream regulators of PTI-responsive gene expression (Petersen *et al.*, 2000;

Asai *et al.*, 2002; Gao *et al.*, 2008; Frei dit Frey *et al.*, 2014). For example, flg22 perception activates MPK4, which through the phosphorylation of an additional signalling partner MAP KINASE SUBSTRATE 1 (MKS1), releases WRKY33 from nuclear complexes. WRKY33 then regulates the transcription of defence-associated genes such as *PHYTOALEXIN DEFICIENT3* (*PAD3*), a key enzyme in the antimicrobial camalexin biosynthetic pathway, by directly interacting with its promoter (Qiu *et al.*, 2008).

1.2.2 Spatial and temporal regulation

Interestingly, these transcriptional responses to biotic stress display distinct spatial and temporal variation. Recent advances in single-cell RNA sequencing (scRNA-seq) methodologies have enabled researchers to probe how pathogen-responsive transcriptional changes vary between cell types and across tissues. These analyses have revealed that different cell types display markedly different levels of transcription of immunity and susceptibility-related genes throughout the infection process (Zhu *et al.*, 2023); details which are lost during the preparation of bulk tissue. Furthermore, priming-associated transcriptional changes occurring in in distal tissues underpin systemic acquired resistance (SAR), a conserved phenomenon in plant defence whereby local pathogen exposure induces systemic broad-spectrum disease resistance (Vlot, Dempsey and Klessig, 2009).

Central to the induction of SAR is the SA-mediated activation of NPR1. Under normal physiological conditions NPR1 is retained in the cytoplasm as a homotetramer linked by disulphide bonds. Upon the activation of immunity, mobile SAR signals such as SA triggers the redox-based monomerization of NPR1, which is catalysed by Thioredoxins (TRXs) (Mou, Fan and Dong, 2003; Tada *et al.*, 2008). Monomeric NPR1 translocates to the nucleus where it activates the expression of *PATHOGENESIS-RELATED* (*PR*) genes via its interaction with TGA class transcription factors (Kinkema, Fan and Dong, 2000; Fan and Dong, 2002; Després *et al.*, 2003). This primes the immune system for subsequent infection at distal sites (Vlot *et al.*, 2021).

Transcriptional changes can occur within minutes following pathogen detection, with the maximum PTI-associated gene expression changes occurring at 2 hours following infection with a disarmed strain of *P. syringae* lacking a T3SS, which cannot deliver virulence effectors into the host to suppress PTI (Lewis *et al.*, 2015; Yu *et al.*, 2017). In particular, the expression of photosynthesis and chloroplast-related genes are significantly downregulated during the initial hours of the PTI response in *A. thaliana* (Lewis *et al.*, 2015). In contrast, wildtype *Pto* DC3000 utilises virulence effectors to rapidly manipulate the transcriptome to suppress host defence responses. For

example, the pathogen induces the expression of genes involved in abscisic acid (ABA) signalling to interfere with SA-associated defences, which promotes bacterial growth (De Torres Zabala *et al.*, 2009; Lewis *et al.*, 2015).

Furthermore, the transcriptional dynamics that underpin PTI can be influenced by the time of day of an infection, as a link between the circadian clock and plant immunity has been firmly established at the transcriptional level. Initial studies identified that the level of resistance to pathogens was dependent upon the time of day of the inoculation, as *A. thaliana* infected in the morning displayed increased resistance (Griebel and Zeier, 2008). It was subsequently found that the expression of many biotic stress-responsive genes associated with PTI, such as *FLS2*, undergo daily transcriptional oscillations in the absence of pathogens, peaking in the morning, which is mediated by the core clock component CIRCADIAN CLOCK ASSOCIATED 1 (CCA1) (Bhardwaj *et al.*, 2011; Zhang *et al.*, 2013). Accordingly, the expression level of biotic stress-responsive genes and the amplitude of corresponding pathogen defence responses was found to be significantly higher upon elicitation of PTI in the morning compared to the evening in *Arabidopsis thaliana* (Korneli, Danisman and Staiger, 2014). It is hypothesised that circadian co-regulation of PTI at the transcriptional level enables the plant host to anticipate infections at times of day when pathogen dispersal and invasion is most likely. Taken together, these studies demonstrate that reprogramming of the transcriptome is an essential component of PTI response to pathogens.

1.3 Overview of the RNA lifecycle

During transcription by RNA polymerase II (RNAP II), nascent pre-mRNA transcripts must undergo a series of processing steps which ultimately regulate their function and expression. These processing reactions are tightly regulated and can be influenced by both physiological and environmental cues. In brief, these stages include the addition of a 5' end cap, (alternative) splicing, 3' end formation (most commonly via poly-adenylation), RNA base editing, export through the nuclear pore complex, translation, and regulated decay (Marquardt, Petrillo and Manavella, 2023).

1.3.1 RNA processing in the nucleus

Almost immediately after a nascent transcript emerges from RNAP II, its 5' end undergoes capping by the covalent addition of a 5' 7-methylguanosine (m7G) cap that protects the transcript from degradation by exonucleases and importantly, facilitates the recruitment of factors that regulate the subsequent processing reactions (Jurado *et al.*, 2014; Ramanathan, Robb and Chan, 2016). The second major processing step involves the removal of intervening regions called introns and the ligation of the remaining regions called exons to form the mature mRNA in a process referred to a splicing. In Eukaryotes, splicing is predominantly catalysed by the spliceosome – a macromolecular complex comprised of multiple protein-ncRNA complexes known as small nuclear ribonucleoprotein complexes (snRNPs) (Wilkinson, Charenton and Nagai, 2020). Splicing is initiated upon the assembly of the U1 snRNP and the U2 auxiliary factor (U2AF) at the 5' and 3' splice sites of an intron respectively, together triggering the recruitment and assembly of additional snRNPs and auxiliary factors on the pre-mRNA which orchestrate the splicing process. At its core, the splicing reaction requires the formation of a covalent bond between the Adenosine residue at the branch point (within the intron) with the 5' splice site, and the subsequent formation of a covalent bond between the 3' hydroxyl group of the upstream exon with the 3' splice site. Highly coordinated cleavage and ligation reactions result in a mature RNA with a contiguous sequence of exons, and the removal of the intron as a lariat structure that is subsequently degraded (Meyer, Koester and Staiger, 2015).

One of the non-snRNP protein complexes that has a fundamental role in the activation of the splicing reaction following snRNP assembly in *A. thaliana* is the MOS4-associated complex (MAC), which is functionally similar to the Nineteen complex (NTC) in humans (Monaghan, Germain, *et al.*, 2010; Meyer, Koester and Staiger, 2015). Interestingly, its founding member MODIFIER OF SNC1, 4 (MOS4), was first identified in a suppressor screen to identify genes that operate downstream of a

gain-of-function mutation in *SNC1* – encoding a Toll/interleukin-1 receptor (TIR) class of NLR that causes a severe autoimmune phenotype. This suggests that MOS4 functions as a positive regulator of immunity (Palma *et al.*, 2007). Many additional MAC components such as the E3 ligases MAC3A and MAC3B, and the putative RNA binding protein MAC5A have also been described to play a role in the regulation of PTI and ETI responses to *P. syringae* pathogens (Monaghan *et al.*, 2009; Monaghan, Xu, *et al.*, 2010). These findings highlight the intimate link between splicing regulation and immune system processes in plants.

Simultaneously to the discovery of Eukaryotic RNA Splicing in the 1970's the process of Alternative Splicing (AS) was described (Berget, Moore and Sharp, 1977; Chow *et al.*, 1977), which offered an explanation as to the function of introns in Eukaryotic genomes. At its most fundamental definition, AS is the process whereby the spliceosome recognises alternative 5' and 3' splice sites to generate mature mRNA with differing combinations of exons, introns and intron fragments (Meyer, Koester and Staiger, 2015) (figure 2). This process increases the diversity of the transcriptome; consequently expanding the protein-coding capacity of Eukaryotic genomes and contributing to proteome plasticity (Marquez *et al.*, 2012, 2015). Pre-mRNA AS can exert two main effects on gene expression in plant cells: i) Quantitative changes in the expression of the substrate mRNA – as certain RNA isoforms may be degraded or sequestered at higher rates (Kalyna *et al.*, 2012; Drechsel *et al.*, 2013; Göhring, Jacak and Barta, 2014); ii) Changes to the function of the protein product by generating alternative protein isoforms with altered primary sequences and domain architecture (Staiger and Brown, 2013). Importantly, the frequency and types of AS can change in response to endogenous physiological and exogenous environmental cues, thus enabling Eukaryotes to rapidly alter gene expression in response to stress. In *A. thaliana*, over 62% of multiexonic genes undergo AS under normal physiological conditions, with this figure increasing to 66% when exposed to various biotic and abiotic stresses (Martín *et al.*, 2021).

RNA splice sites vary in their affinity for splicing factors due to differences in their homology to a conserved consensus sequence. Therefore, splice sites can either be considered 'strong' or 'weak' based on their ability to recruit the splicing machinery, which creates competition between splice sites and results in the differential usage of alternative splice sites. In plants, RNA processing including splicing, primarily occurs co-transcriptionally, meaning that splicing occurs on nascent pre-mRNA during its transcription. This permits functional coupling between transcription and splicing whereby RNAP II can directly influence AS either by the recruitment of splicing factors to the pre-mRNA (recruitment model) or by altering the rate of transcription, which changes the

duration that a particular splice site is presented to the splicing apparatus in the nucleoplasm (kinetic model) (Kufel, Diachenko and Golisz, 2022). AS decisions at weaker splice sites are ultimately determined by the interaction of trans-acting regulatory factors with cis-regulatory elements contained within the pre-mRNA. These elements may be located within exons or introns and are referred to as exonic/intronic splicing enhancers (ESE/ISE) or exonic/intronic splicing silencers (ESS/ISS) depending upon their function to activate or repress a splice site. Generally, trans-acting splicing factors belong to one of two groups called Serine-Arginine rich (SR) proteins, or heterogeneous nuclear ribonucleoparticle proteins (hnRNP) (Meyer, Koester and Staiger, 2015), which can have dual functions to promote or suppress splicing depending on their sequence context. For example, hnRNP binding at a splicing repressor site may block the recruitment of the splicing machinery, resulting in the retention of an alternative exon or intron. Alternatively, hnRNP binding within an splicing enhancer can promote the exclusion of an alternative exon (Wachter, Rühl and Stauffer, 2012).

Alternatively regulated splice site selection can result in different types of AS events including cassette exon skipping, intron retention, alternative 5' splice site or 3' splice site selection. The most common AS event in plants is intron retention (IR) and is particularly responsive to stress. Many intron-retained transcripts encode premature termination codons (PTCs) and are commonly retained within the nucleus. It is hypothesised that IR may provide an important mechanism to create a pool of detained transcripts, which subsequently undergo stress-responsive post-transcriptional splicing to rapidly upregulate the expression of the gene when required (Jia *et al.*, 2020).

Under normal physiological conditions, intron-retained transcripts that encode PTCs will be degraded in the cytosol via the nonsense mediated decay (NMD) pathway – a quality control mechanism that protects Eukaryotic cells against the accumulation of potentially toxic truncated proteins (Maquat, 2005). Interestingly, the suppression of NMD is a key host-directed event during the defence response to pathogens, as this pathway negatively regulates the expression of immunity-associated genes in *A. thaliana* (Gloggnitzer *et al.*, 2014; Shaul, 2015). Mutants deficient in the NMD pathway had enhanced expression of genes involved in SA-mediated defence, and displayed enhanced resistance to *Pto* DC3000 (Rayson *et al.*, 2012). Therefore, it's possible that PTC-containing transcripts generated via IR may be translated into truncated proteins with altered functionality that may modulate biotic stress responses. For example, truncated proteins may exert a dominant negative effect whereby the rare, truncated isoform interferes with the activity of the

canonical protein isoform – consequently masking its phenotype (Staiger and Brown, 2013). Additionally, retained introns that maintain the open reading frame of a transcript can be exported and translated in the cytosol and are referred to as exitrons. Formally known as cryptic introns, exitrons encode proteins with new domains that could gain novel functions (Marquez *et al.*, 2012, 2015).

1.3.2 mRNA export from the nucleus

Due to the compartmentalisation of transcription and translation in Eukaryotes, mature transcripts must transit from the nucleus to the cytoplasm to interact with the ribosomes in order to be translated. The complete sequence of events from mRNA recognition to delivery into the cytoplasm is a highly coordinated process referred to as nuclear RNA export, which requires a variety of RNA export adapters and the nuclear pore complex (NPC) (Germain and Gaouar, 2013). The nuclear membrane is perforated by many openings that are gated by protein factors that regulate the transport of macromolecules into and out of the nucleoplasm (Meier, Richards and Evans, 2017). As nuclear export precedes translation, regulation of export is another mechanism by which plant cells can modulate gene expression and is under tight control.

A central player in nuclear RNA export is the Transcription Export Complex (TREX) which consists of the core THO complex, a hexamer that is conserved between plants and metazoans, along with additional export factors which vary between kingdoms. The core THO complex associates with UAP56, an RNA helicase that is implicated in both alternative splicing and RNA export, which mediates the recruitment of additional export adaptors such as the ALY (*ALLY of AML-1 and LEF-1*) protein family (ALY1 – ALY4) and MOS11 (MODIFIER OF SNC1, 11) (Ehrnsberger, Grasser and Grasser, 2019). The assembly of the TREX complex on mature mRNA generates messenger Ribonucleoparticles (mRNPs) that are designated for unidirectional export into the cytoplasm. Interestingly, mutants in the components of TREX are associated with pleiotropic developmental phenotypes and often compromised immune responses to pathogens, as observed for the *aly* quadruple mutant and the *mos11* loss-of-function mutant in *A. thaliana* (Germain *et al.*, 2010; Pfaff *et al.*, 2018). The specific roles of RNA export adaptor proteins and the level of functional redundancy between them remains unclear, however, some studies are beginning to shed light on this. For instance, all ALY proteins show ubiquitous expression in the nuclei of root and leaf epidermal tissue in *A. thaliana*, but display subtle differences in their sub-nuclear localisation, which may indicate differing functions and RNA substrates for each ALY protein (Uhrig *et al.*, 2004; Pfaff *et al.*, 2018). ALY1 is specifically required to enable RNA-directed DNA methylation (RdDM),

an epigenetic modification that facilitates the transcriptional silencing of transposable elements in the genome (Choudury *et al.*, 2019). Furthermore, the RNA silencing inhibitor P19 from the tomato bushy stunt virus (TBSV), which is required for full virulence, directly interacts with all members of the ALY family in *A. thaliana* via their central RNA recognition motif. Transient expression of P19 caused the re-localisation of only ALY2 and ALY4 from the nucleus to the cytoplasm, further highlighting their differential roles in RNA export and plant-pathogen interactions (Uhrig *et al.*, 2004).

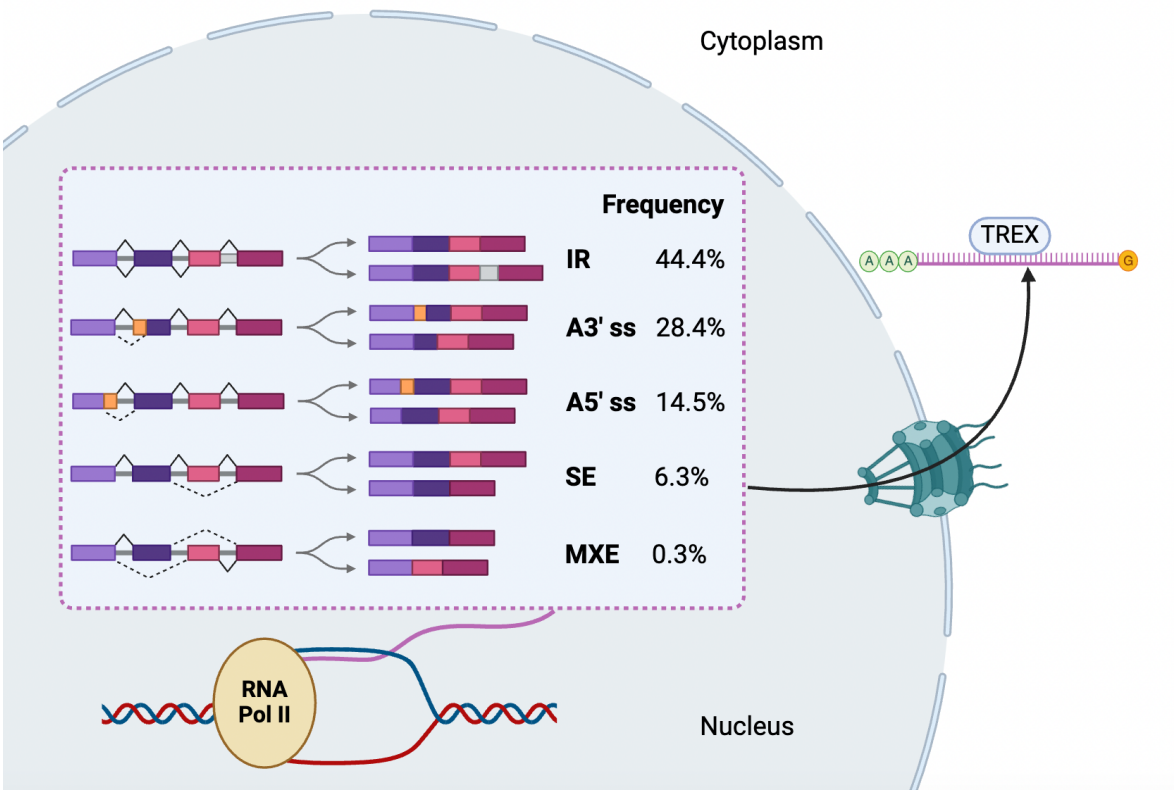

Figure 2. Nuclear mRNA processing and export in plants. During transcription by RNA Polymerase II, nascent transcripts undergo alternative splicing (AS) catalysed by the spliceosome. Types of AS include intron retention (IR); alternative 3' splice site (A3' ss); alternative 5' splice site (A5' ss); skipped exons (SE) – also referred to as cassette exons; mutually exclusive exons (MXE). The frequency of each type of event is listed as described in the most recent release of the *A. thaliana* reference transcriptome (AtRTD3) (Zhang *et al.*, 2022). Mature mRNA transcripts are designated for export via the nuclear pore complex by the transcription export complex (TREX).

1.4 RNA binding proteins regulate PAMP-triggered immunity

Research pertaining to the expression of biotic-responsive genes during PTI has primarily focused on their regulation at the transcriptional level. However, it has become clear that this view is an oversimplification, as post-transcriptional regulation of many biotic-stress responsive genes is also required for an effective plant immune response (Staiger *et al.*, 2013; Bach-Pages *et al.*, 2025).

1.4.1 Structural features of RNA binding proteins

As described in the previous section, maturation of mRNA requires a series of processing steps occurring during and after transcription. These processing reactions are orchestrated by RNA binding proteins (RBPs) and small RNAs, which provide direct points of regulation of the mRNA and thereby influence the expression of the gene (Lee and Kang, 2016). Canonical RBPs are classified as such based on the presence of one or more well-characterised RNA binding domains (RBDs) that physically mediate the interaction with its substrate RNA. Common classes of RBDs encoded by plant genomes include RNA recognition motifs (RRM), K homology (KH) domains, double-stranded RNA-binding domain (dsRBD), and zinc finger domains. Most RBPs possess a modular structure that consists of one or more of these RBDs and their precise arrangement is often critical for the function of the protein (Lunde, Moore and Varani, 2007).

Mechanistically, the amino acid side chains within RBDs facilitate the formation of relatively strong, non-covalent interactions such as hydrogen bonds, salt bridges and weak interactions including hydrophobic interactions and Van der Waals forces with the nucleotide residues or backbone of the RNA substrate (Corley, Burns and Yeo, 2020). Therefore, the sequences of amino acids and nucleotides within the RBD and RNA respectively determine the specificity and strength of the interaction. However, It is also important to note that global analyses of the entire RNA binding proteome of plants have identified hundreds of so called 'non-canonical RBPs' that lack clearly identifiable RBDs – indicating that modes of RNA binding occur beyond the conventional mechanisms (Bach-Pages, Homma, *et al.*, 2020; Liu *et al.*, 2020; Y. Zhang *et al.*, 2023).

Genome-wide analyses have detected almost 200 genes encoding proteins with recognisable RRMs in *A. thaliana* – demonstrating that the RRM domain is the most common type of RBD among canonical RBPs in this species (Lorković and Barta, 2002). Also known as the Ribonucleoprotein (RNP) domain, RRMs are an evolutionarily ancient and ubiquitous protein motifs, as RRM-containing proteins have been identified in all domains of life (Maris, Dominguez and Allain, 2005). Structurally, RRMs consist of two alpha-helices and four beta-sheets arranged in a

$\beta_1\alpha_1\beta_2\beta_3\alpha_2\beta_4$ topology. Two highly conserved sequence motifs within β-sheets 1 and 3 are designated as RNP2 (six amino acids) and RNP1 (eight amino acids) respectively, and are enriched in positively charged, aromatic side chains that form direct contact with the RNA substrate (Burd and Dreyfuss, 1994). RRM-containing proteins are further subdivided into families based on shared structural features such as total number of RRMs and the presence of auxiliary domains that enable these proteins to fulfil their diverse functions relating to RNA processing.

1.4.2 Studying RBP-RNA interactions *in planta*

Efforts to comprehensively profile the RNA binding proteome (RBPome) has culminated in the development of RNA interactome techniques (Bach-Pages, Castello and Preston, 2017). These are RNA-centric approaches which involve covalent crosslinking of the RBPs engaged with an RNA transcript, followed by the isolation of the RBP-RNA complexes through capturing the polyadenylated RNA. The identity of the associated RBPs can be subsequently determined by mass spectrometry or via orthogonal techniques such as an immunoblot. RNA interactome methodologies can provide a global view of the active RBPome during a specific developmental stage or experimental condition (Marondedze *et al.*, 2016; Reichel *et al.*, 2016; Z. Zhang *et al.*, 2017).

One variation called plant RNA interactome capture (ptRIC) has recently been used to profile the early and late flg22-responsive RBPome in mature leaf tissue in *A. thaliana* (Bach-Pages, Chen, *et al.*, 2020). This study revealed that the RNA binding activity of 112 RBPs was significantly altered at 2 hours following elicitation of PTI with flg22. For the majority of these RBPs, this early change in RNA binding activity was not attributed to changes in protein abundance, instead this observation was most likely the result of post-translational modifications (PTMs). These early flg22-responsive RBPs were significantly enriched in PTM sites that are associated with S-nitrosylation (SNO), the covalent attachment of Nitric Oxide to Cysteine residues, and depleted in Lysine Ubiquitination. An enrichment in SNO is particularly notable as a burst of Nitric Oxide occurs rapidly following pathogen detection, and many critical immune signalling proteins such as NPR1 become substrates for SNO – altering their functionality (Borrowman, Kapuganti and Loake, 2023).

Interestingly, many non-canonical RBPs were detected as being flg22-responsive, including many metabolic enzymes (Bach-Pages, Chen, *et al.*, 2020). Subsequent analysis of knockout mutant and overexpression lines of a subset of flg22-responsive RBPs including the canonical RBP RNA HELICASE 11 (RH11), and the metabolic enzyme S-ADENOSYLMETHIONINE SYNTHASE 4 (METK4),

confirmed their functions in resistance and susceptibility to *Pto* DC3000 respectively. These results demonstrate that the interaction of RBPs and RNA in plants is dynamic and highly responsive to elicitor molecules, which supports an emerging model of RBP-mediated immunity whereby RBPs actively orchestrate the remodelling of the transcriptome that occurs during the plant immune response to pathogens (Bach-Pages, Chen, *et al.*, 2020). Furthermore, a growing body of evidence has demonstrated that RBPs with immunity-related functions are implicated in every stage of the mRNA maturation process (Bach-Pages *et al.*, 2025); several key examples are summarised below.

1.4.3 Regulation of RNA stability & translation

Altering the steady-state abundance of mRNA is a strategy used by plant cells to rapidly change the expression of a gene without necessarily changing the rate of its transcription. This type of post-transcriptional regulation can be coordinated with PTI signalling to efficiently induce an appropriate defence response (Staiger *et al.*, 2013). For example, elicitation of PTI in *Phaseolus vulgaris* by a fungal elicitor triggers the down-regulation of a putative cell wall-localised protein (*Pv*PRP1), which is hypothesised to enhance pathogen resistance by increasing the efficiency of cell wall crosslinking during infection (Zhang *et al.*, 1993). This downregulation is thought to be achieved through the activation of a trans-acting protein factor, PRP-BP (*Pv*PRP1 binding protein). PRP-BP is an RBP that binds to the 3' untranslated region (UTR) of the *PvPRP1* transcript upon elicitation of PTI – resulting in its destabilisation and the consequential downregulation of *Pv*PRP1 production (Zhang and Mehdy, 1994).

Sequestering mRNA transcripts in compartments called Processing (P) bodies to prevent their translation by ribosomes is an additional mechanism through which eukaryotes regulate the expression of specific genes. P-bodies are non-membranous cytoplasmic foci that contain RNA-protein particles (RNPs), consisting of translationally repressed mRNA and components of the RNA degradation machinery (Jang, Jang and Wu, 2020). P-bodies are dynamically remodelled in response to biotic stress in *A. thaliana*, as flg22 treatment or infection by a T3SS mutant of *Pto* DC3000, triggers the disassembly of P-bodies in a *FLS2*-dependent manner. Mutants lacking the P-body component proteins DECAPPING 2 (DCP2) and DCP1 had an impaired PTI response and were consequently more susceptible to *Pto* DC3000. Following PAMP perception, activated MPK3/6 phosphorylates DCP1 resulting in an enhanced interaction between DCP1 and the P-body localised exonuclease XRN4, triggering the degradation of specific de-capped transcripts. This mechanism was found to be responsible for the rapid and selective degradation of transcripts encoding negative regulators of immunity (Yu *et al.*, 2019).

1.4.4 Alternative splicing during immune responses

During PAMP-triggered immunity, just over 500 gene transcripts display PTI-responsive changes in alternative splicing (AS) in *A. thaliana* seedlings treated with flg22 for 30 minutes, which demonstrates that splicing is dynamically regulated during the immune response to pathogens (Bazin *et al.*, 2020). AS offers a rapid mechanism to alter gene expression programmes in response to pathogens (Mastrangelo *et al.*, 2012). Summarised below are two well-characterised examples of how alternative splicing can influence the defence response.

AS of key PTI signalling components is crucial for generating an effective defence response. This is illustrated by the Plant Elicitor Peptide (PEP)-induced AS of *CALCIUM-DEPENDENT KINASE 28* (*CPK28*). PEPs are endogenous peptide hormones that are activated by proteolytic cleavage in the apoplast upon PAMP detection to amplify and coordinate tissue-wide innate immune responses to pathogens (Yamaguchi and Huffaker, 2011). The canonical protein isoform of CPK28 (*CPK28.1*) functions as a negative regulator of PTI by phosphorylating BOTRYTIS-INDUCED KINASE 1 (BIK1), a rate-limiting downstream component of PEP signalling, and phosphorylating the E3 ubiquitin ligases PUB25 and PUB26 (PLANT U-BOX PROTEINs). These post-translational modifications stimulate PUB25/26-directed polyubiquitination of BIK1 and its subsequent degradation by the proteosome, maintaining signalling homeostasis (Monaghan *et al.*, 2014; Wang *et al.*, 2018).

A newly discovered regulator of AS called IMMUNO REGULATORY RNA-BINDING PROTEIN (IRR), modulates the strength of PTI by adjusting the levels of functional CPK28 in the cell in response to PEPs. Transient dephosphorylation of IRR upon the activation of PEP signalling causes its dissociation from *CPK28* pre-mRNA, resulting in the production of a PTC-containing intron-retained transcript variant (*CPK28.4*) that encodes a protein with reduced Ca^{2+} stimulated kinase activity (Dressano *et al.*, 2020). Not only does truncated CPK28 facilitate the de-repression of BIK1 activity, but it is also thought to exert a dominant-negative effect by reducing the ability of the functional CPK28 to interact with BIK1 – leading to a further amplification of PTI responses.

CONSTITUTIVE EXPRESSOR OF PATHOGENESIS-RELATED GENES 5 (CPR5), a negative regulator of ETI-associated cell death, belongs to the Transformer 2 subclass of SR splicing factors and has been confirmed to directly bind RNA via its RRM domain (Bowling *et al.*, 1997; Peng *et al.*, 2022). Through a suppressor screen of the *cpr5* mutant, Peng and colleagues demonstrated that CPR5 acts upstream of MAC and CLEAVAGE AND POLYADENYLATION SPECIFICITY FACTOR (CSPF), to regulate pre-mRNA processing within nuclear speckles (Peng *et al.*, 2022). CPR5 directly interacts with

transcripts that are differentially spliced in the *cpr5* loss-of-function mutant such as *AGO1* and *SR34*, which have both been implicated in the immune response (Li *et al.*, 2010; Rigo *et al.*, 2020). Therefore, CPR5 regulates the immune response in *A. thaliana* through its direct effects on AS (Peng *et al.*, 2022).

1.4.5 Regulation of nuclear mRNA export

Interestingly, mutants in several components of the RNA export machinery have been demonstrated to possess altered disease susceptibility phenotypes. One of the first components of the RNA export machinery identified in plants, *MOS2*, was also identified through the *snc1* suppressor screen of the gain-of-function *snc1* (*suppressor of npr1-1, constitutive 1*) allele. The *snc1* mutant possesses an autoimmune phenotype characterised by constitutive defence activation and enhanced disease resistance due to the hyperactivation of the NLR immune receptor that *SNC1* encodes (Monaghan, Germain, *et al.*, 2010). Loss-of-function *mos2* mutants are more susceptible to infection by *P. syringae* pathovar *maculicola* (*Psm*) ES4326, indicating that it serves a positive role in *A. thaliana* the defence response (Zhang *et al.*, 2005). The exact function of MOS2 in plant defence remains to be determined, but it is proposed to be involved in the regulation of RNA processing such as AS and RNA export as MOS2 contains a G-patch domain and two KOW repeats – domains which facilitate RNA binding in other RBPs (Monaghan, Germain, *et al.*, 2010).

Additionally, MOS11 was identified through a suppressor screen of the *snc1* mutant and shares homology with CIP29 (Germain *et al.*, 2010), an RBP involved in the RNA export mechanism in humans (Sugiura, Sakurai and Nagano, 2007). Loss-of-function of *mos11* in the *snc1* background partially abolishes the autoimmunity phenotype observed in *snc1* such as enhanced disease resistance to *Psm* ES4326 (Germain *et al.*, 2010). Despite its putative role in positively regulating ETI, *mos11* single knockout mutants do not show quantitative changes in resistance to *Psm* ES4326, or *Pto* DC3000, but do display impaired RNA export. The level of the SNC1 protein was reduced in the *mos11 snc1* double mutant compared to *snc1*, suggesting that MOS11 may be involved in the export of the *SNC1* mRNA, which consequently impacts its expression (Germain *et al.*, 2010).

Members of the ALY family of RNA export adaptors have also been implicated in the defence responses of multiple plant species. The necrosis and ethylene-inducing peptide 1 (Nep1)-like proteins (NLPs) are produced by taxonomically diverse plant pathogens, and can act as either PAMPs or virulence factors depending on the context of the interaction (Seidl and Ackerveken, 2019). The Oomycete pathogen *Magnaporthe oryzae* secretes $Nep1_{Mo}$, which triggers the HR

response in *N. benthamiana* via the activation of MAPK and WRKY transcription factor signalling (Zhang *et al.*, 2012). Teng and colleagues identified *NbALY916* and its homologue in *A. thaliana ALY4* positively influence $Nep1_{Mo}$-induced activation of defence responses including HR, stomatal closure, ROS accumulation, and changes in immunity-associated gene expression. The *aly4* mutant in *A. thaliana* also displayed reduced $Nep1_{Mo}$-mediated resistance to *Pto* DC3000 compared to WT (Teng *et al.*, 2014). The immunity-associated functions of ALY4 may extend broadly to the other ALY members in *A. thaliana*. This is based on the observation that ALY3 was found to interact with nuclear poly(ADP-Rib) polymerase 1 (PARP1) in a yeast two-hybrid screen (Storozhenko *et al.*, 2001; Germain and Gaouar, 2013). Chemical inhibition of PARP enzyme activity in *A. thaliana* has demonstrated their positive role in the regulation of late PTI responses such as callose deposition (Adams-Phillips, Briggs and Bent, 2009), suggesting that ALY3 may be linked to PTI responses. Together, these studies demonstrate that the export of RNA from the nucleus is a critical step in PTI as plants lacking functional copies of the RBPs that mediate this process have impaired immune responses to pathogens (Germain *et al.*, 2010; Teng *et al.*, 2014).

1.5 Pathogens target host RBPs to suppress immunity

A unifying feature of plant pathogens is their ability to disrupt critical systems within their hosts to suppress the defence response and to create a favourable environment for growth. This interference is achieved at multiple levels through the action of virulence effectors (Ai *et al.*, 2025). Given that RBP-mediated processing of RNA is crucial for the proper functioning of the immune response, unicellular and multicellular plant pathogens have evolved strategies to directly target components of the splicing machinery to disrupt host immunity as a virulence strategy (Bach-Pages *et al.*, 2025).

1.5.1 Oomycete pathogens

The Oomycete pathogens *Phytophthora infestans* and *Phytophthora sojae*, the causal agents of late blight in solanaceous crops and root rot in soybean respectively, both perturb AS during infection by targeting host RBPs (Qiao *et al.*, 2015; Huang *et al.*, 2017, 2020). *P. sojae* deploys the virulence effector *Phytophthora* suppressor of RNA silencing 1 (PSR1) to directly inhibit the activity of PSR1-INTERACTING PROTEIN 1 (PINP1), which contributes to disease progression (Qiao *et al.*, 2015). PINP1, also referred to as pre-mRNA splicing factor 16 (PRP16), belongs to the MUT6 family of DEAD-box RNA helicases that functions in pre-mRNA splicing and sRNA biogenesis. Suppression of the RNA-binding activity of PINP1 either by overexpression of *PRS1* or RNAi silencing of *PINP1* in *A. thaliana,* triggers AS changes in over 5000 genes and particularly intron retention. For example, an intron-retained splice variant of *ALLENE OXIDE CYCLASE (AOC)*, involved in jasmonic acid biosynthesis, that encodes an enzymatically inactive protein isoform, was stimulated in *PINP1* suppressed conditions. The canonical isoform could promote resistance to *Phytophthora* infection, whereas the intron-retained isoform could not. Similar results were found for other genes associated with pathogen defence, demonstrating that *P. sojae* utilises PSR1 to interfere with global intron retention by targeting the host RBP PINP1 as a virulence strategy (Gui *et al.*, 2022).

Transcriptome-wide analysis of alternative splicing in tomato leaves revealed that *P. infestans* can suppress the AS of positive regulators of the immune response, while enhancing the AS of negative regulators. To identify novel virulence effectors that manipulate host AS, Huang *et al.*, (2020) developed a novel luminescence-based reporter system to screen for *P. infestans* effectors which regulate host splicing, termed splicing regulatory effectors (SRE). Amongst the identified proteins, SRE3 and SRE7 directly interact with the host core spliceosome U1-70k subunit to manipulate host AS. For SRE3, this mechanism was proposed to be responsible for SRE3-directed suppression of host immunity (Huang *et al.*, 2020).

1.5.2 Fungal pathogens

Fungal phytopathogens interfere with host trans-kingdom RNA interference (RNAi) pathways as a strategy to enhance virulence (Qiao *et al.*, 2021). However, there are comparatively few examples of fungal virulence effectors directly targeting host RBPs that have been characterised to date. One key example is from the soil-borne pathogen *Verticillium dahliae* – the causal agent of wilt diseases in a range of hosts. *V. dahliae* can suppress immunity-related trans-kingdom RNAi by secreting the VdSSR1 effector into host cells, where it interacts with components of the TREX complex in the nucleus including ALY family proteins. This interaction blocks the association of ALY proteins and UAP56 to form a functional TREX complex, which suppresses the shuttling of microRNA (miRNA) in complex with ARGONAUTE 1 (AGO1) between the nucleus and cytoplasm. Consequently, the delivery of antifungal miRNAs from the cytoplasm of host cells to the *V. dahliae* is limited in the infected host, which increases fungal growth (Zhu *et al.*, 2022).

1.5.3 Parasitic nematodes

Plant-parasitic nematodes also secrete RBP-targeting effectors to interfere with host AS processes. The soybean cyst nematode *Heterodera glycines* and beet cyst nematode *Heterodera schachtii* produce a stylet-secreted virulence effector named 30D08. This effector is secreted into the host upon infection, where it localises to the nucleus and interacts with the auxiliary spliceosomal component SMU2. Transgenic *A. thaliana* plants expressing 30D08 under the control of the SUM2 promoter displayed changes in alternative splicing, which is hypothesised to contribute to pathogen survival (Verma *et al.*, 2018). More recently, the root knot nematode *Meloidogyne incognita* was found to secrete a virulence effector named MiEFF18, that interacts with SmD1, a key component in RNA splicing and quality control pathways (Elvira-Matelot *et al.*, 2016). Ectopic expression of MiEFF18 in *A. thaliana* roots disrupts AS and correlates with the changes in AS observed in the *smd1b* mutant, which has reduced SmD1 functionality. MiEFF18-directed remodelling of the host transcriptome likely contributes to the formation of the characteristic giant cells that are essential for parasitism (Mejias *et al.*, 2021).

1.5.4 Bacterial pathogens

The interaction of the *Pto* DC3000 effector HopU1 with GLYCINE RICH PROTEIN 7 (GRP7) in *A. thaliana* is one of the best studied cases of a bacterial phytopathogen targeting a host RBP (Fu *et al.*, 2007) (figure 3). GRP7 belongs to the hnRNP-like class of splicing factors (Yeap, Namasivayam and Ho, 2014) that modulates the AS of its own mRNA transcript, in addition to its paralogue *At*GRP8, in a negative autoregulatory feedback loop that is under circadian control (Heintzen *et al.*, 1997). *At*GRP7 was identified as a key factor mediating the crosstalk between the circadian clock and PTI, as the master regulator CCA1 functions through *At*GRP7 to regulate resistance to bacterial pathogens (Zhang *et al.*, 2013).

Upon infection with *Pto* DC3000, HopU1 is secreted into host cells via a type III secretion system where it catalyses the ADP-ribosylation of arginine 49 within the RNP1 region of GRP7's N-terminal RRM domain (figure 3a, b). This modification of GRP7 by HopU1 abolishes its RNA binding activity, which consequently suppresses PTI (Jeong *et al.*, 2011) (figure 3c). *grp7* loss-of-function mutants were found to have increased susceptibility to *Pto* DC3000 infection with a corresponding reduction in the amplitude of PTI responses while the opposite is true for *At*GRP7 overexpression lines (*At*GRP7-OX). (Fu *et al.*, 2007; Nicaise *et al.*, 2013). However, this observed increase in resistance of AtGRP7-OX to *Pto* DC3000 was found to be partly dependent upon functional SA signalling. This suggests that AtGRP7 regulates PTI via a SA-dependent, and SA-independent pathway associated with its RNA binding activity (Hackmann *et al.*, 2014). A focused investigation into the mode of action of GRP7 during PTI revealed that GRP7 associates with the PRR FLS2 at the cell surface, in addition to binding to its mRNA transcript. HopU1 was found to specifically block the interaction of GRP7 with *FLS2* mRNA during *Pto* DC3000 infection, which correlated with a reduction in the levels of FLS2 protein (Nicaise *et al.*, 2013). Taken together, these studies highlight the importance of splicing as a mechanism to reprogram the transcriptome during plant defence responses. Pathogens have evolved strategies to target the host splicing machinery to disrupt immune responses.

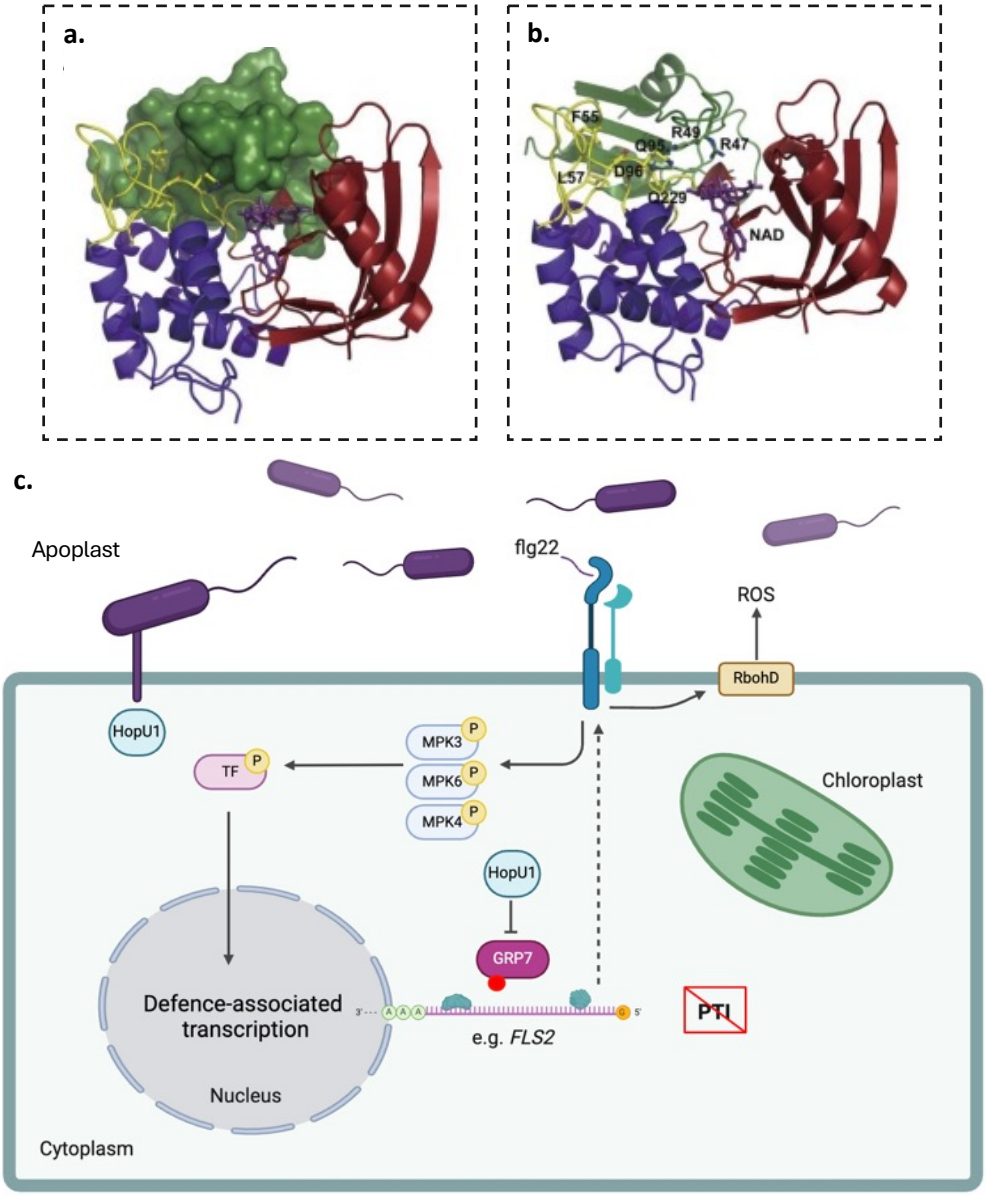

Figure 3. Interaction of HopU1 with the RNA recognition motif (RRM) of GRP7. a) Ribbon representation of the HopU1 crystal structure in association with NAD (purple). The N-terminal domain is coloured blue, and the C-terminal domain is coloured red. The yellow region represents the L1 and L4 loops which are required for substrate recognition and mono-ADP ribosyltransferase activity. Surface representation of the GRP7 RRM is shown in green. **b)** HopU1 residues required for its interaction with GRP7 (F55, L57, Q95, D96, Q229) and the R49 site that is ADP-ribosylated on GRP7 are shown in stick representation. Figure adapted from (Jeong *et al.*, 2011). **c.** After colonising the apoplast, PAMPs derived from *Pseudomonas syringae* pv. *tomato* DC3000 (*Pto* DC3000), such as flg22, are recognised by pattern recognition receptors, triggering a ROS burst in the apoplast and intracellular signalling pathways such as the MAPK cascade to activate PTI through changes in gene expression. During an infection, *Pto* DC3000 delivers the virulence effector HopU1 into the host's cytoplasm via a type 3 secretion system. HopU1 ADP-ribosylates the RNA recognition motif of GLYCINE RICH PROTEIN 7 (GRP7). This blocks the interaction of GRP7 with its RNA targets to suppress PTI. For example, HopU1-mediated suppression of the interaction between GRP7 and *FLS2* correlated with reduced production of ligand-free FLS2 at the cell surface (dashed line) (Nicaise *et al.*, 2013).

1.6 GRP7: An RBP at the crossroads of plant physiology, development, and stress responses

Structurally, GRP7 possesses a single classical RRM-domain at the N-terminus, and a glycine-rich (RGG) region at its C-terminus. Whilst the RRM is responsible for the RNA binding activity of GRP7, RNA binding affinity assays have demonstrated that the RGG domain also contributes to the interaction of GRP7 and substrate RNA as partial RGG deletions reduced the strength of the binding of GRP7 with its own mRNA (Leder *et al.*, 2014).

The first investigations into the cellular functions of GRP7 were in the context of its role in the circadian clock – the endogenous molecular system that maintains synchrony of physiological and developmental processes with the 24-hour day-night cycles (Heintzen *et al.*, 1997; Staiger and Apel, 1999). GRP7 is a slave oscillator in the circadian system, meaning that its transcription undergoes rhythmic cycling that is controlled by the CCA1 clock pathway, with its maximum expression occurring in the subjective evening (Staiger *et al.*, 2003). To maintain its rhythmic cycling, GRP7 represses its own expression post-transcriptionally to rapidly suppress the production of functional GRP7 protein in the cell (Staiger and Apel, 1999).

The underlying mechanism is dependent upon GRP7's role as a regulator of AS and its direct interaction with its own mRNA. High levels of GRP7 trigger the preferential use of a cryptic 5' splice site located within the intron, resulting in the generation of a splice variant containing a PTC, which is subsequently degraded via the NMD pathway. This results in the reduction of GRP7 protein levels, and a return to production of the stable splice variant (Staiger *et al.*, 2003). Interestingly, mathematical models of auxiliary splicing factors suggest that many undergo negative autoregulation through similar mechanisms. This is essential to establish synchronised splicing patterns between cells in a tissue by buffering against transcriptional variation in both the splicing factor and its substrate RNAs. Furthermore, this system enables each cell to adjust the production of the splicing factor based on the cellular load of its substrate RNAs, in that increased binding to substrate RNAs will relieve the negative auto-regulation – resulting in increased production of the splicing factor (Ding *et al.*, 2022).

Since its discovery, GRP7 has been found to have a global effect on pre-mRNA AS dynamics, with many previously identified AS events in *A. thaliana* being affected by the expression level of GRP7 (Streitner *et al.*, 2012; Meyer *et al.*, 2017; Wang *et al.*, 2020). A high proportion of these transcripts are directly bound by GRP7, and these interactions were abolished in an RNA binding-deficient mutant of GRP7 (Streitner *et al.*, 2012). Furthermore, transcriptome-wide profiling of *A. thaliana*

plants constitutively over expressing GRP7 revealed that the expression of a variety of genes involved in abiotic and biotic stress responses were altered in addition to genes involved in the circadian clock. For example, the expression of the SA-responsive genes *PR1*, *PR2*, and *PR5* are all elevated in the overexpression line (Streitner *et al.*, 2010). As GRP7 is ubiquitously expressed in all tissues in *A. thaliana* (Klepikova *et al.*, 2016), this suggests that its functions and activities are conserved across the whole plant.

Interestingly, the RNA binding activity of GRP7 can be directly modulated by external stimuli to influence global AS patterns. This is exemplified by the perception of the endogenous plant signalling peptide RAPID ALKALINIZATION FACTOR 1 (RALF1) by the receptor-like kinase FERONIA (FER). The interaction of RALF1-FER triggers the FER-dependent phosphorylation of 6 amino acid residues within the intrinsically disordered glycine-rich domain of GRP7, which promotes both the nuclear accumulation of GRP7 and enhanced association with components of the spliceosome to influence global AS dynamics (Wang *et al.*, 2020). Additionally, the RALF-FER system also regulates the ability of *A. thaliana* to acclimatise to temperature fluctuations in the environment, as RALF1-induced phosphorylation of GRP7 by FER stimulates the liquid-liquid phase separation (LLPS) of GRP7 and associated RNA to form stress granules. These are cytoplasmic condensates of RNA and protein that inhibit translation of the associated RNA (Xu *et al.*, 2024). Therefore, external stimuli can be transduced into global changes in AS and translation through GRP7, which can have wide-scale impacts on cellular gene expression. Taken together, these studies demonstrate that GRP7 is an important factor involved in plant metabolism and defence responses to pathogens, which is dependent upon its RNA binding activity.

1.7 Methods to study RBPs in plants

As discussed in this chapter, RNA binding proteins (RBPs) are master regulators of RNA processing within eukaryotic cells, having important impacts on gene expression, particularity in response to developmental and environmental cues (Lee and Kang, 2016). Therefore, to fully understand how RBPs regulate gene expression, it is critical to first identify the RNA transcripts that an RBP interacts with and then determine the functional consequence of the interaction. This first step towards understanding RBP function can be achieved via protein-centric methodologies, which rely on the same underlying principle: co-immunoprecipitation of an RBP of interest along with its associated RNA molecules, followed by their subsequent identification.

Currently, there two broad variations of this method referred to as RNA immunoprecipitation (RIP) and cross-linking and immunoprecipitation (CLIP). The former relies on purification of RNA associated with an RBP under native conditions, or following formaldehyde cross-linking, and determination of RNA identity through microarray analysis (RIP-chip) or high-throughput sequencing (RIP-seq) (Hafner *et al.*, 2021). Whilst RIP methods have been successfully deployed to study RBP-RNA interactions in a variety of species, including *A. thaliana* (Terzi and Simpson, 2009), they have two important limitations. Firstly, native RIP can result in the identification of non-specific RNA targets, as stringent wash buffers cannot be used due to the lack of an initial cross-linking step. Secondly, formaldehyde cross-linking simultaneously induces protein-RNA and protein-protein cross-links, which increases the likelihood of identifying indirectly associated RNA (Wheeler, Van Nostrand and Yeo, 2018).

In contrast, CLIP techniques require sample irradiation with UV to induce the formation of irreversible covalent cross-links between the RBP and closely associated RNA. Importantly, UV-induced cross-linking is specific to protein-RNA interactions and does not induce protein-protein cross-links. CLIP-based methods have been extensively reviewed by Hafner et al., (2021). To summarise, a breakthrough was the development of variations of the CLIP protocol that enabled the identification of the RBP binding sites on substrate RNAs with single nucleotide resolution, such as individual-nucleotide resolution CLIP (iCLIP). In the iCLIP workflow, proteolytic degradation of the RBP following the immunoprecipitation of the RBP-RNA complex leaves a peptide scar on the RNA at the crosslink site (CL). As reverse transcriptase tends to terminate at the CL site – this yields a library of cDNAs with the 5’ end corresponding to one nucleotide downstream of the CL site. Subsequent high-throughput sequencing of this library enables the identification of both the RNA targets and the site of interaction of an RBP.

iCLIP was first adapted to *A. thaliana* by the Staiger group (University of Bielefeld) to determine the RNA binding landscape of GRP7 in the context of its role in the circadian clock (Meyer *et al.*, 2017). In this study, GRP7 was found to interact with 858 unique RNA transcripts and had the capacity to interact with all transcript regions. GRP7 showed a slight preference for the 3' UTRs and interacted at sites enriched in uracil and cytosine residues. Interestingly, the authors found that GRP7 has a predominantly repressive effect on its target RNAs, as stable GRP7 over expression lines displayed a dampening in the cyclical expression of circadian-associated genes (Meyer *et al.*, 2017). Since its publication, improvements to the iCLIP workflow have been introduced in an updated version of the protocol, now referred to as iCLIP2. This improved method enables the preparation of higher-complexity libraries and identification of lower-abundance targets due to significant reductions in sample loss during the procedure (Buchbender *et al.*, 2020). iCLIP2 has recently been adapted for *A. thaliana* by the Staiger group, and offers a novel technique to study the RNA binding dynamics of plant RBPs in unprecedented detail (Lewinski, Brüggemann, *et al.*, 2024).

1.8 Thesis aims and rationale

GRP7 is an RNA binding protein that has consistently been identified as an important factor positively regulating plant PAMP-triggered immune responses, which contributes to pathogen resistance (Fu *et al.*, 2007). This immunity-related function is dependent upon its RNA binding activity, indicating that GRP7 exerts its effects by regulating the expression of its targets at the post-transcriptional level (Jeong *et al.*, 2011). Specific targets have been profiled in the context of an elicitor-triggered PTI response, and globally under normal physiological conditions via iCLIP (Nicaise *et al.*, 2013; Meyer *et al.*, 2017; Lewinski, Steffen, *et al.*, 2024). Despite these breakthroughs, many questions relating to its function during PTI remain. For example, it is unknown if the binding targets and/or binding sites of GRP7 are altered during PTI, and what consequences these interactions have on the output of PTI and pathogen resistance.

We hypothesise that the RNA binding landscape of GRP7 does change during PTI, as the expression of many biotic stress-responsive genes is upregulated during PTI. These transcripts could include targets for GRP7 that would not have been identified in the original iCLIP study. For example, *FLS2* mRNA is an experimentally validated binding target of GRP7 during PTI that was not identified in the GRP7 iCLIP dataset (Nicaise *et al.*, 2013; Meyer *et al.*, 2017). Furthermore, we hypothesise that the binding sites of GRP7 will change during PTI due to transcriptional reprogramming. Current evidence suggests that the RNA binding activity and alternative splicing dynamics of GRP7 may be influenced by the ratio of GRP7 to target mRNA, as observed in the regulation of its own transcript (Staiger *et al.*, 2003). Therefore, PTI-associated transcriptome changes may result in new GRP7 binding sites via a similar mechanism. Finally, the functional consequence of GRP7-RNA interactions during PTI remain largely unknown. GRP7 was found to have a predominantly repressive effect on its RNA targets under normal physiological conditions but appears to be required for *FLS2* translation during PTI. Therefore, this project will undertake a focused study using iCLIP2, to characterise the RNA binding dynamics of GRP7 during a flg22-induced PTI response to address these questions. The present research was conducted while iCLIP2 was being adapted for plants by the Staiger lab, which has since been published (Lewinski, Brüggemann, *et al.*, 2024). Additionally, this project will investigate how GRP7 influences the alternative splicing of its target mRNAs, and whether these changes have an impact on the pathogen defence response, to further our understanding of how GRP7 contributes to plant immunity.

This thesis will consist of the following chapters:

- **Chapter 2: Uncovering the RNA interactome of GRP7 during PAMP-triggered immunity**
  In this chapter, we use iCLIP2 to investigate how the RNA interactome of GRP7 changes during a flg22-induced PTI response in *A. thaliana* seedlings. We also perform additional characterisation of the molecular dynamics of GRP7 during PTI.

- **Chapter 3: Investigating the role of GRP7 in PTI-associated alternative splicing**
  We explore how GRP7 affects the post-transcriptional processing of a subset of its targets, and we investigate how alternative protein isoforms generated through alternative splicing can impact the defence response.

- **Chapter 4: ALY3 – an RNA binding protein that functions as a novel susceptibility factor to *Pseudomonas syringae***
  In this chapter, we characterise the role of *ALY3*, a putative GRP7-regulated gene, in the immune response of *A. thaliana* to *Pseudomonas syringae* pv. *tomato* DC3000.

- **Chapter 5: General discussion**
  In this final chapter, I discuss the main findings of this thesis within the context of the literature presented in this introductory chapter and discuss future perspectives within this field.

Chapter 2

Uncovering the RNA interactome of GLYCINE RICH PROTEIN 7 (GRP7) during PAMP-triggered immunity

2.1 Introduction

After gaining entry to a host, pathogens encounter the first layer of the immune system, consisting of cell surface localised receptors called pattern recognition receptors (PRRs), which detect pathogen-associated molecular patterns (PAMPs) and transduce these signals into the cell to trigger PAMP-triggered immunity (PTI) (Dodds and Rathjen, 2010). For example, the elicitor peptide flg22 is derived from the flagellum of bacterial pathogens such as *Pseudomonas syringae* pv. *tomato* DC3000 (*Pto* DC3000) and is detected by the PRR FLAGELLIN SENSITIVE 2 (FLS2) (Chinchilla *et al.*, 2007; Sun *et al.*, 2013). Such interactions ultimately lead to the activation of complex transcriptional networks that result in global changes in gene expression to promote pathogen resistance (Lewis *et al.*, 2015). In Eukaryotes, mRNA processing is an essential step of gene expression that is primarily orchestrated by RNA binding proteins (RBPs), which regulate all stages of the RNA lifecycle from transcription, nuclear mRNA export, translation, and decay (Lee and Kang, 2016). Over recent years, it has become increasingly apparent that many RBPs play a central role in regulating the immune response to pathogens (Staiger *et al.*, 2013).

GLYCINE RICH PROTEIN 7 (GRP7) is an RBP that has been implicated in a range of physiological processes, including the PTI response in *A. thaliana* that depend on its ability to regulate the co-transcriptional and post-transcriptional processing of RNA (Fu *et al.*, 2007; Nicaise *et al.*, 2013). GRP7 and its close paralogue GRP8 belong to the hnRNP-like class of trans-acting splicing factors that regulate alternative splicing in the nucleus (Streitner *et al.*, 2012). Mechanistically, this is achieved by GRP7 binding to cis-regulatory elements on pre-mRNA, which either enhances or suppresses the use of alternative splice sites to generate alternative isoforms (Wachter, Rühl and Stauffer, 2012). This process has been well described in the context of the negative autoregulation of its own pre-mRNA, as elevated levels of GRP7 bind to the 3'UTR and intron of its pre-mRNA to activate a cryptic splice site (Staiger *et al.*, 2003). The resulting intron-retaining isoform is rapidly degraded via the nonsense-mediated decay (NMD) pathway as it encodes a premature termination codon (PTC). As the transcription of GRP7 is directly controlled by the master clock regulator *CIRCADIAN CLOCK-ASSOCIATED 1* (*CCA1*), GRP7 functions within a negative autoregulatory feedback loop that oscillates over the day-night cycle to regulate the outputs of the circadian clock (Schöning *et al.*, 2007; Schmal, Reimann and Staiger, 2013).

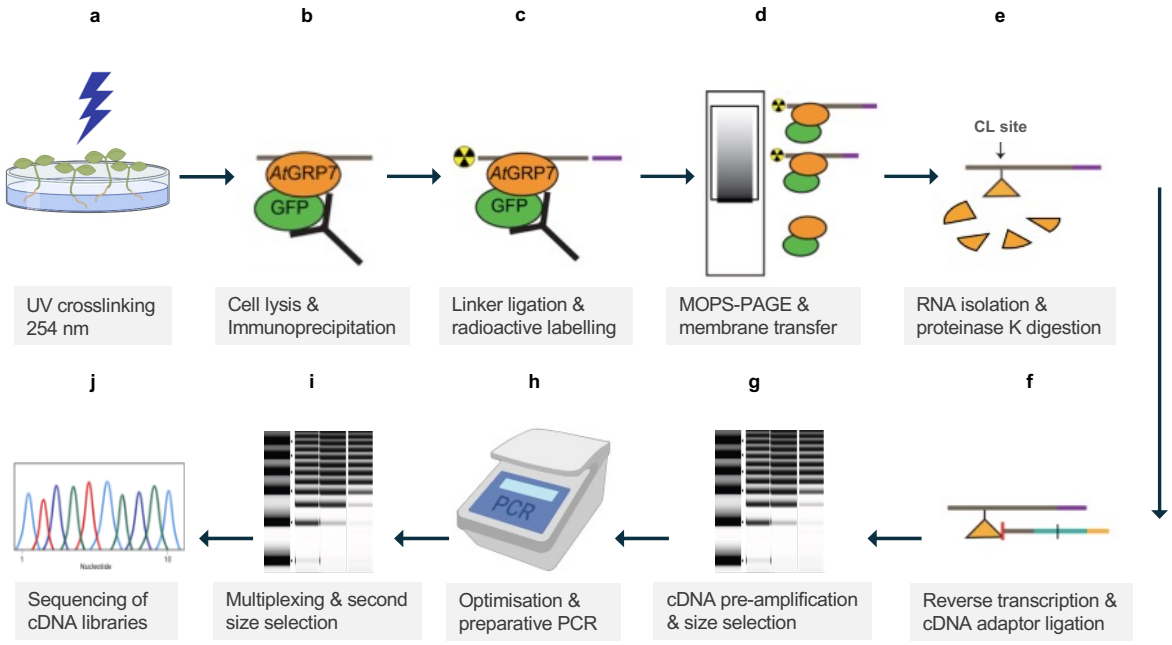

Figure 1. Overview of the plant iCLIP2 protocol. a) Plates of *A. thaliana* seedlings are subjected to UV irradiation at 254 nm to crosslink (CL) RNA-protein interactions, followed by immunoprecipitation of GRP7-GFP with its associated RNA from cell lysates **b, c)** RNA radiolabelling and ligation of the 3' linker, followed by electrophoretic separation to enable the purification and visualisation of GRP7-GFP-RNA complexes via autoradiography **d, e)** Membrane fragments containing desired complexes excised; proteolytic release of RNA leaves a peptide scar at the CL site. **f)** Reverse transcriptase terminates at CL site resulting in a library of cDNA with ends corresponding to the CL site, and a cDNA adaptor is ligated containing the unique molecular identifiers and experiment-specific barcodes. **g)** cDNAs are PCR amplified, and size selected to increase library quality. **h)** cDNA libraries further amplified with primers carrying the necessary adaptors to facilitate Illumina sequencing. **i)** Library concentrations are normalised and multiplexed. A final size selection removes residual primers. **j)** iCLIP2 libraries are sequenced via Illumina sequencing. Reads are processed and aligned to the TAIR10 reference genome to determine GRP7 target identity and binding site. Figure adapted from (Meyer *et al.*, 2017).

Beyond this specific function, GRP7 has been implicated in a range of cellular processes that depend upon its ability to regulate RNA metabolism. High-throughput approaches have demonstrated that GRP7 can modulate AS dynamics on global scale, which can also be influenced by stress exposure (Wang *et al.*, 2020). For example, loss-of-function mutants of GRP7 or RNA binding-deficient mutants display wide-scale changes in AS patterns, with some of these dysregulated transcripts representing direct substrates of GRP7. Interestingly, GRP7 regulates the AS of putative RBPs and other splicing factors – suggesting that GRP7 operates within a complex and highly integrated system to impact transcriptome-wide AS patterns (Streitner *et al.*, 2012). In addition to its role in AS, GRP7 has been found to regulate additional aspects of RNA metabolism and gene expression. For example, differential phosphorylation of GRP7 can regulate stress granule formation to

regulate translation in response to thermal stress (Xu *et al.*, 2024). Together, these studies demonstrate that GRP7 plays a fundamental role in the regulation of RNA metabolism in *A. thaliana.*

Importantly, GRP7 promotes disease resistance to *Pto* DC3000 that is dependent upon its ability to interact with RNA. Crucially, interfering with a single arginine residue within the RNA recognition motif (RRM) of GRP7 through targeted mutagenesis or via the action of the HopU1 virulence effector from *Pto* DC3000 abolishes the RNA binding activity of GRP7, which is sufficient to suppress PTI in *A. thaliana* (Fu *et al.*, 2007; Jeong *et al.*, 2011; Nicaise *et al.*, 2013). Nicaise and colleagues demonstrated a connection between GRP7's function in immunity and the production of PRRs, as HopU1 was found to inhibit the interaction between GRP7 and the *FLS2* mRNA – which correlated with a reduced level of ligand-free FLS2 at the cell surface (Nicaise *et al.*, 2013). Therefore, GRP7 may regulate the translation of important components of the PTI system to promote immunity. Despite these targeted studies, we do not currently understand how GRP7 regulates the transcriptome on a global scale during PTI.

To fully understand how an RBP functions in vivo, it is essential to determine which RNA substrates it interacts with. Advances in protein-centric methodologies such as the development of individual nucleotide crosslinking and immune precipitation (iCLIP) has enabled researchers to identify the RNA substrates of RBPs such as GRP7 (Meyer *et al.*, 2017). Briefly, the iCLIP methodology relies on the formation of UV-induced covalent crosslinks between an epitope-tagged RBP of interest and its substrate RNAs. These RBP-RNA complexes can be immunoprecipitated from tissue lysates using a complementary antibody to the epitope tag. Proteolysis of the RBP leaves a peptide scar at the crosslink site, which interrupts reverse transcription – ultimately yielding cDNA libraries with 5' ends corresponding to one nucleotide downstream of the crosslink site. High-throughput sequencing of these libraries enables the identification of RNA substrates and the interaction site of GRP7 (figure 1) (Hafner *et al.*, 2021).

Meyer and colleagues first adapted iCLIP to plants to profile the RNA binding targets of GRP7 in *A. thaliana* seedlings expressing GFP-tagged GRP7 under the control of its native promoter in a *grp7-1* loss-of-function background. 452 RNA targets were identified with high-confidence, meaning that these transcripts were also identified via an orthogonal RNA immunoprecipitation & sequencing (RIP-seq) method, which included many biotic stress-responsive gene transcripts such as WRKY transcription factors. However, previously confirmed RNA targets of GRP7 such as *FLS2* were not

identified in this dataset. Since this study, further improvements have been made to the original iCLIP method to increase the efficiency of the protocol, which is now called iCLIP2 (Buchbender *et al.*, 2020). Innovations to the protocol workflow significantly increases its sensitivity, due to reduced loss of low-abundance transcripts in the library. When this project was initiated, the Staiger lab was in the process of adapting iCLIP2 to A*. thaliana*, and has since published the full methodology (Lewinski, Brüggemann, *et al.*, 2024).

Aims and rationale

GRP7 is an RNA binding protein that has consistently been identified as an important regulator of plant PAMP-triggered immune responses. This immunity-related function has been related to its RNA binding activity, indicating that GRP7 exerts its effects by regulating the expression of its targets at the post-transcriptional level. We hypothesise that the RNA interactome of GRP7 changes during PTI, as the expression of many biotic stress-responsive genes is upregulated during PTI. These transcripts could become targets for GRP7 that would not have been identified in the original iCLIP study. For example, *FLS2* mRNA is a binding target of GRP7 during PTI that was not identified in the GRP7 iCLIP dataset. Furthermore, we hypothesise that the binding sites of GRP7 will change during PTI due to upregulation of biotic stress-responsive transcripts. Current evidence suggests that the RNA binding and alternative splicing dynamics of GRP7 may be influenced by the ratio of GRP7 to target mRNA, as observed in the regulation of its own transcript. Therefore, PTI-associated transcriptome changes may result in new GRP7 binding sites via a similar mechanism, which could affect RNA processing. In the following chapter, we have conducted a focused study to characterise the binding dynamics of GRP7 during a flg22-induced PTI response.

2.2 Materials and methods

2.2.1 Plant growth conditions

The Arabidopsis thaliana line *AtGRP7::AtGRP7-GFP* (referred to here as GRP7-GFP) expresses A. thaliana GLYCINE RICH PROTEIN 7 (GRP7) under the control of its native promoter, in a *grp7-1* T-DNA mutant background as described previously (Meyer et al., 2017). Seeds were surface sterilised via chlorine gas and sown on MS (Murashige-Skoog; Duchefa) 1% phytoagar plates supplemented with 0.5 g/L MES and 0.5% sucrose. Seeds were stratified at 4°C for 48 hours then transferred to Percival incubators for 14-days and grown under 12-hour light/dark cycles at 20oC with a light intensity of approximately 100 µmol/m2/s.

2.2.2 Flg22 treatment and validation

After 14-days of growth, plates of GRP7-GFP seedlings were flooded with liquid MS growth media containing flg22 (Eurogentec) to a final concentration of 1 µM to elicit PTI, or without flg22 as a mock treatment. For consistency, treatments were applied 9 hours after lights-on (circadian time 9). After 2 hours, each plate was drained and immediately subjected to UV-cross-linking to fix GRP7-RNA interactions by irradiation with 2000 mJ/cm^2 UV light at 254 nm on ice using UVP Cross-linker CL-3000 (AnalytikJenna). Seedlings were immediately harvested and frozen in liquid nitrogen (LN_2). Frozen tissue was subsequently ground to a fine powder using a mortar and pestle in LN_2.

2.2.3 MAPK phosphorylation assay

For the detection of phosphorylated MAPK, total protein was extracted from 50 mg of frozen tissue by adding 200 µL protein extraction buffer (62.5 mM Tris-HCl, 20% glycerol, 2% SDS, 0.1% Beta-mercaptoethanol), followed by heating to 95°C for 5 min and centrifugation to clear debris. Protein extracts were quantified and normalised using the Bradford assay (Thermo Scientific™). 6 µg total protein extracts were mixed with protein loading buffer and heated to 95°C for 5 min, then run on a 12% SDS PAGE gel at 100v for 2 hours. Separated protein was transferred to a PVDF membrane for 1 hr at 100V and 4°C via Western blot in Western transfer buffer (Appendix I. Supplementary table 13).

The membrane was blocked in 5% Bovine Serum Albumin (BSA) dissolved in Tris-buffered saline containing 1% Tween-20 (TBS-T) for 1hr, followed by primary antibody hybridisation overnight with Anti-phospho p44/42 MAPK (cell signalling tech mAb #4370). Secondary antibody Anti-rabbit (Sigma-Aldrich A0545) was subsequently hybridised for 1-hour following removal of primary

antibody and washing 4 times for 10 minutes in TBS-T. Chemiluminescence was recorded following addition of the SuperSignal™ West Femto Maximum Sensitivity Substrate (Thermo Scientific™ ca. 34095) to detect the presence of phosphorylated MPKs.

2.2.4 RT-qPCR quantification of relative gene expression

For the detection of flg22-induced gene expression, total RNA was isolated from approximately 90 mg powdered tissue using the GeneMATRIX Universal RNA Purification Kit (EURx cat. no. E3598), including the on-column DNase digest with DNase I (RNase-free) (New England Biolabs ca. M0303S). Purified RNA was eluted in 40 µL RNase free water. RNA integrity was assessed by running sample aliquots on a 1.5% agarose MOPS/1.3% formaldehyde denaturing gel. RNA samples with good integrity were reverse transcribed to cDNA using Reverse Transcriptase (AMV). Fourfold diluted cDNA was subsequently used in an RT-qPCR reaction using iTaq™ Universal SYBR® Green Supermix (Bio-Rad ca. 1725121) according to the manufacturer's protocol and run on CFX96 Touch Real-Time PCR Detection System (Bio-Rad). Relative gene expression was calculated using the ($2^{-\Delta\Delta Ct}$) method (Livak and Schmittgen, 2001). Primers used for gene expression quantification are listed in (Appendix I. Supplementary table 1).

2.2.5 Plant iCLIP2

Individual nucleotide cross-linking and immunoprecipitation version 2 (iCLIP2) was adapted for *A. thaliana* by the Stagier lab based on the original iCLIP2 protocol for mammalian cell cultures (Buchbender *et al.*, 2020). The *A. thaliana* iCLIP2 protocol and optimisation for GRP7 has recently been published (Lewinski, Brüggemann, *et al.*, 2024). In this section, we describe in detail the methods that were followed to obtain the GRP7 RNA interactome.

Each sample replicate required 20 plates containing approximately 60 seedlings. A total of 3 g of powdered tissue, divided in 500 mg aliquots was required to be processed for each sample. 750 µL cell lysis buffer (Appendix I. Supplementary table 2) was added to each aliquot and vigorously homogenised by vortexing. Tissue aliquots were centrifuged for 10 min at 16,000 xg and 4°C to pellet debris. Supernatants were united and filtered through a 0.45 µm filter (Millex®); a 100 µL aliquot of the lysate was collected and stored as the input for downstream analysis. Cell lysates were then pre-cleared using Sepharose beads to remove non-specific binders before immunoprecipitation with the addition of 25 µL ChromoTek GFP-Trap® Agarose beads (Proteintech) to each pre-cleared lysate, followed by a 1-hour incubation at 4°C with rotation. As a

control immunoprecipitation, a mock precipitation was performed with ChromoTek MBP-Trap (Maltose Binding Protein) Agarose beads (Proteintech) in addition to the GFP-Trap® immunoprecipitation – with the exception that 7 g of total tissue for each treatment condition was processed as described above. Beads were gently pelleted via centrifugation for 1 min at 500 xg and 4°C. An aliquot of the supernatant was also stored for downstream analysis. Beads were subsequently washed four times in 1000 µL wash buffer (Appendix I. Supplementary table 3), followed by two washes in 1000 µL PNK wash buffer (Appendix I. Supplementary table 5). A 50 µL aliquot of the immunoprecipitate was collected and stored for downstream analysis. Beads were pelleted via centrifugation as before and the supernatant was discarded. The beads were resuspended in 100 µL PNK wash buffer followed by a subsequent DNA digestion with 2 µL TURBO™ DNase (Invitrogen™) and a 10 min incubation at 37°C and 1100 rpm. At this stage, for the control immunoprecipitation, an RNase digest was performed simultaneously on a subset of the GFP-Trap® samples by adding 5 µL of a 1/50 dilution of RNase I (Ambion) prepared in PNK wash buffer. All samples were transferred to ice for 3 min, then centrifuged at 500 xg for 2 min 4°C and the supernatant was discarded.

At this stage, the 3' ends of the co-immunoprecipitated RNA fragments were dephosphorylated by T4 Polynucleotide Kinase to enable the ligation of the first linker, which serves as a platform for reverse transcription of the RNA to cDNA. This was performed according to the iCLIP2 protocol (Buchbender *et al.*, 2020), which contains details of the L3-App linker sequence and dephosphorylation procedure. Briefly, the beads were washed, then suspended in 20 µL PNK mix A, containing 1x concentration of PNK buffer (Appendix I. Supplementary table 6) and incubated for 20 min at 37°C. The beads were washed again once with PNK wash buffer, once with the high-salt buffer (Appendix I. Supplementary table 4), then twice more with PNK wash buffer. Next, 38.5 µL ligation mix was added, containing 1x concentration of Ligation buffer (Appendix I. Supplementary table 7) followed by an overnight incubation at 16°C with shaking at 1250 rpm. The composition of the reaction mixtures is described in (Appendix I. Supplementary table 9).

Radiolabelling of the RBP-RNA complexes is critical to visualise both their size and integrity after separation via electrophoresis and subsequent transfer to a nitrocellulose membrane. Furthermore, this step facilitates their isolation and purification (Buchbender *et al.*, 2020). As GRP7 is an abundant protein in our samples, only 20% of the processed beads containing the GRP7-RNA complexes were radiolabelled and recombined with the remaining 80%. This was to limit the amount of radioactive isotope required for each sample. 200 µL (20%) of the beads were collected

and the supernatant was removed. The beads were then re-suspended in 38 µL of PNK mix B (Appendix I. Supplementary table 9), and 2 µL of ^{32}P-γ-ATP was added to each bead aliquot. The bead mix was incubated for 20 minutes at 37°C with shaking at 1100 rpm to radiolabel the 5' end of the RNA fragments. The beads were then washed twice with, and re-suspended in, 800 µL PNK wash buffer and added to the remaining unlabelled 80% bead aliquot. 6 µL of 4 x LDS loading buffer (Pierce™) was added to the beads and heated to 95°C for 10 minutes to elute the RBP-RNA complexes, before pelleting the beads by centrifugation. The supernatant was loaded onto a 4-12 % NuPAGE Bis-Tris gel (Invitrogen™) and run for 60 minutes at 180 V in 1 x MOPS running buffer (Appendix I. Supplementary table 11) on ice. The RBP-RNA complexes were subsequently transferred to a nitrocellulose membrane via a Western blot for 1 hour at 30 V using Western transfer buffer (Appendix I. Supplementary table 13). The nitrocellulose membrane was then rinsed once in 1 x PBS buffer, wrapped in Saran wrap, and exposed to an X-ray film (Fujifilm) at -80°C in an X-ray cassette overnight.

After developing the X-ray film, the autoradiogram served as a template to manually excise membrane segments corresponding to approximately 5 kDa above the expected molecular weight of GRP7-GFP using a scalpel. The membrane fragments were placed in a clean 1.5 mL microcentrifuge tube and submerged in 200 µL PK +SDS buffer (Appendix I. Supplementary table 8), containing 10 µL Proteinase K (20 µg/mL; Roche), and incubated for 60 minutes at 50°C with shaking at 1100 rpm. This step degrades the GRP7-GFP and releases the RNA from the nitrocellulose membrane, leaving a peptide scar on the RNA at the cross-link site. The supernatant was recovered and 200 µL PK -SDS buffer (Appendix I. Supplementary table 8) was added to dilute the SDS to 0.1 % for compatibility with the Zymo spin column. 400 µL phenol/chloroform (pH 7) was added to the supernatant and thoroughly mixed before being transferred to a 2 mL Phase Lock Gel Heavy tube (Avantor). After a 5-minute incubation at 13000 rpm, RNA was isolated as according to the manufacturer's guidelines. The isolated RNA was further purified using the RNA Clean & Concentrator (Zymo Research), processed according to the manufacturer's guidelines and eluted in 12 µL RNase-free H_2O. The reverse transcription and subsequent RNA hydrolysis was performed as described by Buchbender *et al.*, (2020).

The resulting cDNA libraries were subsequently cleaned using MyOne SILANE Dynabeads (Life Technologies) and second linker ligation was performed as described by Buchbender *et al.*, (2020). Briefly, the cDNA hybridises to the ferromagnetic beads, enabling their isolation and purification. Once cleaned, the second L#clip2 oligo was ligated to the 3'OH end of the cDNA (Appendix I.

Supplementary table 10), followed by a second MyOne SILANE clean-up. The second adaptor contains both a unique molecular identifier (UMI) and an experiment-specific barcode, which enables PCR duplicate removal and de-multiplexing *in silico* after sequencing. The clean, ligated cDNAs were then PCR pre-amplified to prevent the loss of unique cDNA reads following a subsequent size selection step with the ProNex Size-Selective Purification System (Promega) to eliminate primer dimers using a sample-to-bead ratio of 1:2.95 v/v. A second PCR amplification is performed for an increasing number of cycles (9, 11, 13) using 1 µL cDNA to identify the optimal cycle number to proceed with the preparative PCR. The PCR products were run on a 12 % TBE polyacrylamide gel and stained with SYBR™ Gold Nucleic Acid Gel Stain (Invitrogen™) (1: 10,000). A preparative PCR was then performed on 10 µL of the cDNA for the appropriate number of cycles to amplify the libraries for sequencing, followed by a second size selection with ProNex beads (Promega) using a sample-to-bead ratio of 1:2.4 v/v. cDNA libraries were then quantified using the Qubit Fluorometric Quantification (Thermo Scientific™) according to the manufacturer's guidelines, and normalised to 10 nM prior to multiplexing. The multiplexed libraries were submitted for Illumina high-throughput sequencing.

2.2.6 iCLIP2 control immunoblot

For the input, supernatant, and immunoprecipitate aliquots that were taken throughout the iCLIP procedure and from the MBP-trap control immunoprecipitation, 4 x LDS loading buffer (Pierce™) was added to each of the aliquots and incubated for 5 minutes at 70°C, then briefly cooled on ice. Samples were loaded onto a 12% SDS polyacrylamide gel and run at 100 V for 2 hours in 1x SDS running buffer (Appendix I. Supplementary table 12). Samples were then transferred to a PVDF membrane by Western blot for 1 hour, 100 v, at 4°C in Western transfer buffer (Appendix I. Supplementary table 13). The membrane was blocked in 2% milk in TBS-T overnight at 4°C. The primary antibody hybridization was performed using anti-GFP (Roche 11814460001) at a 1:1000 dilution in 2% milk in T-BST, 1h. The membrane was washed 3x for 10 min with TBS-T. Second antibody hybridization used anti-mouse (Sigma A0168) at a 1:5000 dilution in 2% milk in T-BST for 1 hour. Membrane washed 4x for 15 min with TBS-T. Chemiluminescence was subsequently recorded following addition of the Clarity Western ECL Substrate (Bio-Rad).

2.2.7 Bioinformatic analysis

Raw sequencing reads were kindly processed by Martin Lewinski (Staiger lab, University of Bielefeld), according to the data analysis pipeline described in the plant iCLIP2 publication (Lewinski, Brüggemann, *et al.*, 2024). To summarise, read quality was evaluated with *FastQC version 0.11.5* then 3' adaptors were trimmed using *cutadapt version 1.16*. Sequencing reads were subsequently demultiplexed into their constituent samples based on their experiment-specific barcodes. Reads containing 14 nucleotides or less were discarded prior to mapping to the *A. thaliana* TAIR10 reference genome using *STAR version 2.6.0a* with a maximum of two mismatches permitted. PCR duplicates were identified as reads that shared the same unique molecular identifier (UMI) and mapped to the same 5' positions and were removed. The -1 position of each uniquely mapped read was extracted as a crosslink site, and the read was subsequently discarded. The *PureCLIP 1.0.4* peak calling algorithm was used to identify significant crosslink sites using all biological replicates simultaneously (Krakau, Richard and Marsico, 2017). *PureCLIP* applies a hidden Markov model that incorporates local fragment density to normalise for transcript expression levels within each sample, to ensure that sites are called based on sharp, statistically unexpected read-start pileups rather than raw coverage. Binding sites were subsequently defined +/- 4 nucleotides adjacent to *PureCLIP* peaks and filtered to retain only those reproducible across at least two of the three replicates.

A final output of the iCLIP2 bioinformatics pipeline is a data frame containing reproducible GRP7 binding sites annotated by transcript region (5' UTR, CDS, intron, 3' UTR). Binding sites were defined based on their presence in at least two out of three biological replicates per condition. To identify condition-specific binding, sites were compared between mock and flg22-treated samples using a binary presence/absence framework, whereby sites detected in one condition but not the other were classified as condition-specific. We note that this approach does not assess differential binding strength at shared sites. Although *PureCLIP* assigns scores to crosslink events, these values are influenced by transcript abundance and library-specific factors and are not directly comparable between conditions without additional normalisation. As such, quantitative differences in binding intensity were not evaluated, and our analysis focuses on reproducible and condition-specific binding site identification rather than differential binding.

Gene ontology (GO) enrichment analyses were performed using ShinyGO (Ge, Jung and Yao, 2020). The set of genes whose transcripts were detected to have conditional GRP7 binding sites was used as a query against a background of all GRP7 targets identified via iCLIP2.

2.2.8 Assay of flg22-induced degradation of GRP7 by immunoblot

A. thaliana GRP7-GFP seedlings were treated with flg22 as described previously (section 2.2.2). 60 mg powdered tissue was mixed with 240 µL protein extraction buffer on ice (Appendix I. Supplementary table 14), then centrifuged for 5 min at 11,000 x G and 4°C to pellet debris. The protein concentrations of the supernatants were subsequently quantified using the Bradford assay (Thermo Scientific™) and normalised with protein extraction buffer. Protein extracts were mixed with protein loading buffer and heated to 95°C for 5 min, then run on 12% SDS PAGE gel in 1x SDS running buffer (Appendix I. Supplementary table 12). Protein was transferred to PVDF membrane by Western blot, followed by blocking in 2% milk powder dissolved in Tris-buffered saline containing 1% Tween-20 (TBS-T) for 1hr. Immunoblot was performed with HRP Anti-GFP antibody (ab6663, Abcam). Chemiluminescence was subsequently recorded following addition of the Clarity Western ECL Substrate (Bio-Rad).

2.2.9 GRP7-GFP confocal microscopy

14-day-old *A. thaliana* GRP7-GFP seedlings were treated with flg22 as described previously (section 2.2.2). After treatment, cotyledons were detached using a scalpel and mounted on slides in liquid MS media. Zeiss LSM 880 Airyscan, with the 40x immersion lens and 488 nm laser wavelength (GFP emission 493 – 598 nm) (Chlorophyl A 647 – 721 nm) was used to acquire Z-stack images of samples. Raw images were processed using Image J.

2.2.10 Phylogenetic tree construction

The *A. thaliana* GRP7 protein sequence (NP_179760.1) was used as a query in an NCBI protein-protein BLAST (BLASTP) search. Orthologues were selected based on a minimum sequence identity threshold of 70% to ensure functional similarity. Sequences were aligned using MAFFT version 7 (Katoh, 2002), and poorly aligned regions were trimmed using TrimAl version 1.5.0 with the automated1 option to improve tree resolution (Capella-Gutiérrez, Silla-Martínez and Gabaldón, 2009). A maximum likelihood phylogenetic tree was then constructed using IQ-TREE with 1,000 bootstrap replicates (Trifinopoulos *et al.*, 2016). The best-fit substitution model was selected automatically using ModelFinder (Kalyaanamoorthy *et al.*, 2017). Bootstrap values were mapped onto the tree to assess branch support and evolutionary divergence among orthologues.

2.3 Results

2.3.1 Flg22 treatment elicited PTI in seedlings

Prior to commencing iCLIP2, it was essential to first validate that PTI was specifically activated in the flg22-treated seedlings prior to UV crosslinking. As previously discussed, the bacterial flagellin peptide fragment flg22 is a potent elicitor of PTI in plants. For this reason, flg22 is routinely used at a concentration of 1 µM to elicit PTI when conducting plant immunity assays and has previously been applied via flood inoculating seedlings with a solution containing the dissolved peptide (Denoux *et al.*, 2008; Bethke *et al.*, 2012). Here, two-week-old *A. thaliana* seedlings were flooded for 2 hours in liquid MS media containing 1 µM of flg22 9 hours after lights-on (circadian time 9). This is was to ensure maximal expression of GRP7-GFP to enhance the yield of co-immunoprecipitated RNA isolated via the iCLIP2 protocol (Heintzen *et al.*, 1997). A mock treatment using liquid MS only was included as a negative control.

A MAPK phosphorylation assay was performed on total protein extracts separated via SDS-PAGE from the treated and mock seedlings following UV crosslinking, to confirm that the flg22 treatment induced PTI. MAPK6 and MAPK3 are rapidly phosphorylated in response to flg22 treatment as a consequence of the elicitor's recognition by FLS2 (Bethke *et al.*, 2012). An immunoblot analysis was performed with Anti-phospho-p44/42 MAPK which specifically recognises phosphorylated MAPK residues (Chung and Sheen, 2017). Initial validations for two independent biological replicates showed no clear difference in the levels of phosphorylation of MAPK6 and MAPK3 detected between the mock and the treated seedlings (figure 2a). This suggested that the flg22 inoculation did not specifically activate PTI in the treated seedlings. This result was unexpected as multiple previous studies have demonstrated that this assay is an effective method to detect the flg22-induced PTI response. Therefore, to determine the source of the error, the treatments were repeated using a fresh stock of flg22 for either 0.5 or 2 hours and compared to the original stock (figure 4b). Again, it was apparent that MAPK6 and MAPK3 were phosphorylated in all treatment groups, including the mock-treated negative control. Interestingly, UV-B and UV-C exposure has previously been demonstrated to trigger the rapid phosphorylation of MAPK6 and MAPK3 in *A. thaliana* as early as 2 minutes after exposure (González Besteiro *et al.*, 2011; González Besteiro and Ulm, 2013). As the MAPK phosphorylation assay described here was performed on UV-C cross-linked material, it is highly likely that the UV treatment activated the phosphorylation of MAPKs in both the mock and flg22-treated seedlings, which masked the effect of the elicitor treatment.

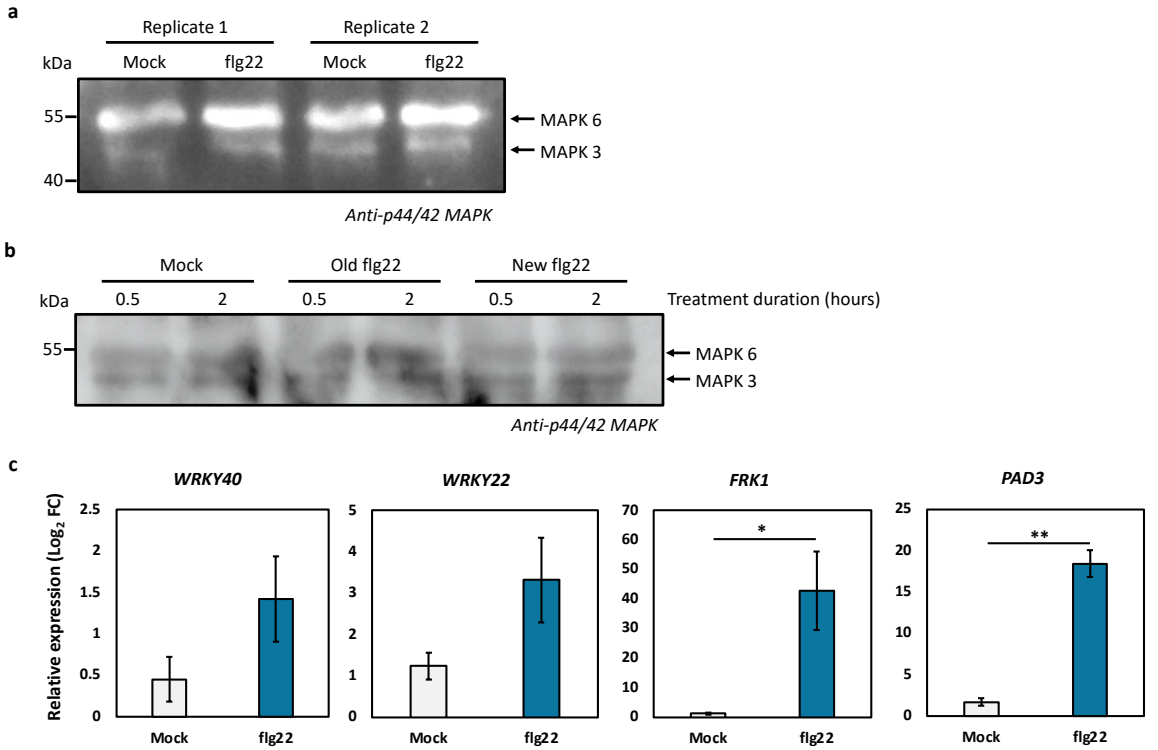

Figure 2. Validation of PTI activation in *A. thaliana* seedlings following flg22 treatment. a) Immunoblot analysis of MPK3 and MPK6 phosphorylation using anti-phospho-p44/42 MAPK following 2-hour submergence in liquid MS media (mock) and liquid MS media containing 1 µM flg22 for two independent biological replicates. **b)** Immunoblot analysis of seedlings mock treated for 0.5 or 2 hours or treated with 1 µM flg22 from an old stock (Biotrend) or a new flg22 stock (Eurogentec). **c)** RT-qPCR detection of PTI-responsive gene expression. *A. thaliana* seedlings were flood treated for 2 hours with liquid MS media (Mock) and liquid MS media containing 1 µM flg22. Cq values normalised to *PP2A*. Relative gene expression changes calculated via $2^{-\Delta\Delta Ct}$ (Livak and Schmittgen, 2001). Error bars represent the mean of 3 independent biological replicates ± SEM. Significance values calculated using a two-tailed T-test. Asterisk indicates significance threshold: **P* < 0.05, ***P* < 0.01.

As an alternative treatment validation, the expression of PTI-responsive genes was quantified via reverse-transcription quantitative PCR (RT-qPCR) using RNA isolated from plant material treated as described above. Four genes that are significantly upregulated at 2 hours following flg22 treatment were selected for this validation (Asai *et al.*, 2002; Denoux *et al.*, 2008). Each target gene was upregulated in the flg22-treated seedlings relative to the mock treated control, with the upregulation of *FRK1* and *PAD3* being significant, indicating that PTI was specifically induced in the flg22-treated seedlings (figure 5c). This further supports the previous observation that the UV cross-linking masked the PTI-associated phosphorylation of the MPK6 and MPK3. Therefore, we proceeded to perform iCLIP2 with these samples.

2.3.2 iCLIP2 Control immunoprecipitation and validation

Before beginning the iCLIP2 protocol, two control experiments must be completed using the whole tissue lysates from the mock and flg22-treated samples. Firstly, an alternative antibody lacking reactivity with the target epitope is used for a control immunoprecipitation (IP) to confirm the absence of background signal. Secondly, a high RNase control is also required to monitor the specificity and quality of RNA-RBP complexes obtained in the pulldown with the GFP-trap beads (Huppertz *et al.*, 2014; Buchbender *et al.*, 2020; Lewinski, Brüggemann, *et al.*, 2024). Cell lysates from mock and flg22-treated *A. thaliana* seedlings were incubated for 1 hour with either MBP-trap beads (maltose binding protein), which do not bind GRP7-GFP-RNA complexes, or GFP-trap beads which specifically bind to GRP7-GFP. One of two independent GFP-trap bead IPs from the mock and flg22-treated samples was treated with a high concentration of RNase I. Co-immunoprecipitated RNA from each IP was radiolabelled to visualise the purified RNA-protein complexes via autoradiography (figure 3a).

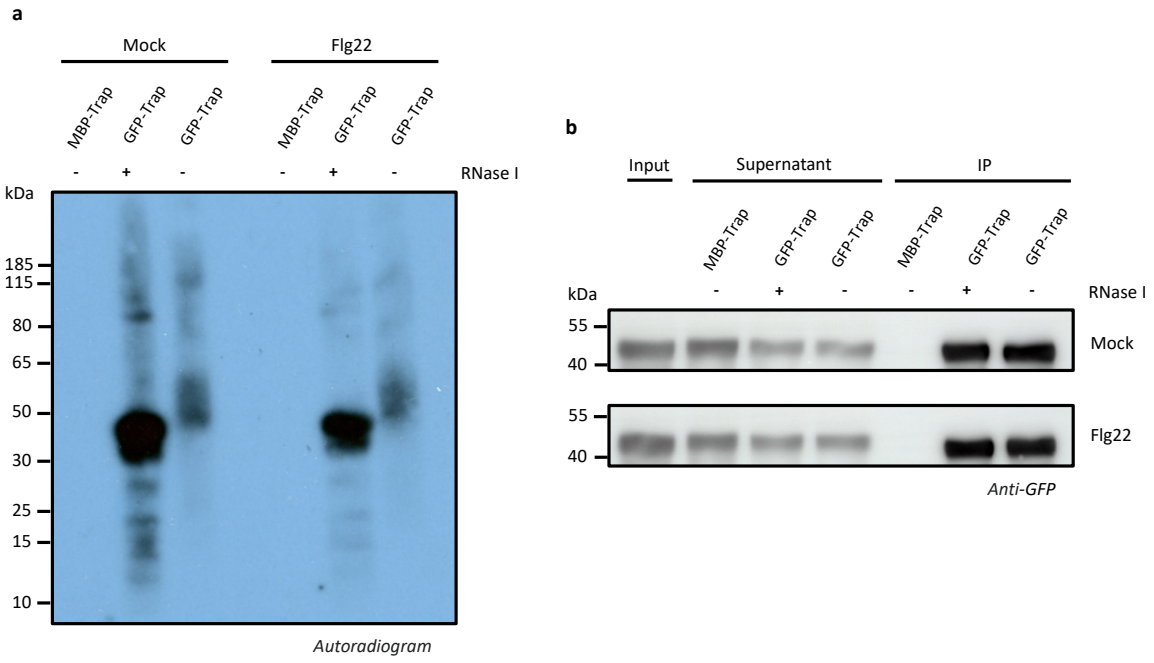

Figure 3. iCLIP2 control immunoprecipitation of *A. thaliana* seedling extracts following a 2-hour mock 1 µM flg22 treatment. a) Autoradiogram of pulldowns from tissue lysates incubated with MBP or GFP-trap beads. One GFP-trap pulldown was subsequently treated with RNase I. 20% of immunoprecipitated RNA-RBP complex was radiolabelled with ^{32}P-γ-ATP. RBP-RNA complexes were separated via neutral pH MOPS-PAGE then transferred to a nitrocellulose membrane by Western Blot. Fujifilm was exposed to the membrane for 14 hours. **b**) Detection of GRP7-GFP in the immuno-precipitate (IP) pulldown and resulting supernatant relative to the whole cell lysate (input). +/- symbols indicate subsequent treatment with RNase I. Immunoblot performed with Anti-GFP primary antibody. Signal was detected via chemiluminescence.

For both mock and flg22-treated tissue, radiolabelled RNA-protein complexes were absent in the MBP-trap bead pulldowns, which indicates that the signal observed in the GFP-trap IP autoradiograms was not background noise caused by non-specific binding. This finding was corroborated by the immunoblot validation which shows an absence of GRP7-GFP in the MBP-trap IP and enrichment in the GFP-trap IPs (figure 3b). Furthermore, the high RNase treatment of the GFP-trap IPs shows a distinct band forming at ~5 kDa above the expected molecular weight of the GRP7-GFP complex (42 kDa), which is absent in the non-RNase treated samples (figure 1a); (Buchbender *et al.*, 2020). This suggests that the signals in the GFP-trap IP, RNase- samples are due to the presence of GRP7-GFP-RNA complexes, which indicates a successful immunoprecipitation.

2.3.3 GRP7-GFP immunoprecipitation and RNA isolation

As the specificity of the IP had been confirmed, an IP of GRP7-GFP was performed using tissue lysates derived from *A. thaliana* seedlings treated with liquid MS (mock) or 1 µM flg22. GFP-trap beads were used as described above. GRP7-GFP-RNA complexes were radiolabelled with ^{32}P-γ-ATP and visualised via autoradiography. For each biological replicate, a clear smear beginning at approximately 40 kDa rising to over 185 kDa was obtained for each treatment group (figure 4a). As the distance that the GRP7-GFP complex migrates through the gel is proportional to the length of the cross-linked RNA, the long smear indicates that high-quality, long RNA was isolated during via the IP. Based on the autoradiograms, the desired membrane regions containing the GRP7-GFP-RNA complexes were manually excised from the membrane. RNA was subsequently liberated via proteolytic digestion, leaving a peptide scar at the cross-link (CL) site. The efficiency of each iCLIP2 IP was assessed via immunoblot with anti-GFP (figure 4b). Despite some variation between replicates, a substantial increase in the levels of GRP7-GFP was detected in the IP+ relative to the input, with a slight reduction in the supernatant. This suggest that the IP successfully enriched for GRP7-GFP. Some lower molecular weight degradation products were observed in the immunoblot, most likely representing free GFP, but these would be purified from the GRP7-GFP-RNA complexes due to the manual excision from the nitrocellulose membrane and will not interfere with downstream processing steps (Lewinski, Brüggemann, *et al.*, 2024).

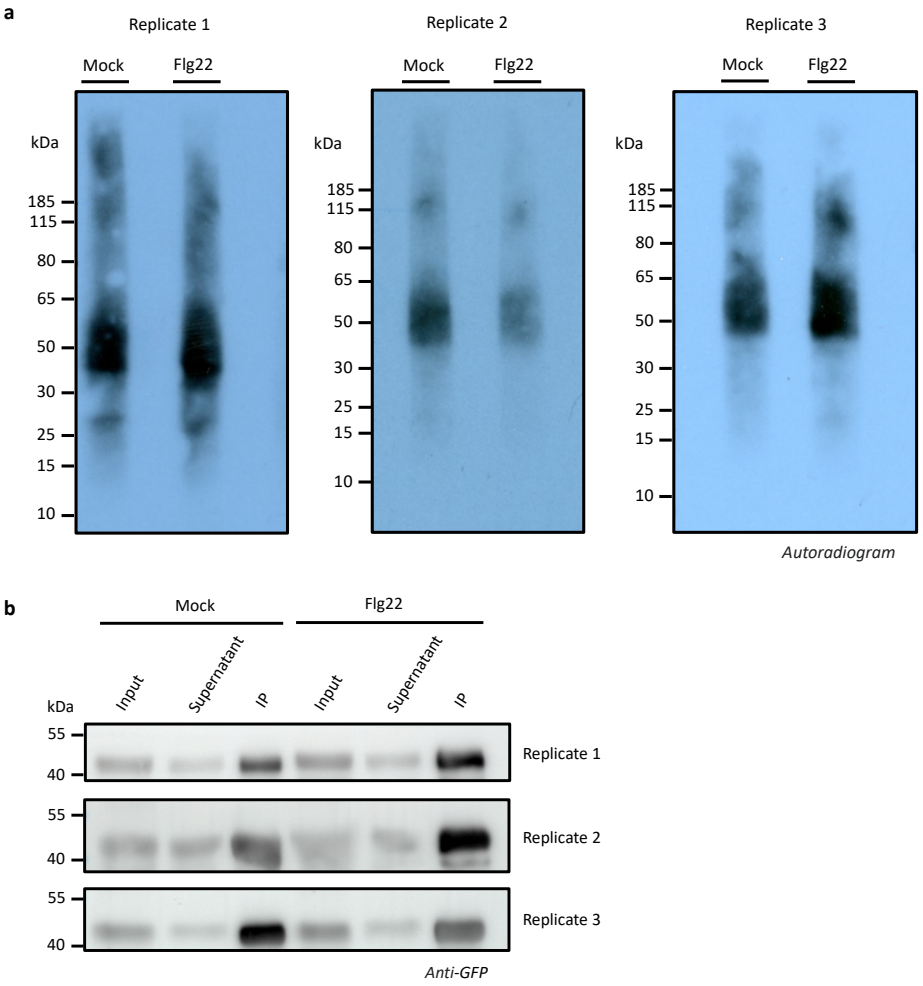

Figure 4. Immunoprecipitation of GRP7-GFP-RNA complexes. a) Autoradiogram of GRP7-GFP-RNA complexes isolated from *A. thaliana* seedlings via anti-GFP immunoprecipitation following 2-hour submergence in liquid MS media lacking (Mock) or containing 1 µM flg22 for three independent biological replicates. 20% of immunoprecipitated RNA was radiolabelled with ^{32}P-γ-ATP. Samples were separated via neutral pH MOPS-PAGE then transferred to a nitrocellulose membrane by Western Blot. Fujifilm was exposed to the membrane for 14 hours. **b)** Immunoblot validation of immunoprecipitation (IP). Levels of GRP7-GFP in the immuno-precipitate (IP+) relative to the whole cell lysate (input) and whole cell lysate after IP (supernatant) for three independent biological replicates were analysed via an Anti-GFP antibody immunoblot.

2.3.4 cDNA library preparation

Isolated RNA was subsequently reverse transcribed into cDNA. As reverse transcriptase tends to terminate cDNA synthesis at the peptide cross-link (CL) sites, this yielded a library of cDNAs with 3' ends corresponding to the CL site. An optimisation PCR was then performed to identify the minimum PCR cycle number required to sufficiently amplify the library for sequencing without over amplification. It was determined that nine cycles were sufficient for all libraries for amplification in the preparative PCR. However, replicate 2 had lower amplification than desired when visualised on a polyacrylamide gel (figure 5a). Therefore, replicate 2 mock (M2) and replicate 2 flg22 (F2) were amplified for 10 and 11 cycles respectively in the preparative PCR. The concentration of each library was then normalised and multiplexed. A final size selection was performed to exclude residual primers prior to sequencing (figure 5b). The results of both gels indicate that the isolation of RNA and generation of cDNA libraries was successful for all three biological replicates.

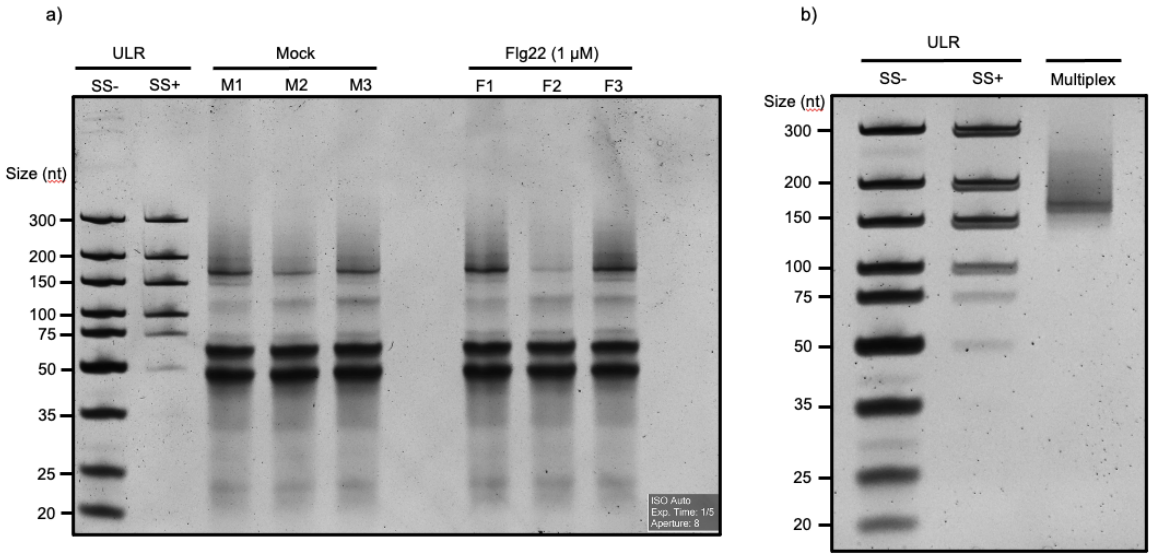

Figure 5. Preparing and multiplexing of iCLIP2 libraries for sequencing. a) Preparative PCR of iCLIP2 cDNA libraries following first size selection. Following the first cDNA pre-amplification step, each iCLIP2 library was size selected. A 300 nt ultra-low-range ladder was also size selected as a control (ULR SS+). Each size selected library was then amplified with 9 cycles preparative PCR. Aliquots of PCR products were separated via polyacrylamide gel electrophoresis, then stained in SYBR Gold. **b)** Multiplexed iCLIP2 libraries submitted for Illumina sequencing. Individual libraries were normalised to 6 nM and pooled prior to a second size selection to remove residual primers. An ultra-low range DNA ladder (ULR), before and after size selection (SS) was included as a control. Pooled, size selected libraries were loaded on a 12% TBE polyacrylamide gel and run as before.

2.3.5. Library sequencing & quality control

The multiplexed iCLIP2 libraries were sequenced via Illumina high-throughput sequencing. Martin Lewinski (Staiger lab, University of Bielefeld) kindly processed the raw reads to determine the identity of the transcripts bound by GRP7 in both experimental conditions in addition to its binding sites according to the iCLIP2 analysis pipeline (Lewinski, Brüggemann, *et al.*, 2024). The number of sequencing reads present at each stage of the analysis pipeline are summarised below in figure 6a. Over three million unique, deduplicated reads were mapped to the *A. thaliana* TAIR10 reference genome indicating good quality libraries were obtained for each sample.

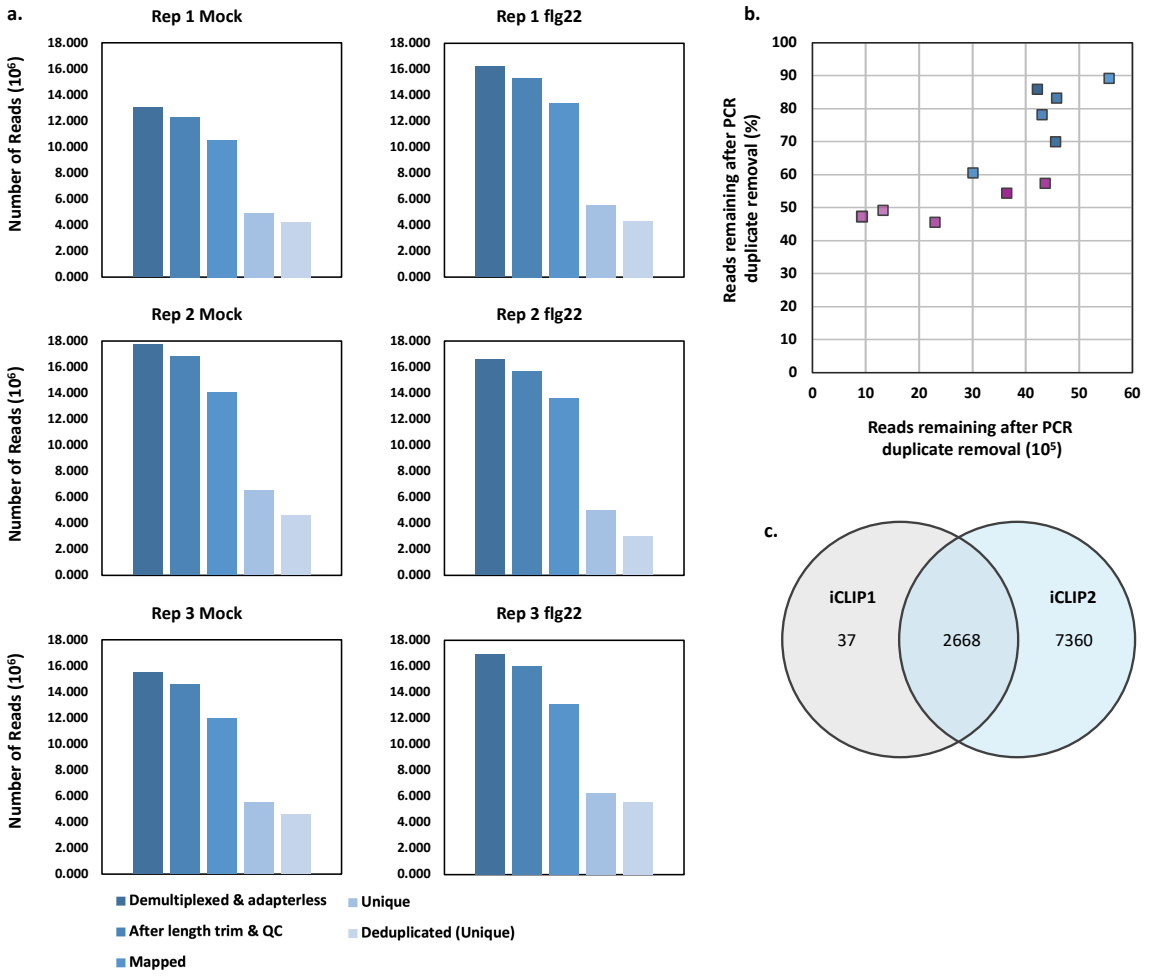

Figure 6. Read statistics of iCLIP2 libraries. a) Total number of reads mapping to the *A. thaliana* TAIR10 genome at each stage of the data analysis pipeline. Total reads generated in each library following demultiplexing and removal of sequencing adapters (Demultiplexed and adapterless). Total reads that passed QC and after 3' adaptors removal (After length trim & QC). Total reads that mapped to the TAIR10 reference genome (Mapped). Total number of mapped reads that map to a unique site in the genome (Unique). Total number of unique reads after removal of PCR duplicates (Deduplicated). **b)** Proportion of reads remaining following PCR duplicate removal from libraries generated via iCLIP2 (blue) (this study), and generated via iCLIP1 (purple) (Lewinski, Brüggemann, *et al.*, 2024). **c)** Comparison of GRP7 RNA targets identified via iCLIP1 (Lewinski, Brüggemann, *et al.*, 2024), and iCLIP2 (this study).

To evaluate the complexity of the libraries that were generated via the iCLIP2 protocol relative to iCLIP1, the proportion of unique reads remaining after PCR duplicate removal (i.e. reads possessing the same unique molecular identifiers) was compared between our iCLIP2 libraries and libraries that were prepared from *A. thaliana* GRP7-GFP seedlings in the subjective evening (LL36) via iCLIP1 (Meyer *et al.*, 2017), which have since been reanalysed and published using the iCLIP2 data analysis pipeline (Lewinski, Brüggemann, *et al.*, 2024). For all biological replicates in our iCLIP2 library, the percentage of retained reads following PCR duplicate removal was substantially higher than for the library generated by iCLIP1 (figure 6b), demonstrating the increased sensitivity of the iCLIP2 protocol due to the reduced loss of reads from targets with lower transcript abundance and or lower GRP7 binding affinity (Buchbender *et al.*, 2020). A relatively higher number of PCR duplicates were obtained in our flg22 replicate 2 library, which was PCR amplified for two additional cycles during the preparative PCR (figure 5, section 2.3.4). This resulted in a lower number of unique, deduplicated reads relative to other samples.

From our analysis, GRP7 was identified to interact with over 10, 000 unique transcripts across both treatment groups – the majority of which were annotated as protein-coding mRNA. These transcripts possessed at least one reproducible binding site that was detected in two or more of the biological replicates. This represents a more than ten-fold increase in the number of RNA targets of GRP7 than previously reported by Meyer and colleagues in the first analysis of GRP7 targets via iCLIP1 (Meyer *et al.*, 2017), and greater than a three-fold increase after reanalysis of the GRP7 iCLIP1 dataset with the improved iCLIP2 data analysis pipeline (Lewinski, Brüggemann, *et al.*, 2024), which highlights the enhanced sensitivity of the iCLIP2 protocol.

To explore the reproducibility of the interactions of GRP7 with its target RNA substrates, we compared the RNA targets of GRP7 that we identified via iCLIP2 in this chapter with the targets that have previously been identified via iCLIP1 (Lewinski, Brüggemann, *et al.*, 2024) (figure 6c). Most of the RNA targets of GRP7 that were identified via iCLIP1 were also identified in our dataset, suggesting that these 2668 targets are bonafide substrates of GRP7. An additional 7360 targets were only identified in our iCLIP2 data, which possibly represent lower abundance and or lower affinity substrates of GRP7 that were detected due to the increased sensitivity of iCLIP2. Less than 2% of the targets identified via iCLIP1 were not detected in our data. Taken together, these findings demonstrate that iCLIP2 successfully generated high complexity libraries which yielded both known and new RNA targets of GRP7.

2.3.6 GRP7 target identification and analysis

In the flg22 treatment condition, GRP7 bound 8,885 unique RNA targets, 718 of which were specific to flg22 (figure 7a; Supplementary Data File 1). These RNA targets primarily consisted of protein-coding mRNA. However, GRP7 was also found to bind to non-coding RNA (ncRNA) species, including long non-coding RNA (lncRNA), antisense lncRNA, small nuclear RNA (snRNA) and small nucleolar RNA (snoRNA). Just under 400 unique ncRNA molecules were identified as being bound by GRP7 in each treatment group, representing approximately 4% of targets. Of which, 93% of these targets were shared between treatment groups. Together, these results suggest that GRP7 may not play a significant role in ncRNA regulation during PTI. However, this could be an avenue for future research.

To understand how PTI activation affects the RNA binding dynamics of GRP7 we compared GRP7 binding to protein-coding transcripts between mock and flg22 across discrete mRNA transcript regions (5'UTR, CDS, intron, 3'UTR). For each region, transcripts were classified as possessing condition-specific binding sites (i.e. at least one binding site detected in exactly one condition) or common binding sites (i.e. detected in both) (figure 7b). From this analysis, we found that GRP7 has a strong preference for the 3'UTRs of its target mRNAs, as over 9,000 unique targets possessed at least one GRP7 binding site within this region, which is consistent with previous findings that GRP7 preferentially interacts with 3'UTRs (Meyer *et al.*, 2017). Out of the entire pool of transcripts with reproducible 3'UTR binding sites, only 1,824 (20%) were detected to have conditional GRP7 binding within this region. In contrast, GRP7 interacted with introns with the lowest frequency in our samples, which was unsurprising as we performed iCLIP2 on bulk tissue containing relatively higher levels of mature, spliced mRNA derived from the cytoplasm. Interestingly, as a proportion of the total set of transcripts possessing a GRP7 binding site within an intron, intronic regions has the highest level of conditional GRP7 binding sites – as 47.2% of these transcripts possessed binding sites that are unique to either the mock or flg22 treatment condition.

Additionally, a relatively high proportion of targets with binding sites within protein coding regions (CDS) and the 5'UTR possessed condition-specific GRP7 binding (39.5% and 36.3% of sites respectively). These findings suggest that PTI-associated function of GRP7 on RNA metabolism may be dependent upon its interactions with introns and protein coding regions of its mRNA substrates. However, it is not possible to conclude this based on positional data alone due to our limited understanding of the relationship between the site of interaction and functional consequences for RNA binding proteins.

A Gene Ontology (GO) enrichment analysis of transcripts having conditional GRP7 binding sites, stratified by transcript region, was conducted against all GRP7 iCLIP2 targets as the background set. This approach ensured that enrichments reflected region-specific binding patterns rather than overall biases in GRP7 target recovery (Appendix I. Supplementary table 15, 16).

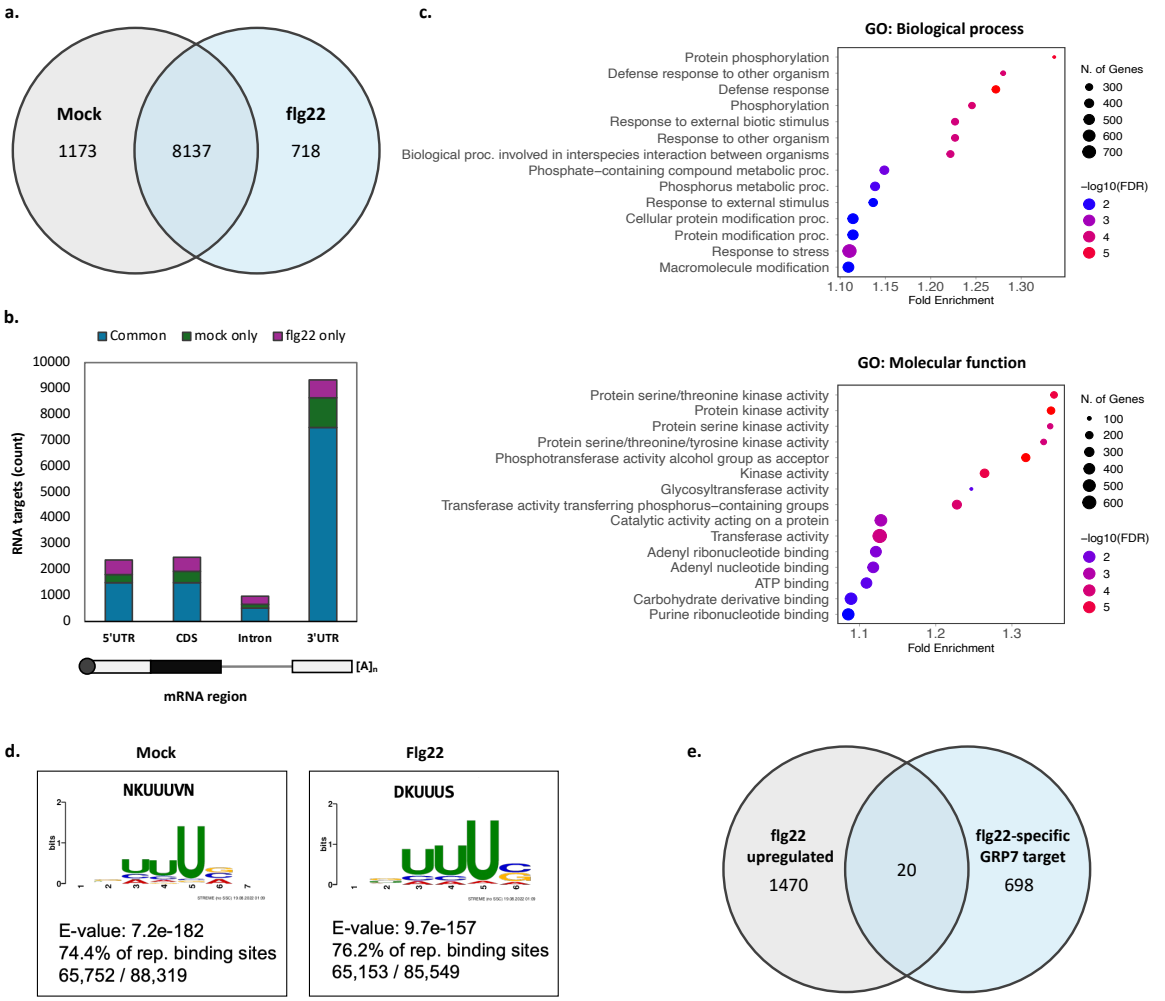

Figure 7. Remodelling of the GRP7 RNA interactome following flg22 treatment. a) Overlap of the RNA targets of GRP7 identified by iCLIP2 in the mock and flg22 treated seedlings. **b)** Comparison of condition-specific GRP7 binding events relative to common GRP7 binding events stratified by transcript region. Total number of transcripts possessing a GRP7 binding event in both treatment groups (blue), unique to the mock-treated condition (green), and unique to the flg22-treated condition (purple). **c)** Gene ontology (GO) term enrichment analysis of transcripts containing flg22-induced conditional GRP7 binding sites. The set of all GRP7 targets identified by iCLIP2 was used as background (FDR cut-off = 0.05). **d)** GRP7 binding site motif for the RNA targets in the mock and flg22 condition identified via MEME analysis. **e)** Overlap between flg22-specific GRP7 targets identified by iCLIP2 and significantly upregulated genes in 2-week-old *A. thaliana* seedlings following a 30 minute-flg22 treatment (Latrasse *et al.*, 2017). Statistical analysis of differences between flg22-upregulated genes and flg22-specific GRP7 targets was performed using Fisher's exact test (Background = 10,028) (observed = 20, expected ≈ 107, odds ratio = 0.15, $P = 1.9 \times 10^{-28}$).

This analysis revealed significant enrichment for biological-process terms related to biotic stress responses (figure 7c). For example, *defence response to other organism* (GO:0098542) was the second most overrepresented term having a fold enrichment of 1.28 (FDR = 6.89×10^{-5}), consistent with GRP7's role as a positive factor in defence against *Pto* DC3000. We also observed enrichment for molecular-function terms such as *protein kinase activity* (GO:0004672; FDR = 1.33×10^{-6}), suggesting that the flg22-specific targets, and common targets with condition-specific GRP7 binding sites encode components of phosphorylation-dependent signalling cascades central to PTI, including receptor-like kinases such as *SOMATIC EMBRYOGENESIS RECEPTOR KINASE 4* (*SERK4*) and MAPK pathway elements such as *MITOGEN-ACTIVATED PROTEIN KINASE 4* (*MPK4*) (Supplementary Data File 1).

2.3.7 flg22-only GRP7 target specificity is not driven by transcriptional changes

It is well documented that the *A. thaliana* transcriptome undergoes substantial changes following the activation of PTI by elicitors such as flg22 (Navarro *et al.*, 2004; Latrasse *et al.*, 2017; Bazin *et al.*, 2020). Therefore, it is possible that the 718 flg22-specific GRP7 targets identified by iCLIP2 were only identified due to their transcriptional upregulation in the PTI activated condition. To test this, the flg22-specific GRP7 targets were compared against a list of 1,490 previously identified genes that are significantly upregulated in *A. thaliana* seedlings following a 30-minute exposure to flg22 (Latrasse *et al.*, 2017) (Supplementary data file 2). From the resulting overlap, only 20 of the flg22-specific GRP7 targets were transcriptionally upregulated after a 30-minute flg22 treatment (figure 7e). Statistical analysis using Fisher's exact test using all GRP7 targets identified by iCLIP2 as a background revealed a highly significant under-representation of overlap ($P = 1.91 \times 10^{-28}$), indicating that GRP7 preferentially binds transcripts that are not strongly transcriptionally induced during early PTI. It is important to note that there are differences in the time points used for our iCLIP2 experiment and for the flg22 differential gene expression experiment (Latrasse *et al.*, 2017) (2 hours vs. 30 minutes). This could influence our analysis and the interpretation of these results.

2.3.8 GRP7 association with known and novel immunity-related RNA targets

We aimed to determine if some of the known targets of GRP7 that have been implicated in immunity such as *FLS2* and *EF-TU RECEPTOR* (*EFR*) are present in our interactome data, and whether the position of GRP7 binding sites along these transcripts differs between mock and flg22 treatment conditions. (Staiger *et al.*, 2003; Nicaise *et al.*, 2013). We identified *FLS2* and *GRP7* mRNA in both datasets, with the location of some GRP7 binding events changing within the first exon of *FLS2* between mock and flg22 (figure 8). However, we did not detect transcripts of *EFR* within either the mock or flg22 treatment groups, possibly suggesting that GRP7 does not strongly interact with the *EFR* mRNA in *A. thaliana* seedlings.

In addition to validating previously reported RNA targets, we identified a wide range of immunity-associated transcripts with many possessing condition-specific GRP7 binding sites in response to flg22 treatment; representative examples are displayed in figure 8. These transcripts encode proteins with established roles in both PTI and ETI, including receptors and co-receptors (BAK1) (Chinchilla *et al.*, 2007), signalling components such as BOTRYTIS-INDUCED KINASE 1 (BIK1) (Lu *et al.*, 2010) and MPK4 (Gao *et al.*, 2008), transcriptional regulators (WRKY40) (Xu *et al.*, 2006), defence metabolite biosynthetic enzymes (PAD3) (Zhou, Tootle and Glazebrook, 1999) and NLR-class resistance proteins such as HOPZ-ACTIVATED RESISTANCE 1 (ZAR1) (Bi *et al.*, 2021). Their binding site profiles suggest that GRP7 may contribute to the fine-tuning of immune responses, possibly by modulating RNA metabolism of these defence-related genes. This expands the repertoire of GRP7 substrate RNAs beyond the well-known targets, underscoring its potential as a central post-transcriptional regulator in *A. thaliana* immunity.

Visualisation of crosslink signal across biological replicates revealed reduced signal intensity in the flg22, replicate 2 sample relative to the others for several loci (Appendix I, Supplementary figure S1). This replicate also exhibited a slightly lower number of unique, deduplicated reads detected in the sequencing quality control stage, consistent with reduced library depth. As crosslink intensity is not directly comparable between samples, this did not affect the identification of reproducible binding sites, which were defined based on presence in at least two biological replicates.

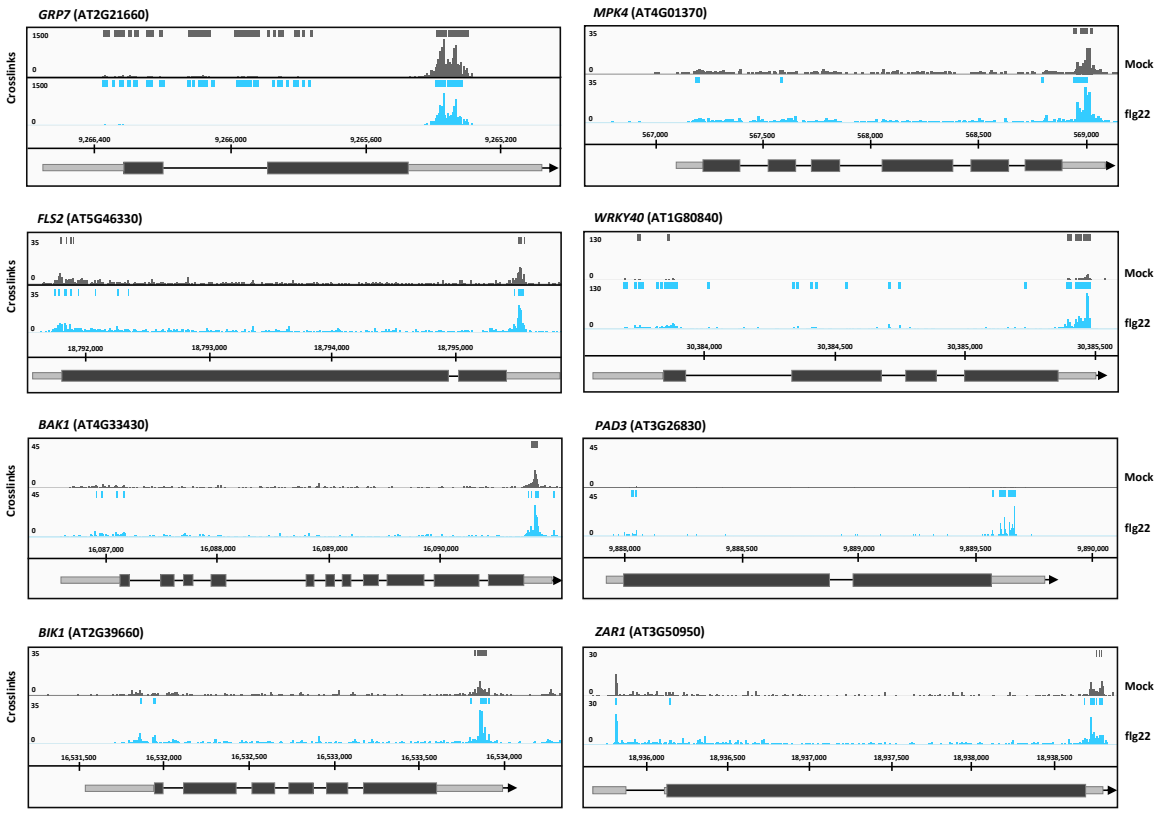

Figure 8. Representative GRP7 binding profiles identified by iCLIP2. iCLIP2 profiles of GRP7 binding on representative immunity-related transcripts under the indicated treatment conditions. (grey = mock; blue = flg22). Crosslinks are displayed relative to the representative mRNA, with y-axis values indicating the number of crosslinks. Reproducible GRP7 binding sites are indicated by bars above each crosslink profile. Grey bars represent 5' UTR and 3' UTR; black bars denote exons and thin lines denote introns.

2.3.9 Assessing flg22-induced changes in the subcellular localisation of GRP7

As we have established that GRP7 may selectively bind to RNA targets following PTI activation that are not differentially expressed during flg22 treatment, we aimed to determine if changes in the localisation of GRP7 could explain this finding. To this end, we used confocal microscopy to assess changes in the subcellular localisation of GRP7 in *A. thaliana* during a flg22-induced PTI response. As before, transgenic *A. thaliana grp7-1* T-DNA seedlings expressing a translational fusion of GRP7-GFP under the control of its native promoter were flood treated with flg22 for 2 hours. We found that the localisation of GRP7-GFP did not show any substantial changes between the mock and flg22 treatment conditions (figure 9), as the GFP signal was detected in both the cytosol, nucleoplasm and nucleolus.

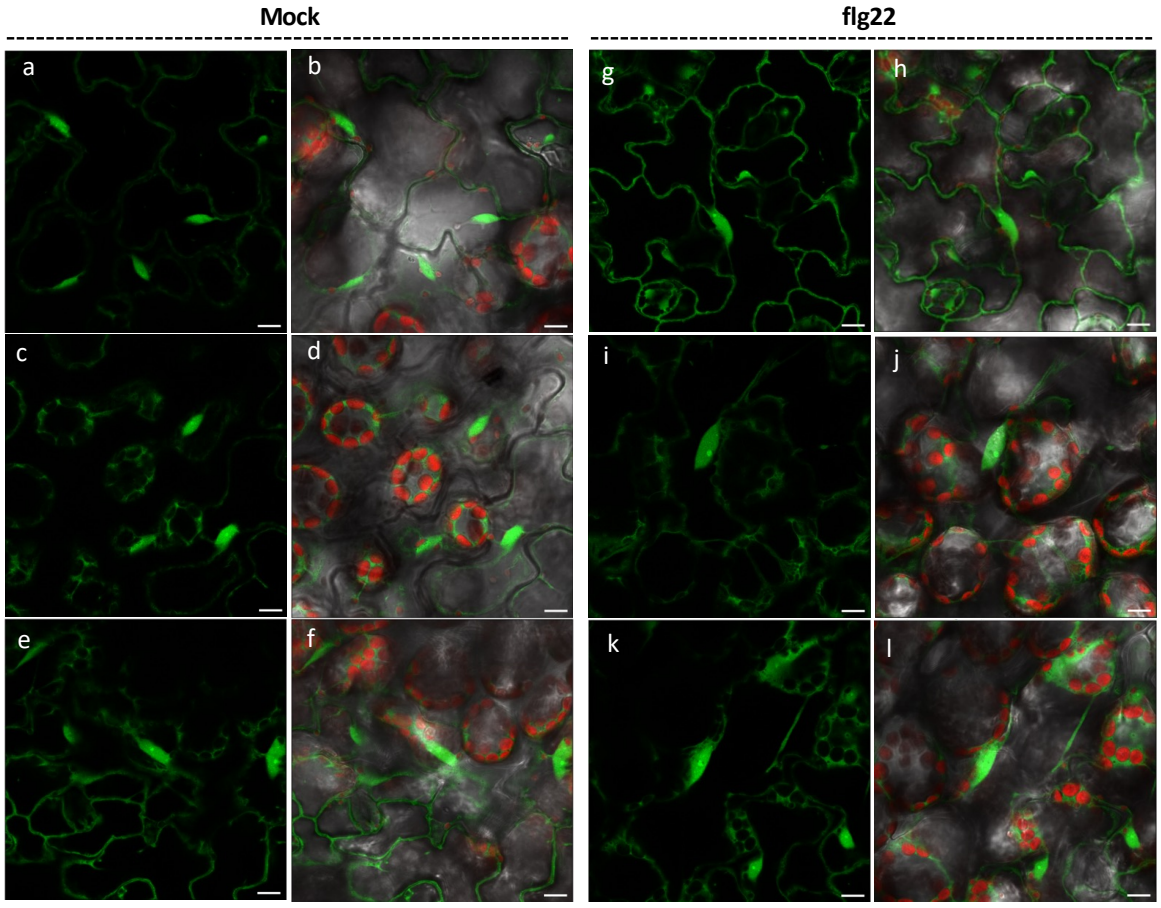

Figure 9. Subcellular localisation of GRP7 during PTI. Two-week old *A. thaliana* GRP7-GFP seedlings flood treated for 2 hours with liquid MS media (Mock) **(a – f)** and liquid MS media containing 1 µM flg22 **(g – i)**. Images of cotyledon epidermal pavement cells acquired using the Zeiss LSM 880 Airyscan, with the 40x immersion lens and 488 nm laser wavelength (GFP emission 493 – 598 nm) (Chlorophyl A 647 – 721 nm). GFP expression is shown in green, chlorophyll autofluorescence is shown in red, and the transmitted light is displayed in greyscale. Each image represents a different biological replicate. Scale bar represents 10 µm.

Therefore, from this data we can conclude that the localisation of GRP7 to the cytoplasm and the nucleus is not affected by flg22 treatment after 2 hours. Anecdotally, we did see evidence of more numerous and intense foci in the nucleus (possibly corresponding to the nucleolus) in the flg22 treated samples. However, further quantitative analyses would need to be performed on a higher number of samples to validate this.

2.3.10 GRP7 is not degraded at 2 hours following PTI activation

It has previously been demonstrated that GRP7 becomes polyubiquitinated following a 30-minute treatment with 100 nM flg22 relative to a water control (Ma *et al.*, 2021). As ubiquitin modifications can be associated with proteolytic turnover of the substrate protein, we aimed to understand if such flg22-induced ubiquitination events can result in the degradation of GRP7 – which could impact its global RNA binding-dynamics. Therefore, the accumulation of GRP7-GFP in seedlings treated with flg22 was analysed by immunoblot relative to a mock-treated control. We did not detect a notable decrease in the protein level of GRP7 between the mock and flg22 treatment conditions across three independent biological replicates (figure 10a). We also analysed a range of total protein masses for one biological replicate to ensure that the immunoblot was not saturated (figure 10b). From these results, we can conclude that flg22 treatment does not trigger the degradation of GRP7 at the time point tested here. This suggests that the flg22-induced ubiquitination of GRP7 may regulate other signalling processes, which may alter its RNA binding dynamics during PTI.

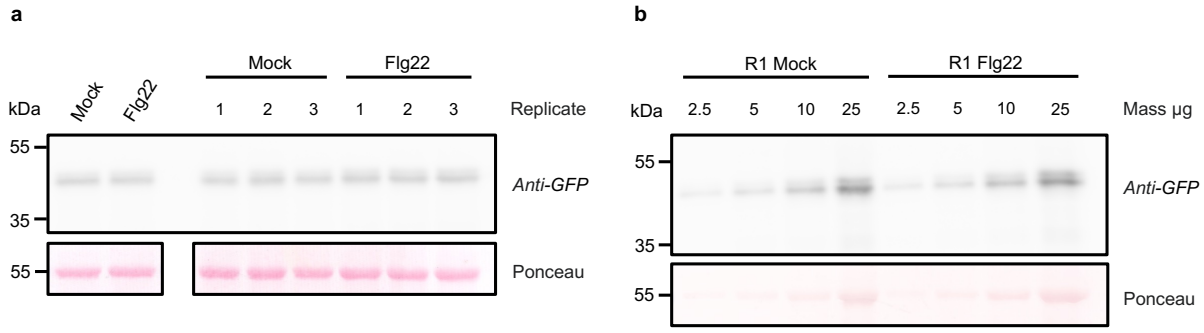

Figure 10. GRP7 protein levels following elicitation of PTI in *A. thaliana* seedlings expressing GRP7-GFP. a) Immunoblot of GRP7-GFP following 2-hour submergence in liquid MS media lacking (Mock) or containing 1 µM flg22. 18 µg of total protein extracts were separated via SDS-PAGE. (left) Combined extracts from three independent biological replicates for each treatment, (right) constituent biological replicates for each treatment. **b)** Increasing mass of total protein from 2.5 µg up to 25 µg for biological replicate 1. Ponceau S staining is used as a loading control.

2.3.11 Phylogenetic analysis of *A. thaliana* GRP7 orthologues in crop species

As GRP7 positively regulates defence against *P. syringae* in *A. thaliana*, we aimed to investigate evolutionary relationships between GRP7 orthologues identified in seventeen economically important crop species, comprising both dicotyledons and monocotyledons. We also assessed the degree of protein sequence conservation of GRP7 orthologues within the RNA recognition motif (RRM), which is targeted by the HopU1 virulence effector protein.

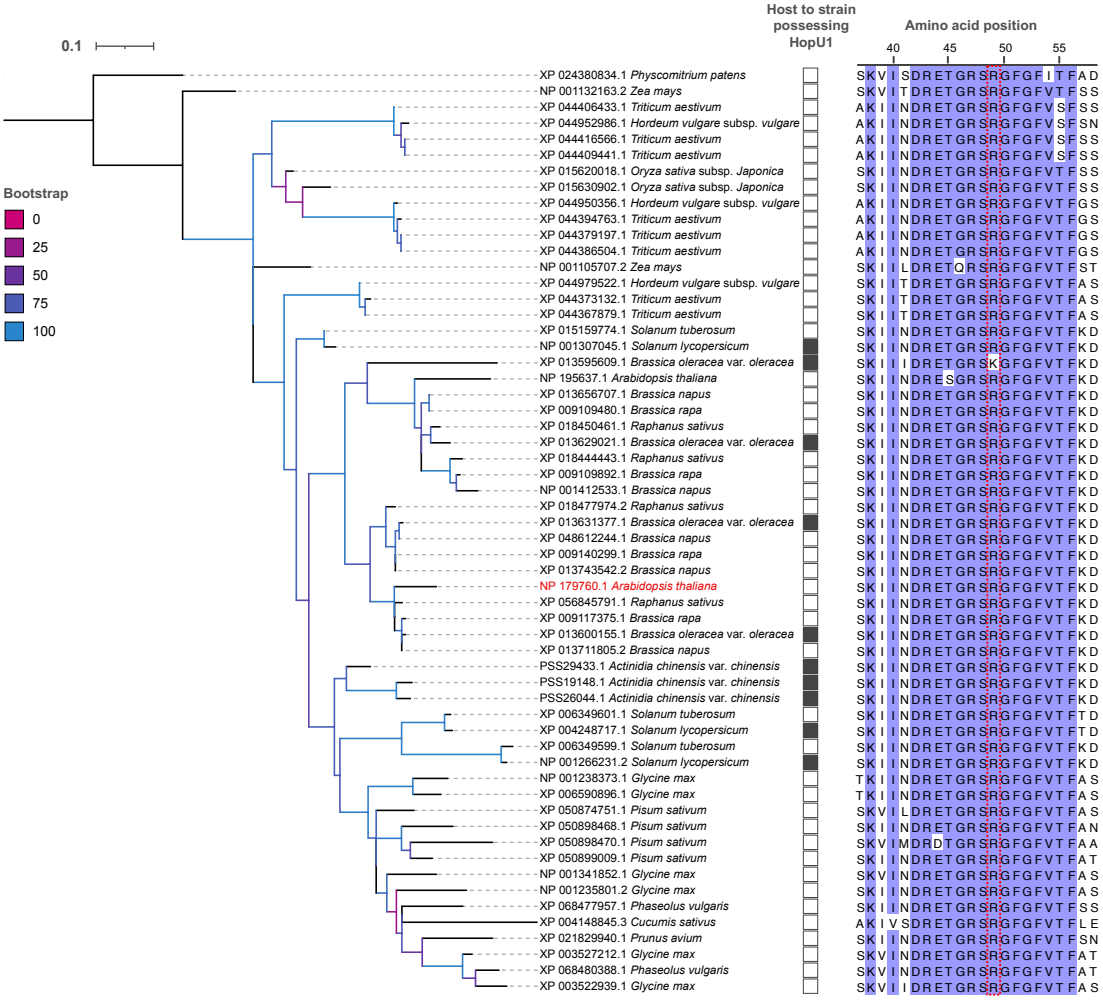

Figure 11. Phylogenetic analysis of *At*GRP7 and *At*GRP8 orthologues in crops. A maximum likelihood (ML) phylogenetic tree was constructed based on the amino acid sequences of *A. thaliana* GRP7 orthologues identified in diverse crop species. *At*GRP7 (NP 179760.1) is highlighted in red. Sequences were aligned using MAFFT with default parameters, and alignment trimming was performed using TrimAl to remove poorly aligned regions. Phylogenetic reconstruction was performed using IQ-TREE with 1000 ultrafast bootstrap replicates to assess branch support (Trifinopoulos *et al.*, 2016). Bootstrap support values are indicated by branch colour; scale bar represents substitutions per site. Hosts of isolation of *P. syringae* strains that possess HopU1 are indicated with a grey box. A multiple sequence alignment of each corresponding GRP7 orthologue showing the RNP1 region of the RNA recognition motif is displayed on the right. Amino acids showing >90 sequence identity are coloured in blue. The arginine (R) residue that is modified by HopU1 is outlined in red.

A maximum likelihood model was used to analyse fifty-eight protein sequences (including GRP7 and GRP8 from *A. thaliana*) that shared at least 70% similarity with the *A. thaliana* GRP7 protein sequence. The topology of the resulting tree broadly corresponded to the separation of monocots and dicots, with the model bryophyte *Physcomitrium patens* used as an outgroup to root the tree (figure 11). We found that most of the crops analysed contained multiple paralogues sharing at least 70% identity with the *A. thaliana* GRP7 sequence, consistent with multiple gene duplication events. As expected, the closest orthologues to *A. thaliana* GRP7 belonged to other members of the Brassicaceae family, including *Brassica rapa* (field mustard), *Brassica oleracea* var. *oleracea* (wild cabbage), *Brassica napus* (rapeseed), and *Raphanus sativus* (radish), supported by a high bootstrap value (91.2%). Even with the large evolutionary distances between the species included in this analysis, the amino acid sequences showed a remarkable level of conservation across orthologues. This indicates the importance of the RNP1 region of the RRM for mediating interaction with substrate RNA and suggests that these orthologues retain functional RNA-binding capacity.

Next, we investigated which of the seventeen crop species in our dataset have been identified as hosts to strains of *P. syringae* possessing HopU1. These included *Brassica oleracea* var. *oleracea*, and *Actinidia chinensis* var. *chinensis* (kiwifruit) that are infected by *P. syringae* pv. *maculicola* 90-32, *P. syringae ICMP 11292* respectively, and *Solanum lycopersicum* (tomato) that is a host to both *P. syringae* pv. *tomato* DC3000 and *P. syringae* pv. *tomato* ICMP2844. Of the ten orthologues identified from these host species, nine had identical RNP1 domains to *A. thaliana* GRP7. Interestingly, one orthologue in *Brassica oleracea* var. *oleracea* has an arginine-49-to-lysine (R49K) substitution in the RNP1 region, which is the residue that is ADP-ribosylated by HopU1 during infection. Additionally, we identified a second substitution event asparagine-41-to-isoleucine (N41I). To the best of our knowledge, the extent to which these amino acid substitutions *Brassica oleracea* var. *oleracea* influence its resistance to *P. syringae* is unknown.

Together, these results demonstrate that GRP7 is an evolutionarily conserved protein due to its prevalence across diverse plant lineages and the strong conservation of its RRM. The presence of identical RNP1 sequences in GRP7 orthologues from crop species that are hosts to *P. syringae* strains possessing HopU1 suggests that these proteins may also be susceptible to HopU1-directed suppression during infection via a mechanism similar to that characterised in *A. thaliana*.

2.4 Discussion

GRP7 is a multifunctional RNA-binding protein that exerts broad control over RNA metabolism and has emerged as a pivotal regulator of immunity in *A. thaliana*. GRP7 is directly targeted by HopU1 – a type III effector secreted by *Pto* DC3000 during infection, which suppresses PTI (Fu *et al.*, 2007). This suppression is caused by the ADP-ribosylation of arginine 49 within the RNA recognition motif (RRM) of GRP7, which has been proven to be indispensable for the RNA binding activity of GRP7, as arginine 49 substitution mutants cannot complement loss of GRP7 function and show PTI responses to *Pto* DC3000 (Jeong *et al.*, 2011). Previous work suggested that GRP7 may regulate the translation of ligand-free receptor-like kinases (RLKs) at the cell surface such as FLS2 (Nicaise *et al.*, 2013), yet a comprehensive characterisation of its RNA interactome during PTI has been lacking. By applying the improved iCLIP2 methodology to seedlings treated with the elicitor peptide flg22, we provide the most extensive dataset to date describing the RNA substrates and binding sites of GRP7 in the context of PTI. These findings substantially expand the known repertoire of GRP7 targets and demonstrate dynamic changes in RNA binding associated with immune activation. Going forward, it will be important to identify which GRP7-RNA interactions are functionally important in the context of PTI, to improve our understanding of how *Pto* DC3000 manipulates the *A. thaliana* via HopU1 during infection.

2.4.1 Expansion of the GRP7 RNA interactome during PTI

Our analysis revealed that GRP7 associates with over 10,000 transcripts in total, representing more than a three-fold increase compared to the original iCLIP study (Meyer *et al.*, 2017), demonstrating the enhanced sensitivity of this improved method, largely due to reduced loss of low-abundance RNA during library preparation (Lewinski, Brüggemann, *et al.*, 2024). Importantly, 718 transcripts were identified as flg22-specific targets, and 2801 additional shared mRNA targets exhibited flg22-dependent shifts in GRP7 binding site positions. GO-term enrichment analyses highlighted strong overrepresentation of stress- and defence-related processes, consistent with the well-established role of GRP7 in promoting resistance to *Pto* DC3000 (Fu *et al.*, 2007; Nicaise *et al.*, 2013). Moreover, the flg22-specific targets and targets with condition-specific GRP7 binding sites encoded receptor-like kinases and MAPK pathway components, suggesting that GRP7 may directly modulate signalling cascades downstream of PAMP perception. Together, these results support a model in which GRP7 contributes to the fine-tuning of immune responses by selectively engaging with transcripts encoding both pattern recognition receptors and intracellular signalling components.

A positional analysis revealed that GRP7 binds preferentially to 3'UTRs, but with notable enrichment of flg22 treatment-specific binding within protein-coding regions and introns. Although intronic binding sites were relatively infrequent, they displayed the highest proportion of condition-specific binding sites. This may indicate a link to PTI-responsive alternative splicing (AS), as GRP7 may conditionally interact with cis-acting splicing regulatory elements (SREs) to modulate AS decisions (Reddy *et al.*, 2013), which is consistent with previous demonstrations of GRP7's role as a splicing regulator (Streitner *et al.*, 2012; Wang *et al.*, 2020).

In contrast, stable interactions with 3'UTRs may underlie the role of GRP7 in post-transcriptional regulation of translation, as shown for *FLS2* and other stress-related targets (Nicaise *et al.*, 2013; Xu *et al.*, 2024). This is further supported by evidence that many 3'UTR interacting RBPs regulate translation by influencing the stability or translatability of an RNA substrate. For example, PUF/PUMILIO (PUM) family proteins target conserved elements within 3'UTRs and negatively regulate gene expression by affecting the stability and translation of their target genes (Hardy and Balcerowicz, 2024). This may indicate that GRP7 regulates the expression of 3'UTR target mRNA at the post-transcriptional level by influencing the stability and translation of such mRNA.

2.4.2 Selective binding of GRP7 to substrate RNA

Interestingly, only a small minority of flg22-specific GRP7 targets corresponded to genes transcriptionally upregulated during early PTI (Latrasse *et al.*, 2017). This significant underrepresentation possibly indicates that the emergence of new GRP7-mRNA interactions is not simply a by-product of transcript abundance. Instead, GRP7 may be actively recruited to a subset of defence-related RNAs through context-dependent mechanisms. We hypothesised that this could be caused by changes in the subcellular localisation of GRP7 or substrate RNA following flg22 treatment, the occurrence of post-translational modifications on GRP7, or a combination of multiple factors.

GRP7 has previously been found to be localised to the nucleus and cytosol in *A. thaliana* (Kim *et al.*, 2008). It is possible that flg22-induced changes in localisation of GRP7 may expose it to different populations of RNA substrates, which could affect its RNA binding activity. For example, GRP7 may accumulate more in the cytoplasm than the nucleus following flg22 treatment, which may facilitate enhanced binding to low-affinity transcripts present in the cytosol. However, in our confocal studies, we found no evidence to support this, which suggests that changes in RNA-binding dynamics are unlikely to be driven by large-scale redistribution of GRP7. We did notice higher

fluorescence signal in the nucleolus in some flg22-treated samples, which may indicate more accumulation in this region. Interestingly, the nucleolus is important for plant immunity and represents a common target for viral and oomycete pathogen effectors (Lee *et al.*, 2024), and GRP7 has been detected with in nucleolar fractions prepared from *A. thaliana* cell cultures (Palm *et al.*, 2016). However, further repeats of this experiment with nucleolar-specific co-staining would be required to quantitatively assess the localisation of GRP7 in the nucleolus. Regardless, the presence of GRP7 in both the nucleus and cytosol is indicative of the range of molecular functions that GRP7 serves in the cell, as nuclear-localised GRP7 would be capable of influencing AS, whereas cytosolic GRP7 may regulate translation and other RNA processing events such as RNA degradation.

Signals at the cell surface can be directly transduced into changes in the RNA binding activity of GRP7, affecting global AS patterns. This has been observed in the RALF1-FERONIA system, whereby the receptor-like kinase FERONIA directly phosphorylates the intrinsically disordered region of GRP7 upon recognition of the signalling peptide RALF1. This enhances the RNA binding activity of GRP7 which alters AS (Wang *et al.*, 2020). In the context of the elicitor-induced PTI response, GRP7 has been found to become polyubiquitinated in *A. thaliana* seedlings following exposure to flg22 (Ma *et al.*, 2021). Mathematical modelling of splicing factors has demonstrated that they can influence AS based on their cellular load (Ding *et al.*, 2022). Polyubiquitination is a PTM that is often associated with proteolytic turnover of the substrate protein and is a critical factor underpinning the plasticity of the proteome during the immune response of plants (Langin, González-Fuente and Üstün, 2023). Therefore, the flg22-induced ubiquitination of GRP7 may indicate that it is degraded, which could influence the RNA binding dynamics of GRP7 within the cell. We found that the accumulation of GRP7 in *A. thaliana* seedlings is not affected by a 2-hour flg22 treatment, which indicates that GRP7 is not being degraded by the proteosome during this period. Or if GRP7 is being degraded, it is rapidly being re-synthesised.

The paradigm of protein ubiquitination has shifted in recent years due to the discovery of the so-called 'ubiquitin code', whereby different types of ubiquitin linkages and topologies are associated with diverse signalling events (Orosa-Puente and Spoel, 2022). This is particularly important in immune signalling processes as demonstrated by the transcriptional activation of SA-responsive genes by NPR1. Following its SA-induced localisation to the nucleus, NPR1 becomes ubiquitinated by the Cullin-RING Ligase 3 (CRL3), which enhances the association of NPR1 with target promoters to facilitate transcription (Skelly *et al.*, 2019). Therefore, it is possible that flg22-assocaited ubiquitination of GRP7 may change its affinity for different transcripts due to its ability to form

complexes with additional RBPs or components of the spliceosome. This hypothesis is supported by the finding that RBPs that display differences in RNA binding activity in response to flg22 are significantly depleted in Lysine ubiquitination, suggesting that ubiquitin-based PTMs may modulate RBP RNA binding activity during PTI (Bach-Pages, Chen, *et al.*, 2020). Unpublished data provided by the Spoel lab (personal communication) has sown that GRP7 is associated with K63-linked chains and infection with *P. syringae* pv. *maculicola* ES4326 results in a -2.14 fold (log2) decrease in this topology. This presents the possibility that virulent pathogens target the ubiquitination of RBPs to disrupt host RNA processing.

2.4.3 Study limitations and future directions

A key limitation of this study is that it only provides a snapshot of the RNA interactome of GRP7 in whole seedlings, specifically 2 hours following flg22 treatment. We know that the initial PTI signalling events and responses occur within minutes of PAMP perception (Yu *et al.*, 2017), so it is possible that important GRP7-RNA interactions induced by flg22 treatment occur before the 2-hour timepoint. However, evidence suggests that type 3 effectors can be delivered into host cells between 1 – 2 hours after inoculation with *Pto* DC3000 (Grant *et al.*, 2000). Therefore, we can hypothesise that any relevant PTI-associated GRP7-RNA interactions that are suppressed by HopU1 can be captured in this dataset. Additionally, comparing flg22-induced changes in the RNA binding dynamics of GRP7 between common targets is challenging in the absence of complementary RNA-seq data prepared from the same samples. This is because changes in the observed number of crosslinks at binding sites could either be caused by differences in the RNA binding site preference and affinity of GRP7, and or by differences in the overall abundance of the substrate RNA transcript.

Furthermore, our iCLIP2 dataset has been prepared from bulk tissue, which masks potentially distinct RNA binding dynamics of GRP7 within different cell populations or cellular compartments. Recent single cell RNA sequencing studies have demonstrated that different cell types within *A. thaliana* leaf tissue undergo markedly different transcriptional responses during infection with *P. syringae* (Zhu *et al.*, 2023). Therefore, it is reasonable to hypothesise that concomitant changes in the RNA binding dynamics of RBPs such as GRP7 would also occur heterogeneously within the leaf tissue. However, this level of spatial resolution is not possible with the current iCLIP2 methodology.

Other technical limitations of iCLIP2 have recently been summarised by Lewinski and colleagues. One key limitation is that while the expression of UV stress-responsive genes is only induced 60 minutes following crosslinking, it is not possible to fully exclude the potential of rapid changes in

RBP-RNA interactions occurring due to UV exposure (Meyer *et al.*, 2017; Lewinski, Brüggemann, *et al.*, 2024). However, the UV exposure will rapidly induce the formation of covalent bonds to fix the RBP-RNA interactions, thus minimising the chance of significant rearrangement of the RNA interactome of GRP7. Additionally, in our experimental setup, the use of a mock-treated control can help account for UV-induced effects and enables us to isolate the effects of the flg22 treatment. In this chapter, we have only investigated the RNA binding dynamics of GRP7 with respect to a flg22-induced PTI response. Going forward, the logical next step would be to explore how wildtype *Pto* DC3000 vs a HopU1 deletion mutant influence the RNA binding activity of GRP7 during infection to identify specific transcripts that are disrupted by HopU1. This could be achieved by replicating the methodology that we have used in this study but replacing the flg22 treatment with the flood-inoculation of *A. thaliana* seedlings with the relevant *P. syringae* strains.

Future work should aim to understand the function of GRP7 orthologues in economically important crops that are also hosts to *P. syringae* strains harbouring HopU1. For example, the orthologue of GRP7 in the solanaceous model *Nicotiana benthamiana*, *Nb*GRP7, has recently been identified as a positive regulator of *R* gene-mediated resistance against the potato cyst nematode *Globodera pallida* and Potato Virus X (PVX). In the case of PVX, the ability of GRP7 to promote extreme resistance is dependent upon the ability of GRP7 to interact with and stabilise the mRNA of Rx1, a CC-NB-LRR immune receptor that confers disease resistance to PVX (Sukarta *et al.*, 2022). This finding provides compelling evidence that GRP7 orthologues can act as conserved hubs in post-transcriptional regulation of immunity across diverse plant lineages. Extending these observations to solanaceous crops such as tomato, and applying innovative methodologies such as iCLIP2, will be essential to determine whether GRP7 orthologues play similar roles in regulating immune responses in economically important species. Ultimately, such approaches may reveal strategies to strengthen crop disease resistance and thereby contribute to global food security.

Our phylogenetic analysis of GRP7 orthologues across seventeen crop species revealed a high degree of evolutionary conservation, particularly within the RNP1 region of the RNA recognition motif (RRM). This motif is indispensable for RNA binding and contains arginine-49, the residue specifically ADP-ribosylated by HopU1 in *A. thaliana* (Jeong *et al.*, 2011). Notably, almost all orthologues examined retained an identical RNP1 sequence, underscoring the evolutionary constraint on this motif and its central role in GRP7 function. However, one orthologue in *B. oleracea* var. *oleracea* displayed an R49K substitution at the HopU1-targeted site. Intriguingly, *B. oleracea* is a host to a strain of *P. syringae* pv. *maculicola* that encodes HopU1. It is possible that

this substitution represents an adaptive event to evade HopU1-directed suppression of RNA binding activity. Despite arginine and lysine having similar physiochemical properties, previous studies have found that $GRP7_{R49K}$ could not restore resistance to *Pto* DC3000 to wildtype levels when cloned into a loss-of-function GRP7 mutant in *A. thaliana*, and had impaired RNA binding activity (Fu *et al.*, 2007). However, the *B. oleracea* orthologue also possessed a simultaneous asparagine-41-to-isoleucine substitution (N41I), which may be required to maintain full RNA binding activity. Therefore, a logical next step would be to clone the RNP1 region from this *B. oleracea* orthologue into *A. thaliana* GRP7 and assess whether this substitution confers resistance to HopU1-mediated modification. If so, this would provide direct evidence that altering the HopU1-target site can preserve GRP7's immune-regulatory function. Such studies could open avenues for engineering HopU1-resistant variants of GRP7 in crops, thereby safeguarding a critical post-transcriptional regulator of immunity against pathogen interference.

From this work, we have identified thousands of potential candidate RNAs for which the direct interaction of GRP7 could influence the immune response to *Pto* DC3000. Therefore, in the following chapter, we will identify a set of high-priority candidates to explore how GRP7 influences their mRNA processing, and how this impacts the defence response to this pathogen.

Chapter 3

Investigating the role of GRP7 in PTI-associated alternative splicing

3.1 Introduction

The differential inclusion of exons and introns during mRNA maturation is a critical co/post-transcriptional process in Eukaryotes that is referred to as alternative splicing (AS). In plants, AS is an important mechanism to enable rapid changes in stress-responsive gene expression without requiring *de novo* transcription (Kufel, Diachenko and Golisz, 2022). A growing number of examples of mRNA isoform switching events resulting from changes in AS, particularly intron retention (IR), have been described to have a significant impact on the outcome of an infection. For example, mRNA encoding the cytoplasmic CALCIUM-DEPENDENT KINASE 28 (CPK28) exists in two major isoforms, the ratio of which is regulated by the splicing factor IMMUNOREGULATORY RNA-BINDING PROTEIN (IRR). The canonical isoform (*CPK28.1*) functions as a negative regulator of PTI through co-ordinating the degradation of BOTRYTIS-INDUCED KINASE 1 (BIK1) via the phosphorylation of the polyubiquitin ligases PUB25/26, which subsequently mark BIK1 for degradation (Dressano *et al.*, 2020). As BIK1 is a key hub within the PTI signalling cascade which directly phosphorylates and activates downstream effectors such as RBOHD, its degradation attenuates PTI (Li *et al.*, 2014). Upon the activation of PTI signalling IRR dissociates from the *CPK28* pre-mRNA triggering the retention of intron 11, which contains a premature-termination codon (PTC). This isoform (*CPK28.4*) encodes a truncated protein product with reduced kinase activity, which enhances PTI signalling outputs due to the re-accumulation of BIK1 (Dressano *et al.*, 2020). This system demonstrates that different protein isoforms of immunity-related genes can pay distinct, and in this case opposing, roles in the defence response of *A. thaliana*.

Furthermore, plant pathogens deploy virulence effectors to target components of the host splicing machinery to disrupt AS and consequently facilitate proliferation in the host. For example, the Oomycete pathogen *Phytophthora sojae* uses the virulence effector PHYTOPHTHORA SUPPRESSOR OF RNA SILENCING 1 (PSR1) to interfere with the activity of pre-mRNA splicing factor PRP16 in its host. This disrupts global AS patterns, which significantly increases the occurrence of IR (Gui *et al.*, 2022). Subsets of these intron-retained isoforms could be translated into truncated proteins, lacking important functional domains with altered activity. When transiently expressed in *N. benthamiana*, intron-retained isoforms significantly altered the susceptibility to *P. sojae*. Such findings highlight the importance of the balance between the translation and degradation of intron-retained transcripts in the immune response (Gloggnitzer *et al.*, 2014; Shaul, 2015). Together, these studies demonstrate that truncated proteins can have important impacts on the defence response.

The RNA binding protein GRP7 belongs to the hnRNP-like class of splicing factors, which has previously been demonstrated to regulate the AS of RNA transcripts *in planta* – some of which GRP7 has been confirmed to directly interact with, such as its own transcript (Staiger *et al.*, 2003). It has since been revealed that GRP7 can regulate the AS of thousands of transcripts in a stress-responsive manner. Interestingly, GRP7's activity as a regulator of AS can be directly modulated downstream of receptor-ligand interactions at the cell surface. For example, the perception of the peptide hormone RAPID ALKALINIZATION FACTOR 1 (RALF1) by the FERONIA receptor-like kinase stimulates the phosphorylation of GRP7, which enhances its RNA binding activity and consequently triggers global changes in AS (Wang *et al.*, 2020). This demonstrates that signalling events at the cell surface can be transduced into changes in AS through GRP7 to regulate cellular responses to stress.

Aims and rationale

In the previous chapter we demonstrated that the RNA interactome of GRP7 changes in response to the elicitor peptide flg22, with 8137 common target transcripts identified in both treatment groups and 718 unique flg22-induced transcript targets. We also demonstrated that the binding sites of GRP7 on the common transcript targets undergoes substantial remodelling following flg22 treatment. For example, over 800 transcripts had at least one condition specific binding site within exonic regions. Therefore, it is possible that GRP7 may affect the AS of its binding targets during a flg22-induced PTI response, as a result of its differential interactions with its mRNA targets, and this may have a quantitative impact on the defence response to *P. syringae.*

Several methods are available to detect isoform switching events caused by changes in alternative splicing. RNA sequencing (RNA-seq) with sufficient read depth, or whole isoform sequencing will enable the detection of isoform abundance and can facilitate the detection of novel isoforms. Additionally, reverse-transcription quantitative PCR (RT-qPCR) provides a targeted approach to assay the expression level of specific isoforms (in this study referred to as isoform-specific qPCR) under different treatment conditions and in different genetic backgrounds to detect changes in alternative splicing (Harvey and Cheng, 2016). In this chapter, we investigate how GRP7 influences the AS of a subset of its flg22-associated targets using isoform-specific qPCR. We also investigate the disease resistance phenotype of the alternative protein isoforms that are encoded by these GRP7-regulated transcripts.

3.2 Materials and methods

3.2.1 Plant growth conditions

The *Arabidopsis thaliana* lines *Atgrp7-1* loss-of-function *AtGRP8* RNAi knockdown (*grp7-1 8i*), *35S::AtGRP7* overexpression (GRP7-OX) were kindly provided by the Staiger lab, University of Bielefeld (Heintzen *et al.*, 1997; Streitner *et al.*, 2008). This line lacks the functional allele of *GRP7* and uses RNAi silencing of *GRP8* to restore its expression to wildtype levels. This is to account for the de-repression of GRP8 production in the *grp7* loss-of-function mutant. All *A. thaliana* seeds were surface sterilised via chlorine gas and sown on half strength MS (Murashige-Skoog; Duchefa) 1% phytoagar plates supplemented with 0.5 g/L MES and 0.5% sucrose at a density of ~40 seedlings per plate. Seeds were stratified at 4°C for 48 hours then transferred to Percival incubators for 14-days and grown under 12-hour light/dark cycles at 20°C with a light intensity of approximately 100 µmol/m^2/s. *Nicotiana benthamiana* was grown in soil for 4 weeks under 16-hour light/dark cycles at 25°C.

3.2.2 Flg22 treatment and RNA extraction

3-week-old seedlings were flooded with liquid MS growth media containing flg22 (Eurogentec) to a final concentration of 1 µM to elicit PTI, or without flg22 as a mock treatment. After 2 hours, each plate was drained, and rosette tissue was immediately harvested and frozen in liquid nitrogen (LN_2). Frozen tissue was subsequently ground to a fine powder using a mortar and pestle in LN_2. RNA was extracted from approximately 100 mg of tissue using the RNeasy Plant Mini Kit (Qiagen). Contaminating DNA was removed from the eluted RNA using the TURBO DNA-free kit (Invitrogen™). cDNA libraries were synthesised from approximately 400 ng of RNA using UltraScript cDNA Synthesis Kit (PCR Biosystems).

3.2.3 Reverse-transcription quantitative PCR (RT-qPCR)

cDNA libraries were synthesised from approximately 400 ng of RNA using UltraScript cDNA Synthesis Kit (PCR Biosystems). qPCR reactions were performed using the Applied Biosystems QuantStudio 5. Each reaction contained diluted cDNA (1:8), SyGreen mix Hi-ROX (PCR Biosystems), and transcript-specific primer pairs (Appendix II. Supplementary table 1). Primer efficiencies were confirmed to fall within an acceptable range of approximately 100% and generate a single amplicon – confirmed through analysis of the PCR product melt curve. Relative quantification of gene expression changes were calculated using the comparative delta Ct method (Livak and Schmittgen, 2001).

For isoform-specific qPCR, relative fold-change of the intron-retained isoforms was calculated with the following formula $2^{-\Delta Ct\ (flg22)} / 2^{-\Delta Ct\ (Mock)}$, where ΔCt = (Ct canonical isoform − Ct intron-retained isoform) (Harvey and Cheng, 2016). Statistical analysis was performed using either a one-way or two-way ANOVA with Tukey's HSD.

3.2.4 Agromonas lux

The CDS of *CPK28.1* (AT5G66210.1), *CPK28.4* (AT5G66210.4), *CIPK3.3* (AT2G26980.3), *CIPK3.2* (AT2G26980.2), *SEN1.1* (AT4G35770.1), *SEN1.4* (AT4G35770.4), were cloned into pJK187 via Golden Gate assembly, then transformed into *Agrobacterium tumefaciens* strain GV3101. Cultures containing each construct were adjusted to a final OD_{600} = 0.5 and prepared into an infiltration solution containing GV3101 P19 (RNA silencing suppressor), and 150 µM Acetosyringone. The two youngest, fully expanded leaves of 4-week-old *N. benthamiana* wild-type plants were infiltrated with an empty vector control (EV) control and the construct of interest in half-leaf zones (Buscaill *et al.*, 2021). After 48hr, plate cultured *Pto* DC3000 ΔhopQ nptII::lux was suspended in sterile distilled water and adjusted to OD_{600} = 0.001 (approximately $1x10^6$ CFU/mL) and pressure infiltrated into agroinfiltrated leaf zones using a needless syringe. At 3 dpi, leaves were detached, and luminescence was recorded using a LAS Imagequant 4000 (General Electric) for 5 min after 2 min incubation in the dark. Mean luminescence was quantified from five distinct 0.59 cm^2 zones within the agroinfiltrated area, avoiding the infiltration site and border regions. Technical replicates were averaged to yield a single luminescence value per biological replicate. Normalised luminescence was calculated by subtracting the mean relative luminescence units (RLU) of the corresponding EV control. Significance was determined using a two-tailed Student's t-test.

3.2.5 Agromonas ROS

Agrobacterium-mediated transient expression was performed as described in section 3.2.4. The ROS assay was performed as described previously (Bach-Pages and Preston, 2018). At 48 hours post-infiltration, 4 mm diameter leaf discs were extracted from agroinfiltrated zones and incubated in Milli-Q water overnight in a 96-well plate under constant light with continuous rotation. Luminol/peroxidase working solutions were prepared with and without 500 nM flg22. Each well was drained before adding the working solutions to each leaf disc. Luminescence was subsequently recorded for 45 minutes, with 1-minute intervals using the Tecan Infinite M200 plate reader. Quantification of total ROS generated in the flg22-treated samples was calculated as the area under the curve (AUC). Significance was determined using a one-way ANOVA with Tukey's HSD.

3.2.6 RT-PCR validation of transient gene expression

Leaf discs (4mm diameter) were extracted from agroinfiltrated zones of *N. benthamiana* leaves two days post-infiltration and pooled from 5 biological replicates. Tissue was flash frozen in 1.5 mL Eppendorf tubes containing 2x steel balls in liquid Nitrogen and homogenised in the TissueLyser II machine (Qiagen). RNA extractions, DNase digest, and cDNA synthesis was performed as described in section 3.2.2. PCR was performed using 1 µL 1:2 diluted cDNA with GoTaq® Green 2x Master Mix (Promega) with the following reaction conditions: 95°C (2 min); 30 cycles of 95°C (30 s), 58°C (30 s), 72°C (30s); final extension 72°C (10 min). PCR products were run on a 2% Agarose TAE gel. Primers are listed in Appendix II, Supplementary table 2.

3.2.7 AlphaFold Multimer modelling of candidate protein interactions

Sequences of full-length and truncated isoforms were obtained from Uniprot.org for CIPK3.3 (Q2V452), CIPK3.2 (A0A178VNR6), CBL9 (Q9LTB8), SEN1.1 (Q38853), SEN1.4 (A0A1P8B5Y0), TRXY1 (Q6NPF9). AlphaFold Multimer models were run using ColabFold v1.5.5: AlphaFold2 using MMseqs2 (REF) with the following parameters: Num relax: 1, template mode: pdb100, model type: alphafold2_multimer_v3, num recycles: 3. The relaxed, highest ranked model for each complex was annotated using PyMOL Molecular Graphics System v2.5.5. Weighted pTM + ipTM scores were calculated with the following formula: (pTM * 0.2) + (ipTM * 0.8) (Evans *et al.*, 2022).

3.2.8 *sen1-1* mutant identification

Genomic DNA was extracted from a *SEN1* T-DNA insertion line obtained from NASC: SALK_020571C (*sen1-1*) as according to the protocol by Chabi Sika and colleagues (Chabi Sika *et al.*, 2015). Precipitated gDNA was re-suspended in sterile distilled water (Milli-Q). PCR reaction mixtures were prepared for each sample containing 12.5 µL GoTaq Green master mix (Promega), 10 µM Forward and reverse primer, 2 µL gDNA, up to 25 µL with PCR grade water. PCR was performed with the following conditions: 94°C (3 min); 34 cycles of 94°C (30 s), 60°C (30 s), 72°C (90s); final extension 72°C (10 min). Two reactions were run for each sample, using the *SEN1*-specific primers and with a gene-specific primer and the SALK primer to detect T-DNA inserts (Appendix II. Supplementary table 3). For RT-PCR detection of mRNA expression in each T-DNA insertion mutant, cDNA libraries were prepared from pooled RNA extracts from three seedlings as described in section 3.2.2. PCRs were set up as described above and run for 24 cycles. *GAPDH* was used as a positive control.

3.2.9 Pathogen infection assay

Col-0 WT and *sen1-1* pathogen susceptibility assays were performed as described by Ishiga and colleagues (Ishiga *et al.*, 2011). A single colony isolate of *P. syringae* pv. *tomato* strain DC3000 (*Pto* DC3000) was grown on LB agar plates for 24 hr at 28°C. Bacteria were harvested and suspended in Milli-Q water then adjusted to an optical density (OD_{600} nm) of 0.02, corresponding to approximately 4 x 10^6 CFU (colony forming units)/mL, and Silwet L-77 was added to a final concentration of 0.025%. MS agar plates containing 6, 3-week-old *A. thaliana* seedlings were fully submerged for 3 min in either the bacterial inoculum, or Milli-Q water containing 0.025% Silwet L-77 as a mock treatment. Seedling rosettes were cut from the agar plate and individually weighed in sterile 2 mL safe-lock Eppendorf tubes containing 2 x steel balls, then homogenised in 1 mL Milli-Q water using the TissueLyser II (Qiagen). Serial dilutions of each sample lysate were performed up to 10^{-8}, then 20 µL of each dilution was plated on LB agar supplemented with Rifampicin (50 µg/ml). Plates were incubated at 28°C for 48 hr. Colony forming units (CFU) was recorded and bacterial growth *in planta* was calculated as CFU/g. Two-tailed T-Tests were performed to assess statistical significance in mean CFU/g between the Col-0 WT and the mutant at each time point.

3.3 Results

3.3.1 Selection of candidate genes

The aim of this chapter was to investigate if GRP7 regulates the AS of its PTI-associated targets. As GRP7 was found to interact with thousands of transcripts in both treatment conditions, a subset of target transcripts were selected as candidates for further analysis. This was accomplished by comparing all GRP7 targets with: i) transcripts that undergo significant changes in alternative splicing *A. thaliana* seedlings following 30 minutes of flg22 exposure (Bazin *et al.*, 2020); ii) transcripts which are alternatively spliced in a *grp7-1 8i* mutant background (Lewinski, Steffen, *et al.*, 2024) (Supplementary data file 3a). GRP8 is a functionally redundant paralogue, so its expression has been reduced to wild-type levels in this line via RNAi. From this analysis, we identified fifteen genes which satisfied our selection criteria (figure 1a). Collectively, these genes are referred to as group I candidates and are summarised in Table 1.

From this pool of candidate genes, six have annotated functions within the plant defence response. These include Hypersensitive-induced response protein 1 (*HIR1*), Penetration 1 (*PEN1*), the Pro-serine rich endogenous peptides 4 & 6 (*PROSCOOP4* & *PROSCOOP6*), Calmodulin-binding protein 60 A (*CBP60A*), and Calcium-dependent protein kinase 28 (*CPK28*). The latter two have well-defined roles within the PTI system of *A. thaliana*. *CBP60A* belongs to a family of Ca^{2+} responsive transcription factors that function downstream of the intracellular Ca^{2+} receptor calmodulin to regulate the expression of PTI-associated genes (Li *et al.*, 2024). *CBP60A* acts as a negative regulator of PTI in *A. thaliana,* as loss-of-function mutants display enhanced resistance to *Pseudomonas syringae* pv. *maculicola* ES4326. This correlates with an increase in both SA accumulation and pathogen-responsive gene expression, which indicates that *CBP60A* functions as a negative regulator of PTI (Truman *et al.*, 2013).

Additionally, as discussed in the introduction to this chapter and in section 1.4.4, *CPK28* primarily functions as a suppressor of PTI signalling due to its role in promoting the degradation of the signalling hub BIK1 (Monaghan *et al.*, 2014). However, the activity of CPK28 is dynamically regulated at the post-transcriptional level in response to PAMP perception, which is coordinated by the RBP IRR. In the presence of a pathogen, IRR modulates the AS of the *CPK28* pre-mRNA to produce an intron-retained isoform that encodes a protein product with impaired kinase activity, thus amplifying the PTI response due to the accumulation of BIK1 (Dressano *et al.*, 2020). However, the relationship between GRP7 and *CPK28* mRNA processing during PTI has not been characterised.

In contrast, *HIR* genes are classically understood to play a key role in resistance (*R*)-gene mediated defence through activating the hypersensitive response (HR) during an infection – a phenotype that is broadly conserved in *A. thaliana* and crops such as *Oryza sativa* and *Triticum aestivum* (Qi *et al.*, 2011; Duan *et al.*, 2013; Li *et al.*, 2019). In *A. thaliana*, HIR1 and HIR2 are plasma membrane-localised proteins that interact with the NB-LRR protein RPS2. In the case of *HIR2*, genetic analyses demonstrated that it is required for RPS2-mediated ETI against strains of *P. syringae* possessing the cognate virulence effector AvrRpt2. Furthermore, overexpressing *HIR1* and *HIR2* enhances basal immunity against *Pto* DC3000 (Qi *et al.*, 2011). *PEN1* encodes syntaxin SYP121, which functions to promote resistance to the biotrophic fungal pathogen *Blumeria graminis f. sp. hordei* – the causal agent of barley powdery mildew (Collins *et al.*, 2003). PEN1 mediates the fusion of exosomes to the plasma membrane, which is required for the timely deposition of callose at infection sites to resist the formation of fungal haustoria (Assaad *et al.*, 2004). Additionally, PEN1 also promoted HR-associated cell death during infection by *Pto* DC3000. *PEN1* is transcriptionally activated during ETI, and *PEN1* loss-of-function mutants display attenuated effector-triggered HR following R-gene detection of *Pto* DC3000 virulence effectors (Johansson *et al.*, 2014). Finally, the SERINE-RICH ENDOGENOUS PEPTIDEs (SCOOPs) are a large family of plant-specific signalling peptides that coordinate development and defence responses. Interestingly, PROSCOOP4 has a direct antimicrobial effect against *Pto* DC3000, significantly reducing its growth on media containing this peptide in a concentration dependent manner (Yu *et al.*, 2020).

Given that the functions of these genes have been characterised with regards to their role in the host defence response to *P. syringae*, we focused on selecting candidates from the pool of group I genes that have no established link to the *A. thaliana* immune system. *SENESCENCE-ASSOCIATED GENE 1* (*SEN1*) represented a candidate of particular interest due to the presence of a flg22-specific GRP7 binding site within the second intron (figure 1b). Interestingly, the position of these condition-specific binding sites corresponds with the location of an alternative intron-retention event that generates an mRNA isoform encoding a premature termination codon (PTC). Furthermore, RNA-seq data provided by the Staiger lab revealed that the proportion of transcripts retaining intron 2 is significantly higher in the *grp7-1 8i* mutant relative to Col-0 WT ($P = 0.00599$) (Lewinski, Steffen, *et al.*, 2024), as can been seen in figure 2b. This suggests that GRP7 promotes splicing of intron 2 from the *SEN1* pre-mRNA. Additionally, *CPK28* was also selected for further analysis in this chapter due to its documented role in the *A. thaliana* PTI response that is dependent upon its alternative splicing (Dressano *et al.*, 2020).

It is well known that exposure to flg22 triggers wide-spread transcriptional changes in *A. thaliana* (Bjornson *et al.*, 2021). Furthermore, in chapter 2, we previously demonstrated that genes that are not differentially expressed following flg22 treatment can become substrates of GRP7. As the alternative splicing data from the *grp7-1 8i* mutant was obtained from plants that were not exposed to biotic stress, other GRP7-regulated candidates are likely present within the pool of GRP7 targets that undergo flg22 changes in alternative splicing – referred to here as differential alternative splicing (DAS). Therefore, these 370 genes were further filtered to identify candidates which have been reported to undergo significant flg22-induced isoform switching events, such that the ratio of the alternative isoforms change following flg22 treatment (Bazin *et al.*, 2020). Additionally, candidates were screened for condition-specific GRP7 binding sites between the mock and flg22 treatments occurring within different regions of the transcript (i.e. a new binding site in a 5' untranslated region), or at different sites within the same region (i.e. different binding sites within an exon).

This further filtering yielded an additional twenty-seven genes that are referred to as group II candidates, which are also summarised in Table 1. Of these group II genes, *CBL-INTERACTING PROTEIN KINASE 3* (*CIPK3*) was also identified as an interesting candidate for further analysis. Again, this was due to the presence of condition-specific GRP7 binding sites in the vicinity of an alternative intron retention event (figure 1b). Together, *CPK28*, *SEN1*, and *CIPK3* were investigated further to determine the role of GRP7 in the pre-mRNA processing of their transcripts, and whether alternative protein isoforms that are predicted to be encoded by these genes affect the immune response.

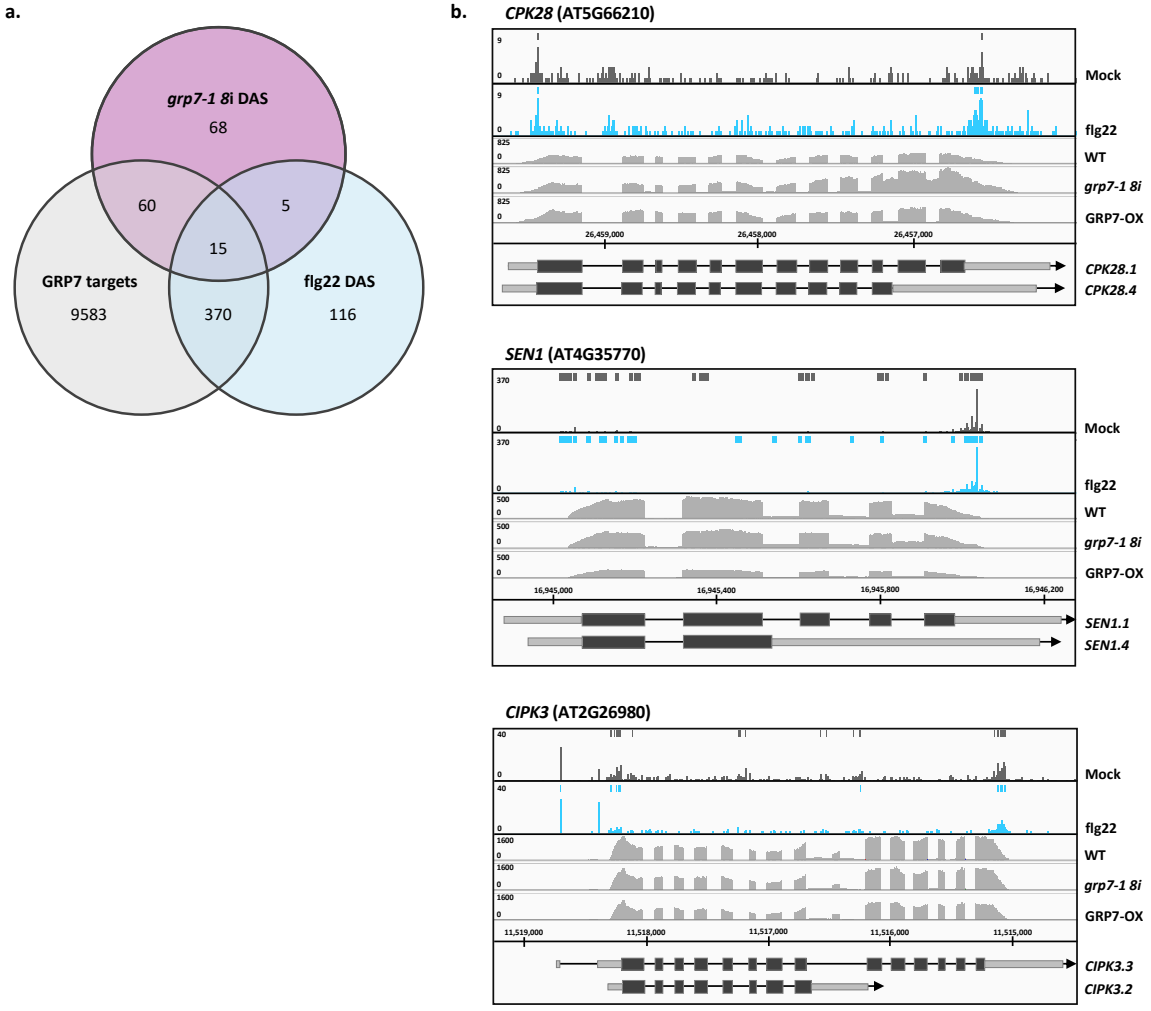

Figure 1. Candidate gene selection from pool of GRP7 targets. a) Three-way overlap between all GRP7 target transcripts with transcripts which undergo differential alternative splicing (DAS) following 1 µM flg22 treatment in *A. thaliana* seedlings for 30 minutes (Bazin *et al.*, 2020), and transcripts which undergo DAS in the *grp7-1 8i* mutant background (Lewinski, Steffen, *et al.*, 2024). **b)** iCLIP2 profile of GRP7 binding on *CPK28*, *SEN1*, and *CIPK3* mRNA in mock treated (top row, grey) and flg22 treated conditions (lower row, blue). The y-axis value indicates crosslink counts. Significant binding sites, indicated by block lines, are mapped to their respective position along the representative pre-mRNA transcript (Exons: black rectangle, Introns: line, 5'/3' untranslated region: grey rectangle). RNA-seq coverage for Col-0 WT, *grp7-1 8i*, and *GRP7-OX* are displayed below the iCLIP2 data (Lewinski, Steffen, *et al.*, 2024). iCLIP2 crosslink counts per replicate are shown in Appendix II, Supplementary figure S1.

Table 1. Candidate GRP7-regulated genes.

Group I Candidates *			Mock				flg22			
AGI Locus	Code	Encodes	5'UTR	CDS	Intron	3'UTR	5'UTR	CDS	Intron	3'UTR
AT1G27020		Uncharacterised protein	X	X		X	X	X	X	X
AT1G68660	CLPS1	ATP-dependent Clp protease adapter protein	X	X		X	X			X
AT1G69840	HIR1	Hypersensitive-induced response protein 1		X		X		X		X
AT2G01180	LPP1	Lipid phosphate phosphatase 1 (Phosphatidic acid phosphatase 1)		X		X	X	X		X
AT2G24600		Ankyrin repeat family protein	X			X	X			X
AT3G11820	PEN1/SYP121	Penetration 1/Syntaxin in plants 121	X	X		X	X	X		X
AT3G57930		Rho GTPase-activating gacO-like protein				X				X
AT4G26400	BTL05	RING-type E3 ubiquitin transferase				X				X
AT4G34150	CALB1	Calcium-dependent lipid-binding protein 1	X	X		X	X	X	X	X
AT4G35770	SEN1	Senescence-associated protein 1	X	X		X	X	X	X	X
AT4G36850		PQ-loop repeat family protein / transmembrane family protein			X	X		X	X	X
AT5G44568	PROSCOOP4	SCOOP (SERINE RICH ENDOGENOUS PEPTIDE) family member		X		X		X		X
AT5G44572	PROSCOOP6	SCOOP (SERINE RICH ENDOGENOUS PEPTIDE) family member				X				X
AT5G62570	CBP60A	Calmodulin-binding protein 60 A				X				X
AT5G66210	CPK28	Calcium-dependent protein kinase 28		X	X			X	X	
Group II Candidates **										
AT1G01490	HMP01	Heavy metal transport/detoxification superfamily protein	X	X	X	X	X	X	X	X
AT1G01550	BPS1	Protein of unknown function (DUF793)	X	X	X	X	X	X	X	X
AT1G08450	CRT3	Calreticulin 3				X		X		X
AT1G14650	PRP21	Pre-mRNA processing factor 21				X				X
AT1G20100		DNA ligase-like protein	X		X	X	X	X	X	X
AT1G53510	MPK18	Mitogen-activated protein kinase 18	X		X	X	X		X	X
AT1G63830		PLAC8 family protein	X			X	X	X		X
AT1G66260	ALY3	RNA-binding (RRM/RBD/RNP motifs) family protein			X	X	X			X
AT1G67060		Peptidase M50B-like protein				X				X
AT2G13790	SERK4	Somatic embryogenesis receptor-like kinase 4				X		X	X	X
AT2G26980	CIPK3	CBL-interacting protein kinase 3		X	X	X			X	X
AT2G30440	TPP	Thylakoid processing peptide	X			X	X	X	X	X
AT2G38870		PR (pathogenesis-related) peptide (PR-6 proteinase inhibitor family)		X		X	X	X	X	X
AT3G01480	CYP38	Cyclophilin 38	X	X		X	X	X		X
AT3G06080	TBL10	TRICHOME BIREFRINGENCE-LIKE 10				X				X
AT3G16220		Putative eukaryotic LigT				X				X
AT3G56130	BLP3	Biotin/lipoyl attachment domain-containing protein		X		X				X
AT4G21410	CRK29	Cysteine-rich RLK (RECEPTOR-like protein kinase) 29				X		X		X
AT4G23850	LACS4	Long-chain acyl-CoA synthetase 4	X			X	X	X	X	X
AT4G32060	MICU	Calcium-binding EF hand family protein	X	X	X	X	X	X	X	X
AT4G33625		Vacuole protein				X				X
AT4G36690	ATU2AF65A	U2 snRNP auxilliary factor, large subunit, splicing factor				X	X			X
AT5G23510		Hypothetical protein				X		X	X	X
AT5G41080	GDPD2	Glycerophosphodiester phosphodiesterase 2				X			X	X
AT5G59960		K-stimulated pyrophosphate-energized sodium pump protein		X		X				X
AT5G63160	BT1	BTB and TAZ domain protein 1	X	X	X	X	X	X	X	X
AT4G19520		Disease resistance protein (TIR-NBS-LRR class) family							X	

* Group I candidates are GRP7 targets identified in both mock and flg22 treatment groups that undergo flg22-induced alternative splicing (Bazin *et al.*, 2020), and are identified to undergo alternative splicing in a *grp7-1 8i* mutant (Lewinski, Steffen, *et al.*, 2024). ** Group II candidates are GRP7 targets that undergo significant isoform switching following flg22 treatment (Bazin *et al.*, 2020). The location of GRP7 binding sites for each candidate are represented by a cross and are categorised into the 5' and 3' untranslated regions (5'/3' UTR), protein coding sequence (CDS), and intronic regions. Novel binding events between the mock and flg22 treatment are indicated by a red cross.

3.3.2 Validating GRP7 mutant and overexpression *A. thaliana* lines

To validate the expression of *GRP7* mRNA in each of the *A. thaliana* lines used in this experiment, cDNA libraries were prepared from total RNA extracted from rosette tissue of 3-week-old plants. The transcript level of *GRP7* was quantified using RT-qPCR and normalised to the housekeeping gene *GLYCERALDEHYDE-3-PHOSPHATE DEHYDROGENASE C2* (*GAPDH*, AT1G13440) and compared to Col-0 WT mock sample (figure 2a). Analysis via a two-way ANOVA showed a significant interaction between the treatment and genotype ($P = 0.00109$) and both main effects were also significant (treatment: $P = 0.00205$; genotype: $P = 1.15\times10^{-14}$). We confirmed a significant reduction in *GRP7* mRNA in the *grp7-1 8i* mutant relative to Col-0 wildtype regardless of flg22 treatment. In contrast, we found that the level of *GRP7* mRNA was significantly higher in two independent GRP7 overexpression lines (D1C and G1D) (Schöning *et al.*, 2007) than in Col-0 wildtype. Interestingly, the flg22 treatment significantly increased *GRP7* mRNA accumulation in both overexpression lines relative to the mock treatment. Together these findings validate the expected phenotypes for each line.

3.3.3 GRP7 regulates the alternative splicing of *CPK28* mRNA

To determine whether GRP7 regulates the alternative splicing of *CPK28* in a flg22-dependent manner, isoform-specific qPCR was performed to detect changes in its splicing ratio following a mock or flg22 treatment in Col-0 wildtype, a *grp7-1 8i* mutant (Streitner *et al.*, 2008), or two GRP7-OX lines (D1C and G1D) (Heintzen *et al.*, 1997). This technique utilised two primer sets that specifically amplify either the canonical splice variant *CPK28.1*, or the intron-retained isoform *CPK28.4* (Dressano *et al.*, 2020) (figure 2b).

To isolate the effect of AS on the relative abundance of each isoform from transcriptional effects, the level of *CPK28.1* was normalised to *CPK28.4* for each sample (figure 2c). A two-way ANOVA detected a significant interaction ($P = 0.023$) between the genotype and treatment, indicating that the treatment effect differed by genotype. The genotype main effect was significant ($P = 4.91\times10^{-4}$), whereas the treatment main effect was not. Post-hoc analysis using Tukey's HSD revealed that the proportion of *CPK28.1* was significantly reduced in the mock-treated *GRP7* mutant and overexpression lines (figure 2c). This trend was also observed for the flg22-treated overexpression lines. Interestingly, the proportion of *CPK28.1* significantly increased in the flg22-treated *grp7-1 8i* mutant when compared to the mock treatment, which reverted to wildtype levels.

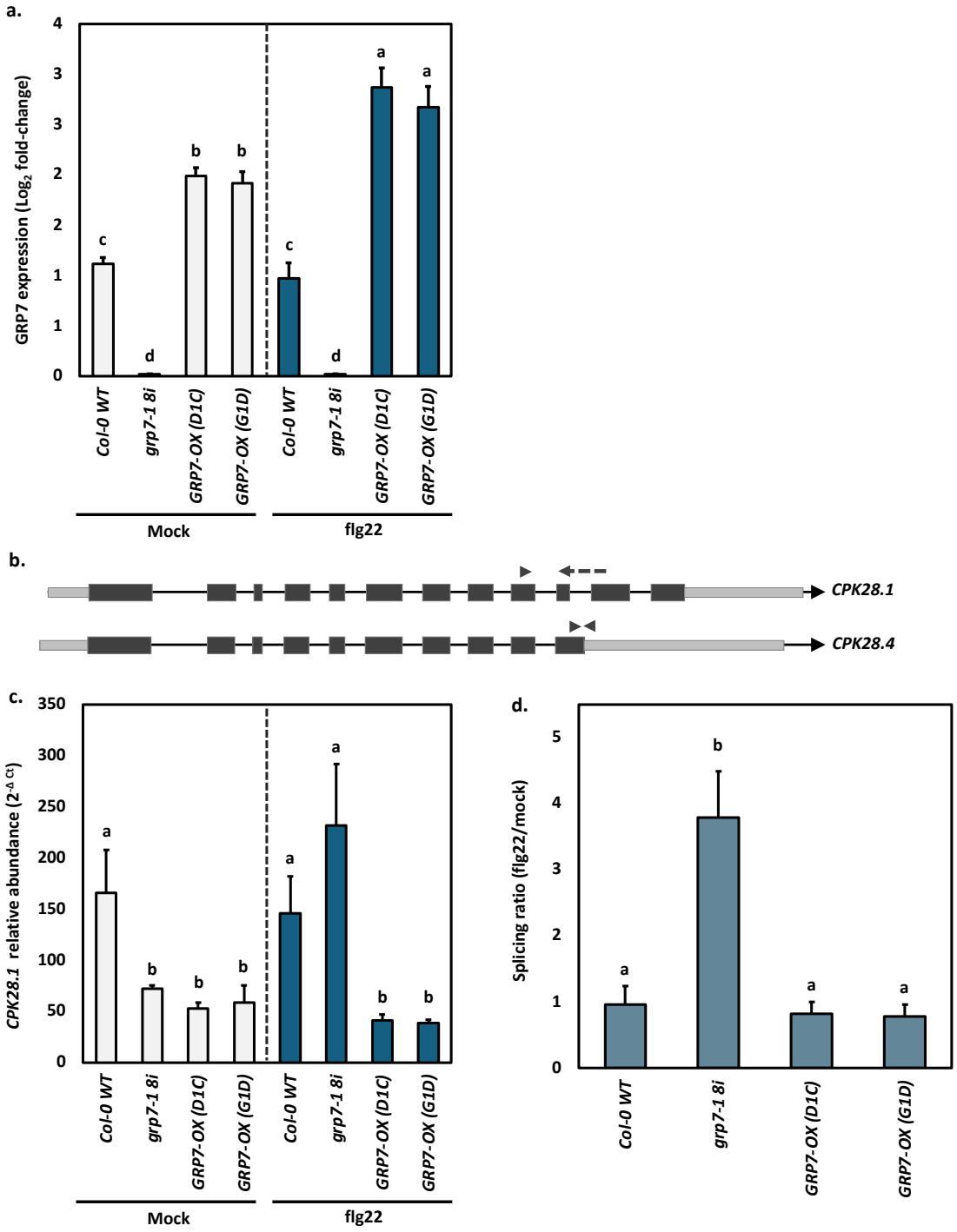

Figure 2. GRP7 differentially regulates the alternative splicing of *CPK28* mRNA following flg22 treatment. a) Validation of *GRP7* expression in each *A. thaliana* line used in this experiment via RT-qPCR. Ct values normalised to *GAPDH*. **b)** mRNA transcript models of canonical *CPK28.1* and intron-retained *CPK28.4* (Exons: black rectangle, Introns: line, 5'/3' untranslated region: grey rectangle). Primer binding sites are shown above each model. **c)** Relative abundance of *CPK28.1* normalised to *CPK28.4* following a 2-hour mock, or 1 µM flg22 treatment in each genotype. Expression levels calculated using the formula $2^{-\Delta Ct}$, where ΔCt = (Ct canonical − Ct intron-retained) (Harvey and Cheng, 2016). **d)** Effect of flg22 treatment on the splicing ratio of *CPK28.1* was calculated for each genotype using the formula $2^{-\Delta Ct\ (flg22)} / 2^{-\Delta Ct\ (Mock)}$. Error bars indicate mean ± SEM (n = 4). Statistical analysis was performed using a two-way ANOVA with Tukey's HSD (a, c), or one-way ANOVA with Tukey's HSD (d). Means not sharing the same letter are significantly different ($P < 0.05$).

We subsequently compared the ratio of the normalised level of *CPK28.1* between the flg22 treatment and mock treatment for each genotype to test how the AS of *CPK28* responds to PTI activation in each genotype (figure 2c). A one-way ANOVA revealed that the relative abundance of the canonical *CPK28.1* isoform significantly increased in the *grp7-1* 8i mutant upon flg22 treatment when compared to Col-0 wildtype (P = 0.0007), while both overexpression lines did not differ significantly from the wildtype. These results suggest that GRP7 is likely required to suppresses the splicing of intron 11 from *CPK28* pre-mRNA only in a PTI-activated context. The relative increase in intron 11 exclusion that was observed in the flg22-treated *grp7-1 8i* mutant appears to be primarily driven by higher levels of *CPK28.1* produced in the flg22 context than in the mock treatment.

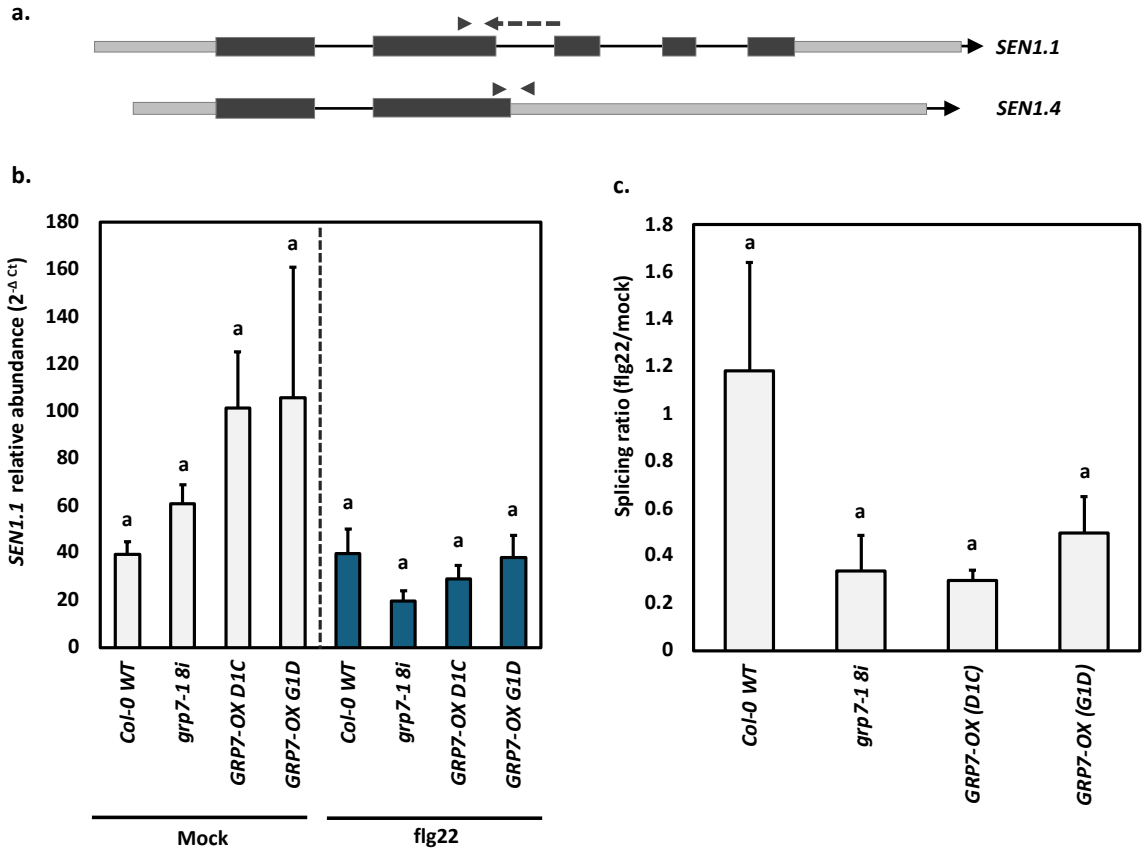

Figure 3. GRP7 does not appear to regulate the alternative splicing of *SEN1* mRNA following flg22 treatment. a) mRNA transcript models of canonical *SEN1.1* and intron-retained *SEN1.4* (Exons: black rectangle, Introns: line, 5'/3' untranslated region: grey rectangle). Primer binding sites are shown above each model. **b)** Relative abundance of *SEN1.1* normalised to *SEN1.4* following a 2-hour mock, or 1 µM flg22 treatment in each genotype. Expression levels calculated using the formula $2^{-\Delta Ct}$, where ΔCt = (Ct canonical − Ct intron-retained) (Harvey and Cheng, 2016). **c)** Effect of flg22 treatment on the splicing ratio of *SEN1.1* was calculated for each genotype using the formula $2^{-\Delta Ct\ (flg22)} / 2^{-\Delta Ct\ (Mock)}$. Error bars indicate mean ± SEM (n = 4). Statistical analysis was performed using a two-way ANOVA with Tukey's HSD (b), or one-way ANOVA with Tukey's HSD (c). Means not sharing the same letter are significantly different ($P < 0.05$).

To assess how GRP7 affects the AS of *SEN1* pre-mRNA during PTI, isoform-specific RT-qPCR primers were designed to amplify across or within the intron 2 splice junction that is regulated by GRP7 (figure 3a) (Lewinski, Steffen, *et al.*, 2024). The expression of the *SEN1.1* transcript normalised to *SEN1.4* slightly increased in the *grp7-1 8i* mutant in the mock condition and slightly decreased in the flg22 condition, whereas both GRP7-OX lines showed increases in the mock condition, but no change in the flg22 condition relative to Col-0 WT (figure 3b). However, these differences are not statistically significant – likely due to a high degree of variation between the four biological replicates potentially masking subtle changes in AS. Additionally, we did not detect any significant flg22-induced changes in the splicing ratio between each genotype, although the mutant and overexpression lines all showed a slight reduction relative to Col-0 WT (figure 3c). We were unable to test how GRP7 influences the AS of *CIPK3* due to issues designing qPCR primers that could specifically amplify alternative CIPK3 mRNA isoforms.

3.3.4 Validation of transient expression of candidate isoforms in *N. benthamiana*

The intron-retained isoforms of *CPK28*, *SEN1*, and *CIPK3* are predicted to encode truncated protein products. Based on protein domain annotations in Uniprot, these truncated protein isoforms lack enzymatic or regulatory domains that are important for the function of the canonical protein isoforms (figure 4a). For CPK28, the intron-retained isoform (*CPK28.4*) lacks two complete C-terminal EF-hand domains that mediate the Ca^{2+}-induced kinase activity of the N-terminal kinase domain, which significantly impedes its function as a negative regulator of PTI (Dressano *et al.*, 2020). In the case of SEN1 and CIPK3, the intron-retained isoforms (*SEN1.4* & *CIPK3.2*) lack enzymatic sulfurtransferase (Rhodanese) domain and a protein-protein interaction domain (NAF) respectively.

Therefore, we aimed to investigate the whether the function of these protein variants alters the PTI response to *Pto* DC3000. To this end, the sequence encoding each protein isoform (canonical and truncated) was cloned into an Agrobacterium expression vector to enable transient expression in *Nicotiana benthamiana*. To confirm that the *A. thaliana* isoforms of *CPK28*, *SEN1*, and *CIPK3* were expressed in agroinfiltrated leaf tissue, we performed RT-PCR using primer pairs that specifically amplify the cDNA derived from the *A. thaliana* transgene (figure 4b). We detected PCR products specifically in the leaf areas infiltrated with *Agrobacterium tumefaciens* GV3101 strains carrying expression constructs containing the isoforms of interest, but not in the empty vector control (EV). This demonstrates that the primers specifically amplify cDNA originating from the target *A. thaliana* transgene mRNA, and not due to off-target amplification of cDNA derived from *N. benthamiana*-

derived mRNA. Additionally, PCR products were only detected in +RT (reverse transcriptase) samples and not in the -RT samples (figure 4b), which indicates that the PCR products are generated reverse transcribed mRNA and not due to amplification of the transgene in the vector from DNA contamination. Together, these results indicate that we could successfully express each *A. thaliana* isoform of interest within the leaves of *N. benthamiana*.

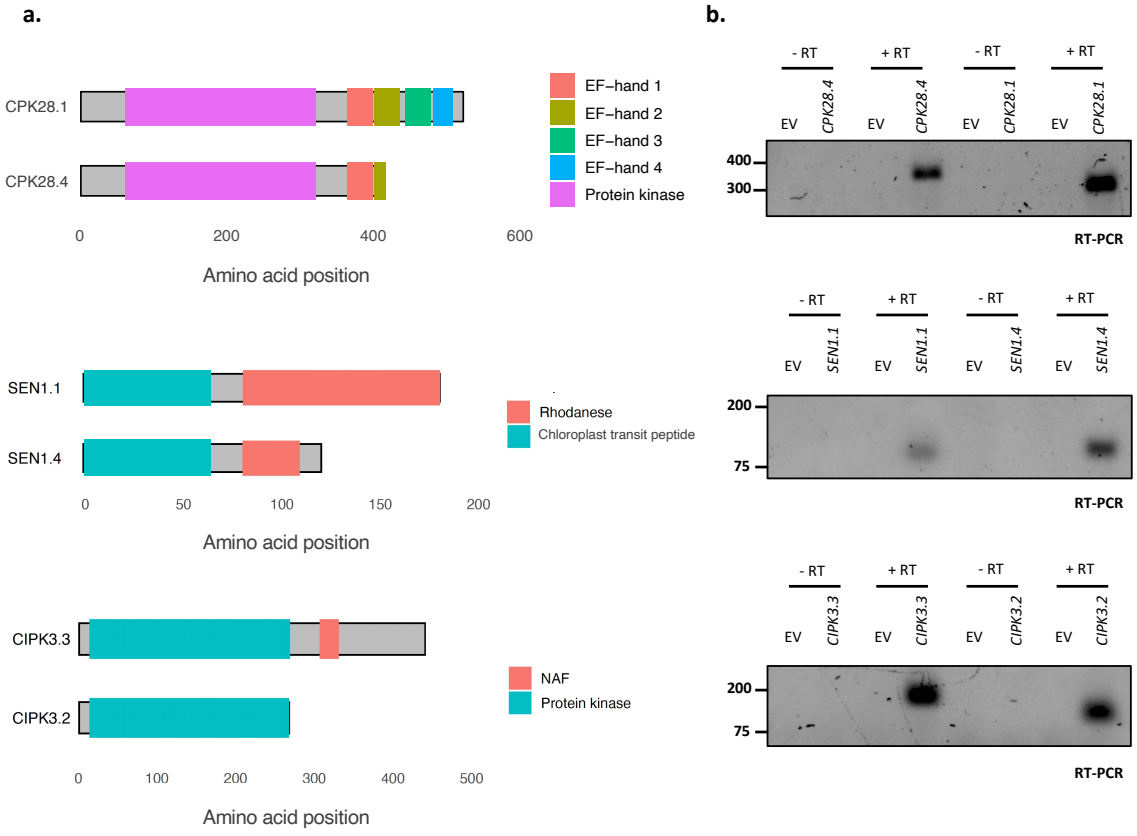

Figure 4. Transient expression of alternative isoforms in *N. benthamiana*. a) Domain structures of protein isoforms of CPK28, SEN1, and CIPK3 encoded by the canonical and intron-retained mRNA isoforms that were transiently expressed in *N. benthamiana* leaves via agroinfiltration. **b)** Transient expression of candidate gene isoforms in *N. benthamiana* leaf tissue at 2 days post-infiltration was validated via RT-PCR. Total RNA was extracted from leaf discs pooled from 5 biological replicates (individual plants) from leaf zones expressing the isoform of interest, or an empty vector (EV) control. RNA was reverse transcribed to cDNA (+RT) and were amplified for 30 cycles. RNA extracts without reverse transcription (-RT) were used as a negative control.

3.3.5 Alternative isoforms influence resistance to *P. syringae*

To determine if these predicted proteins have a quantitative impact on the disease resistance of host plants to *Pto* DC3000, the DNA sequences encoding the full-length and truncated protein isoforms were transiently expressed in *N. benthamiana* via agroinfiltration followed by subsequent infection with *Pto* DC3000 – this method is referred to as Agromonas (Buscaill *et al.*, 2021). Here, the original Agromonas protocol was adapted to use luminescence as a proxy for bacterial growth *in planta* by infecting the agroinfiltrated tissue with *Pto* DC3000 tagged with a lux operon. This technique will be referred to as Agromonas lux. To validate that Agromonas lux is sensitive to detect changes in pathogen resistance or susceptibility caused by the ectopic expression of alternative protein isoforms, CPK28 was used as a control as its ability to modulate the PTI response directly depends upon the relative abundance of the full-length and truncated isoforms (Dressano *et al.*, 2020). However, it is important to note that this response has not been shown in *N. benthamiana*. At three-days post infiltration, the normalised luminescence of leaf tissue expressing *CPK28.1* was found to be significantly higher than tissue expressing *CPK28.4* (figure 5b) ($P = 0.00082$). As CPK28.1 is a negative regulator of PTI, this finding indicated that the assay is sensitive to detect changes in pathogen susceptibility due to the ectopic expression of immunity regulators in an isoform-specific manner.

We subsequently tested the disease resistance phenotype of the full-length and truncated isoforms of *CIPK3* and *SEN1*. Leaves expressing the canonical isoform (*CIPK3.3*) displayed a subtle yet significant increase in luminescence relative to the intron-retained isoform (*CIPK3.2*) following infiltration with lux-tagged *Pto* DC3000 ($P = 0.0397$). This indicates that ectopic expression of *CIPK3.3* increases susceptibility to infection by *Pto* DC300. Transient expression of either *SEN1* isoform did not result in any significant changes in the susceptibility to Pto DC3000 in this heterologous system. Taken together, these results demonstrate that protein isoforms can play a critical role in regulating the immune response to *P. syringae*.

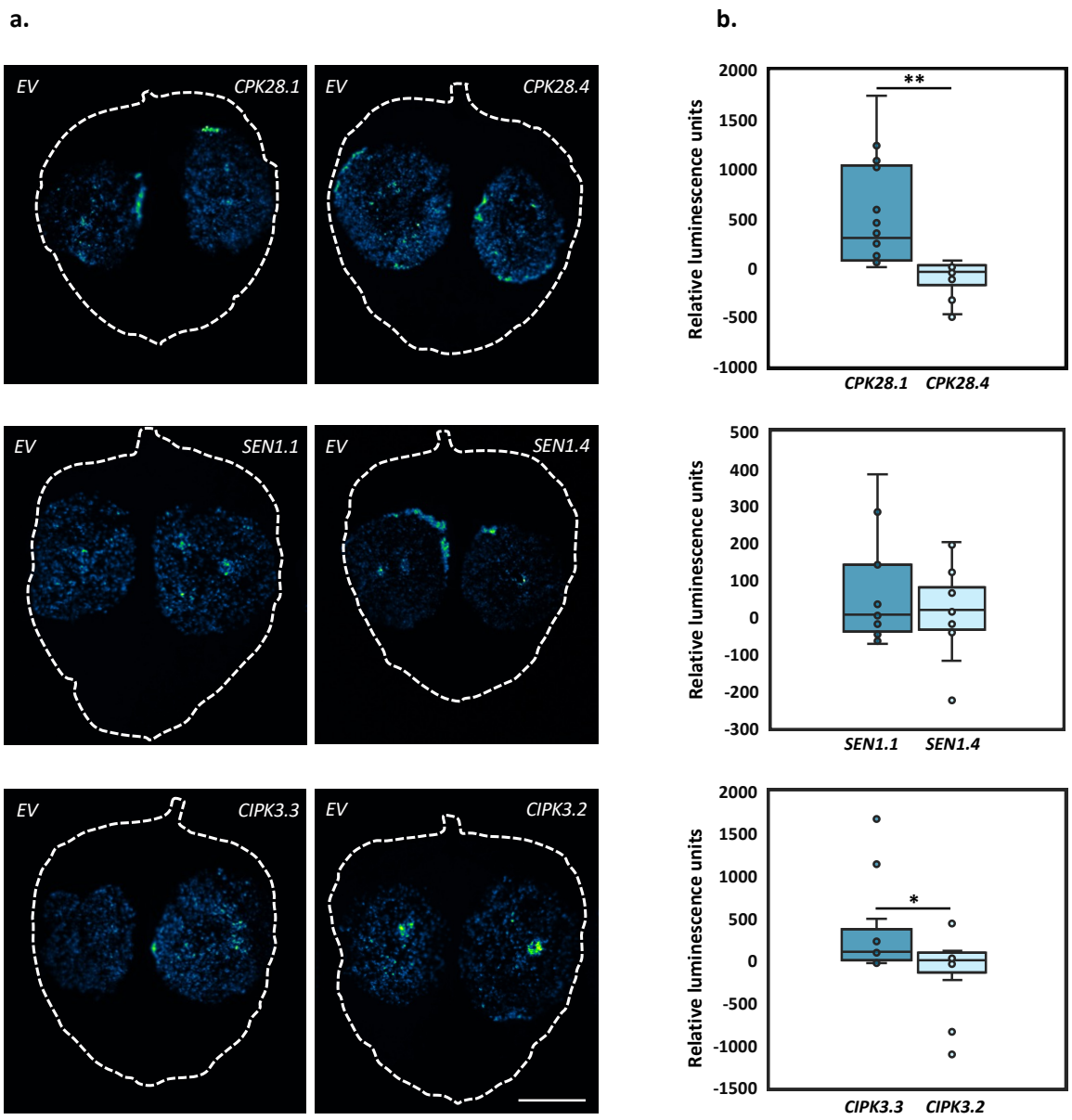

Figure 5. Truncated isoforms alter the resistance of *N. benthamiana* to *Pto* DC3000. a) Representative leaves of 4-week-old *N. benthamiana* transiently expressing the canonical isoforms (CPK28.4, CIPK3.3, SEN1.1) or intron-retained isoforms encoding putative truncated proteins (CPK28.4, CIPK3.2, SEN1.4) (right side of the leaf) or an empty vector (EV) control (left side of the leaf). Leaf tissue was infiltrated with *Pto* DC3000 ΔhopQ nptII::Lux and luminescence was recorded at 3 dpi. Scale bar = 2 cm. White dashed line outlines leaf edge. **b)** Luminescence was quantified from *n* = 13 biological replicates (individual plants), sampled across three independent experiments. For each biological replicate, 5 technical replicates were taken as luminescence measurements from five distinct 0.59 cm² zones within the agroinfiltrated area, avoiding the infiltration site and border regions. Technical replicates were averaged to yield a single value per biological replicate. Normalised luminescence was calculated by subtracting the mean relative luminescence units (RLU) of the corresponding EV control from that of the isoform of interest within each biological replicate. Data are presented as box plots showing the median and interquartile range (IQR) (25th to 75th percentiles). Dark blue: canonical isoform, light blue: truncated isoform. Significance was determined using a two-tailed Student's t-test. Asterisks indicate significance thresholds: **P* < 0.05; ***P* < 0.001.

3.3.6 *CPK28* isoforms differentially influence flg22-induced ROS burst

In order to understand whether canonical or intron-retained isoforms influence the activation of pattern-triggered immunity, we measured the apoplastic reactive oxygen species (ROS) burst in *N. benthamiana* leaves transiently expressing either canonical isoforms (*CPK28.1, CIPK3.3, SEN1.1*), intron-retained isoforms encoding truncated proteins (*CPK28.4, CIPK3.2, SEN1.4*), or an empty vector (EV) control. Leaf discs excised 72 hours post-infiltration were exposed to 500 nM flg22 or mock treatment, and luminescence was monitored as a proxy for ROS production over a 40-minute time course (figure 6a).

Expression of *CPK28.1* significantly suppressed the flg22-induced ROS burst relative to both the EV control and *CPK28.4*, which did not differ from EV (figure 6a, b). This result is consistent with the current model that canonical *CPK28.1 i*soform negatively regulates disease resistance to *Pto* DC3000 by suppressing early PTI responses (Monaghan *et al.*, 2014; Wang *et al.*, 2018). This finding also confirms that the Agromonas ROS assay is sensitive to quantity changes in the flg22-induced PTI response due to ectopic expression of alternative isoforms.

In contrast, *CIPK3.3* displayed a subtle, but non-significant reduction in ROS relative to *CIPK3.2* and EV, indicating that isoform switching of CIPK3 does not markedly alter ROS output under these conditions. This may suggest that the observed differences in disease resistance between *CIPK3* isoforms are likely not caused by early effects on PTI. For SEN1, both the canonical (*SEN1.1*) and intron-retained (*SEN1.4*) isoforms exhibited small increases in ROS production compared to EV; however, these differences were not statistically significant (figure 6b). Together, these results demonstrate that the *CPK28.1* isoform exerts a strong suppressive effect on the flg22-triggered ROS burst, whereas isoform variation in CIPK3 and SEN1 has no significant impact on early PTI-associated ROS accumulation. It is important to note that the data for this experiment represents six biological replicates processed in one experimental replicate and will therefore need to be repeated to confirm the findings presented in this section.

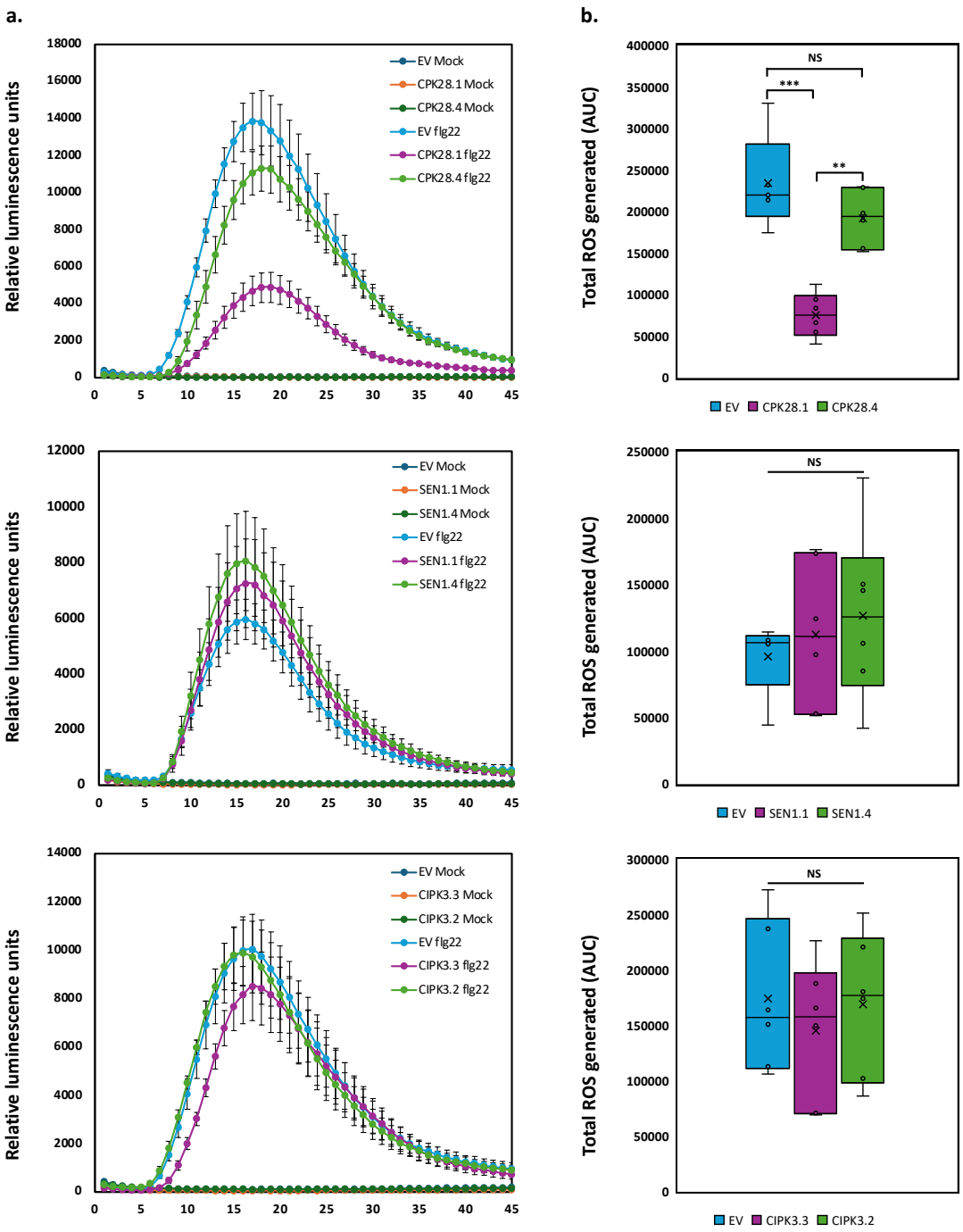

Figure 6. The effect of canonical and truncated protein isoforms on the PTI-associated reactive oxygen species (ROS) burst in the apoplast. a) PAMP-induced production of ROS in *N. benthamiana* leaf tissue transiently expressing either the full-length canonical isoforms (CPK28.1, CIPK3.3, SEN1.1) or intron-retained isoforms encoding putative truncated proteins (CPK28.4, CIPK3.2, SEN1.4) or an empty vector (EV) control at 72 hours post-infiltration, following mock treatment or exposure to 500 nM flg22. Luminescence was quantified from $n = 6$ biological replicates (individual plants). For each biological replicate, 4 technical replicates were taken as luminescence measurements from individual 4 mm discs taken from zones within the agroinfiltrated area. **b)** Quantification of total ROS generated in the flg22-treated samples calculated as the area under the curve (AUC). Data are presented as box plots showing the median and interquartile range (IQR) (25th to 75th percentiles. Significance was determined using a one-way ANOVA with Tukey's HSD. Asterisks indicate significance thresholds: $*P < 0.05$; $**P < 0.001$, $***P < 0.0001$.

3.3.7 Protein-protein interactions may be affected by truncated isoforms

Alterations to the domain architecture of a protein can have substantial consequences for its function, which may result from changes in the enzymatic activity of the protein or due to changes in its ability to interact with partner proteins (Louadi *et al.*, 2021). We hypothesise that relative changes in the accumulation of the truncated protein isoforms may impact host resistance to *Pto* DC3000 due to changes in their ability to interact with other proteins, which may affect the strength of the defence response.

To test this, AlphaFold Multimer (AFM) was used to model the interaction of CIPK3 and SEN1 with their respective protein interactors CALCINEURIN B-LIKE PROTEIN 9 (CBL9) and THIOREDOXIN Y1 (TRXY1) (Henne *et al.*, 2015; Sanyal *et al.*, 2017). This was performed using the peptide sequences of the canonical, full-length isoforms (CIPK3.3 and SEN1.1) and the truncated isoforms (CIPK3.4 and SEN1.4). In the case of the SEN1-TRXY1 interaction, the chloroplast transit sequences were omitted to improve the accuracy of the model as these sequences are cleaved from each protein following their import into the chloroplast (Sidorczuk *et al.*, 2023). For each model, AFM calculates a predicted template modelling (pTM) score and predicted template modelling score at the interface (ipTM), which provide insights into the model's confidence of the overall structure and the protein-protein interaction respectively. A combined, weighted score is used to evaluate the overall quality of the model, and thus the likelihood of the interaction being genuine (Evans *et al.*, 2022). pTM +ipTM scores greater than 0.75 are considered good quality models (Homma, Huang and Van Der Hoorn, 2023).

For CIPK3, the interaction of the full-length isoform with CBL9 had a higher pTM + ipTM score than the truncated isoform (figure 7a). In this model, a substantial portion of the interface between the two proteins includes the NAF domain of CIPK3.3, which is absent in CIPK3.2. This suggests that the presence of the NAF domain is required for a strong interaction of CIPK3.3 with CBL9. Interestingly, although TRXY1 has previously been confirmed to be an interactor of the canonical isoform of SEN1, AFM generated a model with a pTM +ipTM score of 0.3, markedly lower than the 0.75 confidence threshold. However, the model of the interaction of SEN1.4 with TRXY1 had a much higher score of 0.62 (figure 7b). This indicates that the truncated isoform of SEN1 may interact more strongly with TRXY1 than the full-length isoform within the chloroplast. Together, these findings demonstrate that truncated protein isoforms that are generated through alternative splicing may differentially interact with their protein partners.

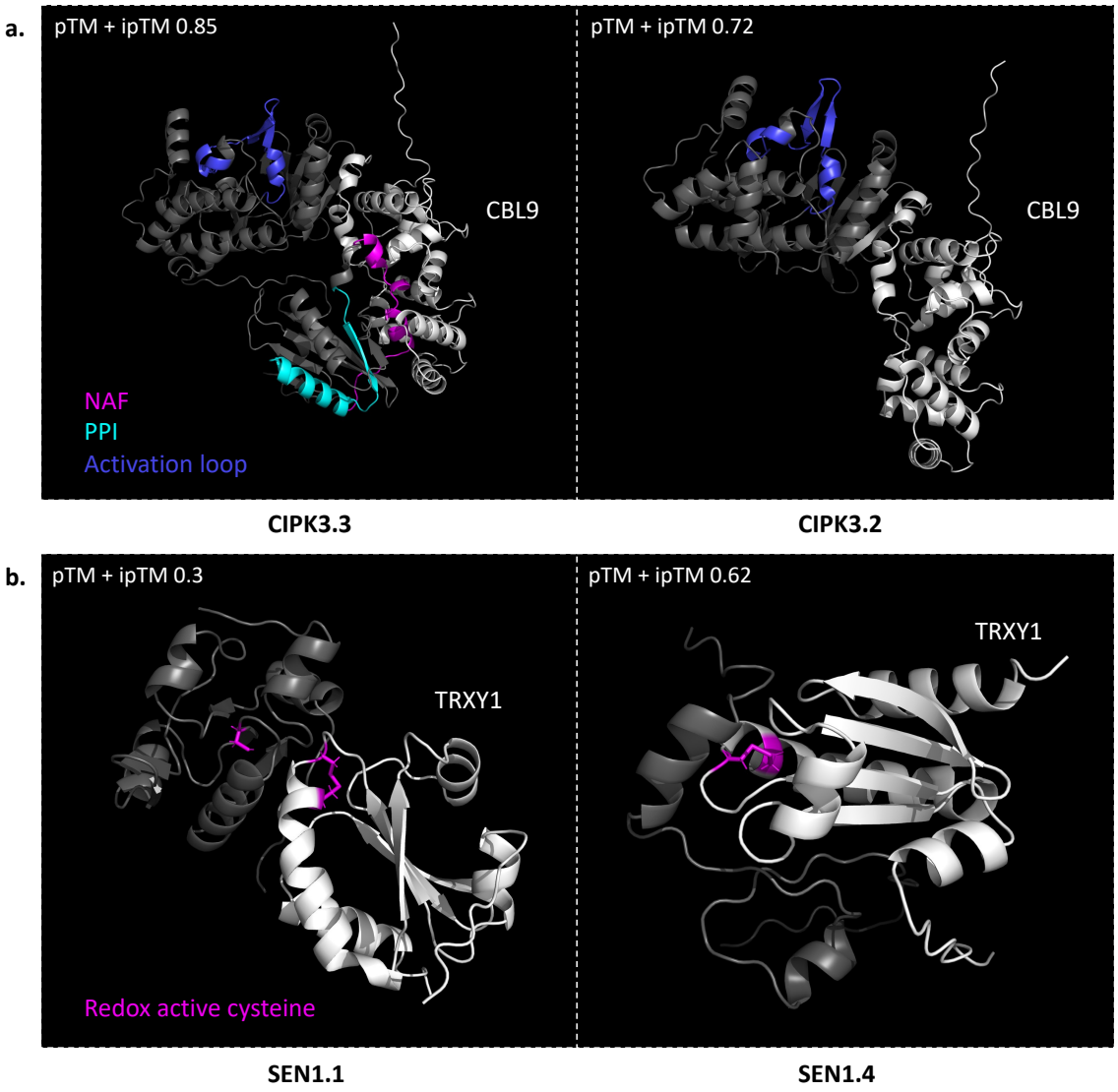

Figure 7. Full-length and truncated proteins are predicted to have different affinities for their protein partners. a) AlphaFold Multimer (AFM) model of the interaction of CIPK3.3 and CIPK3.2 (dark grey) with CBL9 (white). Key motifs include NAF in magenta, PPI (Protein-protein interaction) in cyan, and the kinase activation loop in blue. **b)** AFM model of the interaction of the chloroplast-localised proteins SEN1.1 and SEN1.4 (dark grey) with TRXY1 (white). Redox active cysteine residues are highlighted in magenta. For all models, the weighted total pTM + ipTM scores are displayed.

3.3.8 *SEN1* loss-of-function mutants do not have altered resistance to *Pto* DC3000

As experiments in this chapter were performed in a heterologous system, we aimed to determine whether loss of function of *CIPK3* and *SEN1* in *A. thaliana* would impact its resistance or susceptibility to *Pto* DC3000. However, we were only able to identify a T-DNA insertion mutant from the National Arabidopsis stock Centre (NASC) for *SEN1* (figure 8a). This line was confirmed to contain a homozygous T-DNA insertion within intron 1, which disrupted the production of *SEN1* mRNA (figure 8 b, c). Three-week-old seedlings were flood inoculated with *Pto* DC3000, and

bacterial growth *in planta* was determined at 0-, 2-, and 3-days post-inoculation (dpi). At each time point, we did not detect any significant changes in number of colony forming units (CFU) per gram of tissue. This indicates that *SEN1* does not play an important role in immune response of A. thaliana to *Pto* DC3000. It is important to note that the pathogen susceptibility assay was performed once and will require further replication to confirm this finding.

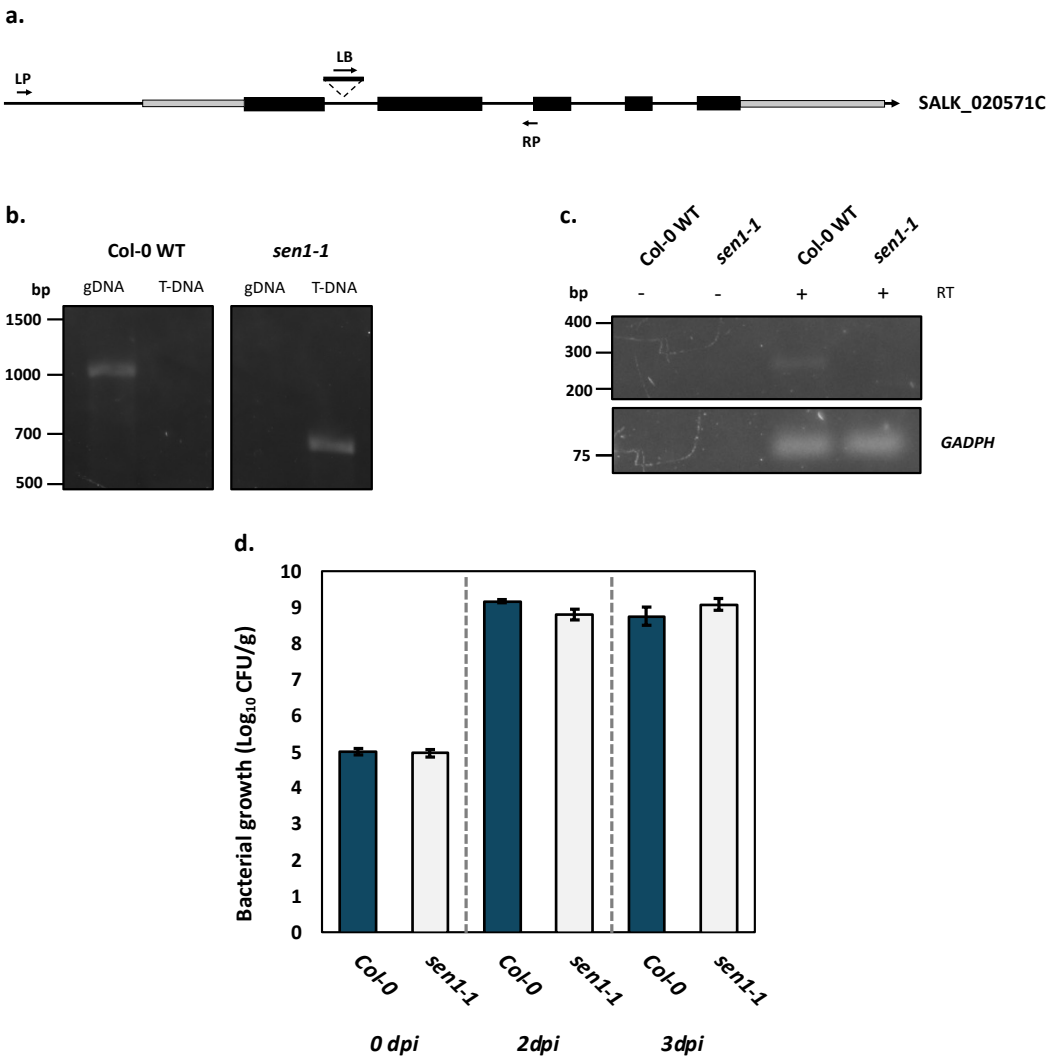

Figure 8. *SEN1* loss-of-function mutants do not display altered disease resistance to *Pto* DC3000. **a)** Locus map of the T-DNA insertion with respect to the representative isoform of *SEN1* SALK_020571C (*sen1-1*). **b)** Detection of homozygous T-DNA insertions for each mutant. Genomic DNA (gDNA) PCRs were performed with gene-specific forward and reverse primer (LP, RP). T-DNA PCRs performed using T-DNA left border (LB) primer and the corresponding gene-specific RP primer. **c)** RT-PCR detection of *SEN1* (AT4G35770) mRNA in the T-DNA insertion mutant compared to Col-0 WT. cDNA libraries were prepared from pooled RNA extracts from three seedlings. *GAPDH* was used as a positive control. **d)** *sen1-1* and Col-0 wildtype seedlings were flood inoculated with *Pto* DC3000 at an inoculum density of 4 x 10^6 CFU. Bacterial growth was quantified at 0-, 2-, and 3-days post inoculation (dpi). Error bars indicate mean ± SEM (n = 6). Two-tailed T-Tests were performed to assess statistical significance in mean CFU/g between the Col-0 WT and mutant at each time point. All biological replicates were from the same experimental replicate.

3.4 Discussion

It is now well established that co-transcriptional processing of RNA at the level of alternative splicing is an essential regulatory layer influencing plant responses to biotic stress (Martín *et al.*, 2021). The transcriptome undergoes extensive changes in alternative splicing in response to elicitors and during infection with pathogens (Bazin *et al.*, 2020). Furthermore, core components of the splicing machinery and accessory splicing factors are targets of pathogen virulence factors as a strategy to suppress host defences to aid pathogen proliferation (Nicaise *et al.*, 2013; Verma *et al.*, 2018; Huang *et al.*, 2020; Gui *et al.*, 2022). Despite this, the extent to which PTI-induced changes in alternative splicing influences the defence response is largely unknown, as relatively few studies have been conducted to investigate the functional consequences of differential alternative splicing events for many genes. Currently, many strategies for crop improvement involve manipulating the expression of canonical isoforms of gene products that influence the immune responses of plants. However, gaining a deeper insight into the relative contributions of specific isoforms may offer novel approaches to enhance the disease resistance characteristics of economically important crops.

As GRP7 has been linked to alternative spicing and plant immunity, we aimed to understand how its function as a regulator of alternative splicing contributes to its role in plant immunity. To this end, candidate genes were selected by overlapping the targets of GRP7 with existing datasets to identify genes that are likely to be regulated at the level of alternative splicing by GRP7 in the context of PTI. From this analysis we identified 42 high-priority candidates, ranging in function, whose AS may quantitatively impact the outcome of an infection.

For a subset of these candidate genes, isoform-specific RT-qPCR was used to quantify changes in the relative levels of specific mRNA isoforms in plant lines possessing elevated or reduced levels of GRP7, with and without flg22 treatment. Additionally, we set out to determine if any of the predicted truncated protein isoforms that result from alternative intron retention events have a functional impact on the immune response to *Pto* DC3000. From these analyses, we provide three main conclusions. First, GRP7 influences the AS of *CALCIUM-DEPENDENT PROTEIN KINASE 28* (*CPK28*) pre-mRNA in a PTI-dependent manner, in a direction consistent with amplification of early PTI outputs. Second, protein isoform identity has measurable consequences for bacterial growth in planta, as full-length CPK28 and CIPK3 protein isoforms enhanced disease susceptibility in our Agromonas lux assay. However, SEN1 isoform expression did not alter susceptibility under the conditions tested, and SEN1 loss-of-function similarly did not alter resistance to *Pto* DC3000 in *A.*

thaliana. Finally, among early PTI readouts, only CPK28 isoform status produced a strong change in the apoplastic ROS burst, pointing to gene and pathway-specific coupling between AS and signalling outputs.

3.4.1 GRP7 promotes a PTI-associated CPK28 splicing state that aligns with defence amplification

Our isoform-specific analyses indicate that, upon flg22 treatment, loss of functional GRP7 in the *grp7-1 8i* mutant shifts *CPK28* splicing towards the canonical *CPK28.1* isoform, whereas in GRP7-proficient contexts the balance favours intron 11 retention (*CPK28.4*) (Section 3.3.3). Because *CPK28.1* promotes BIK1 turnover and dampens PTI, while the intron-retained (IR) *CPK28.4* encodes a truncated kinase with impaired activity that relieves this negative regulation (Dressano *et al.*, 2020), our data support a model in which GRP7 biases *CPK28* mRNA processing towards the IR product during PTI, thereby sustaining early signalling (figure 5). This provides a mechanistic link between GRP7's positive role in immunity and its RNA-binding function and rationalises why disabling GRP7 via HopU1 would suppress PTI (Nicaise *et al.*, 2013).

Functionally, this model is corroborated by our heterologous assays, as ectopic expression of the canonical protein isoform encoded by *CPK28.1* increased *Pto* DC3000 growth relative to CPK28.4, and only CPK28.1 significantly suppressed the flg22-induced ROS burst (Sections 3.3.4–3.3.5). Together, these findings situate GRP7 upstream of a well-defined PTI node, where it can tune receptor-proximal signalling by modulating the fraction of CPK28 that is able to target BIK1 for degradation. Conceptually, this places GRP7 alongside other regulators such as IRR that enforce stress-responsive splicing switches at CPK28 (Dressano *et al.*, 2020), but with the distinction that GRP7's effect emerges specifically in the flg22 context as detected in our assay.

Two non-exclusive mechanisms could account for condition specificity. First, GRP7 binding sites on *CPK28* mRNA may be repositioned or differentially occupied upon PTI induction by flg22, consistent with the observation that the occupancy of GRP7, as defined by the number of adjacent reproducible binding sites, increases within the 3'UTR of *CPK28* following flg22 treatment (Section 3.3.1). Second, it is conceivable that PTI-associated post-translational modification of GRP7 (or of cofactors) could tune its RNA affinity or spliceosomal engagement to influence AS decisions, as is the case for stress-responsive AS mediated through the RALF1-FER-GRP7 module (Wang *et al.*, 2020). Dissecting these possibilities will require mapping of GRP7–RNA contacts across a PTI time course, and testing whether mutating candidate cis-elements around intron 11 re-sets the GRP7 dependence in splicing-reporter assays.

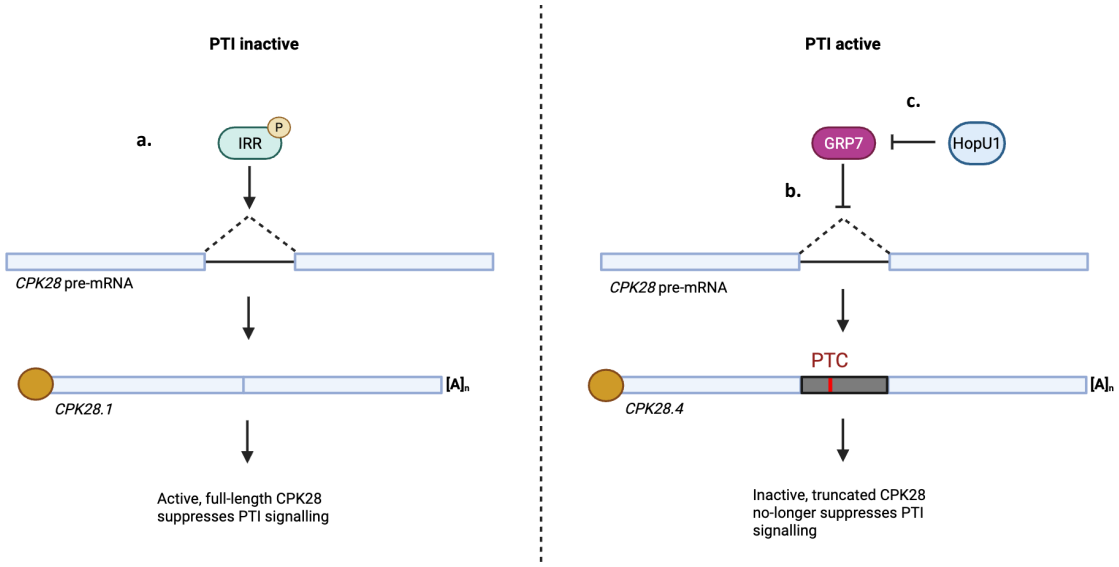

Figure 5. Proposed mechanism of HopU1-medidated interference of GRP7 function through CPK28. a) In a PTI inactive context, phosphorylated IMMUNOREGULATORY RNA-BINDING PROTEIN (IRR) associates with CPK28 pre-mRNA to promote the canonical splicing of intron 11 (thin black line) to produce *CPK28.1*, which encodes a negative regulator of PTI signalling (Dressano *et al.*, 2020). **b)** Under PTI active contexts, GRP7 supresses splicing, resulting in intron 11 inclusion to produce *CPK28.4*. Due to the inclusion of a premature termination codon (PTC), *CPK28.4* encodes a truncated protein isoform that no-longer suppresses PTI signalling. **c)** During an infection with virulent *Pto* DC3000, HopU1 ADP-ribosylates the RNA recognition motif of GRP7, which prevents GRP7 from interacting with RNA. This would bias AS towards the production of *CPK28.1*, which would suppress PTI signalling and enhance pathogen virulence. Schematic representation of RNA (blue boxes: exons; Black line: alternative intron; Grey box: PTC-containing retained intron). Yellow circle represents 5' 7-methylguanosine (m7G) cap.

3.4.2 Isoform identity matters for defence: Behaviours of CPK28 and CIPK3

Our Agromonas lux assays revealed that isoform choice can directly alter bacterial proliferation *in planta*. As expected from previous genetic studies, *CPK28.1* increased susceptibility to *Pto* DC3000 relative to *CPK28.4* (Monaghan *et al.*, 2014; Wang *et al.*, 2018), validating the sensitivity of our assay system (Section 3.3.4). Intriguingly, CIPK3 showed a similar trend as transient expression of the intron-retained isoform that encodes a truncated protein variant (*CIPK3.2*) in *N. benthamiana* conferred greater resistance than the canonical isoform (*CIPK3.3*), despite minimal effects on the early flg22-induced ROS burst (Section 3.3.5).

CBL-Interacting kinases (CIPKs) have a well-established role in responses to abiotic stresses such as drought due to their intimate connection to the ABA signalling pathway (Sanyal *et al.*, 2017). However, the function of CIPKs in plant immunity remains relatively uncharacterised. Calcium (Ca^{2+}) is an important secondary messenger in plant signalling pathways and is recognised by calcium-receptor proteins such as the CALCINEURIN B-LIKE PROTEINS (CBLs). When activated, CBLs interact

with their cognate CIPK protein(s), which phosphorylate downstream protein targets to transduce the signal (Mao *et al.*, 2016). *CIPK3* was selected for analysis in this study due to condition-specific changes in the binding sites of GRP7 to the *CIPK3* transcript between the mock and flg22 treatment conditions. These condition-specific binding sites were localised at an exon-intron boundary that corresponds to an alternative intron retention event that encodes a PTC and is regulated by flg22 treatment (Bazin *et al.*, 2020), which may indicate that GRP7 modulates this event in a PTI-responsive manner.

The altered disease resistance phenotypes that we observed between the two CIPK3 isoforms may be caused by changes in the domain structure of CIPK3. We created an AlphaFold Multimer (AFM) model of the interaction of the full-length and truncated CIPK3 protein isoforms that are encoded by the flg22-regulated *CIPK3* mRNA splice variants the cognate Ca^{2+} receptor CBL9 (Sanyal *et al.*, 2017). In our AFM model, CIPK3.3 was found to strongly interact with CBL9 via its NAF domain – a conserved 21 amino acid motif (named based on the presence of a conserved Asparagine, Alanine, Phenylalanine sequence) that mediates the interaction of CIPKs with their partner CBLs in a Ca^{2+}-dependent manner (Albrecht *et al.*, 2001). In contrast, CIPK3.2 was not predicted to form as stable of an interaction with CBL9 as it lacked the NAF domain, which could perturb downstream signalling events to enhance immunity to *Pto* DC3000.

Additionally, the NAF domain can function as an inhibitor of CIPK kinase activity, as described for an intron-rich homologue of *CIPK3* in *A. thaliana* called *CIPK24*. In the CIPK24 protein, the NAF domain obscures the activation loop of the kinase domain, resulting in an autoinhibited state. Binding of CBL4 in the presence of Ca^{2+} triggers a conformational change that exposes the activation loop, which becomes phosphorylated and can then phosphorylate its downstream targets (Mao *et al.*, 2016). Interestingly, in the AFM model of CIPK3.2, the activation loop is exposed indicating that this isoform may retain its functional kinase activity. Together, these findings suggest that PTI-induced production of the *CIPK3.2* isoform via AS may promote enhanced resistance to *Pto* DC3000 due to its reduced ability to interact with protein partners such as CBL9. Alternatively, the lack of a NAF domain in CIPK3.2 could alleviate its autoinhibition, which may impact downstream phosphorylation events. However, the precise underlying mechanism of this response remains unclear.

Previous studies of *CIPK3* and its close homologues have revealed an association of these signalling proteins with PAMP-triggered immune responses in plants. For example, phosphoproteomic analysis of a *cipk3/9/23/26* quadruple mutant revealed that many PTI-associated proteins were phosphorylated at higher levels than in the *A. thaliana* Col-0 wildtype including MPK6, MPK3 and RBOHD (Yin, Shi and Zhen, 2021). Conversely, phosphorylation of RPM1-INTERACTING PROTEIN4 (RIN4) was downregulated in the *cipk3/9/23/26* quadruple mutant, which is associated with increased resistance to *Pto* DC3000 (Lee *et al.*, 2015; Yin, Shi and Zhen, 2021). Interestingly, the *cipk3* single mutant progenitor possesses a T-DNA insertion in the 3' end of the gene that encodes the NAF domain (Tang *et al.*, 2015). This could mean that the *cipk3* allele could be a gain of function mutant as a protein product from this gene may lack a functional NAF domain and therefore could phenocopy the CIPK3.2 isoform. From this data, the contribution of CIPK3 to the phosphoregulation of immune signalling components remains unclear.

Further evidence specifically implicates the CIPK3-CBL9 signalling module in the regulation of Abscisic Acid (ABA) responses – a phytohormone that is involved in plant responses to abiotic and biotic stress. The active CBL9-CIPK3 complex phosphorylates ABSCISIC ACID REPRESSOR 1 (ABR1), a negative regulator of ABA-responsive gene expression, resulting in the de-repression of ABA-responses. Therefore, the switch between CIPK3 isoforms my help regulate the switch from pre-invasive to post-invasive immunity by regulating stomatal aperture through ABA signalling (Cao, Yoshioka and Desveaux, 2011), which could explain why there is no significant effect of either isoform on early PTI signalling processes such as the flg22-induced ROS burst.

3.4.3 SEN1 does not appear to contribute to defence response to *Pto* DC3000

In this chapter, *SEN1* was selected for further analysis as it has previously been found to be regulated at the level of alternative splicing in response to flg22 and in a GRP7 mutant background (Bazin *et al.*, 2020; Lewinski, Steffen, *et al.*, 2024). Furthermore, the transcription of *SEN1* is strongly induced at 24 hours-post infection with virulent *Pto* DC3000 and avirulent *P. syringae* pv. *tomato* strain 1065 that is dependent upon functional SA signalling, implicating SEN1 in the PTI response to this pathogen (Schenk *et al.*, 2005). From the iCLIP2 analysis of GRP7 binding, we found that the position of GRP7 binding sites changes within an intronic region of the *SEN1* transcript in the flg22 treatment condition relative to the mock condition, which corresponds with an alternative intron-retention event that contains a PTC.

This PTC-containing isoform, *SEN1.4,* is predicted to encode a truncated protein possessing an N-terminal chloroplast transit sequence and an incomplete Rhodanese domain; such domains catalyse the transfer of a sulphur atom from donor molecules to suitable acceptors – impacting cellular redox homeostasis and signalling (Henne *et al.*, 2015). As a marker gene of senescence, *SEN1* is intimately involved in this highly coordinated process of cellular degeneration (Oh *et al.*, 1996; Chung *et al.*, 1997). Senescence is a developmentally coordinated process of cell death that shares similarities to the hypersensitive cell death response (HR) that is induced during effector-triggered immunity, which limits the proliferation of biotrophic and hemibiotrophic pathogens. Both processes are underpinned by the accumulation of SA and ROS (Lee *et al.*, 2012; Yuan *et al.*, 2021; B. Zhang *et al.*, 2023), and share common transcriptional programmes as may senescence-associated transcription factors also co-regulate genes involved in plant immunity (Robatzek and Somssich, 2002). Furthermore, early senescing mutants display enhanced resistance to biotrophic and hemibiotrophic pathogens (Zhang *et al.*, 2020). Therefore, GRP7 may influence the alternative splicing of this *SEN1* in a flg22-responsive manner, which could impact the ratio of the canonical and truncated protein isoforms thereby impacting its enzymatic function in Redox and senescence pathways to influence pathogen defence.

Despite previous RNA-seq data that loss of GRP7 function causes an increase in the abundance of *SEN1* transcripts retaining intron 2 (Lewinski, Steffen, *et al.*, 2024), we were unable to definitively show that GRP7 affects the AS of the *SEN1* mRNA via our isoform-specific RT-qPCR experiments. We detected a high degree of variation between the samples in each genotype, which reduced the power of our statistical analyses – making inferring any solid conclusions from this data challenging. Several possible explanations could account for this variability. For example, spatial and temporal variations in both the expression of *GRP7* and *SEN1* between our experimental setup and the previous RNA-seq experiment could have shifted the window in which intron 2 retention is maximal, such that our sampling captured the trough rather than the peak of the response, thereby diminishing apparent effect sizes and inflating replicate-to-replicate variability in the qPCR. Also, as PTC-containing intron-retained transcripts can be subject to nuclear retention and NMD (Maquat, 2005); modest fluctuations in these pathways, combined with the low absolute abundance of the intron-retained isoform, could amplify stochastic noise in the Ct values – which could contribute to the high degree of variability in our data.

In our transient gene expression assays, expressing either the canonical *SEN1.1* or the intron-retained *SEN1.4* isoform did not measurably change *Pto* DC3000 growth or the early ROS burst in *N. benthamiana* (Sections 3.3.4–3.3.5). Given that SEN1 is predicted to regulate redox homeostasis in the chloroplast (Henne *et al.*, 2015; Moseler *et al.*, 2020), the heterologous expression context and timing of our experiment could mask isoform-specific effects. This may be because *A. thaliana* SEN1 cannot function due to its incompatibility within *N. benthamiana* chloroplast signalling pathways. Additionally, our expression constructs utilised a constitutive promoter, meaning that the dosage of the SEN1 protein may well exceeded its normal levels, which could interfere with its function.

The production of reactive Oxygen and reactive Nitrogen species (ROS, RNS) is a hallmark of plant defence responses to pathogens, directly impacting the proliferation of invading microorganisms and acting as important signalling molecules within the cell (Kuźniak and Kopczewski, 2020). For example, the PTI-induced generation of H_2O_2 in the chloroplasts of *A. thaliana* is required for full immunity to *Pto* DC3000, as this pathogen deploys effectors to actively suppress this response to aid host colonisation (De Torres Zabala *et al.*, 2015). Chloroplasts are major sites of PTI-associated ROS and Nitric Oxide (NO) production, which can affect protein function via post-translational modifications to redox-sensitive Cysteine residues, such as S-nitrosylation (SNO) and can have downstream impacts on nuclear gene expression (Nomura *et al.*, 2012). Interestingly, RBPs that differentially engaged with RNA were enriched in SNO sites following 2 hours of flg22 exposure in *A. thaliana*, suggesting that immunity-induced NO production may impact how RBPs interact with RNA (Bach-Pages, Chen, *et al.*, 2020).

Proteins that possess Rhodanese domains, such as SEN1, are referred to as sulfurtransferases (STRs). To date, 21 STRs have been identified in *A. thaliana*, suggesting that they are involved in a range of molecular pathways and may share functional redundancy between them (Moseler *et al.*, 2020). However, their function in plants remains poorly understood. SEN1, also known as STR15, can directly interact with a class of enzymes called thioredoxins (TRXs) that reverse cysteine oxidation on substrate proteins (Mata-Pérez and Spoel, 2019). Specifically, SEN1 was identified to bind to the thioredoxins TRXY1, TRXM1, TRXF1, and Lilium5 in the plastid of *A. thaliana* protoplasts via bimolecular fluorescence complementation; interactions that are dependent upon the presence of Redox-sensitive cysteine residues within active sites of the TRXs (Henne *et al.*, 2015). Therefore, we aimed to determine if the interaction of SEN1 with its partner TRXs is likely to be affected by the specific protein isoform of SEN1 that participates in the interaction.

TRXY1 was selected for an AFM screen as its X-ray crystal structure exists in the protein data bank. In our AFM model of the SEN1.1-TRXY1 interaction, the redox-sensitive cysteines of both partners were found to localise close to the interaction interface, which corroborates this previous finding that these residues are important in facilitating this interaction (Henne *et al.*, 2015). However, the best pTM + ipTM score obtained for this model was much lower than the 0.75 threshold that is expected of bonafide complexes. This could mean that this interaction is transient, or this complex may be stabilised by a third interactor that is absent in this model such as a substrate protein. Unexpectedly, we found that the predicted complex of the SEN1.4 and TRXY1 had a substantially higher pTM + ipTM score, suggesting that truncated isoform of SEN1 may have a higher affinity for TRXY1 than the full-length isoform. Furthermore, SEN1.4 bound TRXY1 within the vicinity of the redox-sensitive cysteine residues within its active site.

Finally, we tested whether loss of SEN1 function in *A. thaliana* had a bearing on the outcome of an infection with *Pto* DC3000 (Section 3.3.7). We did not detect any significant changes in the level of bacterial growth *in planta* between the *SEN1* loss-of-function allele (*sen1-1*) and Col-0 wildtype. Based on the data presented in this chapter, we conclude that SEN1 does not significantly contribute to the *A. thaliana* defence response to *Pto* DC3000 and likely does not play a role in early PTI-associated responses such as the flg22-induced ROS burst. However, it remains possible that GRP7-mediated changes in the AS of *SEN1* pre-mRNA may exert important effects on other physiological pathways, such as the circadian rhythm, as it has been demonstrated that the accumulation of *SEN1* mRNA fluctuates throughout the day-night cycle – peaking during the dark (Schenk *et al.*, 2005). As our pathogen infection assays were performed approximately 6 hours after lights on, future work should focus on characterising how loss of *SEN1* in *A. thaliana* affects *Pto* DC3000 infection in the subjective morning.

3.4.4 Study limitations and future directions

In this chapter, we aimed to characterise the role of GRP7 in the regulation of PTI-associated AS of its target genes. To this end, we utilised isoform-specific RT-qPCR to investigate how the alternative splicing patterns of a subset of GRP7 targets change in *A. thaliana* expressing elevated or reduced levels of functional GRP7. This required a selection process that utilised existing RNA-seq datasets to identify a subset of candidate genes to investigate experimentally. While this process successfully enabled the identification of 42 candidates, 3 of which were explored in-depth in this chapter, this process was limited by the fact that each dataset was generated using *A. thaliana* tissues of differing ages, and with different flg22 treatment durations. Using isoform-specific RT-

qPCR presented a challenge as this technique required a priori knowledge of the isoforms that are generated for each target gene, to ensure that the primer pairs only amplify the intended target isoform. Although a high-quality reference transcriptome is available for *A. thaliana* that was used to design our primer pairs, AtRTD2 does not contain RNA-seq data from GRP7 mutants and overexpression lines (R. Zhang *et al.*, 2017). In our primer melt-curve validation tests for *CIPK3*, we found that a single amplicon would be generated for the Col-0 wildtype control, but multiple amplicons were detected in either the GRP7 mutant and overexpression lines or in the flg22 treatment condition. This would render the primer pair unsuitable for our assays, which was a particular problem with the CIPK3 isoform assay.

For this experiment, the *grp7-1 8i* mutant was used. This line lacks the functional allele of *GRP7* and uses RNAi silencing of *GRP8* to restore its expression to wildtype levels. This is to account for the de-repression of GRP8 production in the *grp7* loss-of-function mutant. Previous studies have demonstrated that HopU1 ADP-ribosylates both GRP7 and GRP8 (Fu *et al.*, 2007). Therefore, use of a *grp7/grp8* double loss-of-function mutant may have been more suitable in this experiment to replicate the effect of *Pto* DC3000 infection. It is plausible that trends that we have observed in the isoform-specific RT-qPCR assays presented in this chapter may have been more pronounced in a double mutant line, as GRP8 may partially fulfil the role of GRP7 in our experiments. Going forward, a high read-depth RNA-seq experiment should be performed on cDNA libraries generated from Col-0 WT and a *grp7-1/grp8* double mutant with and without treatment with flg22. This will facilitate the detection of GRP7-regulated AS events on a global-scale and enable the characterisation of all 42 candidate genes presented in this chapter.

For the first time, we provide evidence that the AS-based tuning of CPK28 function to derepress PTI is regulated by GRP7 in a flg22-responsive manner. To verify that this regulation is a direct effect of GRP7 interacting with the *CPK28* transcript a reporter system, based on the luciferase splicing reporter assay established by Huang and colleagues could be used. A minimal genomic fragment encompassing the GRP7-responsive intron and flanking exonic sequence (CPK28 intron 11) can be cloned in-frame upstream of firefly luciferase (LUC) and expressed in *A. thaliana* protoplasts and potentially, also in stable lines. Exclusion of the intron restores the LUC open reading frame and yields luminescence upon luciferin addition, whereas intron retention introduces a premature termination codon upstream of LUC, suppressing the luminescence signal (Huang *et al.*, 2020). To establish direct causality, reporters harbouring wildtype sequence could be compared with constructs carrying nucleotide substitutions in candidate cis-elements located where GRP7 binds

as identified in our iCLIP2 data. Loss of the flg22-responsive shift in luminescence upon motif mutation would implicate those elements as functional GRP7 interfaces. Dependence on GRP7 can be tested by co-expressing GRP7, by assaying reporters in GRP7-deficient backgrounds, and by co-expressing HopU1 to acutely suppress endogenous GRP7 activity, followed by quantification of relative luminescence under mock versus flg22 treatment.

With regards to the Agromonas lux assay, the primary limitation is the heterologous context, as we tested the function of *A. thaliana* genes in *N. benthamiana*. It is possible that *CIPK3* and *SEN1* may contribute differently to defence against *Pto* DC3000. Moreover, both full-length and truncated isoforms were expressed from the constitutive *CaMV 35S* promoter, likely exceeding native *A. thaliana* levels and potentially obscuring isoform-specific effects. A central aim, therefore, was to test disease resistance in *A. thaliana* loss-of-function backgrounds. Although we screened T-DNA lines from NASC, no homozygous *cipk3* mutants were recovered. Therefore, a future priority is to generate *cipk3* knockouts and determine whether any enhanced susceptibility or resistance phenotype can be fully complemented by either the canonical or truncated *CIPK3* isoform. While we did successfully isolate a homozygous *sen1* mutant, we did not detect any differences in susceptibility to *Pto* DC3000 relative to wildtype. As noted above, *SEN1* expression appears to be circadian-regulated, rising overnight and declining into the morning, so repeating the infection assay in the subjective morning will be important to assess whether time-of-day masks *SEN1*-dependent phenotypes.

An additional consideration is that agroinfiltration can alter the defence status of leaf tissue and prime the immune system from subsequent infections (Rico *et al.*, 2010). This may underlie the higher luminescence observed at the periphery of infiltration zones, where defence activation can differ from naïve tissue. To minimise this confounding variable, we avoided perimeter regions during lux measurements and normalised all values to an empty-vector control processed in parallel.

Finally, we still do not know how *CIPK3* may function to regulate the disease resistance against *Pto* DC3000 in an isoform-specific manner, which will require further molecular characterisation. Further experiments could be performed using our current transient expression setup in *N. benthamiana*, by performing additional immunity assays using leaf tissue expressing a target isoform. This could include an elicitor or pathogen-induced quantification of callose deposition in the cell wall to test how CIPK3 isoforms influence later PTI responses (Bach-Pages and Preston,

2018). Elucidating the protein-protein interactions of the full-length and truncated CIPK3 isoforms with its respective signalling partner CBL9 would provide further evidence of the molecular function of these alternative isoforms (Henne *et al.*, 2015).

Collectively, our data show that GRP7 links PTI signals to alternative splicing at selected nodes, most clearly with respect to *CPK28*, thereby altering isoform pools to tune early defence outputs. Likewise, our data suggest that the isoform identity of *CIPK3* appears to influence susceptibility to *Pto* DC3000. Taken together with prior studies, these findings establish immunity-associated changes in AS, coordinated by RBPs, as a mechanistic determinant of pathogen resistance via altered protein structure and function, and they open a realistic path to test whether targeted manipulation of cis-elements and RBP activity can be used to enhance disease resistance in crops.

Chapter 4

ALY3 – an RNA binding protein that promotes susceptibility to *Pseudomonas syringae*

4.1 Introduction

As discussed in previous chapters, GRP7 plays a positive role in regulating PTI responses to the bacterial pathogen *Pseudomonas syringae* pv. *tomato* (*Pto*) DC3000 that is dependent upon its ability to interact with RNA (Fu *et al.*, 2007). This is evident from the fact that *Pto* DC3000 produces the HopU1 virulence effector, which ADP-ribosylates Arginine 49 within the RNA recognition motif of GRP7 to inhibit its RNA-binding activity. HopU1-mediated suppression of GRP7 is sufficient to suppress PTI, aiding pathogen proliferation (Jeong *et al.*, 2011; Nicaise *et al.*, 2013). GRP7 belongs to the heterogeneous nuclear ribonucleoprotein-like (hnRNP) class of splicing factors, and its ability to influence AS has been well established (Streitner *et al.*, 2012). Furthermore, the RNA binding activity of GRP7, and by extension its ability to influence AS, can be regulated by external stimuli to impact stress responses (Wang *et al.*, 2020). In the previous chapter, we have demonstrated that GRP7 may directly influence the alternative splicing of a subset of its substrate RNAs, namely *CPK28*. We also confirmed that specific isoforms of the *CPK28* mRNA encode proteins with functionally distinct roles in the defence response to *Pto* DC3000.

Beyond AS, RNA-binding proteins orchestrate every stage of RNA processing, which has significant impacts on gene expression (Prall, Sharma and Gregory, 2019). In addition to its well-established role in AS, GRP7 has been linked to the stress-responsive regulation of translation. For example, the phosphorylation state of the intrinsically disordered domain of GRP7 is regulated by the receptor-like kinase FERONIA in response to temperature stress, which triggers the liquid-liquid phase separation of GRP7 to form stress granules. This sequesters RNA and the translational components in a stalled state to rapidly alter cellular gene expression in response to stress (Xu *et al.*, 2024). Additionally, Nicaise and colleagues identified interactions between GRP7 and components of the translation machinery such as eIF4E and the ribosomal protein S14, and the strength of these interactions could be modulated by flg22 treatment to regulate PTI-responsive translation of *R*-genes such as *FLS2* (Nicaise *et al.*, 2013). Together, these findings suggest that GRP7 may regulate mRNA translation in a PTI-responsive manner to regulate the defence response to *Pto* DC3000.

Aims and rationale

In this chapter we selected an additional subset of genes from our candidate list in chapter 2, which are involved in a range of cellular processes that have the potential to be involved in the defence response to *Pto* DC3000. These represent genes whose transcripts may be regulated at the post-transcriptional level by GRP7 to influence plant immunity. We aimed to assess the contribution of these genes to the defence response by conducting infection assays using the T-DNA insertional mutants of each of the respective genes. For mutants that showed differential resistance to *Pto* DC3000, we performed further characterisation of the role of the gene in the immune response.

4.2 Materials and Methods

4.2.1 Plant growth conditions

Arabidopsis thaliana T-DNA insertion plant lines were requested from the National Arabidopsis Stock Centre (NASC). The gene and respective SALK/SAIL identification codes are summarised in (Appendix III. Supplementary table 1). *A. thaliana* seeds were surface sterilised via chlorine gas and sown on half strength MS (Murashige-Skoog; Duchefa) 0.8% phytoagar plates supplemented with 0.5 g/L MES and 0.5% sucrose. Seeds were stratified at 4°C for 48 hours then transferred to Percival incubators for 21-days and grown under 12-hour light/dark cycles at 20°C with a light intensity of approximately 100 µmol/m^{2}/s. After 1 week of growth, seedlings were thinned out to a density of 6 per plate. For experiments that required mature plants*, A. thaliana* was sown in soil and grown for up to 5 weeks in the same conditions as described above.

4.2.2 T-DNA mutant genotyping

Genomic DNA extractions were performed as according to the protocol by Chabi Sika and colleagues (Chabi Sika *et al.*, 2015). Briefly, for each T-DNA line, mature leaves of 16-22 soil-grown plants were extracted using a scalpel. Each sample was disrupted in 300 µL DNA extraction buffer in the TissueLyser II machine (Qiagen). Precipitated gDNA was re-suspended in sterile distilled water (Milli-Q). PCR reaction mixtures were prepared for each sample containing 12.5 µl GoTaq Green master mix (Promega), 10 µM Forward and reverse primer, 2 µL gDNA, up to 25 µL with PCR grade water. PCR was performed with the following conditions: 94°C (3 min); 34 cycles of 94°C (30 s), 60°C (30 s), 72°C (90s); final extension 72°C (10 min). Two reactions were run for each sample, using the gene-specific primers and with a gene-specific primer and the SALK primer to detect T-DNA inserts (Appendix III. Supplementary table 2). For RT-PCR detection of mRNA expression in each T-DNA insertion mutants, cDNA libraries were prepared from pooled RNA extracts from three seedlings as described in Chapter 3 (section 3.2.2). PCRs were set up as described above and run for 24 cycles. *GAPDH* was used as a positive control.

4.2.3 Pathogen infection assays

For the seedling infection assay, we closely followed the Arabidopsis seedling flood inoculation protocol developed by Ishiga and colleagues (Ishiga *et al.*, 2011). A single colony isolate of *P. syringae* pv. *tomato* strain DC3000 (*Pto* DC3000) was grown on LB agar plates for 24 hr at 28°C. Bacteria were harvested and suspended in Milli-Q water then adjusted to an optical density (OD_{600} nm) of 0.02, corresponding to approximately 4 x 10^{6} CFU (colony forming units)/mL, and Silwet L-

77 was added to a final concentration of 0.025%. MS agar plates containing 6, 3-week-old *A. thaliana* seedlings were fully submerged for 3 min in either the bacterial inoculum, or Milli-Q water containing 0.025% Silwet L-77 as a mock treatment. Seedling rosettes were cut from the agar plate and individually weighed in sterile 2 mL safe-lock Eppendorf tubes containing 2 x steel balls, then homogenised in 1 mL Milli-Q water using the TissueLyser II (Qiagen). Serial dilutions of each sample lysate were performed up to 10^{-8}, then 20 µL of each was plated on LB agar supplemented with Rifampicin (50 µg/ml). Plates were incubated at 28°C for 48 hr. Colony forming units (CFU) was recorded and bacterial growth *in planta* was calculated as CFU/g. Two-tailed T-Tests were performed to assess statistical significance at each time point.

Mature plant infection assays were performed as described by Yao and colleagues (Yao, Withers and He, 2013). 5-week-old *A. thaliana* plants were infiltrated into the abaxial side of the leaf with either *Pto* DC3000 WT or *Pto* DC3000 hrpA- at a density of $0D_{600}$ of 0.0002 corresponding to 1 x 10^5 cells using a needleless syringe. For each time point (0, 2, 3 dpi), four individual plants, each representing one biological replicate, two similar size leaves per plant were infiltrated with each bacterial strain. 2 hr after infiltration, leaves were detached from each plant in the 0-dpi group with a scalpel. One 9 mm leaf disc was extracted from each of the two leaves, then surface sterilised in 70% EtOH for 30 seconds, rinsed twice in Milli-Q water then left to air dry in a sterile laminar flow hood. Leaf discs were the homogenised in 1 mL Milli-Q water using the Tissuelyser II (Qiagen) at max speed for 2 minutes. Serial dilutions of each sample lysate were performed up to 10^{-8}, then 20 µL of each sample was plated on LB agar supplemented with Rifampicin (50 µg/ml). Plates were incubated at 28°C for 48 hr. Colony forming units (CFU) was recorded and bacterial growth *in planta* was calculated as CFU/cm^2. Two-tailed T-Tests were performed to assess statistical significance in mean bacterial growth between the Col-0 WT and the mutant at each time point.

4.2.4 Luminol-based detection of ROS

The quantification of PTI-associated ROS production was performed as previously described (Bach-Pages and Preston, 2018). 4 mm diameter leaf discs were extracted from two leaves of 4-week-old soil-grown *A. thaliana*, this was repeated twelve times for each genotype. Leaf discs were incubated in Milli-Q water overnight in a 96-well plate under constant light with continuous rotation. Luminol/peroxidase working solutions were prepared with and without 500 nM flg22 as described in the protocol. Each well was drained before adding the working solutions to each leaf disc. Luminescence was subsequently recorded for 91 minutes, with 1-minute intervals using the Tecan Infinite M200 plate reader.

4.2.5 MAPK phosphorylation assay

Elicitor-induced phosphorylation of MAPK was quantified via immunoblot as previously described (Chung and Sheen, 2017). Leaf discs extracted from 5-week-old *A. thaliana* Col-0 WT and *aly3-1* were submerged in 5 mL Milli-Q water overnight then subsequently spiked with flg22 to a final concentration of 1 µM for 15 minutes. Leaf tissue was immediately frozen in liquid N_2. Total protein was extracted from 60 mg powdered tissue by mixing with 240 µL protein extraction buffer on ice (Appendix III. Supplementary table 3), then centrifuged for 5 min at 11, 000 xG and 4°C to pellet debris. The protein concentrations of the supernatants were subsequently quantified using the Bradford assay (Thermo Scientific™) and normalised with protein extraction buffer. Protein extracts were mixed with protein loading buffer and heated to 95°C for 5 min, then run on 12% SDS PAGE gel. Protein was transferred to PVDF membrane by Western blot, followed by blocking in 5% BSA/TBS-T. Immunoblot was performed with #4370 antiphospho-p44/p42 MAPK (Erk1/2) (Cell Signalling Tech). Secondary antibody hybridisation was performed using Antirabbit-HRP. Chemiluminescence was subsequently recorded using Imagequant LAS 4000 (GE) following addition of the Clarity Western ECL Substrate (Bio-Rad). Chemiluminescence quantification was performed in Image J.

4.2.6 RT-qPCR quantification of *ALY3* gene expression

cDNA libraries prepared in chapter 3 (sections 3.2.2, 3.2.3) were used in this study to quantify the expression of *ALY3*. qPCR reactions were performed using the StepOnePlus Real-Time PCR system. Each reaction contained diluted cDNA (1:8), SyGreen mix Hi-ROX (PCR Biosystems), and transcript-specific primer pairs (Appendix III. Supplementary table 4). *ALY3* expression was normalised to the geometric mean of *PP2A* & *GAPDH*, relative fold changes were calculated using the comparative delta Ct method (Livak and Schmittgen, 2001).

4.2.7 RNA binding domain prediction

For predicting the amino acid residues within the ALY3 protein (Q94EH8) with RNA binding activity, we used the HybridRNAbind, model (F. Zhang *et al.*, 2023). We also used the AlphaFold 2 prediction of ALY3 as presented in the AlphaFold Protein Structure Database (Jumper *et al.*, 2021; Varadi *et al.*, 2022).

4.3 Results

4.3.1 Screening candidate genes for altered disease resistance

To determine if the candidate GRP7-rgulated genes function in the defence response to *Pto* DC3000, we performed a seedling-based flood inoculation screen of *A. thaliana* seedlings carrying T-DNA insertions within the candidate gene of interest (Ishiga *et al.*, 2017). We selected ten candidate GRP7-regulated genes from chapter 3 (Appendix III. Supplementary table 1), based on the interaction of GRP7 with the RNA transcript, and based on evidence in the literature that the gene or protein product undergoes differential expression in relation to biotic stress (Latrasse *et al.*, 2017; Bassal *et al.*, 2020). Seeds for these genetic lines were obtained from the National Arabidopsis Stock Centre (NASC), which were screened for the presence of homozygous T-DNA insertions within the target gene. From this pool of candidates, only two alleles for *ALLY of AML-1 and LEF-1 3/THO complex subunit 4C* (*ALY3*) were found to possess homozygous T-DNA insertions (figure 1b, e). *ALY3* encodes an RBP that forms a part of the transcription export complex (TREX), which designates mature nuclear mRNA for export to the cytoplasm (Pfaff *et al.*, 2018). We focused on *ALY3* as it is a group II candidate that we had previously identified in chapter 3. Additionally, we have evidence from ptRIC data that the RNA binding affinity of ALY3 changes between infection of *A. thaliana* with WT DC3000 and a mock treatment – indicating that ALY3 may be targeted by a *Pto* DC3000 virulence effector (Preston lab, unpublished).

To confirm that these homozygous T-DNA insertion lines were loss-of-function mutants, we performed an RT-PCR using pooled RNA extracts from each line and Col-0 wildtype The expression of the housekeeping gene *GLYCERALDEHYDE-3-PHOSPHATE DEHYDROGENASE C2* (*GAPDH*) was used as a positive control. *ALY3* mRNA was only detected in the cDNA libraries prepared from Col-0 wildtype and was absent in both *aly3* T-DNA alleles. As the T-DNA insertion is localised within an exon that is common to all transcript isoforms, this demonstrates that *aly3-1* and *aly3-2* do not encode a functional protein product.

Three-week-old seedlings were flood inoculated with *Pseudomonas syringae* pv. *tomato* DC3000 (*Pto* DC3000), and bacterial growth *in planta* was determined at 0, 2, and 3 dpi for the wildtype each *aly3* mutant line (figure 1 g, h). We found that bacterial growth was significantly reduced in the *aly3-1* line at 3 dpi relative to Col-0 wildtype, which suggests that *ALY3* may function as a susceptibility factor to *Pto* DC3000. However, for *aly3-2*, no significant changes in pathogen susceptibility were detected at 2, or 3 dpi.

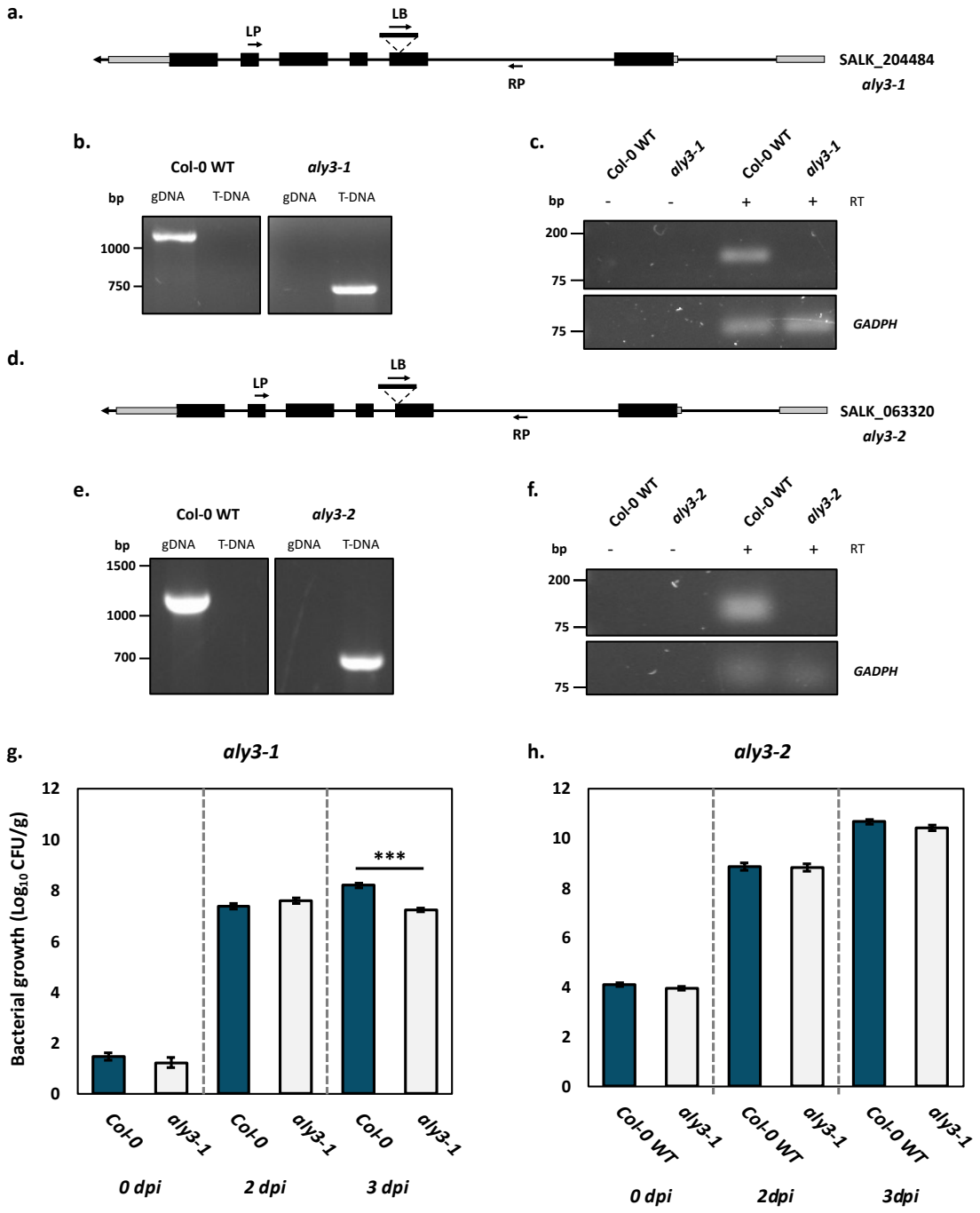

Figure 1. Screening candidate GRP7-regulated genes for altered disease resistance to *Pto* DC3000. **a, d)** Locus maps showing the site of T-DNA insertions with respect to the representative isoform of each ALY3: SALK_204484C (*aly3-1*); SALK_063320 (*aly3-2*). **b, e)** Detection of homozygous T-DNA insertions for each mutant. Genomic DNA (gDNA) PCRs were performed with gene-specific forward and reverse primer (LP, RP). T-DNA PCRs performed using T-DNA left border (LB) primer and the corresponding gene-specific RP primer. **c, f)** RT-PCR detection of *ALY3* (AT1G66260) mRNA in each T-DNA insertion mutants compared to Col-0 WT. cDNA libraries were prepared from pooled RNA extracts from three seedlings. *GAPDH* was used as a positive control. **g, h)** *aly3-1* and *aly3-2* mutants and Col-0 WT seedlings were flood inoculated with *Pto* DC3000 at an inoculum density of 4 x 10^6 CFU. Bacterial growth was quantified at 0-, 2-, and 3-days post inoculation (dpi). Error bars indicate mean ± SEM (n = 6). All biological replicates were from the same experimental replicate. Two-tailed T-Tests were performed to assess statistical significance in mean CFU/g between the Col-0 WT and mutant at each time point (***P < 0.001).

We noticed that the annotated T-DNA insertion site for both alleles mapped to the same locus in the genome (figure 1a, d). When checking for associated polymorphisms, we found that *aly3-2* had additional insertions annotated within protein-coding genes. These included an insertion within the promoter of AT1G33700, which encodes a GBA2-type glucosylceramidase that is hypothesised to function in sphingolipid catabolism and consequently in the acclimatisation to stress (Dai *et al.*, 2020). A second insertion was also annotated to be located within the CDS of AT3G29330, which is predicted to encode a zinc finger RNA-binding-like protein. Finally, there was an insertion within the intergenic region between the 3' UTR of AT1G65483 and AT1G65485. It is possible that these associated insertions in the *aly3-2* line could act epistatically on the enhanced disease resistance phenotype of the *ALY3* mutation. Therefore, the *aly3-2* allele was not used in further experiments.

4.3.2 *ALY3* promotes susceptibility to virulent and avirulent strains of *P. syringae*

After identifying the reduced susceptibility phenotype of the *aly3-1* mutant, we aimed to determine if mature *aly3-1* plants were also more resistant to infection by *P. syringae*. To this end, we performed a second infection assay in which the wildtype strain of *Pto* DC3000 or the type III secretion system-deficient *hrpA*- mutant were pressure infiltrated into the leaves. Similarly to the seedlings, mature *aly3-1* mutants displayed significantly reduced bacterial growth at 3 dpi (figure 2a, b), indicating that *ALY3* promotes susceptibility to both strains of *P. syringae*. Furthermore, the *aly3-1* mutant displayed slightly reduced visual symptoms of necrosis when infected with *Pto* DC3000 at 3 dpi (figure 2d). Together, these findings demonstrate the *ALY3* may play an important, yet undefined role in promoting susceptibility to *P. syringae*. However, additional replication of this experiment will be required to confirm these results.

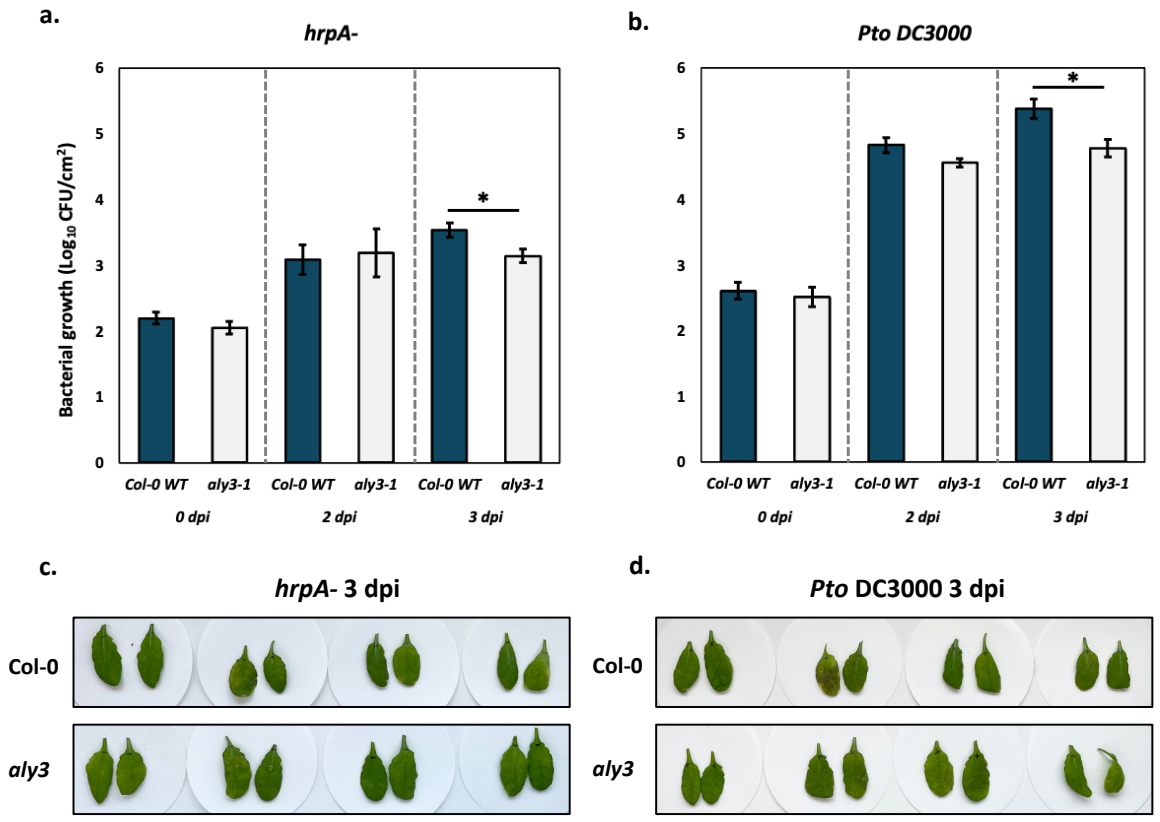

Figure 2. *ALY3* promotes susceptibility to *Pto* DC3000 in mature plants. a, b) Quantification of bacterial growth in 5-week-old *A. thaliana* Col-0 WT and *aly3-1* mutant following pressure infiltration with *P. syringae* DC3000 *hrpA*- and *Pto* DC3000 WT at a density of 1 x 10^5 colony forming units per mL (CUF/mL). Bacterial growth was determined at 0-, 2-, and 3-days post inoculation (dpi) Error bars indicate mean ± SEM (n = 4). All biological replicates were from the same experimental replicate. Two-tailed T-Tests were performed to assess statistical significance in mean CFU/g between the Col-0 WT and mutant at each time point (*P < 0.05). **c, d)** Leaf images from Col-0 WT and *aly3* mutant plants, infiltrated with *P. syringae* DC3000 *hrpA*- (c), and *Pto* DC3000 WT (d) at 3 dpi.

4.3.3 *ALY3* negatively regulates MAPK functioning

To gain a better understanding of which sector of the immune system that *ALY3* functions in, we performed two standard immunity assays, the luminol-based detection of reactive oxygen species (ROS) generation in the apoplast, and the immunoblot detection of elicitor-induced MAPK phosphorylation.

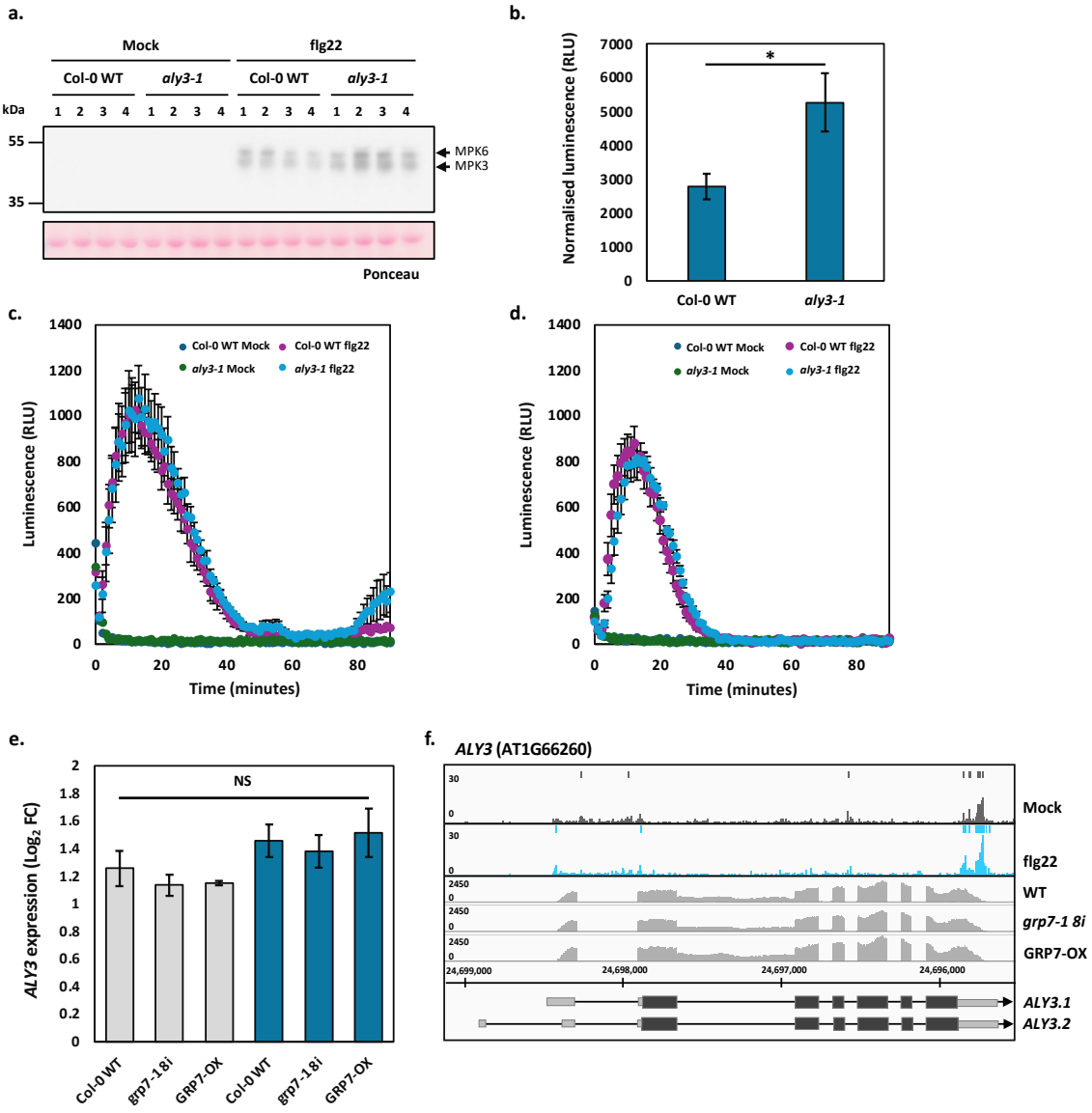

Figure 3. Molecular characterisation of *ALY3* function and regulation during a flg22-induced PTI response in *A. thaliana*. a) Detection of flg22-induced phosphorylation of MPK6 & MPK3. Leaf discs from *n* = 4 biological replicates were incubated overnight in water and treated with flg22 to a final concentration of 1 µM for 15 minutes. Phosphorylated MPK6/3 were detected by immunoblot using anti-phospho-p44/42 MAPK antibodies. **b)** Quantification of MPK6/3 phosphorylation by Image J following background subtraction. Data represent mean ± SEM (*n* = 4). Statistical significance was assessed using a two-tailed T-test (*P* = 0.039). **c, d)** flg22-induced reactive oxygen species (ROS) burst in 4-week-old *A. thaliana* Col-0 WT and *aly3-1* following 500 nM flg22 treatment. Luminescence was recorded from *n* = 6 biological replicates each. **e)** RT-qPCR analysis of *ALY3* gene expression in Col-0 WT, *grp7-1 8i*, and *GRP7-OC* (*D1C*) seedlings following a 2-hour

(Figure 3 continued) mock (grey) or 1 µM flg22 (blue) treatment. Ct values normalised to the geometric mean of *PP2A* and *GAPDH*. Relative fold-change calculated using $2^{-\Delta Ct}$ (Livak and Schmittgen, 2001). Data represent mean ± SEM (*n* = 3). Statistical analysis was performed using a two-way ANOVA with Tukey's HSD. **f)** iCLIP2 profile of GRP7 binding *ALY3* mRNA in mock and flg22 conditions. (y-axis = crosslink counts), with significant binding sites, indicated by block lines. RNA-seq coverage for Col-0 WT, *grp7-1 8i*, and *GRP7-OX* is shown below (Lewinski, Steffen, *et al.*, 2024).

It has previously been demonstrated that a paralogue of *ALY3*, *ALY4*, mediates the elicitor-induced generation of ROS during ETI responses in *A. thaliana* (Teng *et al.*, 2014). Therefore, we hypothesised that *ALY3* may function as a negative regulator of the elicitor-induced ROS burst. To test this, we used a chemiluminescence-based assay to track the flg22-induced generation of ROS over time in leaf tissue from Col-0 wildtype and *aly3-1* mutant plants (Bach-Pages and Preston, 2018). However, we detected no substantial differences in the flg22-induced ROS response between the *aly3-1* mutant and Col-0 wildtype (figure 3c, d), as both genotypes displayed a characteristic rapid rise in ROS generation between 0 and 20 minutes followed by a steady decline. This effect was observed in two independent experiments.

MAPKs play crucial roles in early PTI signalling and are rapidly phosphorylated following the recognition of pathogen elicitors by PRRs (Asai *et al.*, 2002). Therefore, we aimed to assess if the flg22-induced phosphorylation of MAPKs is compromised or enhanced in the *aly3-1* relative to Col-0 wildtype. We used an immunoblot to quantify the relative level of phosphorylated MAPKs in the *aly3-1* mutant following elicitation of PTI with flg22 (Chung and Sheen, 2017). After 15 minutes of flg22 treatment, the phosphorylation of two MAPKs that regulate PTI, MPK6 and MPK3 (Asai *et al.*, 2002), showed higher levels of phosphorylation in the *aly3-1* mutant (figure 3a). Subsequent quantification of chemiluminescence between the two genotypes confirmed a significant increase in MPK3 and MPK6 phosphorylation in the *aly3-1* mutant relative to Col-0 WT following flg22 exposure (figure 3b) (P = 0.039). These findings suggest that the *aly3-1* mutant has enhanced elicitor-induced MAPK signalling. However, it is important to note that this finding will need to be replicated with an independent loss-of-function allele.

4.3.4 GRP7 does not modulate the expression of *ALY3* mRNA

From the iCLI2P dataset we generated in chapter 2, we know that GRP7 interacts with the transcript of *ALY3*, with only subtle changes in the position of GRP7 binding sites between the mock and flg22 treatment conditions (figure 4f), (Appendix III, Supplementary figure S1). However, it is unclear how GRP7 would regulate the splicing of this transcript, as the annotated isoforms of *ALY3* only appear to differ in their 5' untranslated regions. As demonstrated in chapter 2, GRP7 preferentially binds

to the 3' UTRs of mRNA, which could indicate that GRP7 regulates processing reactions such as alternative polyadenylation, which can impact transcript stability. Therefore, we aimed to assess if the total expression level of *ALY3* mRNA is modulated by GRP7 following PTI induction. To this end, we used RT-qPCR to quantify the abundance of *ALY3* mRNA in mock or flg22-treated *grp7-1* 8i GRP7-OX, relative to Col-0 wildtype. We found that there was no significant change in the abundance of the *ALY3* RNA in the different genotypes (figure 3e). These results suggest that GRP7 does not play a direct role in modulating the stability and/or accumulation of the *ALY3* transcript.

4.3.5 Predicting the RNA binding regions of ALY3

Despite being predicted to bind to RNA, the structure of ALY3 and the presence of *bona fide* RNA binding domains have not been experimentally determined. Therefore, we used a sequence-based computational model, HybridRNAbind (F. Zhang *et al.*, 2023), to predict the RNA-binding residues (RBRs) within the ALY3 protein. This model was selected due to its ability to predict RBRs within structured and intrinsically disordered regions of proteins, which is critical for the accurate identification of RBRs within ALY3, as it is predicted to possess both highly structured and disordered domains by AlphaFold 2 (figure 4a). An RNA propensity score is assigned to each residue in the protein, which range between 0 – 1 (figure 4b). Propensity scores of 0.5 and above indicate that the residue is predicted to bind to RNA. This model correctly predicted RNA binding residues within the annotated RNA recognition motif (RRM) between residues 107 – 184, as annotated in the UniProt database. Additionally, the model also predicted RBRs within the N- and C-terminal disordered regions of ALY3. This analysis provides further evidence that ALY3 can bind to RNA, and that the intrinsically disordered regions of ALY3 may also play a crucial role in facilitating this.

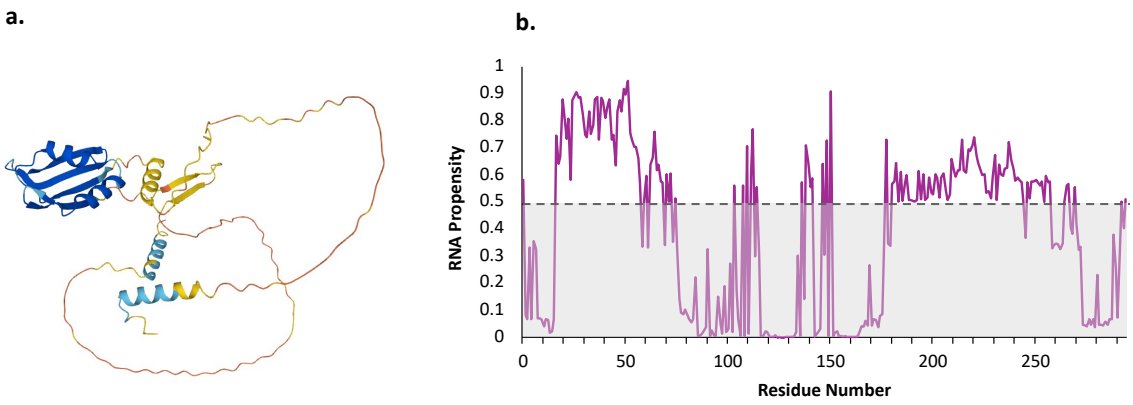

Figure 4. ALY3 predicted structure and RNA-binding residues. a) AlphaFold 2 structural prediction of ALY3. Regions with high per-residue confidence scores (pLDDT) are coloured blue, low scores are coloured yellow and orange. **b)** Per-residue prediction of RNA binding HybridRNAbind (F. Zhang *et al.*, 2023). Residues with an RNA propensity ≥ 0.5 are predicted to bind to RNA.

4.4 Discussion

Over the past decade, accumulating evidence has demonstrated that RNA binding proteins (RBPs) serve as master regulators of plant immunity through their roles in RNA processing and, consequently, gene expression (Woloshen, Huang and Li, 2011; Bach-Pages, Chen, *et al.*, 2020). In previous chapters, we explored the function of GRP7 in the immune response with respect to its activity as a regulator of alternative splicing. However, this function may also derive from the ability of GRP7 to regulate additional RNA processing events. For example, previous research has shown that GRP7 may influence the translation of essential immune system components such as the flg22 receptor-like kinase FLS2 in a PTI-responsive manner (Nicaise *et al.*, 2013). Therefore, additional candidate GRP7-regulated genes may also have as-of-yet unknown functions within the defence response to *Pto* DC3000. In this chapter we tested whether ALY3, an RBP that is associated with the transcription export complex (TREX), modulates defence against *Pto* DC3000. Our data demonstrates that loss of *ALY3* function reduces bacterial growth and suggest that *ALY3* constrains early MAPK activation without detectably altering the primary apoplastic ROS burst.

4.4.1 *ALY3* may promote susceptibility to *Pto* DC3000 by enhancing MAPK signalling

Loss of *ALY3* function in the *aly3-1* line reduced the level of bacterial growth *in planta* at three days post-infiltration, suggesting that *ALY3* may encodes a pathogen susceptibility factor. Such a phenotype may be caused by ALY3 being the target of a pathogen effector to support *Pto* DC3000 proliferation, or by loss of ALY3 resulting in enhancement of immunity-related processes. Consequently, loss-of-functional ALY3 would reduce the ability of the pathogen to colonise the host. Interestingly, host ALY proteins are coopted by viruses to facilitate viral RNA export from the nucleus, and thus act as susceptibility factors to viral infection. Quadruple loss-of-function of *ALY* genes has been demonstrated to increase the resistance of *A. thaliana* to Cauliflower Mosaic Virus (CaMV), as viral 35S RNAs could not be exported from the host nuclei. Specifically, *ALY1* and *ALY3*, in addition to *MOS11*, were required for viral RNA export (Kubina *et al.*, 2021).

However, in subsequent infection assays we detected reduced bacterial growth in *aly3-1* inoculated with either *Pto* DC3000 wildtype or *hrpA*-, which lacks secreted virulence effectors. Notably, visual symptoms were also slightly attenuated in *aly3-1* at 3 dpi when compared with Col-0 wildtype. These findings support a model in which *ALY3* negatively regulates basal defence rather than being a target of a type-3 secreted virulence effector.

Consistent with this interpretation, elicitor-induced phosphorylation of MPK3 and MPK6 was significantly higher in *aly3-1* relative to Col-0 wildtype within 15 minutes of exposure to flg22. MAPKs are understood to promote the immune response of plants, and are activated in the very initial phases of PTI through a sequence of upstream kinase phosphorylation events (Asai *et al.*, 2002). Therefore, we infer that ALY3 normally dampens MAPK signalling, such that its loss permits a stronger or more sustained early MAPK response that translates into reduced bacterial proliferation. It is unclear why the level of flg22-induced phosphorylation of MPK3 and MPK6 is enhanced in the *aly3-1* mutant. It is conceivable that ALY3 negatively regulates the nuclear export of *MPK3* and *MPK6* mRNA, and thus *ALY3* mutants have impaired MAPK activity. Alternatively, ALY3 may modulate the expression of other factors that control the phosphorylation status of MPK3 and MPK6. For example, ALY3 may promote the nuclear export and expression of *MAP KINASE PHOSPHATASE 1* (*MKP1*), which negatively regulates basal resistance to *Pto* DC3000 by dephosphorylating MPK6 (Anderson *et al.*, 2011). Therefore, loss of ALY3 function would result in an increase in MPK1 expression and consequently reduced levels of elicitor-induced phosphorylation of MPK6. Further experimentation will be required to evaluate these hypotheses.

It is important to note that in a previous replicate of this experiment, a slight, non-significant reduction in flg22-induced MAPK phosphorylation was observed in *aly3-1* relative to Col-0 WT. However, this data was not included in the final analysis due to the limited number of biological replicates (n = 2) and variability in loading control signal intensity across samples. Furthermore, repeat analysis of the same samples yielded inconsistent levels of MAPK phosphorylation in both genotypes, indicating reduced assay reliability. For these reasons, the dataset was excluded from this thesis.

Four *ALY* paralogues are encoded by the *A. thaliana* genome, which share partially redundant roles within the nuclear mRNA export pathway. They are all constituents of the transcription export complex (TREX), a multiprotein complex that is deposited on mature RNA that designates them for export from the nucleoplasm, thus performing a crucial role in regulating gene expression (Ehrnsberger, Grasser and Grasser, 2019). *ALYs* have been demonstrated to regulate stress-responsive gene expression in multiple plant species. For example, *ALY4* and its orthologue in *N. benthamina NbALY916*, share close homology to *ALY3*. Both ALY4 and NbALY916 mediate the expression of genes involved in ETI-associated defence responses to the Nep1 peptide – a putative virulence effector from the fungal pathogen *Magnaporthe oryzae* (Teng *et al.*, 2014; Fang, Peng and Fan, 2017). Mutations in either *ALY4* or *NbALY916*, impaired Nep1-induced defence responses,

which resulted in reduced stomatal closure, lower levels of hypersensitive cell death, and reduced ROS production. Accordingly, the expression of ROS generating genes such as *RbohD* was impaired in the *aly4* mutants. Interestingly, *aly4* mutants were significantly more sensitive to infection with *Pto* DC3000, and showed accelerated tissue necrosis (Teng *et al.*, 2014). This indicates that *ALY4* has a positive effect on pathogen-induced defence responses, which contrasts with the apparent negative role of *ALY3* in the defence response of *A. thaliana* that we have described. The relationship between the RNA export activity of *ALYs* and their role in immunity remains unclear but is most likely related to the altered expression of pathogen-responsive genes.

With regards to the regulation of *ALY3* expression by GRP7, we assessed the steady-state accumulation of *ALY3* mRNA in a GRP7 loss-of-function mutant and a GRP7 overexpression line treated with and without the elicitor peptide flg22. We found that GRP7 did not appear to have a significant effect on the accumulation of the *ALY3* transcript, which indicates that the interaction of GRP7 and the *ALY3* transcript does not affect its steady-state abundance. Future studies should quantify the relative abundance, localisation, protein-protein and protein-RNA interactions of ALY3 in different *GRP7* genetic backgrounds to explore if GRP7 affects the translation or function of *ALY3*.

4.4.2 Study limitations and future directions

We confirmed that both *aly3-1* and *aly3-2* carry homozygous T-DNA insertions and lack detectable *ALY3* mRNA, consistent with loss of ALY3 function. However, upon further investigation, *aly3-2* harbours additional insertion events; to avoid potential confounding effects, we did not pursue this allele further. Consequently, subsequent analyses in this chapter focus only on *aly3-1*. While the enhanced resistance phenotype observed is consistent with disruption of *ALY3*, definitive causality should be established by genetic complementation of *aly3-1* with a wild-type *ALY3* allele under the control of its native promoter and generating an independent, clean loss-of-function allele to repeat these experiments with.

Additionally, we could explore if the altered resistance to *Pto* DC3000 is dependent upon the RNA-binding activity of *ALY3*, by transforming the *aly3-1* mutant with an RNA binding-deficient allele of *aly3*. However, this may be challenging as, based on our HybridRNAbind model, large regions of the protein are predicted to mediate the interaction of ALY3 with its substrate RNAs including the intrinsically disordered regions. This corroborates previous findings that the disordered regions of ALY1 were required in addition to the RRM for full RNA-binding activity (Pfaff *et al.*, 2018). We could complement the *aly3-1* mutant with different alleles of *ALY3* lacking either the N- or C- terminal

intrinsically disordered regions or lacking the central RRM domain. If RNA binding is important for function, we would expect to see an intermediate disease resistance phenotype in these transformants relative to the full *aly3-1* mutant and Col-0 wildtype.

As discussed previously, we hypothesise that the increased resistance of the *aly3* mutant to infection by *P. syringae* may be caused in part by an increase in flg22-activated MPK3/MPK6 signalling. However, we have not demonstrated a causal link between the loss of *ALY3* and the observed increase in MAPK activity. Therefore, to validate this hypothesis, it will be important to demonstrate that ALY3 can modulate the expression of *MPK3* and *MPK6*, and to investigate if ALY3 is involved in regulating the nuclear export and/or stability of their mRNA. In the short-term, we could assay the change in *MPK3* and *MPK6* expression via RT-qPCR in the *aly3-1* mutant to determine if the increase in flg22-induced MAPK phosphorylation is due to higher expression of these genes. Furthermore, RNA-immunoprecipitation (RIP)-qPCR following UV crosslinking could be performed to detect a physical interaction between ALY3 and *MPK3/MPK6* mRNA (Mermaz, Liu and Song, 2018). This experiment would require an GFP-tagged ALY3 protein for the immunoprecipitation step, which could be sourced from Pfaff and colleagues as this line already exists (Pfaff *et al.*, 2018).

In the long term, omics-based approaches could be deployed to generate an in-depth understanding of the role of ALY3 in the context of the immune response in *A. thaliana*. For example, RNA-seq analysis could be performed to identify genes that display differential expression between the *aly3-1* mutant and Col-0 wildtype, with and without activating PTI via flg22 treatment. Additionally, we could assess the RNA interactome of ALY3 using iCLIP2 using the same experimental approach that we used for GRP7 in chapter 2 (Reichel *et al.*, 2024). Again, this procedure would require a GFP-tagged ALY3 *A. thaliana* line.

Finally, we did not identify a link between GRP7 and the stability of the *ALY3* transcript. Therefore, future studies should investigate if GRP7 can influence the translation of *ALY3*. This could be achieved by quantifying the accumulation of GFP-tagged ALY3 protein *in planta* in different GRP7 genetic backgrounds via an immunoblot. For example, we could perform a genetic cross between the ALY3-GFP (Pfaff *et al.*, 2018) and the *grp7-1 8i* mutant that we have used in this thesis (Staiger lab). This would enable us to evaluate the hypothesis that GRP7 negatively regulates the translation of ALY3 to promote resistance to *Pto* DC3000.

Together, the findings presented in this chapter demonstrate the *ALY3* represents an interesting gene for further characterisation of its role in the immune system of *A. thaliana*. For example, it would be particularly interesting to test if *ALY3* loss-of-function mutants show enhanced resistance to other pathogens such as fungi and oomycetes. As this gene appears to promote susceptibility to *Pto* DC3000, *ALY3* could potentially be a promising target for gene editing in crops to enhance their resistance to infection by *P. syringae*. However, this would first require the identification of functionally conserved orthologues in economically important species of crops.

Chapter 5

General Discussion

5.1 Overview

Land plants have evolved highly complex gene expression programmes to cope with biotic stress that are regulated at the transcriptional and post-transcriptional level (Aerts *et al.*, 2022). RNA binding proteins (RBPs) are master regulators of RNA processing that orchestrate all stages of mRNA maturation and thus have large effects on biotic stress-responsive gene expression (Staiger *et al.*, 2013; Lee and Kang, 2016). GRP7 has been linked to a multitude of physiological and stress responses in the model plant *A. thaliana* through its role as a regulator of alternative splicing and due to its function in mRNA translation (Staiger *et al.*, 2003; Streitner *et al.*, 2012; Wang *et al.*, 2020; Xu *et al.*, 2024). Its importance in the PTI response is highlighted by the fact that it is targeted by the *Pto* DC3000 virulence effector HopU1 to suppress immunity and therefore represents a key factor in the PTI response (Fu *et al.*, 2007). However, how GRP7 executes this function is currently unclear. Therefore, this thesis aimed to utilise cutting-edge techniques at the forefront of RNA biology to deepen our understanding of the role of GRP7 in the PTI response, and to further our understanding of how post-transcriptional processing of RNA influences the defence response to pathogens. In this chapter, I will summarise the key findings of this thesis and describe how this work could impact long-term goals to achieve durable disease resistance in crops.

5.2 Identification of the GRP7 interactome during PTI

GRP7 and its close paralogue GRP8 are unique among RBPs in *A. thaliana*, as they are the only known RBPs to be directly targeted by a virulence effector from *Pto* DC3000 to suppress immunity (Fu *et al.*, 2007). Specifically, this involves the inhibition of the RNA binding activity of GRP7 by the enzymatic addition of ADP ribose to the RNA recognition motif by the HopU1 effector (Jeong *et al.*, 2011). This demonstrates that GRP7 regulates RNA metabolic processes that are crucial in the immune response to this pathogen. Specific, targeted studies have investigated the interaction between GRP7 and the transcript encoding the immune receptor *FLS2* and determined that GRP7 may promote its translation at the cell surface to enhance PTI (Nicaise et al., 2013). However, prior to this work we did not know how the RNA interactome of GRP7 is influenced by eliciting PTI, and whether the interactions between GRP7 and its substrates had a quantitative impact on the defence response to *Pto* DC3000.

Individual nucleotide crosslinking and immunoprecipitation (iCLIP) is a laboratory technique that enables the global identification of the RNA substrates and specific interaction sites for an RBP of interest (Hafner *et al.*, 2021). The initial iCLIP version 1 methodology was first used in plants to identify the RNA targets of GRP7 in *A. thaliana* seedlings under normal physiological conditions (Meyer *et al.*, 2017). Since its publication, large improvements to the workflow to reduce sample loss have greatly increased the sensitivity of the technique, now referred to as iCLIP2 (Buchbender *et al.*, 2020; Lewinski, Brüggemann, *et al.*, 2024). Therefore, we aimed to use iCLIP2 to assess how the RNA interactome of GRP7 changes during a flg22-induced PTI response to improve our understanding of how GRP7 promotes immunity to *Pto* DC3000.

To the best of our knowledge, this is one of the first studies to investigate stress-responsive RNA interactome changes for any RBP in plants and thus provides a framework for studying how the RNA binding dynamics of other RBPs can be investigated during stress. In chapter 2, we found that GRP7 interacts with thousands of transcripts across both treatment groups, which is substantially more targets than were previously identified in the iCLIP1 analysis of GRP7 owing to the higher sensitivity of the iCLIP2 technique (Meyer *et al.*, 2017). GRP7 interacted with 718 unique RNAs in the flg22 treatment condition – primarily at the 3’ UTRs of transcripts. We speculate that this may indicate that GRP7 plays a role in regulating the translation of these RNAs, as 3’ UTR-interacting RBPs can regulate RNA stability or translation (Hardy and Balcerowicz, 2024). Furthermore, an increasing body of evidence demonstrates that dynamic remodelling of the translatome is an important factor underpinning gene expression changes during PTI (Son and Park, 2023). Therefore,

GRP7 may influence elicitor-responsive gene expression by regulating the translation of a subset of its target transcripts. Additionally, we determined that over half of the 718 flg22-specific RNA substrates of GRP7 were likely present in both the mock and flg22 treatment conditions, suggesting that GRP7 can selectively bind to RNA between treatment conditions (chapter 2). This is most likely caused by flg22-responsive post-translational modifications to GRP7 such as ubiquitination, which could alter its RNA binding activity or its interactions with partner RBPs. However, further studies will be required to evaluate this hypothesis.

The work presented in chapter 2 provides a strong foundation to fully understand the role of GRP7 in the PTI response to *Pto* DC3000 and sets out a novel methodology for researchers to explore how immune signals can be transduced into changes in the activity of RNA binding proteins. Future work should characterise how the proteome of *A. thaliana* is affected by GRP7 in response to flg22 treatment to identify genes whose expression, translation, or the domain architecture of the encoded protein is influenced by their interaction with GRP7. As a longer-term aim, researchers should explore adapting iCLIP2 to crops to investigate the role of GRP7 orthologues in such species. For example, *Solanum lycopersicum* and *Brassica rapa* both possess orthologues of GRP7 that contain the arginine residue that is targeted by HopU1. And both species are infected by pathovars of *P. syringae* that contain the HopU1 effector (Sarkar *et al.*, 2006), suggesting that a common virulence strategy exists in both species. This may enable the identification of new components of the PTI response to bacterial pathogens, which could facilitate the development of crops with enhanced disease resistance.

5.3 Alternative splicing as a mechanism to fine-tune PTI

Alternative splicing (AS) is a ubiquitous Eukaryotic RNA maturation event that predominantly occurs co-transcriptionally in plants, which increases the diversity of the proteome and regulates gene expression via downstream post-transcriptional events such as nonsense-mediated decay (NMD) (Kufel, Diachenko and Golisz, 2022). AS is ultimately controlled by the interaction of trans-acting splicing factors with cis-regulatory elements on pre-mRNA, and can be regulated in response to external cues such as the detection of pathogens (Meyer, Koester and Staiger, 2015).

GRP7 belongs to a class of hnRNP-like splicing factors and has been found to autoregulate the AS of its own transcript, and can affect global AS patterns in response to stress (Staiger *et al.*, 2003; Streitner *et al.*, 2012; Wang *et al.*, 2020). From our iCLIP2 dataset, we identified that common GRP7 targets in the mock and flg22 treatment groups had flg22-reponsive GRP7 binding sites predominantly within exons. As has been well established, the *A. thaliana* transcriptome undergoes dynamic remodelling at the level of transcription and AS, this suggested GRP7 may be involved in regulating PTI-responsive AS (Bazin *et al.*, 2020).

Intron retention (IR) is a common type of AS event in plants, which often results in the inclusion of a premature termination codon (PTC). This can influence gene expression by rendering the transcript susceptible to degradation by the NMD pathway, or results in its retention in the nucleus. However, the NMD pathway has been found to be downregulated during periods of stress, and mutations in NMD pathway regulators are associated with enhanced pathogen resistance. This implies that IR plays an important, and yet largely uncharacterised role in the pathogen defence response. Indeed, there are several examples of IR-containing splice variants that promote disease resistance to *Pto* DC3000. For example, RPS4 belongs to the Toll/interleukin-1 receptor (TIR) class of NLRs that triggers ETI upon the detection of the AvrRps4 effector produced by *Pto* DC3000. Interestingly, perception of AvrRps4 triggers a significant increase in the proportion of RPS4 transcripts possessing a retained intron (Zhang and Gassmann, 2007). Both the canonical splice variant, and isoforms containing retained introns are required for full resistance to *Pto* DC3000. Complementing the *rps4* mutant with intron-deficient *RPS4* does not restore pathogen resistance, suggesting that the protein products of the IR-containing isoforms have functional significance in the defence response (Zhang and Gassmann, 2003). Furthermore, the canonical splice variant of *CALCIUM-DEPENDENT KINASE 28* (*CPK28*) encodes a negative regulator of the flg22-induced PTI response. During PTI, an intron-retained transcript is dynamically generated via alternative splicing that encodes a truncated protein that functions as a positive regulator of the PTI response. This

PTI-associated switch in the AS of *CPK28* is directly regulated by an RNA-binding protein called IMMUNOREGULATORY RNA-BINDING PROTEIN (IRR) (Dressano *et al.*, 2020). Together, these studies demonstrate that immunity associated AS events can be directly regulated via the interaction of RBPs and pre-mRNA and do have a functional consequence for the pathogen defence response that depends on the protein products encoded by intron-retained transcripts.

In our iCLIP2 dataset, we found that many of the flg22-assoicated target transcripts of GRP7, including *CPK28*, *CBL-INTERACTING KINASE 3* (*CIPK3*)*, SENESCENCE-ASSOCIATED GENE 1* (*SEN1*), have previously been identified to undergo biotic stress-induced changes in AS. A key finding of this thesis is that *CPK28* is regulated at the level of AS by GRP7 in a flg22-dependent manner. Crucially, this provides the first clear linkage between the function of GRP7 as a regulator of AS and the *A. thaliana* defence response to *Pto* DC3000.

For *CIPK3* and *SEN1*, we identified condition-specific changes in the location of reproducible GRP7 binding sites within regions adjacent to alternative IR events. In the *A. thaliana* reference transcriptome, this differential IR created two populations of transcripts that are predicted to encode either full-length or truncated protein products due to the inclusion of PTCs within the retained introns. In chapter 3, we demonstrated that the CIPK3 isoforms contribute differently to resistance against *Pto* DC3000 when transiently expressed in *N. benthamiana*, which we hypothesise reflects changes in domain architecture that alter interactions with downstream partners, such as CBL9, and thereby altering cell signalling cascades. Whether GRP7 enforces this CIPK3 isoform switch via PTI-responsive AS remains an open question, requiring splicing reporter assays and endogenous genetic tests in *A. thaliana*. In contrast, the effects of *SEN1* on pathogen resistance were not detectable under our conditions, and despite prior evidence of GRP7 affecting IR in *SEN1*, we did not detect any significant effects in our isoform-specific RT-qPCR assay. As discussed in chapter 3, further work is needed to clarify the mechanisms that underpin the altered disease resistance phenotypes that we have observed. Specifically, researchers will need to study in further detail the function and regulation of *CIPK3* in *A. thaliana*, which due to timing constraints, was not completed in this thesis.

Transcriptome remodelling at the level of AS is a well-documented phenomenon that occurs in response to stress, with IR representing the most common form of AS event in plants (Martín *et al.*, 2021). However, the functional consequences of specific instances of IR remain poorly understood, particularly in the context of the immune response to pathogens. The findings in this thesis support

previous reports that the translation of intron-retained transcripts generates truncated protein variants with altered functionality to impact the defence response to pathogens (Zhang and Gassmann, 2003, 2007; Dressano *et al.*, 2020; Gui *et al.*, 2022). This represents a largely unexplored area for future study, which could be exploited to provide novel strategies to engineer enhanced disease resistance into crops. Gene editing technologies could be deployed to abolish or enhance a splice site to promote the production of a splice variant that enhances immunity to a pathogen. For example, targeted edits could be made to *CIPK3* to abolish 5' splice site of intron 8, which could lead to the enhanced production of the intron retained variant that promotes increased resistance to *Pto* DC3000.

5.4 RNA binding proteins as targets for crop improvement

Plant pathogens pose a significant threat to global food security, which is severely exasperated by climate change. Fluctuations in temperature, precipitation, and atmospheric CO_2 levels affect pathogen-host interactions and can cause changes in the geographic range of a pathogen (Singh *et al.*, 2023). Therefore, there is an urgent need to develop new technologies and strategies to sustainably combat plant diseases to ensure crop yields can continue to meet demand. Genes encoding RBPs could represent promising targets for enhancing the disease resistance of crops, due to their capacity to influence the regulation of stress-responsive gene expression at the post-transcriptional level. Recently, Bach-Pages and colleagues demonstrated that RBPs in *A. thaliana* differentially engage with RNA during a flg22-induced PTI response. Phenotyping of some of the flg22-responsive RBPs including canonical RBPs such as RNA HELICASE 11 (RH11) and non-canonical RBPs such as S-ADENOSYLMETHIONINE SYNTHASE 4 (METK4), revealed mutants in both genes display increased susceptibility to infection by *Pto* DC3000 (Bach-Pages, Chen, *et al.*, 2020). This demonstrates that RBPs represent an untapped resource for gene editing to create disease resistant crops.

In chapter 4, we screened additional candidate GRP7-regulated genes to identify candidates that influence the resistance of *A. thaliana* to *Pto* DC3000. We identified *ALY3* as a novel factor that appears to be involved in the normal function of the PTI system, as a loss-of-function *ALY3* mutant was found to be less susceptible to infection by wildtype and a type 3 secreted effector-deficient strain of *Pto* DC3000. As mentioned in chapter 4, this finding must be validated by further experiment replication and through phenotyping an additional loss-of-function allele and a functional complementation line. ALY3 is an RBP that regulates mRNA export from the nucleus as it is a component of the THO/TREX complex. We found that the magnitude of the flg22-induced

MAPK response was enhanced in the *aly3-1* mutant, suggesting that ALY3 represses MAPK signalling, which may cause the enhanced disease resistance phenotype that we observed. We hypothesise that this may be caused by a reduction in the expression of MPK3 and MPK6, as ALY3 may promote its export from the nucleus. Therefore, *ALY3* could represent a promising target for engineering enhanced resistance to *Pto* DC3000 in crops. However, this would first require the identification of orthologues, and an understanding of their functional conservation in crops.

GRP7 and its orthologues have been shown to be important factors of the immune response to diverse pathogens and represent a possible target for crop improvement. In this thesis, we have demonstrated that the RNA interactome of GRP7 substantially changes during the PTI response, with the flg22-associated targets of GRP7 significantly enriched in transcripts involved in the biotic stress response. Going forward, researchers should explore how PTI-induced changes in the *A. thaliana* proteome and transcriptome are disrupted in a *GRP7* loss-of-function mutant. Comparing which transcripts and proteins are affected by the expression of *GRP7* with the flg22-associated targets of GRP7 that we have identified in this thesis will enable the global identification candidates that are post-transcriptionally regulated by GRP7.

Furthermore, our phylogenetic analysis in Chapter 2 shows that GRP7 is widely conserved across monocots and dicots, with Brassicaceae orthologues clustering with *A. thaliana* GRP7, and all retained the characteristic RNP1 motif within the RRM. Notably, nine of ten GRP7 orthologues from crop hosts of HopU1-positive *P. syringae* strains (including those that host *Pto* DC3000) all possess a conserved arginine 49 residue sequence with *A. thaliana* that is ADP-ribosylated by HopU1, implying that HopU1-directed suppression may occur via the same mechanism as has been identified in *A. thaliana* (Jeong *et al.*, 2011). Intriguingly, we found that *Brassica oleracea* var. *oleracea* harbours natural substitutions in RNP1, R49K and N41I, suggesting that HopU1 evasion may be achievable without abolishing RNA binding. Coupled with our finding that GRP7 regulates *CPK28* splicing in a flg22-dependent manner (Chapter 3), these observations point to actionable routes to enhance resistance to *Pto* DC3000 through allele mining and precision editing. For example, targeted editing of R49 and N41 guided by naturally occurring variants to create HopU1-resistant, yet RNA-binding-competent GRP7, and functional validation of edited alleles using splicing reporter assays alongside disease assays in relevant crop backgrounds. If successful, such edits would preserve GRP7's pro-immune AS functions while evading effector interference, providing a tractable strategy to bolster crop immunity.

5.5 Conclusions

In summary, the work presented in this thesis provides a novel insight into the function of RBPs during the *A. thaliana* immune response to the bacterial pathogen *Pseudomonas syringae* pv. *tomato* DC3000. This work also adds to the growing body of evidence that plant RBPs represent promising targets for engineering durable disease resistance in crops to a range of pathogenic microorganisms. From this thesis we can draw the following conclusions about the role of GRP7 in PAMP-triggered immunity:

- The RBP GRP7 interacts with thousands of transcripts during a flg22-induced PTI response, with a significant enrichment in transcripts encoding factors relating to the biotic stress response and protein kinase signalling.
- Many of the flg22-associated targets of GRP7 have previously been reported to undergo changes in alternative splicing following biotic stress exposure.
- GRP7 influences the AS of *CALCIUM-DEPENDENT PROTEIN KINASE 28* (*CPK28*) pre-mRNA in a PTI-dependent manner, in a direction consistent with amplification of early PTI outputs.
- Protein isoform identity can have measurable impacts on the defence response to *P. syringae* pv. *tomato* DC3000.
- Mutants in the RNA export factor of *ALY3* display increased resistance to infection by *P. syringae* pv. *tomato* DC3000, which could be linked to the reduced activity of MPK3.
- RBPs such as GRP7 and ALY3 represent promising candidates for improving the disease resistance characteristics of crops.

Appendices

Appendix I – supplementary data for chapter 2

Appendix II – supplementary data for chapter 3

Appendix III – supplementary data for chapter 4

Appendix IV – statement of collaborative contributions

Appendix I.

Supplementary Table 1. List of RT-qPCR primers used to validate PTI-activation in flg22-treated seedlings.

Gene		Forward	Reverse
AT1G80840	*WRKY40*	GATCCACCGACAAGTGCTTT	AGGGCTGATTTGATCCCTCT
AT3G26830	*PAD3*	ACGAGCATCTTAAGCCTGGA	TCGGTCATTCCCCATAGTGT
AT3G23240	*ERF1*	TCGGCGATTCTCAATTTTTC	ACAACCGGAGAACAACCATC
AT4G01250	*WRKY22*	ATGTCTGGGCATGGCGAA	GTGCTTCCGGCGAGAGAAT
AT2G19190	*FRK1*	CAGCGCAAGGACTAGAG	CTTCGCTTGGAGCTTCT
AT1G13320	*PP2A*	CGATAGTCGACCAAGCGGTT	TACCGAACATCAACATCTGG

Supplementary Table 2. iCLIP2 cell lysis buffer.

Component	Concentration
Trizma base (Tris)-HCl pH 7.5	50 mM
NaCl	150 mM
DTT	5 mM
$MgCl_2$	4 mM
SDS	1 %
Sodium deoxycholate	0.25 %
IGEPAL	0.25 %
Roche complete protease inhibitors	1:100 (v/v)
PMSF	1 mM
Ribolock	5 µL/mL

Supplementary Table 3. iCLIP2 wash buffer.

Component	Concentration
Tris-HCl pH 7.5	50 mM
NaCl	500 mM
DTT	2 mM
$MgCl_2$	4 mM
SDS	1 %
Sodium deoxycholate	0.5 %
Urea	2 M
IGEPAL	0.5 %
Roche complete protease inhibitors	1:100 (v/v)

Supplementary Table 4. iCLIP2 high-salt buffer.

Component	Concentration
Tris-HCl pH 7.4	50 mM
NaCl	1 M
EDTA	1 mM
IGEPAL	1 %
SDS	0.1 %
Sodium deoxycholate	0.5%

Supplementary Table 5. iCLIP2 PNK wash buffer.

Component	Concentration
Tris-HCl pH 7.4	20 mM
$MgCl_2$	10 mM
Tween-20	0.2 %

Supplementary Table 6. iCLIP2 5x PNK buffer.

Component	Concentration
Tris-HCl pH 6.5	350 mM
$MgCl_2$	50 mM
DTT	25 mM

Supplementary Table 7. iCLIP2 4x ligation buffer.

Component	Concentration
Tris-HCl pH 7.8	200 mM
$MgCl_2$	40 mM
DTT	40 mM

Supplementary Table 8. iCLIP2 PK buffer.

Component	(+ SDS) Concentration	(- SDS) Concentration
Tris-HCl pH 7.4	100 mM	100 mM
NaCl	50 mM	50 mM
EDTA	1 mM	1 mM
SDS	0.2 %	-

Supplementary Table 9. iCLIP2 Polynucleotide kinase & linker ligation reaction mixes (volumes per sample).

Component	PNK mix A	PNK mix B	Ligation mix
H_2O	14.5 µL	31 µL	17.5 µL
Ribolock	0.5 µL	1 µL	1 µL
T4 PNK (Thermo)	1 µL	2 µL	-
5 x PNK	4 µL	-	-
Buffer A (Thermo)	-	4 µL	-
RNA ligase (NEB)	-	-	2 µL
4 x ligation buffer	-	-	10 µL
PEG 8000	-	-	8 µL

Supplementary table 10. List of L#clip2.0 primers used in the preparation of each library.

Sample	Name	Sequence
Replicate 1 Mock	L01clip2.0	/5Phos/NNNNATCACGNNNNNAGATCGGAAGAGCGTCGTG/3ddC/
Replicate 1 flg22	L02clip2.0	/5Phos/NNNNCGATGTNNNNNAGATCGGAAGAGCGTCGTG/3ddC/
Replicate 2 Mock	L05clip2.0	/5Phos/NNNNACAGTGNNNNNAGATCGGAAGAGCGTCGTG/3ddC/
Replicate 2 flg22	L06clip2.0	/5Phos/NNNNGCCAATNNNNNAGATCGGAAGAGCGTCGTG/3ddC/
Replicate 3 Mock	L08clip2.0	/5Phos/NNNNACTTGANNNNNAGATCGGAAGAGCGTCGTG/3ddC/
Replicate 3 flg22	L09clip2.0	/5Phos/NNNNGATCAGNNNNNAGATCGGAAGAGCGTCGTG/3ddC/

Supplementary table 11. Components of 20x MOPS buffer.

Component	Concentration
MOPS	50 mM
Tris	50 mM
SDS	0.1 %
EDTA	1 mM

Supplementary table 12. Components of the SDS running buffer for polyacrylamide gel electrophoresis.

Component	Concentration
Tris	25 mM
Glycine	192 mM
SDS	0.1 %

Supplementary table 13. Components of the transfer buffer for Western blots.

Component	Concentration
Tris	25 mM
Glycine	192 mM
Methanol	20 %

Supplementary table 14. Protein extraction buffer for GRP7 immunoblot.

Component	Concentration
Tris-HCl pH 7.4	25 mM
NaCl	150 mM
EDTA	1 mM
IGEPAL	1 %
Glycerol	5 %
Roche complete protease inhibitors	1:50 (v/v)

Supplementary table 15. Gene ontology enrichment analysis statistics for biological process.

Enrichment FDR	Genes	Pathway Genes	Fold Enrichment	Pathway
6.70E-06	210	1182	1.33650236	GO:0006468 protein phosphorylation
6.89E-05	231	1178	1.28007226	GO:0098542 defense response to other organism
2.78E-06	326	1704	1.2720084	GO:0006952 defense response
6.89E-05	282	1591	1.24561897	GO:0016310 phosphorylation
0.000108653	297	1485	1.22691951	GO:0043207 response to external biotic stimulus
0.000108653	297	1485	1.22691951	GO:0051707 response to other organism
0.000111314	302	1507	1.2218136	GO:0044419 biological proc. involved in interspecies interaction between organisms
0.004031439	387	2189	1.14885891	GO:0006796 phosphate-containing compound metabolic proc.
0.007257241	396	2232	1.13860875	GO:0006793 phosphorus metabolic proc.
0.011024535	370	1947	1.13652232	GO:0009605 response to external stimulus
0.011024535	485	2934	1.11420503	GO:0006464 cellular protein modification proc.
0.011024535	485	2935	1.11420503	GO:0036211 protein modification proc.
0.0009303	744	3953	1.11033782	GO:0006950 response to stress
0.011024535	518	3300	1.1091961	GO:0043412 macromolecule modification

Supplementary table 16. Gene ontology enrichment analysis statistics for molecular function.

Enrichment FDR	Genes	Pathway Genes	Fold Enrichment	Pathway
9.34E-06	167	865	1.35527515	GO:0004674 protein serine/threonine kinase activity
1.33E-06	201	1111	1.35133678	GO:0004672 protein kinase activity
0.000116906	127	633	1.35024233	GO:0106310 protein serine kinase activity
0.000111367	135	678	1.34169064	GO:0004712 protein serine/threonine/tyrosine kinase activity
1.33E-06	235	1275	1.31821639	GO:0016773 phosphotransferase activity alcohol group as acceptor
1.26E-05	259	1472	1.2641283	GO:0016301 kinase activity
0.018766057	95	629	1.24682363	GO:0016757 glycosyltransferase activity
6.57E-05	282	1705	1.22782441	GO:0016772 transferase activity transferring phosphorus-containing groups
0.0017106	475	2793	1.12807852	GO:0140096 catalytic activity acting on a protein
0.000168308	637	4144	1.12656262	GO:0016740 transferase activity
0.007454459	406	2525	1.12151346	GO:0032559 adenyl ribonucleotide binding
0.008603842	408	2536	1.11803086	GO:0030554 adenyl nucleotide binding
0.018766057	389	2411	1.10918052	GO:0005524 ATP binding
0.030065825	472	2865	1.08889963	GO:0097367 carbohydrate derivative binding
0.041520544	455	2796	1.08527865	GO:0032555 purine ribonucleotide binding

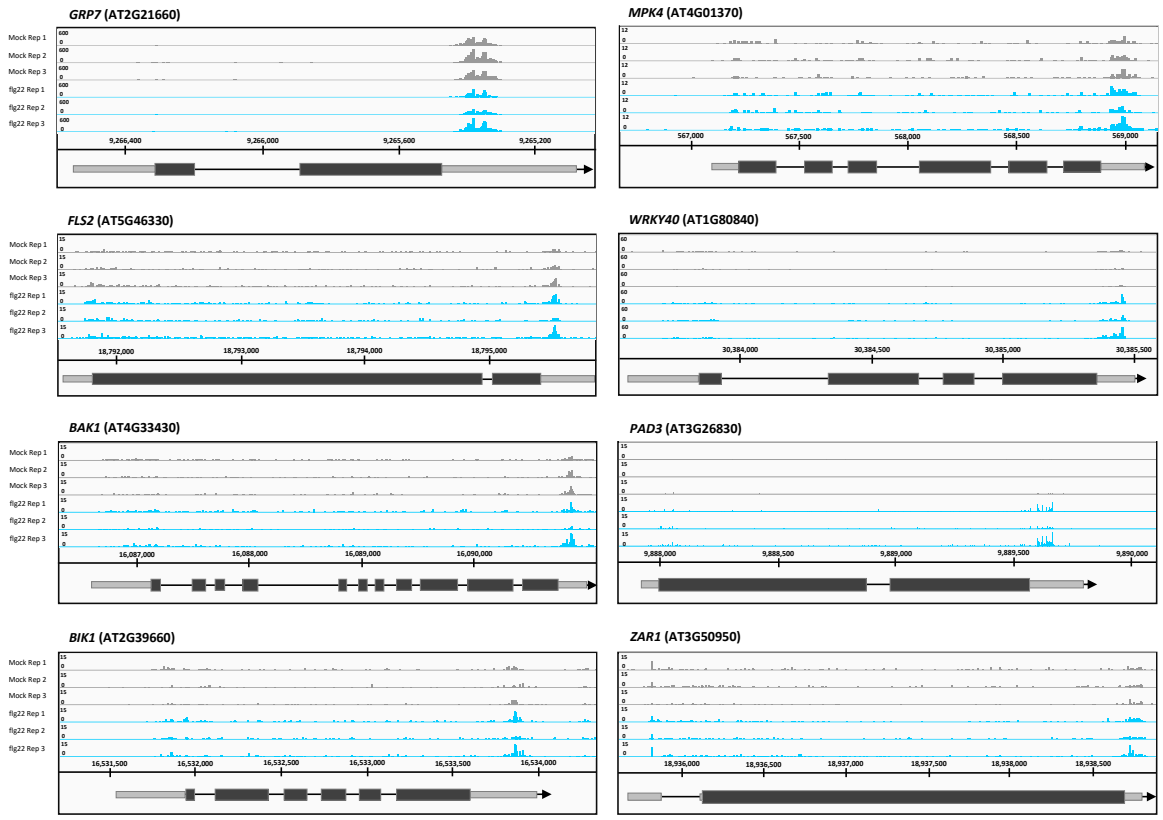

Supplementary figure S1. iCLIP2 peak tracks for individual replicates. iCLIP2 crosslink profiles of GRP7 binding on gene transcripts shown in figure 8 in each replicate. Crosslinks are displayed relative to the representative mRNA, with the y-axis values indicating the number of crosslinks.

Supplementary data files can be viewed by accessing the following link.

Supplementary data files

Appendix II.

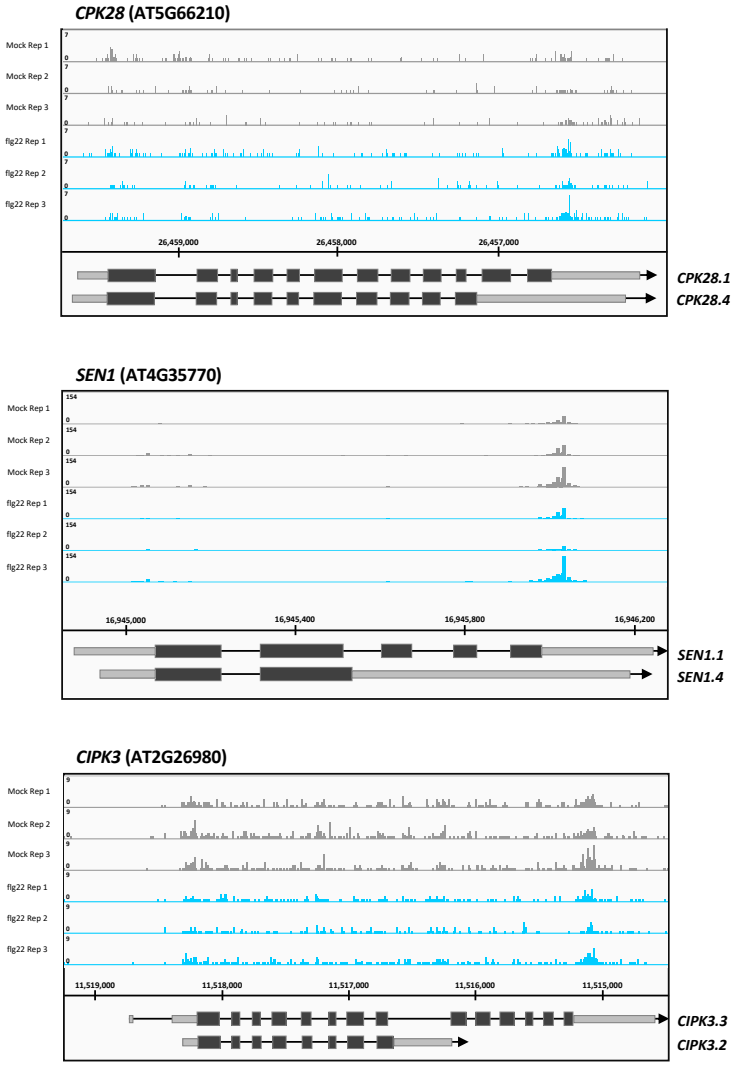

Supplementary figure S1. iCLIP2 peak tracks for individual replicates. iCLIP2 crosslink profiles of GRP7 binding on gene transcripts shown in Figure 1b in each replicate. Crosslinks are displayed relative to the representative mRNA, with the y-axis values indicating the number of crosslinks.

Supplementary Table 1. List of primers used to validate the *grp7-1 8i* mutant and GRP7-OX lines, and primers used for isoform-specific RT-qPCR.

Gene		**Forward**	**Reverse**
AT2G21660	*GRP7*	CCTTCGCTCAATACGGCGACG	GGTGACGAATCCGAATCCCCTTG
AT5G66210.1	*CPK28.1*	TTGATGCGATTGATGTGGAT	GCTATCAATCGCTTCAAG
AT5G66210.4	*CPK28.4*	GCATCTCTGGGGGTATCAGA	CACAACGGCTCATTATGAAA
AT4G35770.1	*SEN1.1*	CGCTATCTCGACGTGAGGAC	TCTTAACCATTCCTGATCCGACT
AT4G35770.4	*SEN1.4*	TCCGACTAGAGCCATCAACG	CCTGCAACGGTTTTGGCTTG

Supplementary Table 2. List of primers used for RT-PCR validation of Agrobacterium-mediated transient gene expression of candidate gene isoforms in *N. benthamiana*.

Gene		**Forward**	**Reverse**
AT5G66210.1	*CPK28.1*	ACCAAGGCCTCTACCAAACG	CCTCCTTCGCACAACTCCAT
AT5G66210.4	*CPK28.4*	CTACACCTACGTCGCCATCC	CAACGGCTGCATCTTTCTCG
AT4G35770.1	*SEN1.1*	CGCTATCTCGACGTGAGGAC	TCTTAACCATTCCTGATCCGACT
AT4G35770.4	*SEN1.4*	GCAACGACAACAAGCAGAGG	GTCCTCACGTCGAGATAGCG
AT2G26980.3	*CIPK3.3*	TGTGGTCATGCGGTGTTGTA	TGCGGTGTTACACGAGTCAT
AT2G26980.2	*CIPK3.2*	CATGTGGTCATGCGGTGTTG	TTCATGGCACCGAGTGAGAG

Supplementary table 3. Primers used for genotyping the *sen1-1* T-DNA insertion mutant [1].

Gene		**Forward**	**Reverse**
AT4G35770	*SEN1*	GCCAATTACCAACACGAAGAGG	GCCTCTGCTGCAACATTTCC
AT1G13440	*GAPDH*	TCTCGATCTCAATTTCGCAAAA	CGAAACCGTTGATTCCGATTC
AT4G35770	SALK_020571C	ACGACACAGAAACAAACCTCG	TTCTTAACCATTCCTGCAACG
SALK LB		ATTTTGCCGATTTCGGAAC	

[1] Gene-specific primers were designed using Signal Salk T-DNA primer design tool (O'Malley, Barragan and Ecker, 2015).

Appendix III.

Supplementary table 1. List of candidate genes and corresponding T-DNA insertion mutants that were genotyped in this study.

AGI	Description	NASC ID	SALK ID
AT4G19520	Probable disease resistance protein	N663793	SALK_118667C
AT4G36690	U2AF6A: Splicing factor U2 auxiliary factor 65 kDa subunit A	N677273	SALK_144790C
AT2G24600	Ankyrin repeat family protein	N600250	SALK_100250
AT1G66260	ALY3: THO complex subunit 4C	N693274	SALK_204484C
AT1G15520	ABCG40: ABC transporter G family member 40	N667586	SALK_148565C
AT4G25080	CHLM: Magnesium protoporphyrin IX methyltransferase	N610265	SALK_110265
AT2G24600	Ankyrin repeat family protein	N600250	SALK_100250
AT5G62570	Calmodulin-binding protein 60 A	N574113	SALK_074113
AT2G41560	CBP60A: Calcium-transporting ATPase 4	N608323	SALK_108323
AT2G05440	GRP9: Glycine rich protein 9	N619828	SALK_119828

Supplementary table 2. Primers used for genotyping T-DNA insertion mutants [1].

Gene		Forward	Reverse
AT4G19520	SALK_118667C	TAACCTTTTCAGGTTTTGGGG	CAAAGCGATGAGATAGGGATG
AT4G36690	SALK_144790C	CACAAAGACCACCAAACAACC	GCGAAAAGATGTCTGAATTCG
AT2G24600	SALK_100250	TTGTTCCACTCAACTCCCAAG	CCTCCCAAGCATTTTTCCTAG
AT1G66260	SALK_204484C	GTCTCCCAGAAGGACCTGAAC	AAAGCCTGAAAATGTGTGTGG
AT1G15520	SALK_148565C	ATCTCAAGAAGCGGCTTTAGG	AACCACACCCAAGAAACCTTC
AT4G25080	SALK_110265	CAGCAGAAATATCGGAAGCAG	ACAATGACGAGTGACCACCTC
AT2G24600	SALK_100250	TTGTTCCACTCAACTCCCAAG	CCTCCCAAGCATTTTTCCTAG
AT5G62570	SALK_074113	GAGCAGTTCCAGAGATTGTCG	GGAAGTTCAGACTCGGGGTAC
AT2G41560	SALK_108323	TTGTTCAAAAGGCAGCTCTTC	GCTACCAGACGTTGCTTTGTC
AT2G05440	SALK_119828	ATCCACGTCAGTAGCCATGAG	AATATGTTACGTTGCATGCCC
SALK LB		ATTTTGCCGATTTCGGAAC	

[1] Gene-specific primers were designed using Signal Salk T-DNA primer design tool (O'Malley, Barragan and Ecker, 2015).

Supplementary table 3. Protein extraction buffer components.

Component	Concentration
Tris-HCl pH 7.4	25 mM
NaCl	150 mM
EDTA	1 mM
IGEPAL	1 %
Glycerol	5 %
Roche complete protease inhibitors	1:50 (v/v)

Supplementary table 4. Primers used for RT-qPCR quantification of *ALY3* expression.

Gene		Forward	Reverse
AT1G66260	*ALY3*	GAGACGCCTTCCACTCCAAC	ACTGGCTTCTTTCCACCTCG
AT1G13440	*GAPDH*	TCTCGATCTCAATTTCGCAAAA	CGAAACCGTTGATTCCGATTC

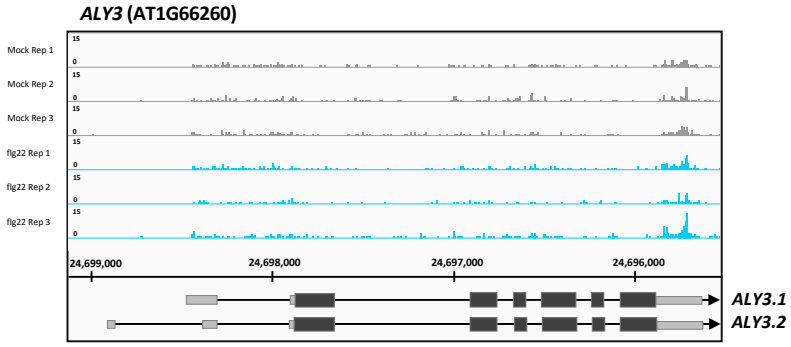

Supplementary figure S1. iCLIP2 peak tracks for individual replicates. iCLIP2 crosslink profiles of GRP7 binding on *ALY3* mRNA shown in Figure 3f in each replicate. Crosslinks are displayed relative to the representative mRNA, with the y-axis values indicating the number of crosslinks.

Appendix IV.

Statement of Collaborative Contributions

Certain aspects of the work presented in this thesis were carried out with the assistance of collaborators, whose contributions I gratefully acknowledge:

- In chapter 2, the iCLIP2 experiment was conducted by Brett Wadley in the Staiger Lab at the University of Bielefeld under the supervision of Professor Dorothee Staiger and Dr Marlene Reichel.
- The bioinformatic analysis for identifying GRP7 binding events was conducted by Dr. Martin Lewinski.
- The confocal analysis of GRP7 localisation was carried out by Sarah Skinner under the supervision of Brett Wadley and Professor Gail Preston.
- In chapter 4, the *A. thaliana aly3-1* T-DNA mutant genotyping and seedling infection assay with *Pto* DC3000 was performed by Sarah Skinner, supervised by Brett Wadley and Professor Gail Preston.

References

Adams-Phillips, L., Briggs, A.G. and Bent, A.F. (2009) 'Disruption of Poly(ADP-ribosyl)ation Mechanisms Alters Responses of Arabidopsis to Biotic Stress', *Plant Physiology*, 152(1), pp. 267–280. Available at: https://doi.org/10.1104/pp.109.148049.

Aerts, N. *et al.* (2022) 'Transcriptional regulation of plant innate immunity', *Essays in Biochemistry*. Edited by K. Kanyuka and K. Hammond-Kosack, 66(5), pp. 607–620. Available at: https://doi.org/10.1042/EBC20210100.

Ai, G. *et al.* (2025) 'A catalogue of virulence strategies mediated by phytopathogenic effectors', *Fundamental Research*, 5(2), pp. 663–673. Available at: https://doi.org/10.1016/j.fmre.2023.10.026.

Albrecht, V. *et al.* (2001) 'The NAF domain defines a novel protein–protein interaction module conserved in Ca2+-regulated kinases', *The EMBO Journal*, 20(5), pp. 1051–1063. Available at: https://doi.org/10.1093/emboj/20.5.1051.

Anderson, J.C. *et al.* (2011) 'Arabidopsis MAP Kinase Phosphatase 1 (AtMKP1) negatively regulates MPK6-mediated PAMP responses and resistance against bacteria', *The Plant Journal*, 67(2), pp. 258–268. Available at: https://doi.org/10.1111/j.1365-313X.2011.04588.x.

Asai, T. *et al.* (2002) 'MAP kinase signalling cascade in Arabidopsis innate immunity', *Nature*, 415(6875), pp. 977–983. Available at: https://doi.org/10.1038/415977a.

Assaad, F.F. *et al.* (2004) 'The PEN1 Syntaxin Defines a Novel Cellular Compartment upon Fungal Attack and Is Required for the Timely Assembly of Papillae', *Molecular Biology of the Cell*, 15(11), pp. 5118–5129. Available at: https://doi.org/10.1091/mbc.e04-02-0140.

Bach-Pages, M., Homma, F., *et al.* (2020) 'Discovering the RNA-Binding Proteome of Plant Leaves with an Improved RNA Interactome Capture Method', *Biomolecules*, 10(4), p. 661. Available at: https://doi.org/10.3390/biom10040661.

Bach-Pages, M., Chen, H., *et al.* (2020) 'Proteome-wide Profiling of RNA-Binding Protein Responses to flg22 Reveals Novel Components of Plant Immunity'. bioRxiv, p. 2020.09.16.299701. Available at: https://doi.org/10.1101/2020.09.16.299701.

Bach-Pages, M. *et al.* (2025) 'RNA-binding proteins orchestrating immunity in plants', *The Plant Journal*, 123(5), p. e70433. Available at: https://doi.org/10.1111/tpj.70433.

Bach-Pages, M., Castello, A. and Preston, G.M. (2017) 'Plant RNA Interactome Capture: Revealing the Plant RBPome', *Trends in Plant Science*, 22(6), pp. 449–451. Available at: https://doi.org/10.1016/j.tplants.2017.04.006.

Bach-Pages, M. and Preston, G.M. (2018) 'Methods to Quantify Biotic-Induced Stress in Plants', in C. Medina and F.J. López-Baena (eds) *Host-Pathogen Interactions*. New York, NY: Springer New York (Methods in Molecular Biology), pp. 241–255. Available at: https://doi.org/10.1007/978-1-4939-7604-1_19.

Bassal, M. *et al.* (2020) 'Reshaping of the Arabidopsis thaliana Proteome Landscape and Co-regulation of Proteins in Development and Immunity', *Molecular Plant*, 13(12), pp. 1709–1732. Available at: https://doi.org/10.1016/j.molp.2020.09.024.

Bazin, J. *et al.* (2020) 'Role of MPK4 in pathogen-associated molecular pattern-triggered alternative splicing in Arabidopsis', *PLOS Pathogens*, 16(4), p. e1008401. Available at: https://doi.org/10.1371/journal.ppat.1008401.

Berget, S.M., Moore, C. and Sharp, P.A. (1977) 'Spliced segments at the 5' terminus of adenovirus 2 late mRNA*', *Proceedings of the National Academy of Sciences*, 74(8), pp. 3171–3175. Available at: https://doi.org/10.1073/pnas.74.8.3171.

Bethke, G. *et al.* (2012) 'Activation of the Arabidopsis thaliana Mitogen-Activated Protein Kinase MPK11 by the Flagellin-Derived Elicitor Peptide, flg22', *Molecular Plant-Microbe Interactions®*, 25(4), pp. 471–480. Available at: https://doi.org/10.1094/MPMI-11-11-0281.

Bhardwaj, V. *et al.* (2011) 'Defence responses of Arabidopsis thaliana to infection by Pseudomonas syringae are regulated by the circadian clock', *PloS One*, 6(10), p. e26968. Available at: https://doi.org/10.1371/journal.pone.0026968.

Bi, G. *et al.* (2021) 'The ZAR1 resistosome is a calcium-permeable channel triggering plant immune signaling', *Cell*, 184(13), pp. 3528-3541.e12. Available at: https://doi.org/10.1016/j.cell.2021.05.003.

Bjornson, M. *et al.* (2021) 'The transcriptional landscape of Arabidopsis thaliana pattern-triggered immunity', *Nature Plants*, 7(5), pp. 579–586. Available at: https://doi.org/10.1038/s41477-021-00874-5.

Boller, T. and Felix, G. (2009) 'A Renaissance of Elicitors: Perception of Microbe-Associated Molecular Patterns and Danger Signals by Pattern-Recognition Receptors', *Annual Review of Plant Biology*, 60(1), pp. 379–406. Available at: https://doi.org/10.1146/annurev.arplant.57.032905.105346.

Borrowman, S., Kapuganti, J.G. and Loake, G.J. (2023) 'Expanding roles for S-nitrosylation in the regulation of plant immunity', *Free Radical Biology and Medicine*, 194, pp. 357–368. Available at: https://doi.org/10.1016/j.freeradbiomed.2022.12.009.

Boutrot, F. and Zipfel, C. (2017) 'Function, Discovery, and Exploitation of Plant Pattern Recognition Receptors for Broad-Spectrum Disease Resistance', *Annual Review of Phytopathology*, 55(Volume 55, 2017), pp. 257–286. Available at: https://doi.org/10.1146/annurev-phyto-080614-120106.

Bowling, S.A. *et al.* (1997) 'The cpr5 mutant of Arabidopsis expresses both NPR1-dependent and NPR1-independent resistance.', *The Plant Cell*, 9(9), pp. 1573–1584. Available at: https://doi.org/10.1105/tpc.9.9.1573.

Buchbender, A. *et al.* (2020) 'Improved library preparation with the new iCLIP2 protocol', *Methods*, 178, pp. 33–48. Available at: https://doi.org/10.1016/j.ymeth.2019.10.003.

Burd, C.G. and Dreyfuss, G. (1994) 'Conserved Structures and Diversity of Functions of RNA-Binding Proteins', *Science*, 265(5172), pp. 615–621. Available at: https://doi.org/10.1126/science.8036511.

Buscaill, P. *et al.* (2019) 'Glycosidase and glycan polymorphism control hydrolytic release of immunogenic flagellin peptides', *Science*, 364(6436), p. eaav0748. Available at: https://doi.org/10.1126/science.aav0748.

Buscaill, P. *et al.* (2021) 'Agromonas: a rapid disease assay for *Pseudomonas syringae* growth in agroinfiltrated leaves', *The Plant Journal*, 105(3), pp. 831–840. Available at: https://doi.org/10.1111/tpj.15056.

Cao, F.Y., Yoshioka, K. and Desveaux, D. (2011) 'The roles of ABA in plant–pathogen interactions', *Journal of Plant Research*, 124(4), pp. 489–499. Available at: https://doi.org/10.1007/s10265-011-0409-y.

Capella-Gutiérrez, S., Silla-Martínez, J.M. and Gabaldón, T. (2009) 'trimAl: a tool for automated alignment trimming in large-scale phylogenetic analyses', *Bioinformatics*, 25(15), pp. 1972–1973. Available at: https://doi.org/10.1093/bioinformatics/btp348.

Chabi Sika, K. *et al.* (2015) 'A simple and efficient genomic DNA extraction protocol for large scale genetic analyses of plant biological systems', *Plant Gene*, 1, pp. 43–45. Available at: https://doi.org/10.1016/j.plgene.2015.03.001.

Chinchilla, D. *et al.* (2007) 'A flagellin-induced complex of the receptor FLS2 and BAK1 initiates plant defence', *Nature*, 448(7152), pp. 497–500. Available at: https://doi.org/10.1038/nature05999.

Choudury, S.G. *et al.* (2019) 'The RNA Export Factor ALY1 Enables Genome-Wide RNA-Directed DNA Methylation', *The Plant Cell*, 31(4), pp. 759–774. Available at: https://doi.org/10.1105/tpc.18.00624.

Chow, L.T. *et al.* (1977) 'An amazing sequence arrangement at the 5' ends of adenovirus 2 messenger RNA', *Cell*, 12(1), pp. 1–8. Available at: https://doi.org/10.1016/0092-8674(77)90180-5.

Chung, B.-C. *et al.* (1997) 'The promoter activity of sen 1, a senescence-associated gene of Arabidopsis, is repressed by sugars', *Journal of Plant Physiology*, 151(3), pp. 339–345. Available at: https://doi.org/10.1016/S0176-1617(97)80262-3.

Chung, H.S. and Sheen, J. (2017) 'MAPK Assays in Arabidopsis MAMP-PRR Signal Transduction', in L. Shan and P. He (eds) *Plant Pattern Recognition Receptors: Methods and Protocols*. New York, NY: Springer, pp. 155–166. Available at: https://doi.org/10.1007/978-1-4939-6859-6_12.

Collins, N.C. *et al.* (2003) 'SNARE-protein-mediated disease resistance at the plant cell wall', *Nature*, 425(6961), pp. 973–977. Available at: https://doi.org/10.1038/nature02076.

Corley, M., Burns, M.C. and Yeo, G.W. (2020) 'How RNA-Binding Proteins Interact with RNA: Molecules and Mechanisms', *Molecular Cell*, 78(1), pp. 9–29. Available at: https://doi.org/10.1016/j.molcel.2020.03.011.

Cui, H., Tsuda, K. and Parker, J.E. (2015) 'Effector-Triggered Immunity: From Pathogen Perception to Robust Defense', *Annual Review of Plant Biology*, 66(1), pp. 487–511. Available at: https://doi.org/10.1146/annurev-arplant-050213-040012.

Cunnac, S., Lindeberg, M. and Collmer, A. (2009) 'Pseudomonas syringae type III secretion system effectors: repertoires in search of functions', *Current Opinion in Microbiology*, 12(1), pp. 53–60. Available at: https://doi.org/10.1016/j.mib.2008.12.003.

Dai, G.-Y. *et al.* (2020) 'The Arabidopsis AtGCD3 protein is a glucosylceramidase that preferentially hydrolyzes long-acyl-chain glucosylceramides', *Journal of Biological Chemistry*, 295(3), pp. 717–728. Available at: https://doi.org/10.1016/S0021-9258(17)49930-3.

De Torres, M. *et al.* (2006) 'Pseudomonas syringae effector AvrPtoB suppresses basal defence in Arabidopsis', *The Plant Journal*, 47(3), pp. 368–382. Available at: https://doi.org/10.1111/j.1365-313X.2006.02798.x.

De Torres Zabala, M. *et al.* (2009) 'Antagonism between salicylic and abscisic acid reflects early host–pathogen conflict and moulds plant defence responses', *The Plant Journal*, 59(3), pp. 375–386. Available at: https://doi.org/10.1111/j.1365-313X.2009.03875.x.

De Torres Zabala, M. *et al.* (2015) 'Chloroplasts play a central role in plant defence and are targeted by pathogen effectors', *Nature Plants*, 1(6), p. 15074. Available at: https://doi.org/10.1038/nplants.2015.74.

Denoux, C. *et al.* (2008) 'Activation of defense response pathways by OGs and Flg22 elicitors in Arabidopsis seedlings', *Molecular plant*, 1(3), pp. 423–445. Available at: https://doi.org/10.1093/mp/ssn019.

Després, C. *et al.* (2003) 'The Arabidopsis NPR1 Disease Resistance Protein Is a Novel Cofactor That Confers Redox Regulation of DNA Binding Activity to the Basic Domain/Leucine Zipper Transcription Factor TGA1', *The Plant Cell*, 15(9), pp. 2181–2191. Available at: https://doi.org/10.1105/tpc.012849.

Ding, F. *et al.* (2022) 'Dynamics and functional roles of splicing factor autoregulation', *Cell Reports*, 39(12), p. 110985. Available at: https://doi.org/10.1016/j.celrep.2022.110985.

Dodds, P.N. and Rathjen, J.P. (2010) 'Plant immunity: towards an integrated view of plant–pathogen interactions', *Nature Reviews Genetics*, 11(8), pp. 539–548. Available at: https://doi.org/10.1038/nrg2812.

Drechsel, G. *et al.* (2013) 'Nonsense-Mediated Decay of Alternative Precursor mRNA Splicing Variants Is a Major Determinant of the Arabidopsis Steady State Transcriptome', *The Plant Cell*, 25(10), pp. 3726–3742. Available at: https://doi.org/10.1105/tpc.113.115485.

Dressano, K. *et al.* (2020) 'Dynamic regulation of Pep-induced immunity through post-translational control of defence transcript splicing', *Nature Plants*, 6(8), pp. 1008–1019. Available at: https://doi.org/10.1038/s41477-020-0724-1.

Duan, Y. *et al.* (2013) 'Wheat hypersensitive-induced reaction genes TaHIR1 and TaHIR3 are involved in response to stripe rust fungus infection and abiotic stresses', *Plant Cell Reports*, 32(2), pp. 273–283. Available at: https://doi.org/10.1007/s00299-012-1361-6.

Ehrnsberger, H.F., Grasser, M. and Grasser, K.D. (2019) 'Nucleocytosolic mRNA transport in plants: export factors and their influence on growth and development', *Journal of Experimental Botany*, 70(15), pp. 3757–3763. Available at: https://doi.org/10.1093/jxb/erz173.

Elvira-Matelot, E. *et al.* (2016) 'The Nuclear Ribonucleoprotein SmD1 Interplays with Splicing, RNA Quality Control, and Posttranscriptional Gene Silencing in Arabidopsis', *The Plant Cell*, 28(2), pp. 426–438. Available at: https://doi.org/10.1105/tpc.15.01045.

Evans, R. *et al.* (2022) 'Protein complex prediction with AlphaFold-Multimer'. bioRxiv, p. 2021.10.04.463034. Available at: https://doi.org/10.1101/2021.10.04.463034.

Fan, W. and Dong, X. (2002) 'In Vivo Interaction between NPR1 and Transcription Factor TGA2 Leads to Salicylic Acid–Mediated Gene Activation in Arabidopsis', *The Plant Cell*, 14(6), pp. 1377–1389. Available at: https://doi.org/10.1105/tpc.001628.

Fang, Y.-L., Peng, Y.-L. and Fan, J. (2017) 'The Nep1-like protein family of Magnaporthe oryzae is dispensable for the infection of rice plants', *Scientific Reports*, 7(1), p. 4372. Available at: https://doi.org/10.1038/s41598-017-04430-0.

Frei dit Frey, N. *et al.* (2014) 'Functional analysis of Arabidopsisimmune-related MAPKs uncovers a role for MPK3 as negative regulator of inducible defences', *Genome Biology*, 15(6), p. R87. Available at: https://doi.org/10.1186/gb-2014-15-6-r87.

Fu, Z.Q. *et al.* (2007) 'A type III effector ADP-ribosylates RNA-binding proteins and quells plant immunity', *Nature*, 447(7142), pp. 284–288. Available at: https://doi.org/10.1038/nature05737.

Gao, M. *et al.* (2008) 'MEKK1, MKK1/MKK2 and MPK4 function together in a mitogen-activated protein kinase cascade to regulate innate immunity in plants', *Cell Research*, 18(12), pp. 1190–1198. Available at: https://doi.org/10.1038/cr.2008.300.

Ge, S.X., Jung, D. and Yao, R. (2020) 'ShinyGO: a graphical gene-set enrichment tool for animals and plants', *Bioinformatics*, 36(8), pp. 2628–2629. Available at: https://doi.org/10.1093/bioinformatics/btz931.

Germain, H. *et al.* (2010) 'MOS11: A New Component in the mRNA Export Pathway', *PLOS Genetics*, 6(12), p. e1001250. Available at: https://doi.org/10.1371/journal.pgen.1001250.

Germain, H. and Gaouar, O. (2013) 'mRNA export: threading the needle', *Frontiers in Plant Science*, 4. Available at: https://doi.org/10.3389/fpls.2013.00059.

Gloggnitzer, J. *et al.* (2014) 'Nonsense-Mediated mRNA Decay Modulates Immune Receptor Levels to Regulate Plant Antibacterial Defense', *Cell Host & Microbe*, 16(3), pp. 376–390. Available at: https://doi.org/10.1016/j.chom.2014.08.010.

Göhre, V. *et al.* (2008) 'Plant Pattern-Recognition Receptor FLS2 Is Directed for Degradation by the Bacterial Ubiquitin Ligase AvrPtoB', *Current Biology*, 18(23), pp. 1824–1832. Available at: https://doi.org/10.1016/j.cub.2008.10.063.

Göhring, J., Jacak, J. and Barta, A. (2014) 'Imaging of Endogenous Messenger RNA Splice Variants in Living Cells Reveals Nuclear Retention of Transcripts Inaccessible to Nonsense-Mediated Decay in Arabidopsis', *The Plant Cell*, 26(2), pp. 754–764. Available at: https://doi.org/10.1105/tpc.113.118075.

González Besteiro, M.A. *et al.* (2011) 'Arabidopsis MAP kinase phosphatase 1 and its target MAP kinases 3 and 6 antagonistically determine UV-B stress tolerance, independent of the UVR8 photoreceptor pathway', *The Plant Journal*, 68(4), pp. 727–737. Available at: https://doi.org/10.1111/j.1365-313X.2011.04725.x.

González Besteiro, M.A. and Ulm, R. (2013) 'Phosphorylation and Stabilization of Arabidopsis MAP Kinase Phosphatase 1 in Response to UV-B Stress*', *Journal of Biological Chemistry*, 288(1), pp. 480–486. Available at: https://doi.org/10.1074/jbc.M112.434654.

Grant, M. *et al.* (2000) 'The *RPM1* plant disease resistance gene facilitates a rapid and sustained increase in cytosolic calcium that is necessary for the oxidative burst and hypersensitive cell death', *The Plant Journal*, 23(4), pp. 441–450. Available at: https://doi.org/10.1046/j.1365-313x.2000.00804.x.

Griebel, T. and Zeier, J. (2008) 'Light Regulation and Daytime Dependency of Inducible Plant Defenses in Arabidopsis: Phytochrome Signaling Controls Systemic Acquired Resistance Rather Than Local Defense', *Plant Physiology*, 147(2), pp. 790–801. Available at: https://doi.org/10.1104/pp.108.119503.

Gui, X. *et al.* (2022) 'Phytophthora effector PSR1 hijacks the host pre-mRNA splicing machinery to modulate small RNA biogenesis and plant immunity', *The Plant Cell*, 34(9), pp. 3443–3459. Available at: https://doi.org/10.1093/plcell/koac176.

Hackmann, C. *et al.* (2014) 'Salicylic acid-dependent and -independent impact of an RNA-binding protein on plant immunity', *Plant, Cell & Environment*, 37(3), pp. 696–706. Available at: https://doi.org/10.1111/pce.12188.

Hafner, M. *et al.* (2021) 'CLIP and complementary methods', *Nature Reviews Methods Primers*, 1(1), pp. 1–23. Available at: https://doi.org/10.1038/s43586-021-00018-1.

Hardy, E.C. and Balcerowicz, M. (2024) 'Untranslated yet indispensable—UTRs act as key regulators in the environmental control of gene expression', *Journal of Experimental Botany*. Edited by P. Manavella, 75(14), pp. 4314–4331. Available at: https://doi.org/10.1093/jxb/erae073.

Harvey, S.E. and Cheng, C. (2016) 'Methods for Characterization of Alternative RNA Splicing', *Methods in molecular biology (Clifton, N.J.)*, 1402, pp. 229–241. Available at: https://doi.org/10.1007/978-1-4939-3378-5_18.

Heintzen, C. *et al.* (1997) '*At* GRP7, a nuclear RNA-binding protein as a component of a circadian-regulated negative feedback loop in *Arabidopsis thaliana*', *Proceedings of the National Academy of Sciences*, 94(16), pp. 8515–8520. Available at: https://doi.org/10.1073/pnas.94.16.8515.

Henne, M. *et al.* (2015) 'Sulfurtransferase and thioredoxin specifically interact as demonstrated by bimolecular fluorescence complementation analysis and biochemical tests', *FEBS Open Bio*, 5(1), pp. 832–843. Available at: https://doi.org/10.1016/j.fob.2015.10.001.

Homma, F., Huang, J. and Van Der Hoorn, R.A.L. (2023) 'AlphaFold-Multimer predicts cross-kingdom interactions at the plant-pathogen interface', *Nature Communications*, 14(1), p. 6040. Available at: https://doi.org/10.1038/s41467-023-41721-9.

Huang, J. *et al.* (2017) 'An oomycete plant pathogen reprograms host pre-mRNA splicing to subvert immunity', *Nature Communications*, 8(1), p. 2051. Available at: https://doi.org/10.1038/s41467-017-02233-5.

Huang, J. *et al.* (2020) 'Phytophthora Effectors Modulate Genome-wide Alternative Splicing of Host mRNAs to Reprogram Plant Immunity', *Molecular Plant*, 13(10), pp. 1470–1484. Available at: https://doi.org/10.1016/j.molp.2020.07.007.

Huppertz, I. *et al.* (2014) 'iCLIP: Protein–RNA interactions at nucleotide resolution', *Methods*, 65(3), pp. 274–287. Available at: https://doi.org/10.1016/j.ymeth.2013.10.011.

Ishiga, Y. *et al.* (2011) 'Arabidopsis seedling flood-inoculation technique: a rapid and reliable assay for studying plant-bacterial interactions', *Plant Methods*, 7(1), p. 32. Available at: https://doi.org/10.1186/1746-4811-7-32.

Ishiga, Y. *et al.* (2017) 'Pseudomonas syringae Flood-inoculation Method in Arabidopsis', *BIO-PROTOCOL*, 7(2). Available at: https://doi.org/10.21769/BioProtoc.2106.

Jang, G.-J., Jang, J.-C. and Wu, S.-H. (2020) 'Dynamics and Functions of Stress Granules and Processing Bodies in Plants', *Plants*, 9(9), p. 1122. Available at: https://doi.org/10.3390/plants9091122.

Jeong, B. *et al.* (2011) 'Structure Function Analysis of an ADP-ribosyltransferase Type III Effector and Its RNA-binding Target in Plant Immunity *', *Journal of Biological Chemistry*, 286(50), pp. 43272–43281. Available at: https://doi.org/10.1074/jbc.M111.290122.

Jia, J. *et al.* (2020) 'Post-transcriptional splicing of nascent RNA contributes to widespread intron retention in plants', *Nature Plants*, 6(7), pp. 780–788. Available at: https://doi.org/10.1038/s41477-020-0688-1.

Johansson, O.N. *et al.* (2014) 'Role of the penetration-resistance genes PEN1, PEN2 and PEN3 in the hypersensitive response and race-specific resistance in Arabidopsis thaliana', *The Plant Journal*, 79(3), pp. 466–476. Available at: https://doi.org/10.1111/tpj.12571.

Jones, J.D.G. and Dangl, J.L. (2006) 'The plant immune system', *Nature*, 444(7117), pp. 323–329. Available at: https://doi.org/10.1038/nature05286.

Jumper, J. *et al.* (2021) 'Highly accurate protein structure prediction with AlphaFold', *Nature*, 596(7873), pp. 583–589. Available at: https://doi.org/10.1038/s41586-021-03819-2.

Jurado, A.R. *et al.* (2014) 'Structure and Function of Pre-mRNA 5'-End Capping Quality Control and 3'-End Processing', *Biochemistry*, 53(12), pp. 1882–1898. Available at: https://doi.org/10.1021/bi401715v.

Kalyaanamoorthy, S. *et al.* (2017) 'ModelFinder: fast model selection for accurate phylogenetic estimates', *Nature Methods*, 14(6), pp. 587–589. Available at: https://doi.org/10.1038/nmeth.4285.

Kalyna, M. *et al.* (2012) 'Alternative splicing and nonsense-mediated decay modulate expression of important regulatory genes in Arabidopsis', *Nucleic Acids Research*, 40(6), pp. 2454–2469. Available at: https://doi.org/10.1093/nar/gkr932.

Katoh, K. (2002) 'MAFFT: a novel method for rapid multiple sequence alignment based on fast Fourier transform', *Nucleic Acids Research*, 30(14), pp. 3059–3066. Available at: https://doi.org/10.1093/nar/gkf436.

Kim, J.S. *et al.* (2008) 'Glycine-rich RNA-binding protein7 affects abiotic stress responses by regulating stomata opening and closing in Arabidopsis thaliana', *The Plant Journal*, 55(3), pp. 455–466. Available at: https://doi.org/10.1111/j.1365-313X.2008.03518.x.

Kinkema, M., Fan, W. and Dong, X. (2000) 'Nuclear Localization of NPR1 Is Required for Activation of PR Gene Expression', *The Plant Cell*, 12(12), pp. 2339–2350.

Klepikova, A.V. *et al.* (2016) 'A high resolution map of the Arabidopsis thaliana developmental transcriptome based on RNA-seq profiling', *The Plant Journal*, 88(6), pp. 1058–1070. Available at: https://doi.org/10.1111/tpj.13312.

Korneli, C., Danisman, S. and Staiger, D. (2014) 'Differential Control of Pre-Invasive and Post-Invasive Antibacterial Defense by the Arabidopsis Circadian Clock', *Plant and Cell Physiology*, 55(9), pp. 1613–1622. Available at: https://doi.org/10.1093/pcp/pcu092.

Krakau, S., Richard, H. and Marsico, A. (2017) 'PureCLIP: capturing target-specific protein–RNA interaction footprints from single-nucleotide CLIP-seq data', *Genome Biology*, 18(1), p. 240. Available at: https://doi.org/10.1186/s13059-017-1364-2.

Kubina, J. *et al.* (2021) 'Nuclear export of plant pararetrovirus mRNAs involves the TREX complex, two viral proteins and the highly structured 5' leader region', *Nucleic Acids Research*, 49(15), pp. 8900–8922. Available at: https://doi.org/10.1093/nar/gkab653.

Kufel, J., Diachenko, N. and Golisz, A. (2022) 'Alternative splicing as a key player in the fine-tuning of the immunity response in Arabidopsis', *Molecular Plant Pathology*, 23(8), pp. 1226–1238. Available at: https://doi.org/10.1111/mpp.13228.

Kuźniak, E. and Kopczewski, T. (2020) 'The Chloroplast Reactive Oxygen Species-Redox System in Plant Immunity and Disease', *Frontiers in Plant Science*, 11, p. 572686. Available at: https://doi.org/10.3389/fpls.2020.572686.

Langin, G., González-Fuente, M. and Üstün, S. (2023) 'The Plant Ubiquitin–Proteasome System as a Target for Microbial Manipulation', *Annual Review of Phytopathology*, 61(1), pp. 351–375. Available at: https://doi.org/10.1146/annurev-phyto-021622-110443.

Latrasse, D. *et al.* (2017) 'MAPK-triggered chromatin reprogramming by histone deacetylase in plant innate immunity', *Genome Biology*, 18(1), p. 131. Available at: https://doi.org/10.1186/s13059-017-1261-8.

Leder, V. *et al.* (2014) 'Mutational definition of binding requirements of an hnRNP-like protein in Arabidopsis using fluorescence correlation spectroscopy', *Biochemical and Biophysical Research Communications*, 453(1), pp. 69–74. Available at: https://doi.org/10.1016/j.bbrc.2014.09.056.

Lee, D. *et al.* (2015) 'Phosphorylation of the Plant Immune Regulator RPM1-INTERACTING PROTEIN4 Enhances Plant Plasma Membrane H+-ATPase Activity and Inhibits Flagellin-Triggered Immune Responses in Arabidopsis[OPEN]', *The Plant Cell*, 27(7), pp. 2042–2056. Available at: https://doi.org/10.1105/tpc.114.132308.

Lee, K. and Kang, H. (2016) 'Emerging Roles of RNA-Binding Proteins in Plant Growth, Development, and Stress Responses', *Molecules and Cells*, 39(3), pp. 179–185. Available at: https://doi.org/10.14348/molcells.2016.2359.

Lee, S. *et al.* (2012) 'A NAC transcription factor NTL4 promotes reactive oxygen species production during drought-induced leaf senescence in Arabidopsis', *The Plant Journal*, 70(5), pp. 831–844. Available at: https://doi.org/10.1111/j.1365-313X.2012.04932.x.

Lee, S. *et al.* (2024) 'Nucleolar actions in plant development and stress responses', *Plant, Cell & Environment*, p. pce.15099. Available at: https://doi.org/10.1111/pce.15099.

Lewinski, M., Steffen, A., *et al.* (2024) 'Arabidopsis thaliana GLYCINE RICH RNA-BINDING PROTEIN 7 interaction with its iCLIP target LHCB1.1 correlates with changes in RNA stability and circadian oscillation', *The Plant Journal*, 118(1), pp. 203–224. Available at: https://doi.org/10.1111/tpj.16601.

Lewinski, M., Brüggemann, M., *et al.* (2024) 'Mapping protein–RNA binding in plants with individual-nucleotide-resolution UV cross-linking and immunoprecipitation (plant iCLIP2)', *Nature Protocols*, pp. 1–52. Available at: https://doi.org/10.1038/s41596-023-00935-3.

Lewis, L.A. *et al.* (2015) 'Transcriptional Dynamics Driving MAMP-Triggered Immunity and Pathogen Effector-Mediated Immunosuppression in Arabidopsis Leaves Following Infection with Pseudomonas syringae pv tomato DC3000', *The Plant Cell*, 27(11), pp. 3038–3064. Available at: https://doi.org/10.1105/tpc.15.00471.

Li, L. *et al.* (2014) 'The FLS2-Associated Kinase BIK1 Directly Phosphorylates the NADPH Oxidase RbohD to Control Plant Immunity', *Cell Host & Microbe*, 15(3), pp. 329–338. Available at: https://doi.org/10.1016/j.chom.2014.02.009.

Li, L.-S. *et al.* (2024) 'CBP60b clade proteins are prototypical transcription factors mediating immunity', *Plant Physiology*, 196(2), pp. 1489–1501. Available at: https://doi.org/10.1093/plphys/kiae349.

Li, S. *et al.* (2019) 'The hypersensitive induced reaction 3 (HIR3) gene contributes to plant basal resistance via an EDS1 and salicylic acid-dependent pathway', *The Plant Journal*, 98(5), pp. 783–797. Available at: https://doi.org/10.1111/tpj.14271.

Li, Y. *et al.* (2010) 'Identification of MicroRNAs Involved in Pathogen-Associated Molecular Pattern-Triggered Plant Innate Immunity', *Plant Physiology*, 152(4), pp. 2222–2231. Available at: https://doi.org/10.1104/pp.109.151803.

Liu, J. *et al.* (2020) 'Comparative analysis of RNA-binding proteomes under Arabidopsis thaliana-Pst DC3000-PAMP interaction by orthogonal organic phase separation', *International Journal of Biological Macromolecules*, 160, pp. 47–54. Available at: https://doi.org/10.1016/j.ijbiomac.2020.05.164.

Livak, K.J. and Schmittgen, T.D. (2001) 'Analysis of Relative Gene Expression Data Using Real-Time Quantitative PCR and the 2−ΔΔCT Method', *Methods*, 25(4), pp. 402–408. Available at: https://doi.org/10.1006/meth.2001.1262.

Lorković, Z.J. and Barta, A. (2002) 'Genome analysis: RNA recognition motif (RRM) and K homology (KH) domain RNA-binding proteins from the flowering plant Arabidopsis thaliana', *Nucleic Acids Research*, 30(3), pp. 623–635. Available at: https://doi.org/10.1093/nar/30.3.623.

Louadi, Z. *et al.* (2021) 'DIGGER: exploring the functional role of alternative splicing in protein interactions', *Nucleic Acids Research*, 49(D1), pp. D309–D318. Available at: https://doi.org/10.1093/nar/gkaa768.

Lu, D. *et al.* (2010) 'A receptor-like cytoplasmic kinase, BIK1, associates with a flagellin receptor complex to initiate plant innate immunity', *Proceedings of the National Academy of Sciences*, 107(1), pp. 496–501. Available at: https://doi.org/10.1073/pnas.0909705107.

Lunde, B.M., Moore, C. and Varani, G. (2007) 'RNA-binding proteins: modular design for efficient function', *Nature Reviews Molecular Cell Biology*, 8(6), pp. 479–490. Available at: https://doi.org/10.1038/nrm2178.

Ma, X. *et al.* (2021) 'Ubiquitylome analysis reveals a central role for the ubiquitin-proteasome system in plant innate immunity', *Plant Physiology*, 185(4), pp. 1943–1965. Available at: https://doi.org/10.1093/plphys/kiab011.

Maldonado-Bonilla, L.D. *et al.* (2014) 'The Arabidopsis Tandem Zinc Finger 9 Protein Binds RNA and Mediates Pathogen-Associated Molecular Pattern-Triggered Immune Responses', *Plant and Cell Physiology*, 55(2), pp. 412–425. Available at: https://doi.org/10.1093/pcp/pct175.

Mao, J. *et al.* (2016) 'Mechanisms and Physiological Roles of the CBL-CIPK Networking System in Arabidopsis thaliana', *Genes*, 7(9), p. 62. Available at: https://doi.org/10.3390/genes7090062.

Maquat, L.E. (2005) 'Nonsense-mediated mRNA decay in mammals', *Journal of Cell Science*, 118(9), pp. 1773–1776. Available at: https://doi.org/10.1242/jcs.01701.

Maris, C., Dominguez, C. and Allain, F.H.-T. (2005) 'The RNA recognition motif, a plastic RNA-binding platform to regulate post-transcriptional gene expression', *The FEBS Journal*, 272(9), pp. 2118–2131. Available at: https://doi.org/10.1111/j.1742-4658.2005.04653.x.

Marondedze, C. *et al.* (2016) 'The RNA-binding protein repertoire of Arabidopsis thaliana', *Scientific Reports*, 6(1), p. 29766. Available at: https://doi.org/10.1038/srep29766.

Marquardt, S., Petrillo, E. and Manavella, P.A. (2023) 'Cotranscriptional RNA processing and modification in plants', *The Plant Cell*, 35(6), pp. 1654–1670. Available at: https://doi.org/10.1093/plcell/koac309.

Marquez, Y. *et al.* (2012) 'Transcriptome survey reveals increased complexity of the alternative splicing landscape in Arabidopsis', *Genome Research*, 22(6), pp. 1184–1195. Available at: https://doi.org/10.1101/gr.134106.111.

Marquez, Y. *et al.* (2015) 'Unmasking alternative splicing inside protein-coding exons defines exitrons and their role in proteome plasticity', *Genome Research*, 25(7), pp. 995–1007. Available at: https://doi.org/10.1101/gr.186585.114.

Martín, G. *et al.* (2021) 'Alternative splicing landscapes in Arabidopsis thaliana across tissues and stress conditions highlight major functional differences with animals', *Genome Biology*, 22(1), p. 35. Available at: https://doi.org/10.1186/s13059-020-02258-y.

Mastrangelo, A.M. *et al.* (2012) 'Alternative splicing: Enhancing ability to cope with stress via transcriptome plasticity', *Plant Science*, 185–186, pp. 40–49. Available at: https://doi.org/10.1016/j.plantsci.2011.09.006.

Mata-Pérez, C. and Spoel, S.H. (2019) 'Thioredoxin-mediated redox signalling in plant immunity', *Plant Science*, 279, pp. 27–33. Available at: https://doi.org/10.1016/j.plantsci.2018.05.001.

Meier, I., Richards, E.J. and Evans, D.E. (2017) 'Cell Biology of the Plant Nucleus', *Annual Review of Plant Biology*, 68(Volume 68, 2017), pp. 139–172. Available at: https://doi.org/10.1146/annurev-arplant-042916-041115.

Mejias, J. *et al.* (2021) 'The root-knot nematode effector MiEFF18 interacts with the plant core spliceosomal protein SmD1 required for giant cell formation', *New Phytologist*, 229(6), pp. 3408–3423. Available at: https://doi.org/10.1111/nph.17089.

Mermaz, B., Liu, F. and Song, J. (2018) 'RNA Immunoprecipitation Protocol to Identify Protein–RNA Interactions in Arabidopsis thaliana', in M. Bemer and C. Baroux (eds) *Plant Chromatin Dynamics: Methods and Protocols*. New York, NY: Springer, pp. 331–343. Available at: https://doi.org/10.1007/978-1-4939-7318-7_19.

Meyer, K. *et al.* (2017) 'Adaptation of iCLIP to plants determines the binding landscape of the clock-regulated RNA-binding protein AtGRP7', *Genome Biology*, 18(1), p. 204. Available at: https://doi.org/10.1186/s13059-017-1332-x.

Meyer, K., Koester, T. and Staiger, D. (2015) 'Pre-mRNA Splicing in Plants: In Vivo Functions of RNA-Binding Proteins Implicated in the Splicing Process', *Biomolecules*, 5(3), pp. 1717–1740. Available at: https://doi.org/10.3390/biom5031717.

Monaghan, J. *et al.* (2009) 'Two Prp19-Like U-Box Proteins in the MOS4-Associated Complex Play Redundant Roles in Plant Innate Immunity', *PLoS Pathogens*. Edited by J.L. Dangl, 5(7), p. e1000526. Available at: https://doi.org/10.1371/journal.ppat.1000526.

Monaghan, J., Germain, H., *et al.* (2010) 'Dissecting plant defence signal transduction: modifiers of snc1 in Arabidopsis', *Canadian Journal of Plant Pathology*, 32(1), pp. 35–42. Available at: https://doi.org/10.1080/07060661003621001.

Monaghan, J., Xu, F., *et al.* (2010) 'Two Putative RNA-Binding Proteins Function with Unequal Genetic Redundancy in the MOS4-Associated Complex', *Plant Physiology*, 154(4), pp. 1783–1793. Available at: https://doi.org/10.1104/pp.110.158931.

Monaghan, J. *et al.* (2014) 'The Calcium-Dependent Protein Kinase CPK28 Buffers Plant Immunity and Regulates BIK1 Turnover', *Cell Host & Microbe*, 16(5), pp. 605–615. Available at: https://doi.org/10.1016/j.chom.2014.10.007.

Moseler, A. *et al.* (2020) 'Novel insights into the diversity of the sulfurtransferase family in photosynthetic organisms with emphasis on oak', *New Phytologist*, 226(4), pp. 967–977. Available at: https://doi.org/10.1111/nph.15870.

Mou, Z., Fan, W. and Dong, X. (2003) 'Inducers of Plant Systemic Acquired Resistance Regulate NPR1 Function through Redox Changes', *Cell*, 113(7), pp. 935–944. Available at: https://doi.org/10.1016/S0092-8674(03)00429-X.

Mukhi, N. *et al.* (2021) 'Perception of structurally distinct effectors by the integrated WRKY domain of a plant immune receptor', *Proceedings of the National Academy of Sciences*, 118(50), p. e2113996118. Available at: https://doi.org/10.1073/pnas.2113996118.

Navarro, L. *et al.* (2004) 'The Transcriptional Innate Immune Response to flg22. Interplay and Overlap with Avr Gene-Dependent Defense Responses and Bacterial Pathogenesis', *Plant Physiology*, 135(2), pp. 1113–1128. Available at: https://doi.org/10.1104/pp.103.036749.

Ngou, B.P.M. *et al.* (2021) 'Mutual potentiation of plant immunity by cell-surface and intracellular receptors', *Nature*, 592(7852), pp. 110–115. Available at: https://doi.org/10.1038/s41586-021-03315-7.

Nicaise, V. *et al.* (2013) 'Pseudomonas HopU1 modulates plant immune receptor levels by blocking the interaction of their mRNAs with GRP7', *The EMBO Journal*, 32(5), pp. 701–712. Available at: https://doi.org/10.1038/emboj.2013.15.

Nomura, H. *et al.* (2012) 'Chloroplast-mediated activation of plant immune signalling in Arabidopsis', *Nature Communications*, 3(1), p. 926. Available at: https://doi.org/10.1038/ncomms1926.

Oh, S.A. *et al.* (1996) 'A senescence-associated gene of Arabidopsis thaliana is distinctively regulated during natural and artificially induced leaf senescence', *Plant Molecular Biology*, 30(4), pp. 739–754. Available at: https://doi.org/10.1007/BF00019008.

O'Malley, R.C., Barragan, C.C. and Ecker, J.R. (2015) 'A User's Guide to the Arabidopsis T-DNA Insertional Mutant Collections', *Methods in molecular biology (Clifton, N.J.)*, 1284, pp. 323–342. Available at: https://doi.org/10.1007/978-1-4939-2444-8_16.

Orosa-Puente, B. and Spoel, S.H. (2022) 'Harnessing the ubiquitin code to respond to environmental cues', *Essays in Biochemistry*. Edited by F. Theodoulou et al., 66(2), pp. 111–121. Available at: https://doi.org/10.1042/EBC20210094.

Palm, D. *et al.* (2016) 'Proteome distribution between nucleoplasm and nucleolus and its relation to ribosome biogenesis in *Arabidopsis thaliana*', *RNA Biology*, 13(4), pp. 441–454. Available at: https://doi.org/10.1080/15476286.2016.1154252.

Palma, K. *et al.* (2007) 'Regulation of plant innate immunity by three proteins in a complex conserved across the plant and animal kingdoms', *Genes & Development*, 21(12), pp. 1484–1493. Available at: https://doi.org/10.1101/gad.1559607.

Pandey, S.P. and Somssich, I.E. (2009) 'The Role of WRKY Transcription Factors in Plant Immunity', *Plant Physiology*, 150(4), pp. 1648–1655. Available at: https://doi.org/10.1104/pp.109.138990.

Pecher, P. *et al.* (2014) 'The Arabidopsis thaliana mitogen-activated protein kinases MPK3 and MPK6 target a subclass of 'VQ-motif'-containing proteins to regulate immune responses', *New Phytologist*, 203(2), pp. 592–606. Available at: https://doi.org/10.1111/nph.12817.

Peng, S. *et al.* (2022) 'CONSTITUTIVE EXPRESSER OF PATHOGENESIS-RELATED GENES 5 is an RNA-binding protein controlling plant immunity via an RNA processing complex', *The Plant Cell*, 34(5), pp. 1724–1744. Available at: https://doi.org/10.1093/plcell/koac037.

Peng, Y., van Wersch, R. and Zhang, Y. (2018) 'Convergent and Divergent Signaling in PAMP-Triggered Immunity and Effector-Triggered Immunity', *Molecular Plant-Microbe Interactions®*, 31(4), pp. 403–409. Available at: https://doi.org/10.1094/MPMI-06-17-0145-CR.

Petersen, M. *et al.* (2000) '*Arabidopsis* MAP Kinase 4 Negatively Regulates Systemic Acquired Resistance', *Cell*, 103(7), pp. 1111–1120. Available at: https://doi.org/10.1016/S0092-8674(00)00213-0.

Pfaff, C. *et al.* (2018) 'ALY RNA-Binding Proteins Are Required for Nucleocytosolic mRNA Transport and Modulate Plant Growth and Development', *Plant Physiology*, 177(1), pp. 226–240. Available at: https://doi.org/10.1104/pp.18.00173.

Prall, W., Sharma, B. and Gregory, B.D. (2019) 'Transcription Is Just the Beginning of Gene Expression Regulation: The Functional Significance of RNA-Binding Proteins to Post-transcriptional

Processes in Plants', *Plant and Cell Physiology*, 60(9), pp. 1939–1952. Available at: https://doi.org/10.1093/pcp/pcz067.

Qi, Y. *et al.* (2011) 'Physical Association of *Arabidopsis* Hypersensitive Induced Reaction Proteins (HIRs) with the Immune Receptor RPS2*', *Journal of Biological Chemistry*, 286(36), pp. 31297–31307. Available at: https://doi.org/10.1074/jbc.M110.211615.

Qiao, Y. *et al.* (2015) 'Phytophthora effector targets a novel component of small RNA pathway in plants to promote infection', *Proceedings of the National Academy of Sciences*, 112(18), pp. 5850–5855. Available at: https://doi.org/10.1073/pnas.1421475112.

Qiao, Y. *et al.* (2021) 'Small RNAs in Plant Immunity and Virulence of Filamentous Pathogens', *Annual Review of Phytopathology*, 59(Volume 59, 2021), pp. 265–288. Available at: https://doi.org/10.1146/annurev-phyto-121520-023514.

Qiu, J. *et al.* (2008) 'Arabidopsis MAP kinase 4 regulates gene expression through transcription factor release in the nucleus', *The EMBO Journal*, 27(16), pp. 2214–2221. Available at: https://doi.org/10.1038/emboj.2008.147.

Ramanathan, A., Robb, G.B. and Chan, S.-H. (2016) 'mRNA capping: biological functions and applications', *Nucleic Acids Research*, 44(16), p. 7511. Available at: https://doi.org/10.1093/nar/gkw551.

Rayson, S. *et al.* (2012) 'A Role for Nonsense-Mediated mRNA Decay in Plants: Pathogen Responses Are Induced in Arabidopsis thaliana NMD Mutants', *PLOS ONE*, 7(2), p. e31917. Available at: https://doi.org/10.1371/journal.pone.0031917.

Reddy, A.S.N. *et al.* (2013) 'Complexity of the Alternative Splicing Landscape in Plants', *The Plant Cell*, 25(10), pp. 3657–3683. Available at: https://doi.org/10.1105/tpc.113.117523.

Reddy, V.S. and Reddy, A.S.N. (2004) 'Proteomics of calcium-signaling components in plants', *Phytochemistry*, 65(12), pp. 1745–1776. Available at: https://doi.org/10.1016/j.phytochem.2004.04.033.

Reichel, M. *et al.* (2016) 'In Planta Determination of the mRNA-Binding Proteome of Arabidopsis Etiolated Seedlings', *The Plant Cell*, 28(10), pp. 2435–2452. Available at: https://doi.org/10.1105/tpc.16.00562.

Reichel, M. *et al.* (2024) 'Revealing the Arabidopsis AtGRP7 mRNA binding proteome by specific enhanced RNA interactome capture', *BMC Plant Biology*, 24(1), p. 552. Available at: https://doi.org/10.1186/s12870-024-05249-4.

Rico, A. *et al.* (2010) 'Agroinfiltration Reduces ABA Levels and Suppresses Pseudomonas syringae-Elicited Salicylic Acid Production in Nicotiana tabacum', *PLoS ONE*. Edited by H.A. El-Shemy, 5(1), p. e8977. Available at: https://doi.org/10.1371/journal.pone.0008977.

Rigo, R. *et al.* (2020) 'The Arabidopsis lncRNA ASCO modulates the transcriptome through interaction with splicing factors', *EMBO reports*, 21(5), p. e48977. Available at: https://doi.org/10.15252/embr.201948977.

Robatzek, S. and Somssich, I.E. (2002) 'Targets of AtWRKY6 regulation during plant senescence and pathogen defense', *Genes & Development*, 16(9), pp. 1139–1149. Available at: https://doi.org/10.1101/gad.222702.

Sanyal, S.K. *et al.* (2017) 'Arabidopsis CBL interacting protein kinase 3 interacts with ABR1, an APETALA2 domain transcription factor, to regulate ABA responses', *Plant Science*, 254, pp. 48–59. Available at: https://doi.org/10.1016/j.plantsci.2016.11.004.

Sarkar, S.F. *et al.* (2006) 'Comparative Genomics of Host-Specific Virulence in *Pseudomonas syringae*', *Genetics*, 174(2), pp. 1041–1056. Available at: https://doi.org/10.1534/genetics.106.060996.

Sarris, P.F. *et al.* (2015) 'A Plant Immune Receptor Detects Pathogen Effectors that Target WRKY Transcription Factors', *Cell*, 161(5), pp. 1089–1100. Available at: https://doi.org/10.1016/j.cell.2015.04.024.

Schenk, P.M. *et al.* (2005) 'The SEN1 gene of Arabidopsis is regulated by signals that link plant defence responses and senescence', *Plant Physiology and Biochemistry*, 43(10), pp. 997–1005. Available at: https://doi.org/10.1016/j.plaphy.2005.09.002.

Schmal, C., Reimann, P. and Staiger, D. (2013) 'A Circadian Clock-Regulated Toggle Switch Explains AtGRP7 and AtGRP8 Oscillations in Arabidopsis thaliana', *PLoS Computational Biology*. Edited by C.V. Rao, 9(3), p. e1002986. Available at: https://doi.org/10.1371/journal.pcbi.1002986.

Schöning, J.C. *et al.* (2007) 'Auto-regulation of the circadian slave oscillator component AtGRP7 and regulation of its targets is impaired by a single RNA recognition motif point mutation', *The Plant Journal*, 52(6), pp. 1119–1130. Available at: https://doi.org/10.1111/j.1365-313X.2007.03302.x.

Seidl, M.F. and Ackerveken, G.V. den (2019) 'Activity and Phylogenetics of the Broadly Occurring Family of Microbial Nep1-Like Proteins', *Annual Review of Phytopathology*, 57(Volume 57, 2019), pp. 367–386. Available at: https://doi.org/10.1146/annurev-phyto-082718-100054.

Shaul, O. (2015) 'Unique Aspects of Plant Nonsense-Mediated mRNA Decay', *Trends in Plant Science*, 20(11), pp. 767–779. Available at: https://doi.org/10.1016/j.tplants.2015.08.011.

Sidorczuk, K. *et al.* (2023) 'Characterization of signal and transit peptides based on motif composition and taxon-specific patterns', *Scientific Reports*, 13(1), p. 15751. Available at: https://doi.org/10.1038/s41598-023-42987-1.

Singh, B.K. *et al.* (2023) 'Climate change impacts on plant pathogens, food security and paths forward', *Nature Reviews Microbiology*, 21(10), pp. 640–656. Available at: https://doi.org/10.1038/s41579-023-00900-7.

Skelly, M.J. *et al.* (2019) 'Dynamic ubiquitination determines transcriptional activity of the plant immune coactivator NPR1', *eLife*, 8, p. e47005. Available at: https://doi.org/10.7554/eLife.47005.

Son, S. and Park, S.R. (2023) 'Plant translational reprogramming for stress resilience', *Frontiers in Plant Science*, 14, p. 1151587. Available at: https://doi.org/10.3389/fpls.2023.1151587.

Spoel, S.H. and Dong, X. (2012) 'How do plants achieve immunity? Defence without specialized immune cells', *Nature Reviews Immunology*, 12(2), pp. 89–100. Available at: https://doi.org/10.1038/nri3141.

Spoel, S.H. and Dong, X. (2024) 'Salicylic acid in plant immunity and beyond', *The Plant Cell*, 36(5), pp. 1451–1464. Available at: https://doi.org/10.1093/plcell/koad329.

Staiger, D. *et al.* (2003) 'The circadian clock regulated RNA-binding protein AtGRP7 autoregulates its expression by influencing alternative splicing of its own pre-mRNA', *The Plant Journal*, 33(2), pp. 361–371. Available at: https://doi.org/10.1046/j.1365-313X.2003.01629.x.

Staiger, D. *et al.* (2013) 'Emerging role for RNA-based regulation in plant immunity', *New Phytologist*, 197(2), pp. 394–404. Available at: https://doi.org/10.1111/nph.12022.

Staiger, D. and Apel, K. (1999) 'Circadian clock-regulated expression of an RNA-binding protein in Arabidopsis: characterisation of a minimal promoter element', *Molecular and General Genetics MGG*, 261(4), pp. 811–819. Available at: https://doi.org/10.1007/s004380050025.

Staiger, D. and Brown, J.W.S. (2013) 'Alternative Splicing at the Intersection of Biological Timing, Development, and Stress Responses', *The Plant Cell*, 25(10), pp. 3640–3656. Available at: https://doi.org/10.1105/tpc.113.113803.

Storozhenko, S. *et al.* (2001) 'Arabidopsis coactivator ALY-like proteins, DIP1 and DIP2, interact physically with the DNA-binding domain of the Zn-finger poly(ADP-ribose) polymerase 1', *Journal of Experimental Botany*, 52(359), pp. 1375–1380. Available at: https://doi.org/10.1093/jexbot/52.359.1375.

Streitner, C. *et al.* (2008) 'The small glycine-rich RNA binding protein *At* GRP7 promotes floral transition in *Arabidopsis thaliana*', *The Plant Journal*, 56(2), pp. 239–250. Available at: https://doi.org/10.1111/j.1365-313X.2008.03591.x.

Streitner, C. *et al.* (2010) 'Global transcript profiling of transgenic plants constitutively overexpressing the RNA-binding protein AtGRP7', *BMC Plant Biology*, 10(1), p. 221. Available at: https://doi.org/10.1186/1471-2229-10-221.

Streitner, C. *et al.* (2012) 'An hnRNP-like RNA-binding protein affects alternative splicing by in vivo interaction with transcripts in Arabidopsis thaliana', *Nucleic Acids Research*, 40(22), pp. 11240–11255. Available at: https://doi.org/10.1093/nar/gks873.

Sugiura, T., Sakurai, K. and Nagano, Y. (2007) 'Intracellular characterization of DDX39, a novel growth-associated RNA helicase', *Experimental Cell Research*, 313(4), pp. 782–790. Available at: https://doi.org/10.1016/j.yexcr.2006.11.014.

Sukarta, O.C.A. *et al.* (2022) 'GLYCINE-RICH RNA-BINDING PROTEIN 7 potentiates effector-triggered immunity through an RNA recognition motif', *Plant Physiology*, 189(2), pp. 972–987. Available at: https://doi.org/10.1093/plphys/kiac081.

Sun, T. *et al.* (2015) 'ChIP-seq reveals broad roles of SARD1 and CBP60g in regulating plant immunity', *Nature Communications*, 6(1), p. 10159. Available at: https://doi.org/10.1038/ncomms10159.

Sun, Y. *et al.* (2013) 'Structural Basis for flg22-Induced Activation of the Arabidopsis FLS2-BAK1 Immune Complex', *Science*, 342(6158), pp. 624–628. Available at: https://doi.org/10.1126/science.1243825.

Tada, Y. *et al.* (2008) 'Plant Immunity Requires Conformational Charges of NPR1 via S-Nitrosylation and Thioredoxins', *Science*, 321(5891), pp. 952–956. Available at: https://doi.org/10.1126/science.1156970.

Tang, R.-J. *et al.* (2015) 'Tonoplast CBL–CIPK calcium signaling network regulates magnesium homeostasis in Arabidopsis', *Proceedings of the National Academy of Sciences*, 112(10), pp. 3134–3139. Available at: https://doi.org/10.1073/pnas.1420944112.

Tao, Y. *et al.* (2003) 'Quantitative Nature of Arabidopsis Responses during Compatible and Incompatible Interactions with the Bacterial Pathogen Pseudomonas syringae [W]', *The Plant Cell*, 15(2), pp. 317–330. Available at: https://doi.org/10.1105/tpc.007591.

Teng, W. *et al.* (2014) 'ALY proteins participate in multifaceted Nep1Mo-triggered responses in Nicotiana benthamiana and Arabidopsis thaliana', *Journal of Experimental Botany*, 65(9), pp. 2483–2494. Available at: https://doi.org/10.1093/jxb/eru136.

Terzi, L.C. and Simpson, G.G. (2009) 'Arabidopsis RNA immunoprecipitation', *The Plant Journal*, 59(1), pp. 163–168. Available at: https://doi.org/10.1111/j.1365-313X.2009.03859.x.

Trifinopoulos, J. *et al.* (2016) 'W-IQ-TREE: a fast online phylogenetic tool for maximum likelihood analysis', *Nucleic Acids Research*, 44(W1), pp. W232–W235. Available at: https://doi.org/10.1093/nar/gkw256.

Truman, W. *et al.* (2013) 'The CALMODULIN-BINDING PROTEIN60 Family Includes Both Negative and Positive Regulators of Plant Immunity', *PLANT PHYSIOLOGY*, 163(4), pp. 1741–1751. Available at: https://doi.org/10.1104/pp.113.227108.

Tsuda, K. and Somssich, I.E. (2015) 'Transcriptional networks in plant immunity', *New Phytologist*, 206(3), pp. 932–947. Available at: https://doi.org/10.1111/nph.13286.

Uhrig, J.F. *et al.* (2004) 'Relocalization of Nuclear ALY Proteins to the Cytoplasm by the Tomato Bushy Stunt Virus P19 Pathogenicity Protein', *Plant Physiology*, 135(4), pp. 2411–2423. Available at: https://doi.org/10.1104/pp.104.046086.

Varadi, M. *et al.* (2022) 'AlphaFold Protein Structure Database: massively expanding the structural coverage of protein-sequence space with high-accuracy models', *Nucleic Acids Research*, 50(D1), pp. D439–D444. Available at: https://doi.org/10.1093/nar/gkab1061.

Verma, A. *et al.* (2018) 'The novel cyst nematode effector protein 30D08 targets host nuclear functions to alter gene expression in feeding sites', *New Phytologist*, 219(2), pp. 697–713. Available at: https://doi.org/10.1111/nph.15179.

Vlot, A.C. *et al.* (2021) 'Systemic propagation of immunity in plants', *New Phytologist*, 229(3), pp. 1234–1250. Available at: https://doi.org/10.1111/nph.16953.

Vlot, A.C., Dempsey, D.A. and Klessig, D.F. (2009) 'Salicylic Acid, a Multifaceted Hormone to Combat Disease', *Annual Review of Phytopathology*, 47(Volume 47, 2009), pp. 177–206. Available at: https://doi.org/10.1146/annurev.phyto.050908.135202.

Wachter, A., Rühl, C. and Stauffer, E. (2012) 'The Role of Polypyrimidine Tract-Binding Proteins and Other hnRNP Proteins in Plant Splicing Regulation', *Frontiers in Plant Science*, 3. Available at: https://doi.org/10.3389/fpls.2012.00081.

Wang, C. and Luan, S. (2024) 'Calcium homeostasis and signaling in plant immunity', *Current Opinion in Plant Biology*, 77, p. 102485. Available at: https://doi.org/10.1016/j.pbi.2023.102485.

Wang, Jinlong *et al.* (2018) 'A Regulatory Module Controlling Homeostasis of a Plant Immune Kinase', *Molecular Cell*, 69(3), pp. 493-504.e6. Available at: https://doi.org/10.1016/j.molcel.2017.12.026.

Wang, L. *et al.* (2009) 'Arabidopsis CaM Binding Protein CBP60g Contributes to MAMP-Induced SA Accumulation and Is Involved in Disease Resistance against Pseudomonas syringae', *PLOS Pathogens*, 5(2), p. e1000301. Available at: https://doi.org/10.1371/journal.ppat.1000301.

Wang, L. *et al.* (2020) 'RALF1-FERONIA complex affects splicing dynamics to modulate stress responses and growth in plants', *Science Advances*, 6(21), p. eaaz1622. Available at: https://doi.org/10.1126/sciadv.aaz1622.

Wheeler, E.C., Van Nostrand, E.L. and Yeo, G.W. (2018) 'Advances and challenges in the detection of transcriptome-wide protein–RNA interactions', *WIREs RNA*, 9(1), p. e1436. Available at: https://doi.org/10.1002/wrna.1436.

Wilkinson, M.E., Charenton, C. and Nagai, K. (2020) 'RNA Splicing by the Spliceosome', *Annual Review of Biochemistry*, 89(Volume 89, 2020), pp. 359–388. Available at: https://doi.org/10.1146/annurev-biochem-091719-064225.

Williams, S.J. *et al.* (2014) 'Structural Basis for Assembly and Function of a Heterodimeric Plant Immune Receptor', *Science*, 344(6181), pp. 299–303. Available at: https://doi.org/10.1126/science.1247357.

Woloshen, V., Huang, S. and Li, X. (2011) 'RNA-Binding Proteins in Plant Immunity', *Journal of Pathogens*, 2011, p. e278697. Available at: https://doi.org/10.4061/2011/278697.

Xu, F. *et al.* (2024) 'Phase separation of GRP7 facilitated by FERONIA-mediated phosphorylation inhibits mRNA translation to modulate plant temperature resilience', *Molecular Plant*, 17(3), pp. 460–477. Available at: https://doi.org/10.1016/j.molp.2024.02.001.

Xu, X. *et al.* (2006) 'Physical and Functional Interactions between Pathogen-Induced *Arabidopsis* WRKY18, WRKY40, and WRKY60 Transcription Factors', *The Plant Cell*, 18(5), pp. 1310–1326. Available at: https://doi.org/10.1105/tpc.105.037523.

Yamaguchi, Y. and Huffaker, A. (2011) 'Endogenous peptide elicitors in higher plants', *Current Opinion in Plant Biology*, 14(4), pp. 351–357. Available at: https://doi.org/10.1016/j.pbi.2011.05.001.

Yao, J., Withers, J. and He, S.Y. (2013) 'Pseudomonas syringae Infection Assays in Arabidopsis', in A. Goossens and L. Pauwels (eds) *Jasmonate Signaling*. Totowa, NJ: Humana Press (Methods in Molecular Biology), pp. 63–81. Available at: https://doi.org/10.1007/978-1-62703-414-2_6.

Yeap, W.-C., Namasivayam, P. and Ho, C.-L. (2014) 'HnRNP-like proteins as post-transcriptional regulators', *Plant Science*, 227, pp. 90–100. Available at: https://doi.org/10.1016/j.plantsci.2014.07.005.

Yin, Z., Shi, J. and Zhen, Y. (2021) 'Quantitative Phosphoproteomics of cipk3/9/23/26 Mutant and Wild Type in Arabidopsis thaliana', *Genes*, 12(11), p. 1759. Available at: https://doi.org/10.3390/genes12111759.

Yu, X. *et al.* (2017) 'From Chaos to Harmony: Responses and Signaling upon Microbial Pattern Recognition', *Annual Review of Phytopathology*, 55(Volume 55, 2017), pp. 109–137. Available at: https://doi.org/10.1146/annurev-phyto-080516-035649.

Yu, X. *et al.* (2019) 'Orchestration of Processing Body Dynamics and mRNA Decay in Arabidopsis Immunity', *Cell Reports*, 28(8), pp. 2194-2205.e6. Available at: https://doi.org/10.1016/j.celrep.2019.07.054.

Yu, Z. *et al.* (2020) 'The Brassicaceae-specific secreted peptides, STMPs, function in plant growth and pathogen defense', *Journal of Integrative Plant Biology*, 62(4), pp. 403–420. Available at: https://doi.org/10.1111/jipb.12817.

Yuan, M. *et al.* (2021) 'PTI-ETI crosstalk: an integrative view of plant immunity', *Current Opinion in Plant Biology*, 62, p. 102030. Available at: https://doi.org/10.1016/j.pbi.2021.102030.

Zaidi, S.S.-A. *et al.* (2020) 'Engineering crops of the future: CRISPR approaches to develop climate-resilient and disease-resistant plants', *Genome Biology*, 21(1), p. 289. Available at: https://doi.org/10.1186/s13059-020-02204-y.

Zhang, B. *et al.* (2023) 'Salicylic acid accelerates carbon starvation-induced leaf senescence in *Arabidopsis thaliana* by inhibiting autophagy through Nonexpressor of pathogenesis-related genes 1', *Plant Science*, 336, p. 111859. Available at: https://doi.org/10.1016/j.plantsci.2023.111859.

Zhang, C. *et al.* (2013) 'Crosstalk between the Circadian Clock and Innate Immunity in Arabidopsis', *PLOS Pathogens*, 9(6), p. e1003370. Available at: https://doi.org/10.1371/journal.ppat.1003370.

Zhang, F. *et al.* (2023) 'HybridRNAbind: prediction of RNA interacting residues across structure-annotated and disorder-annotated proteins', *Nucleic Acids Research*, 51(5), pp. e25–e25. Available at: https://doi.org/10.1093/nar/gkac1253.

Zhang, H. *et al.* (2012) 'The Nicotiana benthamiana Mitogen-Activated Protein Kinase Cascade and WRKY Transcription Factor Participate in Nep1Mo-Triggered Plant Responses', *Molecular Plant-Microbe Interactions®*, 25(12), pp. 1639–1653. Available at: https://doi.org/10.1094/MPMI-11-11-0293.

Zhang, R. *et al.* (2017) 'A high quality Arabidopsis transcriptome for accurate transcript-level analysis of alternative splicing', *Nucleic Acids Research*, 45(9), pp. 5061–5073. Available at: https://doi.org/10.1093/nar/gkx267.

Zhang, R. *et al.* (2022) 'A high-resolution single-molecule sequencing-based Arabidopsis transcriptome using novel methods of Iso-seq analysis', *Genome Biology*, 23(1), p. 149. Available at: https://doi.org/10.1186/s13059-022-02711-0.

Zhang, S. *et al.* (1993) 'Fungal Elicitor-Induced Bean Proline-Rich Protein mRNA Down-Regulation Is Due to Destabilization That Is Transcription and Translation Dependent.', *The Plant Cell*, pp. 1089–1099. Available at: https://doi.org/10.1105/tpc.5.9.1089.

Zhang, S. *et al.* (2022) 'Action Mechanisms of Effectors in Plant-Pathogen Interaction', *International Journal of Molecular Sciences*, 23(12), p. 6758. Available at: https://doi.org/10.3390/ijms23126758.

Zhang, S. and Mehdy, M.C. (1994) 'Binding of a 50-kD Protein to a U-Rich Sequence in an mRNA Encoding a Proline-Rich Protein That Is Destabilized by Fungal Elicitor.', *The Plant Cell*, pp. 135–145. Available at: https://doi.org/10.1105/tpc.6.1.135.

Zhang, X.-C. and Gassmann, W. (2003) 'RPS4-Mediated Disease Resistance Requires the Combined Presence of RPS4 Transcripts with Full-Length and Truncated Open Reading Frames', *The Plant Cell*, 15(10), pp. 2333–2342. Available at: https://doi.org/10.1105/tpc.013474.

Zhang, X.-C. and Gassmann, W. (2007) 'Alternative Splicing and mRNA Levels of the Disease Resistance Gene *RPS4* Are Induced during Defense Responses', *Plant Physiology*, 145(4), pp. 1577–1587. Available at: https://doi.org/10.1104/pp.107.108720.

Zhang, Y. *et al.* (2005) 'MOS2, a Protein Containing G-Patch and KOW Motifs, Is Essential for Innate Immunity in *Arabidopsis thaliana*', *Current Biology*, 15(21), pp. 1936–1942. Available at: https://doi.org/10.1016/j.cub.2005.09.038.

Zhang, Y. *et al.* (2020) 'Genetic Network between Leaf Senescence and Plant Immunity: Crucial Regulatory Nodes and New Insights', *Plants*, 9(4), p. 495. Available at: https://doi.org/10.3390/plants9040495.

Zhang, Y. *et al.* (2023) 'Plant phase extraction: A method for enhanced discovery of the RNA-binding proteome and its dynamics in plants', *The Plant Cell*, 35(8), pp. 2750–2772. Available at: https://doi.org/10.1093/plcell/koad124.

Zhang, Z. *et al.* (2017) 'mRNA Interactome Capture from Plant Protoplasts', *Journal of Visualized Experiments : JoVE*, (125), p. 56011. Available at: https://doi.org/10.3791/56011.

Zhou, N., Tootle, T.L. and Glazebrook, J. (1999) 'Arabidopsis *PAD3* , a Gene Required for Camalexin Biosynthesis, Encodes a Putative Cytochrome P450 Monooxygenase', *The Plant Cell*, 11(12), pp. 2419–2428. Available at: https://doi.org/10.1105/tpc.11.12.2419.

Zhu, C. *et al.* (2022) 'A fungal effector suppresses the nuclear export of AGO1–miRNA complex to promote infection in plants', *Proceedings of the National Academy of Sciences*, 119(12), p. e2114583119. Available at: https://doi.org/10.1073/pnas.2114583119.

Zhu, J. *et al.* (2023) 'Single-cell profiling of Arabidopsis leaves to Pseudomonas syringae infection', *Cell Reports*, 42(7). Available at: https://doi.org/10.1016/j.celrep.2023.112676.